

Title	The application of machine learning and 3D photogrammetry for cold-water coral habitat classification in the NE Atlantic
Authors	de Oliveira, Larissa Macêdo Cruz
Publication date	2023
Original Citation	de Oliveira, L. M. C. 2023. The application of machine learning and 3D photogrammetry for cold-water coral habitat classification in the NE Atlantic. PhD Thesis, University College Cork.
Type of publication	Doctoral thesis
Rights	© 2023, Larissa Macêdo Cruz de Oliveira. - https://creativecommons.org/licenses/by-nc-nd/4.0/
Download date	2025-07-04 01:57:59
Item downloaded from	https://hdl.handle.net/10468/14482

Ollscoil na hÉireann, Corcaigh
National University of Ireland, Cork



**The application of machine learning and 3D
photogrammetry for Cold-water Coral habitat
classification in the NE Atlantic**

Thesis presented by

Larissa Macêdo Cruz de Oliveira, BSc (Hons) in Geology

ORCID: <https://orcid.org/0000-0003-4806-0048>

for the degree of

Doctor of Philosophy

University College Cork

School of Biological, Earth & Environmental Sciences

Head of School/Department: Prof. Astrid Wingler

Supervisor(s): Prof. Andrew Wheeler, Dr Aaron Lim & Prof. Luis A. Conti

February, 2023

Table of Contents

Table of Contents	ii
List of Figures.....	vi
List of Tables.....	xiii
List of Abbreviations	xiv
Declaration	xvi
Acknowledgements	xvii
Outline.....	xx
Abstract	xxi
1. Introduction	1
1.1 Cold-Water Corals.....	1
1.1.1 The Importance Of Corals And Cold-Water Coral Reefs	1
1.1.2 Definition And Development Of Cold-Water Corals.....	2
1.1.3 Global Distribution Of Cold-Water Corals	6
1.1.4 The Role Of Cold-Water Corals In Local Biodiversity	8
1.2 Study areas	9
1.2.1 Porcupine Bank Canyon	9
1.2.2 Piddington Mound.....	10
1.3 High-Resolution Mapping Trends For Cold-Water Coral Environments.....	12
1.3.1 Photogrammetry	13
1.3.2 Structure-from-Motion (SfM)	14
1.3.3 Automated Classification Of Coral Reefs	21
1.4 Rationale	23
1.5 Aims And Research Questions	26
1.6 References	30
2. 3D Classification of Cold-Water Coral Reefs: A Comparison of Classification Techniques for 3D Reconstructions of Cold-Water Coral Reefs and Seabed	56
Abstract.....	58
2.1 Introduction	59
2.2 Materials and Methods.....	62
2.2.1 Study Area	62
2.2.2 Video Survey and Data Collection	64
2.2.3 3D Reconstruction Using Structure-From-Motion (SfM) Photogrammetry.....	65
2.2.4 Classification Methods	66
2.3 Results	72
2.3.1 Coral and Seabed Distribution in the Porcupine Bank Canyon	72

2.3.2	Multiscale Geometrical Classification (MGC).....	73
2.3.3	Colour and Geometrical Classification (CGC).....	76
2.3.4	Object-Based Image Classification (OBIA).....	78
2.4	Discussion.....	79
2.4.1	Classification results.....	80
2.4.2	Comparison Within 3D Classifications.....	82
2.4.3	Cost and Data Loss Related to Representing 3D Objects as 2D.....	84
2.4.4	Main Advantages and Disadvantages of the 3D Workflows Identified Within This Study	86
2.5	Conclusions.....	88
2.6	References.....	89
2.7	Supplementary materials.....	105
3.	High-resolution 3D Mapping Of Cold-Water Coral Reefs Using Machine Learning.....	107
	Abstract.....	109
3.1	Introduction.....	110
3.2	Study Area.....	114
3.3	Materials and Methods.....	116
3.3.1	Photogrammetry.....	116
3.3.2	Multiclass Classification Of 3D Point Clouds.....	118
3.4	Results.....	125
3.4.1	3D Reconstructions.....	125
3.4.2	Multiclass Classification Results.....	126
3.5	Discussion.....	134
3.5.1	Machine Learning And 3D Reconstructions Of Coral Reef Environments.....	135
3.5.2	Classifier Performance.....	135
3.5.3	Sample Size And Accuracy Variation.....	139
3.6	Conclusions.....	141
3.7	References.....	143
3.8	Supplementary Materials.....	155
3.8.1	Supplementary overview of the classification algorithms used in the study.....	157
3.8.2	Overview of the Performance assessment.....	160
4.	Cold-Water Coral Spatial Relationships Based On The Analysis Of High-Resolution Photogrammetry And Terrain Descriptors.....	162
	Abstract.....	164
4.1	Introduction.....	165
4.2	Materials and Methods.....	168
4.2.1	Study area.....	168

4.2.2	Structure-from-Motion Photogrammetry.....	169
4.2.3	Data Segmentation And Classification	169
4.2.4	Terrain Variable Extraction From Digital Elevation Model (DEM)	171
4.2.5	Point Pattern Spatial Analysis	172
4.3	Results	175
4.3.1	Geomorphometric Characterisation Of The Terrain	175
4.3.2	Facies Distribution Analysis.....	178
4.4	Discussion	191
4.5	Conclusions.....	198
4.6	References	199
5.	Developing Mobile Applications with Augmented Reality and 3D Photogrammetry for Visualisation of Cold-Water Coral Reefs and Deep-Water Habitats	215
	Abstract.....	217
5.1	Introduction.....	218
5.2	Materials and Methods.....	223
5.2.1	Data Acquisition.....	223
5.2.2	3D Models with Structure-from-Motion Photogrammetry.....	225
5.2.3	Three-Dimensional Android APP Development	226
5.3	Results	227
5.3.1	Photogrammetry	227
5.3.2	The Coral APP	230
5.4	Discussion	233
5.5	Conclusions.....	236
5.6	References	238
6.	Conclusions	250
6.1	Concluding remarks	250
6.2	Future Directions	259
	Appendix I.....	260
	Chapter 2.....	265
	Chapter 3.....	267
	Chapter 4.....	269
	Chapter 5.....	273
	Appendix II.....	274
	Appendix III.....	275
	Appendix IV	278
	Appendix V	280
	Appendix VI	282

Appendix VII 284
Appendix VIII..... 285
Appendix IX..... 289

List of Figures

Figure 1.1: Illustration of a CWC mound cycle proposed in Roberts et. al (2006). Mound cycle stages reflecting the environmental change during recurrent glacial cycles. Extracted from Roberts et. al (2006).....	5
Figure 1.2: Global distribution of Cold-water Corals as of 2004. Scleractinia in red. Extracted from: Freiwald A, Rogers A, Hall-Spencer J, Guinotte JM, Davies AJ, Yesson C, Martin CS, Weatherdon LV (2021). Global distribution of cold-water corals (version 5.1). Fifth update to the dataset in Freiwald et al. (2004) by UNEP-WCMC, in collaboration with Andre Freiwald and John Guinotte. Cambridge (UK): UN Environment Programme World Conservation Monitoring Centre.....	7
Figure 1.3 Location of Porcupine Bank Canyon and Belgica Mound Province Special Areas of Conservation (SAC) studied herein.....	11
Figure 1.4: Standard Structure-from-Motion workflow for the production of georeferenced dense point clouds. Inputs and outputs are shown in red. From the top right to bottom right: valid image matches generated from key point correspondence, sparse point cloud, dense point cloud. Image extracted from Smith et al. (2016).	16
Figure 1.5: An overview of high-resolution data formats. Point cloud data (top) can be transformed into meshes by interpolation, gridding of the point cloud into a 2D plane can generate 2.5D rasters such as digital elevation models (DEMs) Extracted from D'Urban et al. (2020).	18
Figure 2.1: Study site (in red)—The Porcupine Bank Canyon study area on the Irish continental margin west of Ireland	63
Figure 2.2: Workflow for 3D model reconstruction and applications of each output data within this study.	66
Figure 2.3: Map showing the location of the Porcupine Bank Canyon on the Irish continental shelf and the location of each SfM reconstructed dense cloud produced in this study and its respective	

class distribution with manual annotation. Blue represents seabed and orange represents coral.
.....73

Figure 2.4: Classifier accuracy in relation to the number of scales. The classifier ID is placed on the top of each bar. In the MGC method, scale is defined as the neighbourhood size of pixels to which the classifiers compute each metrics.74

Figure 2.5: Confusion matrices representing the MGC classification results for each dense cloud reconstruction. Confusion matrices show the accuracy score and the relationship between the referenced data and the classification. The “Actual class” on the y-axis refers to the manually annotated data, whereas the “Predicted class” on the x-axis relates to the classification output. The main diagonal of the matrices lists the correctly classified percentage of points per class. The colour scale bar on the right of each confusion matrix represents the number of points.75

Figure 2.6: Model F - Results of classification using the MGC method – (A) Dense cloud (B) Classification output. Model with predominance of black corals (*Leiopathes sp.*). Red is seabed and blue is coral. Model A – Results of classification using the MGC method – (A) Dense cloud (B) Classification output. Model with predominance of coral rubble patterns. Red is seabed and blue is coral.76

Figure 2.7: Results of classification using CGC method—(A) Dense cloud and (B) classification output with CGC method.....77

Figure 2.8: Confusion matrices representing the CGC classification results for each dense cloud reconstruction. The “Actual class” on the y-axis refers to the manually annotated data, whereas the “Predicted class” on the x-axis relates to the classification output. The main diagonal of the matrices lists the correctly classified percentage of points per class. The colour scale bar on the right of each confusion matrix represents the number of points.78

Figure 2.9: Results of classification using OBIA method—(A) Orthomosaic, (B) output of the multi-resolution automated segmentation, and (C) manual classification.79

Supplementary Figure 2.10. Workflow for the Multiscale Geometrical Classification (MGC). ...105

Supplementary Figure 2.11: Workflow for the Colour and Geometrical Classification method (CGC)	105
Supplementary Figure 2.12: Workflow for the method 2D Object-based Image classification (OBIA)	106
Figure 3.1: Map of the study site (A): Porcupine Seabight location relative to Ireland. The blue box indicates the location of the Belgica Mound Province (BMP) Special Area of Conservation (SAC) (B) Close view of the Porcupine Seabight and BMP with the Piddington Mound. (C) Bathymetric map of the Moira Mounds and location of the Piddington Mound Area (red box) within adjacent mounds.	115
Figure 3.2: (A) Original 3D dense cloud reconstruction of the on-mound section of the Piddington Mound (B) its relative ground-truth labels (C) Percentage class distribution of the reconstructed area.	126
Figure 3.3: Bar plot showing the $f1$ accuracy results of all 18 classifiers grouped by algorithm type. Light blue bars represent classifiers trained in group 2 (dataset 2, 10,000 samples) and dark blue bars represent classifiers trained in group 1 (dataset 1, 1,000 samples). The red dotted line indicates $f1 < 60\%$ threshold. Run times (in minutes) for group 1 (orange) and group 2 (green) represented in the secondary axis on the right are plotted against $f1$ accuracy.	127
Figure 3.4: Classification outputs of the top four performing classifiers ($f1$ score $> 90\%$). (A) Classification output of the GBT classifier GBT_GS_1_10000, $f1$ score: 95.1% (B) Classification output of the RF classifier RF_GS_2_10000, $f1$ score: 94.2% (C) Classification output of the MLP classifier MLP_GS_7_10000, $f1$ score: 92.3% (D) Classification output of the KNN classifier KNN_GS_1_10000, $f1$ score: 91.6%.	131
Figure 3.5: Difference of class distribution from the ground-truth labels against the classification output labels of the top four performing classifiers ($f1$ score $> 90\%$). (A) Difference of classification output vs. ground truth of the GBT classifier GBT_GS_1_10000, $f1$ score: 95.1% (B) Difference of classification output vs. ground truth of the RF classifier RF_GS_2_10000, $f1$ score: 94.2% (C)	

Difference of classification output vs. ground truth of the MLP classifier MLP_GS_7_10000, *f1* score: 92.3% (D) Difference of classification output vs. ground truth of the KNN classifier KNN_GS_1_10000, *f1* score: 91.6%.....132

Figure 3.6: ROC curves of the four best-performing classifiers (*f1* > 90%). The name of the classifiers and their *f1* score obtained on the first accuracy assessment were placed on the top of their respective graph. The AUC score for each label is placed on the lower right side of each graph. Label 1 = LCV, label 2 = SD, label 3 = DCF, label 4 = CR. (A) ROC curve of GBT classifier GBT_GS_1_10000, *f1* score: 95.1% (B) ROC curve of the RF classifier RF_GS_2_10000, *f1* score: 94.2% (C) ROC curve of the output of the MLP classifier MLP_GS_7_10000, *f1* score: 92.3% (D) ROC curve of the KNN classifier KNN_GS_1_10000, *f1* score: 91.6%.133

Figure 3.7: ROC curve of the worst performing classifiers (*f1* < 60%). The name of the classifiers and their *f1* score obtained on the first accuracy assessment were placed on the top their respective graph. The AUC score for each label is placed on the lower right side of each graph. Label 1 = LCF, label 2 = SD, label 3 = DCF, label 4 = CR. (A) ROC curve of MLP classifier MLP_GS_6_1000, *f1* score: 50.6% (B) ROC curve of the MLP classifier MLP_GS_1_1000, *f1* score: 58.1% (C) ROC curve of output of the MLP classifier MLP_GS_1_10000, *f1* score: 58.08% (D) ROC curve of the LR classifier LR_GS_1_1000, *f1* score: 59.6%.....134

Figure 4.1: Spatial distribution of geomorphometric variables at 50cm/pixel resolution. (A) Orthomosaic (B) Hill shaded DEM (C) Slope (D) Curvature (E) Eastness (F) Northness (G) Rugosity (Arc-Chord Ratio) (H) BPI calculated with a 3x3 kernel size (I) Vector Ruggedness Measure (VRM) at 50 cm/pixel (J) VRM at 3.39mm/pixel.177

Figure 4.2: (A) Slope view of the hill shaded DEM overlaid with Euclidean radius buffers of DC (yellow) and LC facies (green) (B) Percentage of each of the four facies found in the study area. Percentages of each facies: SD = 49%, CR = 38.8%, LC = 8.9% and DC = 3.3%. (C) South facing view of the hill shaded DEM overlaid with Euclidean radius buffers (spheres) of DC and LC facies. Spheres not to scale (D) Distribution of LC and DC facies object sizes (euc_rad) relative to depth (centroid_z). (E) Box plots of Euclidean radii distribution of LC (green), DC (yellow)179

Figure 4.3: Violin box plots showing the distribution of abiotic (terrain) variables for each facies at 50cm/pixel resolution. (A) Depth (m) (B) Slope (C) Bathymetry Position Index (BPI) (D) Curvature (E) Northness (F) Eastness (G) Vector Ruggedness Measure (VRM) (H) Rugosity index (Arc-Chord Ratio).182

Figure 4.4: Spearman’s Correlation coefficient (SCC) matrix for the entire study area (left). Only coefficients that were significant at the level of 95% were included.....183

Figure 4.5: Subplots of Spearman’s correlation coefficients for each facies , where green= LC, orange= DC, blue = CR, and red= SD.184

Figure 4.7: Estimated density function in relation to terrain covariates (rho_{hat}) for (A) live coral (LC) facies (B) and dead coral (DC) facies and respective density estimate plots. The grey area on rho_{hat} plots represents the 95% confidence envelope.186

Figure 4.8: Kernel estimate intensity plots of number of points per m² (sigma=1) of Live coral (LC) facies (left) and Dead coral (DC) facies (right) separated in (A) LC facies all sizes (B) DC facies all sizes (C) LC of small size (Euclidean radius ≤ 0.17m) (D) DC of small size (E) LC of medium size (Euclidean radius ≤ 0.33 m) (F) DC of medium size (G) LC of large sizes (Euclidean radius ≤ 0.49m) (H) DC of large sizes.188

Figure 4.9: Scatter plots showing the High-Low clustering (Getis-Ord General G) results of (A) Live coral (LC) facies (B) Dead coral (DC) facies. Gi Z-score (X axis) shows the intensity of the clustering vs. depth (y-axis). The sizes of the circles represent the relative Euclidean radii of the facies sphere.189

Figure 4.10: L-function plots showing the clustering likelihood in relation to the distance of each point (r(m)) of (A) Live coral (LC) facies and (B) dead coral (DC) facies. The grey shaded area represents the confidence interval of 95% from 999 Montecarlo simulations (nrank=25).190

Figure 5.1: Location of the study site in the Piddington Mound, Belgica Mound Province area relative to the Irish margin. Upper left: extracted HD video frame of the study site.224

Figure 5.2: Generalised workflow of the methodology from the video acquisition to the APP development.	225
Figure 5.3: Workflow of the platforms used in the development of the Android APP.....	226
Figure 5.4: Demonstration of AR APP integration with the mobile phone and QR Code of two models. The background image shows the map of the study area in relation to Ireland and the QR Code for interaction: (a) demonstration of APP visualisation of Model D and (b) demonstration of APP visualisation of Model B.	230
Figure 5.5: Three-dimensional models of CWC: Model A with 1,124,301 faces and 4,177,311 vertices at a resolution of 297,749.21 faces/area (m ²); Model B with 462,589 faces and 232,453 vertices at a resolution of 31,825.87 faces/area (m ²); Model C with 6,285,480 faces and 3,154,610 vertices at 292,660.99 faces/area (m ²); Model D with 44,000 faces and 22,122 vertices at 4108.31 faces/area (m ²), with A extracted from C.	231
Figure 5.6: Relationship of the number of faces (x-axis) and number of vertices (blue trend line) in relation to the size of the APP in MB (y-axis).	233
Figure 5.7: View of Model A (297,749.21 faces/m ² resolution) and Model D (4,108.31 faces/m ² resolution) from Unity 3D desktop. Here, it is possible to see the resolution differences between models.....	234
Figure 5.8: Interactive map for the AR app visualisation. After downloading the APP (APK) on their phone, the user can open app and scan the QR Code (left) on the map.....	236
Figure 0.1 Class distribution of each 3D model reconstructed from the Porcupine Bank Canyon (PBC)	265
Figure 0.2 Accuracy comparison between the Multiscale Geometric Classification method (MGC) and the Colour Geometrical Classification (CGC) method	265
Figure 0.3 Workflow of the study design developed for Chapter 3.....	267
Figure 0.4 Examples of the four facies categorised in the study.....	268

Figure 0.5: Getis Ord Gi hotspot results for the Dead coral facies (left) and Live coral facies (right)	269
Figure 0.6 Ripley's K function plots for Live coral facies (left) and Dead coral facies (right). The shaded grey area represents the 95% confidence bands	270
Figure 0.7 Ripley's K functions for Live coral facies (left) and Dead coral facies (right)	270
Figure 0.8 Berman's Z2 tests for the density in function of covariate tests of Live Coral facies (Rhohat function)	271
Figure 0.9 Figure 0.7 Berman's Z2 tests for the density in function of covariate tests of Dead Coral facies (Rhohat function)	272
Figure 0.10: Coral APP flyer used in outreach events in 2022	273
Figure 0.1: Results of the MSc project (1) an image from the Piddington Mound dataset, (2) the ground-truth dense labels manually created of this image (3) the dense labels created for this image using the Fast-MSS algorithm (4) An image overlay of the ground truth image and the actual image, and () An image overlay of the Fast-MSS image and the actual image (Credits: David Dalton, MSc student)	276

List of Tables

Table 2.1: Accuracy metrics for Method 1 – Multiscale Geometrical Classification (MGC), Method 2 - Colour and Geometrical Classification (CGC) and Method 3 – Object-based Image Classification (OBIA).....	83
Table 2.2: Percentage of class distribution results for each habitat and each class in 2D and 3D	85
Table 3.1: Class label definitions used in the study	118
Supplementary Table 3.2: Summary of <i>f1</i> accuracies results of the top performing classifiers in group 1 and group 2. The first column “Classifiers” shows the given names of each classifiers. Names ending at “1000” indicates the number of samples to which the classifiers were trained i.e. Group 1. Similarly, classifier names ending in “10000” indicates this version of the classifier was trained on Group 2, i.e. 10000 samples.	155
Table 4.1: Definition of each facies used in the study.....	170
Table 4.2: Geomorphometric variables extracted from the DEM, the neighbourhood (kernel) size and the resolution of the DEM from which the variables were extracted.....	171
Table 5.1: Metadata of each 3D model used in the study.	228
Table 0.1 Total of video frames per ROV transect used in the 3D reconstructions of the study area analysed in Chapter 3,4 and 5	260
Table 0.2: Comparison among frame extraction tools to analyse the impact of frame extraction on the photogrammetry reconstruction workflow	262
Table 0.3 Summary of comparisons among the MGC, CGC and OBIA methods	266

List of Abbreviations

AIC	Akaike's Information Criterion
ANN	Approximate Nearest Neighbours
ASH	Aragonite saturation horizon
AUC	Area Under the Receiver Operating Curve
AUV	Autonomous Underwater Vehicle
BPI	Bathymetric Positioning Index
BMP	Belgica Mound Province
CNN	Convolutional Neural Networks
CWC	Cold-water coral
DEM	Digital Elevation Model
ENAW	Eastern North Atlantic Water
GBT	Gradient Boosted Trees
GCP	Ground Control Point
HD	High definition
LR	Logistic Regression
ML	Machine Learning
MBES	Multibeam echosounder
MLP	Multilayer Perceptron
MOW	Mediterranean Outflow Water
MPA	Marine Protected Area
MVS	Multi-view stereo
KNN	k-Nearest Neighbours
OBIA	Object-based Image Analysis
PPA	Point Pattern Analysis
PCF	Pair Correlation Function
PSU	Practical Salinity Unity
PPM	Point Pattern Modelling
PBC	Porcupine Bank Canyon

RANSAC	Random Sample Consensus
AIC	Akaike's Information Criterion
ANN	Approximate Nearest Neighbours
RF	Random Forest
ROC	Receiver Operating Characteristic
ROV	Remotely Operated Vehicle
SAC	Special Areas of Conservation
SDGs	Sustainable Development Goals
SBES	Single Beam echosounder
SIFT	Scale Invariant Feature Transform
SfM	Structure-from-Motion
SVM	Support Vector Machines
SSS	Side-scan sonar
VRM	Vector Ruggedness Measure
°C	Celsius
3D	Three-dimensional

Declaration

This is to certify that the work I am submitting is my own and has not been submitted for another degree, either at University College Cork or elsewhere. All external references and sources are clearly acknowledged and identified within the contents. I have read and understood the regulations of University College Cork concerning plagiarism and intellectual property.



Signed

Larissa Macedo Cruz de Oliveira, author.



Signed

Prof. Andy Wheeler, supervisor of research.



Signed

Dr. Aaron Lim, co-supervisor of research.



Signed

Prof Luis Conti, co-supervisor of research.

Acknowledgements

To my supervisors Prof Andy Wheeler, Dr Aaron Lim and Prof Luis Conti, I will be forever grateful for the guidance and support. Thank you for fostering my interest in marine sciences, seabed mapping and cold-water corals. Thank you for sharing your wisdom and for trusting me to conduct this research. Andy, thank you for your academic guidance, extensive and passionate knowledge about life and deep-water habitats. Aaron, your life has changed massively in the past 4 years and yet, you always made time to help and provide massive guidance throughout my PhD. Thank you for believing in my potential, sometimes more than I believed it myself, for the crucial ‘mental clearing up’ meetings and for life mentorship. You are the example of dedication, positivity, creativity, focus and knowledge that I will carry with me going forward.

I would not be here if it wasn't for my parents Antonio and Gloria. Thank you for making a massive effort to provide us with education and for being my example of dedication and perseverance. *Mainha, obrigada pela sua positividade inabalável, por ser um exemplo de resistência, por me trazer o colo de mãe quando eu preciso e por sempre me apoiar nas minhas aventuras. Painho, obrigado por me mostrar o que astúcia, pelos muitos conselhos acadêmicos e de vida e por despertar em mim a vontade de investigar o mundo.*

Thank you to Nathalie Macêdo and Lucas Macêdo. Nathalie, thank you for being a role model of discipline and tenacity. You inspired me to also become a doctor but ‘not that kind of doctor’. Lucas, thank you for showing me how to take things lightly, ‘except during a weights session’.

I also would like to thank the amazing people in the Marine Geosciences Research group: Ger Summers, Luke O'Reilly, John Appah, Audrey Recouvreur, Alicia Cardenas, Felix Butschek, Riccardo Arosio and former members, Ruaihri (Rasher) Strachan, Evan O'Mahony, Guillaume Michel, Siobáhn Burke, Stephanie Dunne and Kimberly Harris. Ger and Luke, I am grateful for sharing the PhD journey with you. Thank you for all the ‘I can relate’ chats and great moments. With you I understood the meaning of the word ‘banter’. Thank you to the amazing people I have met along these 4 years: Ninon Robin, Aude Cincotta, Mohit Tunwal, Naomi O'Reilly, Daniel Falk, Juergen Lang, Juan Cuenca, Julia Terra, Luisa Andrade, Hannah Binner, Bea Carazo, Aaron Quigley, Dan Cirtina, Valentina Rossi, Tiffany Slater and Marta Cabello. Thank you Ninon, Aude, Audrey and Moe for sharing great experiences with me and using your ‘posdoc wisdom’ to tell me it's all going to be okay at the end.

An especial thank you to Ed, a mentor and a friend, for the much-needed hours of chat and cuppas that helped me during the three lockdowns. Thank you, John Boyd, from SmartSea School for trusting me with passing on the knowledge I gathered during the PhD. Thank you Veerle Huvenne, for the opportunity to contribute to your

research cruises and thank you David Price the valuable contribution during the final bend. To Dave Dalton, thank you for choosing to work in one of the ‘this is so exciting’ side projects, and trusting me to supervise you.

My journey would not be the same without the people I share most of my days with: thank you, Carol, for the countless ‘bat helps’ and for sharing the hard and good times with me. One day we will publish ‘that paper’ together. Thank you, Mari, Isa, Jonathan for being by my side in so many moments of this journey, most of which involved food and laughter. Most gladly. Thank you, Olly, for the countless draft readings and support. I would not have gotten this far without your companionship of all of you. I thank my long-time friends, Fernanda, Marina, Juliana, Gabi, Sami and Hiana, Joyce, Guida, Matias for always being a phone call away. *To Tia Cintia, minha segunda mãe, muito obrigada por me mostrar a beleza da força e o belo das coisas.*

I also would like to thank the Science Foundation of Ireland, the Irish Research Council and the Marine Institute for funding the research that led to this PhD thesis. Thank you to the scientists and crew members who made the research cruises possible. Especial thanks to the *Holland 1* ROV pilots for taking our aims as their own during expeditions. Thank you to CAPES Foundation and the Ministry of Education, in Brazil, for awarding me with my first undergraduate scholarship and granting me the life-changing opportunity to experience science without borders. This body of work would not be here without you all.

Thank you to the School of BEES and UCC staff members who contributed to my experience in UCC. Dr. Pat Meere, Eileen McCarthy and Cliona Maher for helping me to progress in my research career path. Thank you to the UCC staff, Christine Dennehy, Elaine Kelly, Phil Fogarty, Mary McSweeney and Gillian Aughney for providing administrative assistance and looking after all the students.

Finally, the COVID-19 pandemic will be marked in our lives forever. I dedicate this thesis to my Tio Ze and Tia Neide and all those who are no longer with us. Tio and Tia, I could not say goodbye to you, but my thoughts are with you, always.

Thank you all!

Obrigada,

Go raibh maith agat

Larissa

*Vou mostrando como sou
E vou sendo como posso
Jogando meu corpo no mundo
Andando por todos os cantos
E pela lei natural dos encontros
Eu deixo e recebo um tanto
E passo aos olhos nus
Ou vestidos de lunetas
Passado, presente
Participo sendo o mistério do planeta*

Acabou Chorare, Novos Baianos

Outline

This thesis comprises five chapters. Chapter 1 provides an overview of the components of the seabed habitats and mapping technologies studied. Chapters 2–5 present four studies about the use of high-resolution mapping techniques to investigate deep-water seabed habitats. These four chapters follow the formatting requirements of specific journals for publication. [Chapter 2](#) presents a paper that has been published in the journal *Frontiers in Marine Sciences*. [Chapter 3](#) presents a study that has been published in the journal *Frontiers in Environmental Sciences*. [Chapter 4](#) presents a study that is prepared for submission to *Scientific Reports*. [Chapter 5](#) presents a study that has been published in *Geosciences MDPI*. Each chapter is presented as a complete study, with references and supplementary information following the main text in each case. Chapter 6 presents the concluding remarks, summary of main findings, directions for future research as well as limitations of this line of study.

This thesis contains eight appendices. Appendix I provides additional data acquired and processed in support of Chapters 2, 3, 4 and 5. Appendix II to VIII provide a summary of curricular and extracurricular activities carried out during the PhD of the candidate, namely: list of peer-reviewed papers, supervised projects, academic roles, grants and awards, conference presentations, research cruises and courses completed during the PhD, in that order.

Author contributions are outlined according to the [Contributor Roles Taxonomy \(CRediT\)](#) author statement. UK English is used throughout the thesis.

Abstract

Cold-water coral reefs are complex structural habitats that represent one of the most important deep marine ecosystems. As three-dimensional habitats with high structural complexity, they provide ecosystem services that influence species abundance and biodiversity, being indicators of ecosystem health. These habitats are considered hotspots of biodiversity around the globe, especially in cold and deep waters between 50 and 4000 metres depth. Similar to their tropical counterparts, these habitats are subject to several climate and anthropogenic threats.

Over the last two decades, research efforts to identify, map and manage these environments have increased along with the advances in data acquisition. Technologies such as remotely underwater vehicles are equipped with high-resolution sensors that generate gigabytes to terabytes of data. However, data analysis methods are being outpaced by acquisition technologies and there is a latency in the extraction of meaningful information from large datasets. Furthermore, the fine-scale heterogeneity promoted by the three-dimensional scleractinian coral branching structure is often overlooked, being reduced to a two-dimensional scale.

This thesis explores methods that can advance seabed mapping to further understand cold-water coral reef habitat features in the deep sea considering their natural, three-dimensional structure and posed data analysis demands given the current technologies. The key aims of the research were to:

- i) develop an unprecedented 3D imaging classification workflow for CWC habitats of Ireland whilst analysing the suitability and transferability of 2D and 3D data to represent these habitats in high-resolution;
- ii) quantify facies distribution and spatial variability;
- iii) link image data to processes driving CWC reef development;
- iv) develop new forms of visualisation of 3D data of underwater environments;
- v) derive meaningful information from dense optical datasets.

Here, CWC reef habitats in the Porcupine Bank Canyon and the Belgica Mound Province, in the Porcupine Seabight, SW of Ireland were reconstructed in 3D using Structure-from-Motion (SfM) photogrammetry. Point clouds, meshes, orthomosaics and digital elevation models (DEMs) were produced at sub-centimetric resolution. Four different classification workflows were developed and analysed, namely: Multiscale Geometrical Classification (MGC); Colour and Geometrical Classification (CGC); Object-Based Image Classification (OBIA) and; Machine Learning Multiclass classification (MLMC). These first three workflows provided a binary (coral, seabed) classification with accuracy ranging 56 to 74% and provided the analysis of the percentage class distribution for each habitat in 2D and 3D. Results show that there is an impact in mapping CWC in 3D and 2D of at least a tenth of order of magnitude. The MLMC method provided a multiclass (live coral, dead coral, coral rubble, and sediments and dropstones) classification of the 3D point cloud which achieved *f1* scores of up to 95.1%. DEMs and classification results were used to assess local and regional CWC patterns in relation to terrain features, facies size and facies distribution. Further investigation revealed that CWC are not randomly distributed within CWC reefs, instead their distribution may be driven by local geomorphometric properties. Aiming to raise awareness and facilitate the interaction of humans with deep-water environments, an application for visualisation of 3D models of CWC in mobile phones was developed. This thesis demonstrates how SfM and machine learning can be used to quantify CWC facies and understand CWC reef habitats.

1. Introduction

1.1 Cold-Water Corals

1.1.1 The Importance Of Corals And Cold-Water Coral Reefs

Cold-water coral (CWC) reefs are amongst the Earth's most diverse ecosystems. Once thought to be restricted to shallow, warm waters, coral reefs have been found in cold, dark waters around the globe (Freiwald et al., 2004; Henry and Roberts, 2017; Mortensen et al., 1995; Roberts et al., 2009). It is acknowledged that CWCs are the most three-dimensionally complex habitats in the deep ocean, acting as niches for many organisms (Roberts et al., 2006). Their sheltering capabilities promote them to comparable biodiversity to that of tropical coral reefs (Henry and Roberts, 2017; Roberts et al., 2006). It is estimated that coral reefs cover approximately 0.1-0.5% of the ocean floor (Moberg and Folke, 1999), however, they accommodate up to one third of marine species (Reaka-Kudla, 1997). There is an inherent economical value to CWC ecosystems as they hold increased biodiversity and biological resources (Freiwald et al., 2004) acting as nurseries to fish and other benthic species (Costello et al., 2005; Fosså et al., 2002; Rogers, 1999). Their value is directly linked to commercial fisheries (Costanza et al., 1996) which generates several hundreds of millions of euros per year (Foley et al., 2010). In Ireland, CWC habitats contribute to rich ecosystems that together form Irish ocean resources, which represent a valuable portion of the economy, having a turnover of €6.2 billion and employing around 34,132 people as of 2018 (Inter-Departmental Marine Coordination Group, 2018).

Apart from the estimated social-economical value, CWC reefs play an important role to global biogeochemical and carbon cycling (Burke et al., 2011; Henry and Roberts, 2017; Oevelen et al., 2009; Titschack et al., 2009). In the Træna coral field in Norway, for example, CWC reefs had carbon, respiration and oxygen consumption rates over an order of magnitude higher than noncoral areas (Cathalot et al., 2015). And because of their longevity over geological times, global distribution and physical structure, they can carry records of climate events, being important predictors on the characterisation of paleo-environments (Mangini et al., 1998; Roberts et al., 2006).

1.1.2 Definition And Development Of Cold-Water Corals

CWCs are azooxanthellate cnidarians, meaning that they do not have a symbiotic relationship with zooxanthellate algae which are microscopic photosynthetic organisms that provide nutrients to zooxanthellate corals. For that reason, CWCs do not depend on sunlight and therefore are not restricted to the photic zone, contrary to their tropical counterparts. CWCs comprise Scleractinia (stony corals), Octocorallia (soft corals), Antipatharia (black corals) and Stylasteridae (hydrocorals) (Roberts et al., 2009). Scleractinian CWC are sessile, filter-feeding, benthic organisms with an aragonitic calcium carbonate skeleton (Cairns, 1995). As of 2017, there are 711 azooxanthellate scleractinian species documented in the world (Henry and Roberts, 2017). However, only six are major reef framework-building species. These include: *Madrepora oculata*, *Lophelia pertusa* (synonymised to *Desmophyllum pertusum* in Addamo et al. (2016)), *Solenosmilia variabilis*, *Goniocorella dumosa*, *Enallopsammia profunda*, and *Bathelia candida*.

Among CWCs, *Lophelia pertusa* is the most common and well known framework-forming species (Freiwald and Wilson, 1998). The phenotype of *L. pertusa* is characterised by a white to light red colour variations (Rogers, 1999) and is usually known to form dendroid colony developments that can reach several metres across, branches can anastomose, which can strengthen the framework (Lim, 2017). *Lophelia pertusa* build-ups are documented to occur with common elements of reef formations, such as the secretion of carbonate skeleton that forms a 3D relief above the seafloor and therefore alters the local hydrodynamic and sedimentary regimes. Consequently, this enriches the biodiversity and biomass associated with the framework compared to the surrounding (Freiwald et al., 2002), thus leading to a diversity 'hotspot' in an otherwise featureless environment. Studies have found that the diversity of taxa associated with *L. pertusa*, for example, was 3 times higher than in surrounding soft-bottom areas (Mortensen et al., 1995).

Madrepora oculata is also a cosmopolitan species of azooxanthellate corals that often occurs with *L. pertusa* and has an important role in reef framework formation

(Freiwald and Wilson, 1998). Similar to *L. pertusa*, *M. oculata* is known to be widespread, reaching the geographical extent of CWC occurrences (Rogers, 1999).

CWCs are known to thrive under specific environmental conditions. The temperature ranges to which CWCs are found range between 4° to 13° Celsius (°C). These ranges are usually found in shallow waters (c.50 to c.1000 metres depth) at high latitudes, and at greater depths (up to 4000 metres) at low latitudes (Roberts et al., 2006). There is also a relationship between CWC occurrences and the depth of the aragonite saturation horizon (ASH) (Cairns, 2007; Dorschel et al., 2005), high-current speeds (Frederiksen et al., 1992; Roberts et al., 2003) and increased values of dissolved organic matter (Freiwald and Wilson, 1998). CWCs have been found in areas with current speeds of $> 100 \text{ cm s}^{-1}$ (Frederiksen et al., 1992; Lim et al., 2020b; Rogers, 1999). *L. pertusa* in particular, seems tolerant to different salinities, varying from 35-37 PSU (de Haas et al., 2009; Freiwald et al., 2004; Gass and Roberts, 2006) or sometimes lower between 34-35 PSU in Norwegian fjords (Flögel et al., 2014; Rogers, 1999). In Irish waters around the Porcupine Seabight, these temperature and salinities are found in Mediterranean Outflow Water (MOW) and the Eastern North Atlantic Water (ENAW) water masses which are often linked to CWC development (Appah et al., 2020; Mazzini et al., 2012; O'Reilly et al., 2022).

CWC can occur as isolated colonies, in small patch reefs, thickets or large reefs to giant carbonate mounds up to 300 metres high (Freiwald et al., 1999; Roberts et al., 2006). Driven by specific hydrodynamic conditions and food supply that favour coral growth, these reefs and mounds tend to occur in groups and form kilometre-wide provinces (Roberts et al., 2006; Wheeler et al., 2007).

The initial coral settlement requires a hard substrate on which larvae can attach to (Dorschel et al., 2005; Wilson, 1979a). In sand-dominated areas, the hard substrate can be small, such as a pebble or a worm tube (Rogers, 1999). From the initial settlement, and given favourable conditions, CWC grow until its branches collapse from the initial attachment point by breaking or falling over. The broken colony can then serve as a larger attachment to further growth (Rogers, 1999; Wilson, 1979a). As CWC are sessile and can baffle current-suspended sediments, their role is directly linked to carbonate mound development in the North Atlantic (de Haas et al., 2009;

Dorschel et al., 2005; Wheeler et al., 2007, 2008). Hence, CWC density is also an indication of different mound stages. It is noted, for example, that the presence of coral thickets in mounds indicate healthy and growing carbonate mounds (Dorschel et al., 2005; Wilson, 1979a). These thickets are formed after the initial settlement, when coral starts to grow and amalgamate with other colonies (Lim, 2017). Similarly, it is indicated that mound reaches maturity when colonising filter-feeders cover most of the mound (Dorschel et al., 2005). It is acknowledged that CWC reef growth starts from an initial larvae settlement, progressing into a colony and, when these colonies become interlaced, they form a thicket (Lim, 2017; Squires, 1964). When significant amounts of debris and sediment accumulate around the base of the thicket, it becomes a coppice (Squires, 1964). The coppice, or a number of coppices with accumulated debris can develop into coral bank (Squires, 1964) or reef as per definition of Roberts et al. (2009). Late stages of the mound development may be indicated by mound coalescence leading to clusters of mounds (De Mol et al., 2005; Freiwald et al., 1999).

It is noteworthy that CWC carbonate mound size is not exclusively influenced by ideal conditions for CWC growth, rather, it may be related to the resilience through alternated periods of favourable conditions and sedimentological hiatus and erosion through time (Dorschel et al., 2005; Wheeler et al., 2007). As such, CWC carbonate mounds are defined as “large structures formed by successive periods of coral reef development, sedimentation and (bio)erosion” (Roberts et al., 2006, 2009). CWC mound stages have been defined using many aspects of growth and morphology, often being referred as ‘active’ or ‘retired’ mounds (Roberts et al., 2006) or as by ‘developed’ or ‘inherited’ mounds (Wheeler et al., 2007) or “mature” and “immature” (Freiwald et al., 1999) given their stage and CWC activity. In the North Atlantic, the cyclic nature of mound development is emphasised by stages of initial growth, development, retirement and recolonization linked with glacial and interglacial periods that favour each of these stages (Figure 1.1).

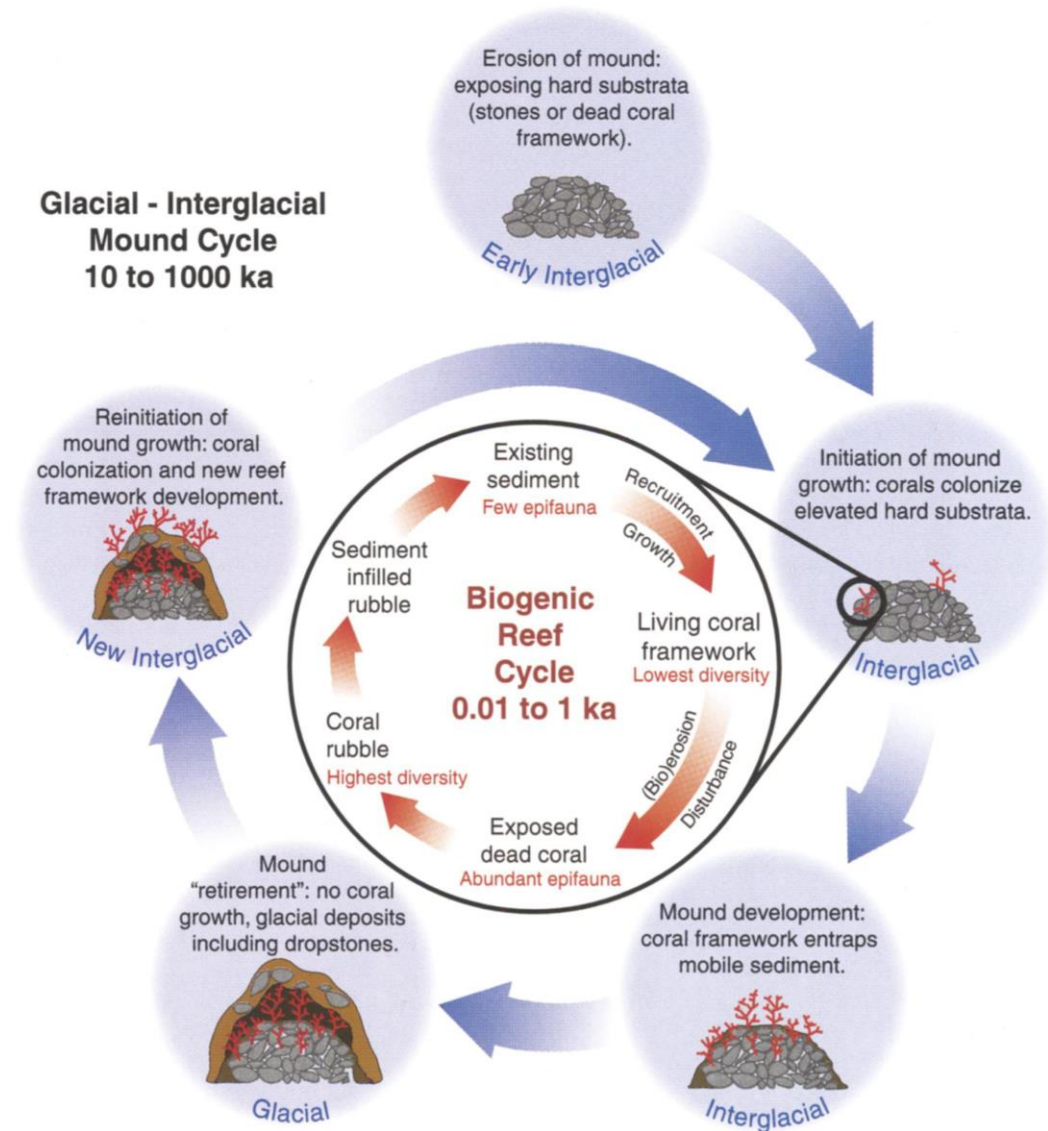


Figure 1.1: Illustration of a CWC mound cycle proposed in Roberts et. al (2006). Mound cycle stages reflecting the environmental change during recurrent glacial cycles. Extracted from Roberts et. al (2006).

Many CWC mound and reef growth models have been put forward since the 1960s (De Mol et al., 2005; Dorschel et al., 2005; Douarin et al., 2014; Hovland and Thomsen, 1997; Squires, 1964; Wilson, 1979a). While some models emphasise the importance the hydrodynamic regimes such as current direction and speed (De Mol et al., 2005; Dorschel et al., 2005, 2007), others emphasise the importance of sedimentological processes such as sediment supply (Foubert et al., 2011; Wheeler et al., 2007), erosion and seabed temperatures (Roberts et al., 2003). Nonetheless, CWCs are frequently

documented in areas with locally accelerated currents (Wheeler et al., 2008) or with internal tidal waves that enhance food supply (Frederiksen et al., 1992; Mortensen et al., 2001; Roberts et al., 2003). Conversely, a few studies document that fast-flowing bottom currents may restrict food supply and larvae settlement, whilst high sediment rates can lead to complete mound burial (Kenyon et al., 2003). In submarine canyons, mound growth is facilitated by bottom currents and the influence of canyon morphology on the hydrodynamic regime as the irregular topography around the canyon edge may cause speed enhancement (Mazzini et al., 2012).

However, current studies agree that CWC mound development is unlikely to be linked to hydrocarbon seepage as previously hypothesised (Hovland et al., 1994; Hovland and Thomsen, 1997) due to a lack of conclusive supporting evidence. Over the years, it has become more accepted that CWC reef development is controlled by the interaction local hydrography and sedimentary dynamics such as current dynamics, temperature, pH, salinity, food and sediment supply (Davies et al., 2010; Dorschel et al., 2005; Roberts et al., 2006; Wheeler et al., 2007). As such, the development of large mounds represents a balance among bottom current speeds, mound growth rates and sedimentation rates (Foubert et al., 2011; Kenyon et al., 2003) facilitating successive reef development to construct large mound structures.

1.1.3 Global Distribution Of Cold-Water Corals

Although reaching a similar level of biodiversity to that of tropical coral reefs, CWC are more globally distributed across wider latitudinal ranges than their tropical counterparts (Henry and Roberts, 2017). The first occurrence was documented in 1948 by Le Denois (Le Danois, 1948) along Bay of Biscay. Although a few studies claim that their first occurrence dates back in 1755, in the *Natural History of Norway* book written by Enrich Pontoppidan (Pontoppidan, 1755). It is however, well accepted that CWC have been known since the 18th century (Roberts et al., 2006).

Over the following centuries and with the advance of mapping technologies, CWC occurrence has been documented in fjords (Fosså et al., 2002; Jonsson et al., 2004; Rüggeberg et al., 2011), along continental shelves (Leverette and Metaxas, 2006;

Mortensen et al., 1995), ridges, slopes, troughs (Freiwald et al., 1999; Guinan et al., 2009; Savini and Corselli, 2010), carbonate mounds (Hall-Spencer et al., 2009; Hovland et al., 1994; Mienis et al., 2006; Wheeler et al., 2005a, 2007; White, 2007; Wilson, 1979b) and submarine canyons (De Mol et al., 2011; Huvenne et al., 2011; Orejas et al., 2009). Although there is a higher density of CWC occurrences in the North Atlantic, it is well acknowledged that this reflects the research efforts in this region (Freiwald et al., 2004; Lim et al., 2020b; Roberts 2006) (Figure 1.2). CWCs have been found in tropical waters in the southern hemisphere like off the coast of Brazil (Barbosa et al., 2019; Kitahara, 2007) and are known to have the highest species diversity around the Philippines and the Indian Ocean (Cairns, 2007; Roberts et al., 2006). As research and technology advance, these numbers are prone to increase as we can now reach pristine areas with remotely assisted technologies.

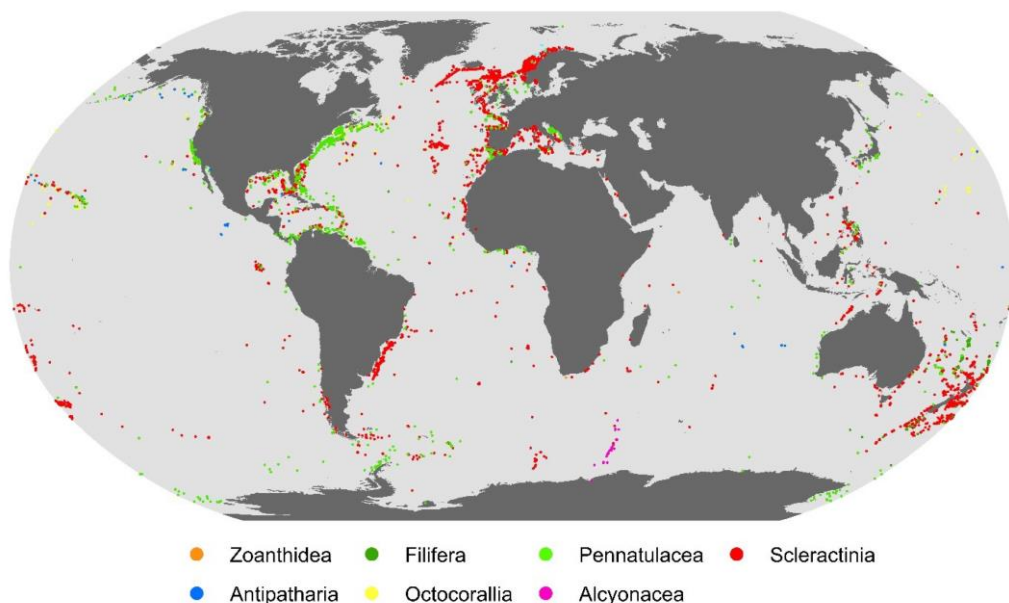


Figure 1.2: Global distribution of Cold-water Corals as of 2004. Scleractinia in red. Extracted from: Freiwald A, Rogers A, Hall-Spencer J, Guinotte JM, Davies AJ, Yesson C, Martin CS, Weatherdon LV (2021). Global distribution of cold-water corals (version 5.1). Fifth update to the dataset in Freiwald et al. (2004) by UNEP-WCMC, in collaboration with Andre Freiwald and John Guinotte. Cambridge (UK): UN Environment Programme World Conservation Monitoring Centre.

Scleractinian CWCs, apart from being senescent, slow growing organisms, are also especially vulnerable to physical and chemical damage (Clark, 2006; Freiwald et al., 2004; Hall-Spencer et al., 2002; Hennige et al., 2020; Roberts et al., 2000).

Multifactorial experiments estimated that about 70% of known scleractinian CWC are expected to be exposed to ocean acidification effects by the end of the century (Büscher et al., 2017). There has also been a growing concern about the environmental sensitivity of deep-water ecosystems to hydrocarbon exploration and bottom trawling (Althaus et al., 2009; Hall-Spencer et al., 2002; Huvenne et al., 2016; Long et al., 1999; Paradis et al., 2017; Puig et al., 2012; Rogers, 1999; Wheeler 2005b). In Irish waters, a decline of CWC (*Madrepora oculata*) cover over 4 years has already been documented (Bohlukos et al., 2019). The conservation of CWC started to emerge as an compelling environmental issue since 1990 (Foley et al., 2010; Roberts, 1997; Rogers, 1999), with the first EU Habitats Directive provisions to protect CWCs. More recently, in 2021, the United Nations has proclaimed a Decade of Ocean Science for Sustainable Development Goals (SDGs) from 2021-2030 to support efforts to reverse the decline in ocean health.

1.1.4 The Role Of Cold-Water Corals In Local Biodiversity

Apart from being hotspots of biodiversity in deep sea environments, CWC also provide distinct macro to micro habitats that introduce local spatial heterogeneity to the region (Jonsson et al., 2004; Mortensen et al., 1995; Savini et al., 2014). Mortensen et al. (1995) divided *L. pertusa* colonies into four different microhabitats: the smooth surface of living *Lophelia*, the detritus laden surface of dead *Lophelia*, the cavities inside the dead *Lophelia* made by boring sponges and the free space between coral branches. These were defined based on the percentage cover of stones and coral debris. It was noted that the diversity of fauna of the soft bottom and the rubble was low. On the other hand, the diversity of taxa associated with live and dead *Lophelia* was 3 times as high than on the surrounding soft bottom (Mortensen et al., 1995). Similarly, Jonsson et al. (2004) found that the abundance of organisms on reef and rubble habitats is twice as higher than in gravel and sediment habitats. Savini et al. (2014) found five dominant seafloor features and thirteen microhabitats in video data of the northern Ionian Margin, which highlights the existing substrate heterogeneity

and structural complexity of these environments at colony-scales (Buhl-mortensen et al., 2015; Kazanidis et al., 2021).

Structural complexity is defined as the physical three-dimensional structures of an ecosystem (Graham and Nash, 2013). These structures are provided by the physical shape of any living organism, such as trees, kelps and corals. For that reason, they are often termed as 'ecosystem engineers' or 'foundation species' (Burns et al., 2015b; Jones et al., 1994). Structural complexity is often termed as rugosity, a measure of variability or complexity of a surface calculated as a ratio of the distance along a surface to the linear distance (Storlazzi et al., 2016). Generally, structural complexity is also addressed as substrate or habitat heterogeneity (De Leo et al., 2014; Ismail et al., 2018; Kazanidis et al., 2021) or 'habitat architecture' (Buhl-Mortensen et al., 2015).

These fine-scale measurements of structural complexity, surface area and 3D volume metrics are particularly relevant for estimating ecosystem services of corals (Burns et al., 2015a; Fukunaga and Burns, 2020; House et al., 2018; Price et al., 2019; Urbina-barreto et al., 2020). These metrics are critical indicators of reef building capacity (Moberg and Folke, 1999; Urbina-barreto et al., 2020) and biodiversity (Graham et al., 2006), as well as contributing to primary measures of coral reef monitoring such as biomass, growth rate and carbonate production (Cocito et al., 2003; Fisher et al., 2007).

1.2 Study areas

The work carried out herein was applied in two areas: the Porcupine Bank Canyon and the Piddington Mound, located in the Porcupine Seabight, southwest of Ireland (Figure 1.3).

1.2.1 Porcupine Bank Canyon

The Porcupine Bank Canyon (PBC), located southwest of Ireland is shaped by the Porcupine Seabight to the southeast and the Rockall Trough to the north. The PBC is an approximately 63 km long and 29 km wide canyon, being one of the largest submarine canyons in the Irish margin (Dorschel et al., 2010). The canyon is up to 800

m deep, striking approximately NE-SW, oblique to the west flank of the Porcupine Bank (Elliott et al., 2006). The PBC is a tectonically controlled, asymmetric canyon (Shannon, 1991) that comprises three confluent axial channels (Elliott et al., 2006). The canyon is influenced by strong bottom currents of up to 114 cm s^{-1} , the highest ever recorded current speed in a CWC habitat (Lim et al., 2020b). These currents influence the distribution of benthic fauna and contribute to (bio) erosion in the canyon, thus influencing coral rubble development (Lim et al., 2020b; Mortensen et al., 1995; O'Reilly et al., 2022). Although the main framework building CWC in the canyon is *L. pertusa* there is a high biodiversity in the canyon that is thought to be influenced by the MOW and ENAW (Appah et al., 2020). The interaction of these water masses with the canyon morphology promotes localised upwelling which brings enriched particle supply to the canyon, contributing to the development of ecological hotspots in the canyon lip and adjacent areas (Mazzini et al., 2012; O'Reilly et al., 2022).

1.2.2 Piddington Mound

The Porcupine Seabight is an approximately 150 km long and 65 km wide embayment between the Porcupine Bank and the Irish shelf formed in Middle to Late Jurassic (Dorschel et al., 2005). The Porcupine Seabight harbours three giant carbonate mounds: Belgica, Hovland and Magellan mound provinces, dated from the Late Pliocene/Pleistocene (Kenyon et al., 1998). The Belgica Mound Province (BMP), located in the eastern part of the Porcupine Seabight, comprises approximately 35 exposed conical, ellipsoidal, elongated mounds aligned mainly at a NNW-SSW orientation (Wheeler et al., 2007) measuring up to 200 metres high and up to 4 km wide (Dorschel et al., 2005). The surface morphology of the BMP is characterised by ridges covered in corals, which turn into coral banks driven by sediment transportation that provide support for coral colonies (Wheeler et al., 2007). The BMP has been divided into four main regions based on the morphology: northern area, upslope, midslope and downslope areas (Wheeler et al., 2011). The heights of the mounds found in each of these regions vary, with downslope and upslope areas being dominated by smaller, so called Moira mounds (Wheeler et al., 2007).

Within the BMP, these small-sized mound features called the Moira Mounds (Foubert et al., 2011; Huvenne et al., 2005; Wheeler et al., 2011), occur from 900 to 1080 metres depth reaching up to 10 metres in height (Spezzaferri et al., 2012). They have a clearly defined morphology, with slope gradients of 15-20° (Foubert et al., 2011; Spezzaferri et al., 2012; Wheeler et al., 2011). It is postulated that the mound surface morphology of the Moira Mounds is created by a spatial organisation where colonies tend to distance themselves from their neighbours, as closer colonies would be under a competitive and reduced food supply regime (Masson et al., 2003; Wheeler et al., 2007). It is also suggested that these small mounds may reflect mound formation under stressed conditions rather than the otherwise predicted initial stage of mound growth (Foubert et al., 2011)

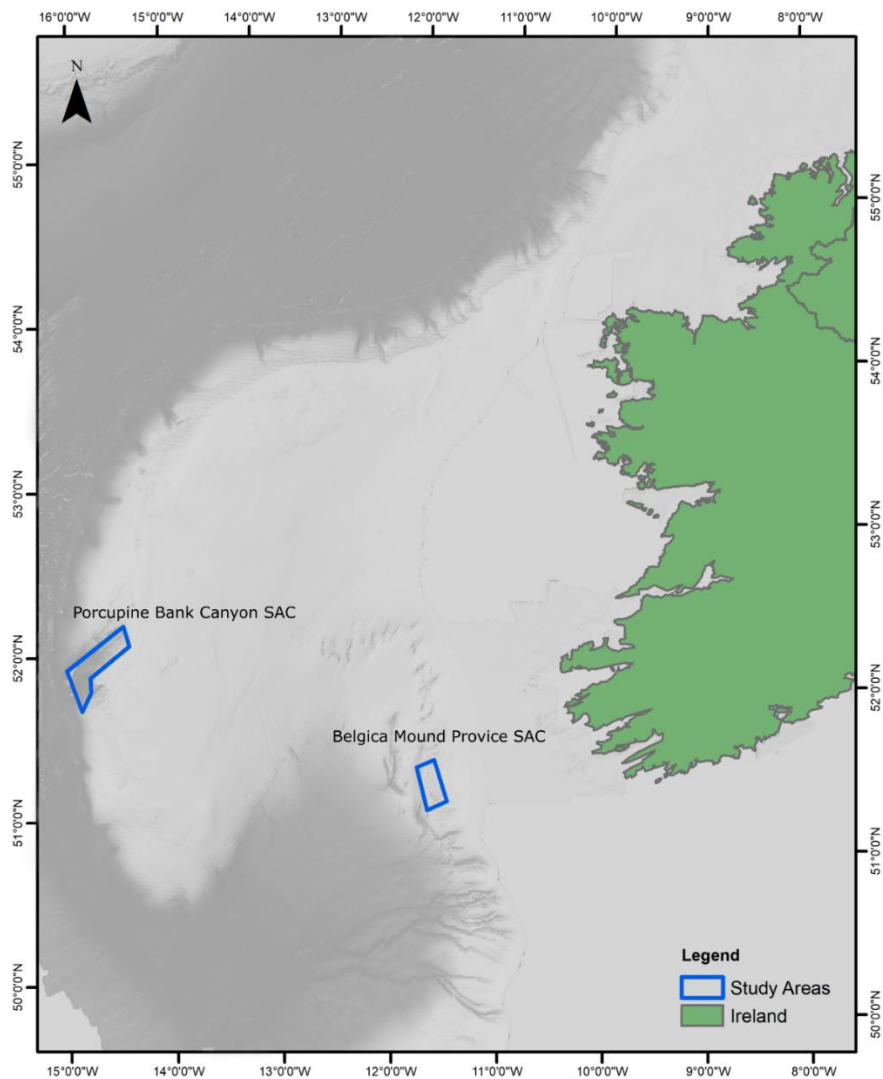


Figure 1.3 Location of Porcupine Bank Canyon and Belgica Mound Province Special Areas of Conservation (SAC) studied herein

1.3 High-Resolution Mapping Trends For Cold-Water Coral Environments

Mapping deep-sea habitats is a well-known global challenge (Baker and Harris, 2012; Brandt et al., 2014; Lim et al., 2020a). Efforts to map these habitats have increased over the past decade (Brown et al., 2011; Davies et al., 2017), especially with European mapping projects such as MAREANO (Marine Areal Database for Norwegian Coasts and Sea Areas) (Buhl-Mortensen et al., 2015) in Norway, INFOMAR (Integrated Mapping for the Sustainable Development of Ireland's Marine Resource) (<https://www.infomar.ie/>) in Ireland, and global initiatives such as Nippon Foundation, GEBCO (General Bathymetric Chart of Oceans) and Seabed 2030 (GEBCO, 2017) that have committed to map 100% of the oceans until 2030.

Regional mapping expeditions using single beam (SBES) and multibeam echosounder (MBES) bathymetry, side-scans sonars (SSS), have been used to identify mound features on the seabed (Freiwald et al., 1999; Huvenne et al., 2002; Savini and Corselli, 2010; Wheeler et al., 2007). These acoustic methods are often used to locate and quantify CWC reef formations and to place these and other geomorphological features in a wider seascape context (Schlacher et al., 2010).

Robotic exploration of remote environments extends the reach to areas where direct human exploration is impractical (Eustice et al., 2004). New data acquisition technologies such as Remotely Operated Vehicles (ROVs) and Autonomous Underwater Vehicles (AUV) and quantitative image methods are increasing the ability to map these habitats (Kwasnitschka et al., 2013; Pizarro et al., 2009). These robotic underwater vehicles are considered the most advanced platforms for automated mapping and surveying of deep-sea environments (Negahdaripour and Madjidi, 2003).

ROVs, which were initially developed for military use, have become critical multi-functional tools for deep-sea mapping (Kwasnitschka et al., 2013). ROVs are tethered to the vessel, having a continuous physical link between the vessel or platform whilst reaching up to 6000 metres depth capacity. ROVs are fully controllable and

manoeuvred by human personnel, thus providing a high level of real-time surveying control. World-class ROVs can be equipped with high-definition cameras, MBES echosounder systems and robotic arms, often being tailored to the survey needs.

AUVs represent a step forward to progressively more common autonomous technologies (Danson, 2002; Wakita et al., 2010). AUVs are untethered robots equipped with multiple sensors that are able to survey autonomously for long periods of time, from 2.5 days to 15 days depending on payload (Kongsberg 2010). Their main advantage is that the vessel does not have to follow the survey design of the AUV, which allows the vessel to undertake other surveying activities, thus maximising survey efficiency and productivity (Chance et al., 2000).

1.3.1 Photogrammetry

Acoustic methods such as MBES, SBES provide information about the regional morphology of the environments, being widely used for evaluating large and meso-scale natural benthic habitat characteristics over large areas (Negahdaripour and Madjidi, 2003). Optical methods, on the other hand, enable the investigation of fine-scale community characteristics over local areas which suits ocean exploration, mapping, inspection, thus complementing acoustic methods (Negahdaripour and Madjidi, 2003; Schoening et al., 2016). Optical imaging is considered a bridge between acoustic data and physical data e.g. sediment sampling which provides high spatial resolution but low sampling rate, acting as the midpoint between spatial resolutions intrinsic to acoustic and physical data collection (Schoening et al., 2016; Shihavuddin et al., 2013).

Remote sensing applications in general have progressed significantly and such advance is brought forward with the application of photogrammetry and Structure-from-Motion (SfM) techniques (Carrivick et al., 2016; Nyimbili et al., 2016; Westoby et al., 2012; Wolf et al., 2014).

Photogrammetry has been defined as “the art, science and technology of obtaining reliable information about physical objects and the environment through process of

recording, measuring and interpreting photographic images and pattern of recorded radiant electromagnetic energy and other phenomena” (American Society for Photogrammetry and Remote Sensing *apud* Schenk, (2005); Wolf et al. (2014). The first experiments using photogrammetry for topographic mapping date back to 1849 under the leadership of Colonel Aime Laussedat of the French Army Corps of Engineers (Ragey, 1952). Until the beginning of the 21st century, photogrammetry was used extensively by the military for reconnaissance to the mass production of maps (Wolf et al., 2014). Advancements in techniques and instrumentation continued through the 21st century with the popularisation of digital cameras and unmanned hardware (Wolf et al., 2014). In marine sciences, Bythell et al. (2001) was among the first to use photogrammetry in coral reefs for ecological studies whilst highlighting advantages related to minimal costs and the non-destructive nature of the method. The use of the technique has increased substantially as computer resources become more accessible (Lavy et al., 2015; Pizarro et al., 2017; Storlazzi et al., 2016).

1.3.2 Structure-from-Motion (SfM)

SfM is thought to have been developed in the 1990s with the first feature matching algorithms for visual motion perception (Lowe, 1999; Spetsakis and Aloimonos, 1991). Although there are similarities between conventional photogrammetry and SfM, several aspects of SfM have an entire different origin, which come instead from advances in 3D computer vision algorithms (Carrivick et al., 2016; Smith et al., 2016). Whilst traditional photogrammetric methods require the location and camera poses or the location of ground control points for scene triangulation, SfM uses feature matching algorithms such as Scale Invariant Feature Transform (SIFT) (Lowe, 1999) and bundle adjustments to do a similar process (Carrivick et al., 2016; Westoby et al., 2012). A further difference between SfM and traditional photogrammetry methods is that the first produces fully 3D data, which are otherwise only possible with laser scanning methods (Carrivick et al., 2016).

The fundamental concept of SfM photogrammetry is the reconstruction of a scaled 3D model of a given object or scene from a series of overlapping images (Figure 1.4). The term ‘structure -from-motion’, strictly speaking, refers to only one element of the workflow (Carrivick et al., 2016; Smith et al., 2016) which actually accounts for a set of principle steps:

- 1) Feature detection: detecting image features or keypoints using algorithms such as SIFT (Lowe, 1999, 2004)
- 2) Key point correspondence: identifying correspondences of keypoints in the set of different images. K-d Trees and approximate nearest neighbours (ANNs) are common algorithms used (Carrivick et al., 2016)
- 3) Identifying geometrically consistent matching: filter keypoints to identify geometrically inconsistent keypoint correspondences. Random Sample Consensus (RANSAC) algorithms (Fischler and Bolles, 1981) are commonly used in this step.
- 4) Structure-from-Motion: estimating 3D scene geometry, camera pose and calibration parameters using bundle adjustment methods (Granshaw, 1980). The term “bundle” refers to the group of light rays that connects the 3D points to the camera centres, and ‘adjustment’ refers to the minimised non-linear cost functions that reflects the measured error (Smith et al., 2016).
- 5) Scale and georeferencing: include field measurements and known coordinates to scale and georeference the model.
- 6) Refinement of parameter values: optimise the parameters of the bundle adjustment using ground control points (GCPs).
- 7) Multi-view stereo (MVS) image matching: Final step of the workflow which increases the density of point cloud by at least two orders of magnitude. There is a wide variety of MVS approaches (Carrivick et al., 2016), including voxel based methods, surface evolution based methods, patch-based MVS and depth-maps (model combining the distance between the camera viewpoint and the 3D scene objects).

For that reason, the method can also be commonly addressed as SfM-MVS to account for the MVS algorithms used at the final stage (Carrivick et al., 2016; Smith et al., 2016).

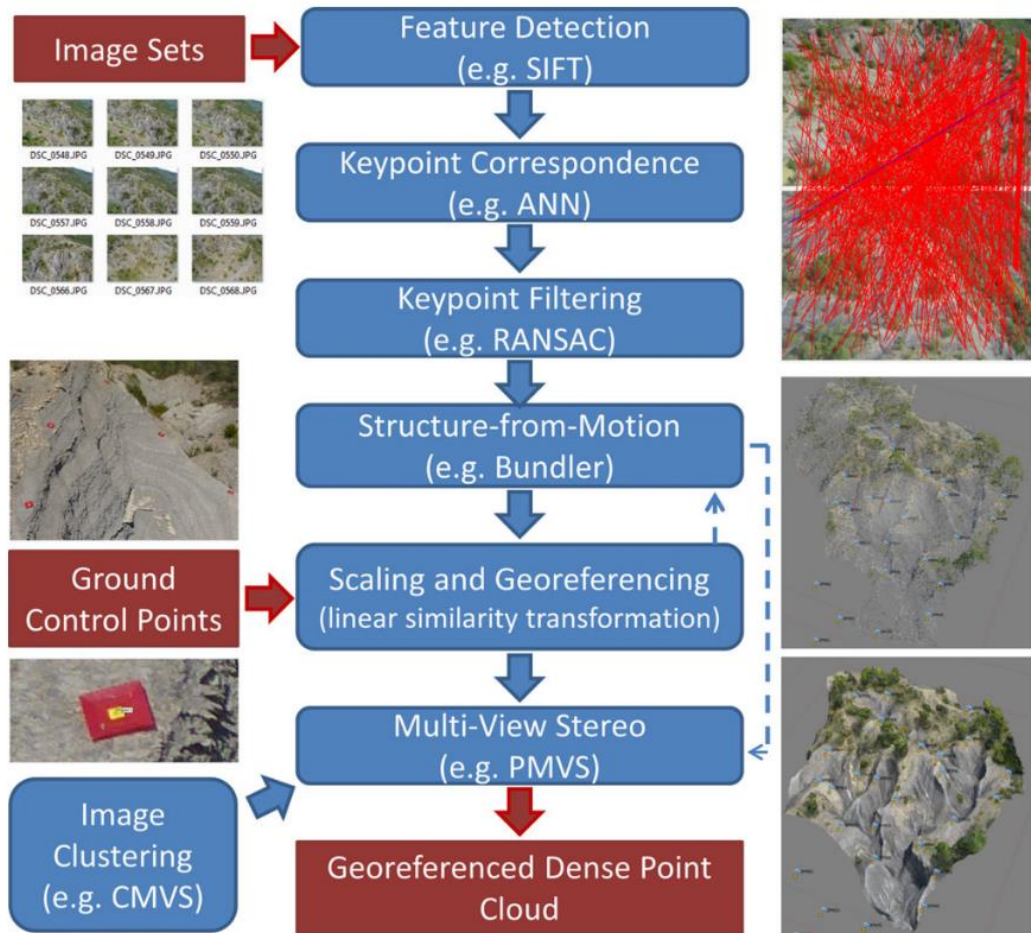


Figure 1.4: Standard Structure-from-Motion workflow for the production of georeferenced dense point clouds. Inputs and outputs are shown in red. From the top right to bottom right: valid image matches generated from key point correspondence, sparse point cloud, dense point cloud. Image extracted from Smith et al. (2016).

1.3.2.1 SfM products

SfM produces four main products: point clouds; meshes; orthomosaics and digital elevation models. SfM derived point clouds and texture surfaces are inherently multi-dimensional, generally containing, X, Y, Z, colour and texture which are transformed into orthomosaics and DEMs (Carrivick et al., 2016; Wolf et al., 2014). A brief description of each SfM product is given as follows:

3D point clouds

A point cloud is a collection of individual points where each point contains X, Y, Z coordinates describing their position in a 3D space (D'Urban Jackson et al., 2020). The SfM process produces a sparse point cloud and reconstructed camera poses (Carrivick et al., 2016) which is then transformed into a dense point cloud on the MSV step. Point clouds are the first product of the SfM process, that the following processes build upon (D'Urban Jackson et al., 2020) (Figure 1.5). It is a versatile dataset that can be used to compute terrain descriptors (Robert et al., 2017; Van Audenhaege et al., 2021) and determine changes in structures by aligning point clouds obtained within different time intervals (Ferrari et al., 2021).

Digital Elevation Models (DEMs)

DEMs are the projection of 3D dense cloud onto a 2D plane (Carrivick et al., 2016). Thus, the 3D structure is gridded and rasterised into 2.5D. Regularly gridded DEMs comprise square pixels of constant spatial resolution in which each pixel is assigned with a depth value (Quincey et al., 2014; Westoby et al., 2012). Experts also discuss the terminology related to this dimensionality reduction, which is often termed as either 2D or 2.5D, given that depth information continues integrated to the pixel even though it is in a coarse resolution (Koch and Heipke, 2006; Turner, 1997). The loss of information associated with the 2D projection is considered a trade-off between maximising field sampling and data handling (Carrivick et al., 2016; Fukunaga et al., 2020). The DEM is a simplified yet useful data product of which fine-scale habitat metrics can be extracted (Fukunaga et al., 2020; Leon et al., 2015). DEMs, both derived from bathymetry and SfM, serve as a proxy to study the geomorphic features of single coral mounds and model coral spatial distribution (Price et al., 2019; Savini et al., 2020, 2014)

Orthomosaics

The SfM workflow produces a georectified and mosaicked image data by merging original images through differential rectification process which eliminates image displacements caused by image tilt and terrain relief (Wolf et al., 2014). The orthomosaic may be georeferenced provided the addition of field coordinates in the

previous SfM step. SfM-derived orthomosaics are presently underused in geosciences (Carrivick et al., 2016). However, these datasets are useful to investigate spatial associations in the data. High-resolution mapping studies of coral reefs have successfully used orthomosaics in combination with DEMs to build classification frameworks and derive spatial zonation of benthic facies (Burns et al., 2015a; Conti et al., 2019; Lim et al., 2017).

3D Meshes

3D meshes are triangulated surfaces from point cloud data. It is a 'closed surface' polygonal model created from interpolation of the points in the point cloud, often using Delaunay triangulation (Shewchuk, 2002). Some software may also opt to use depth map information to build meshes (Agisoft, 2019). A textured mesh can be produced from reprojecting the orthophotos onto the mesh (Smith et al., 2016). A few studies have reservations in using meshes due to their triangulated nature (Ferrari et al., 2021) and limited file formats. However, studies have successfully used 3D meshes to derive structural complexity measures complementing DEM measures (Fukunaga and Burns, 2020; Young et al., 2018). Similar to 3D point clouds, meshes have also been used to detect structural changes over time (Ferrari et al., 2021)

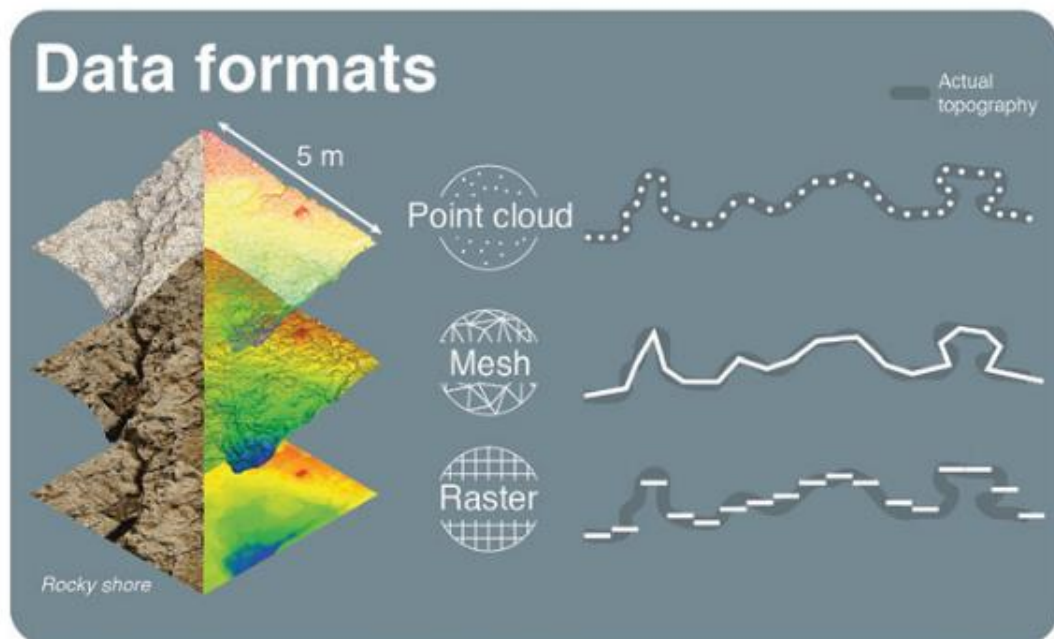


Figure 1.5: An overview of high-resolution data formats. Point cloud data (top) can be transformed into meshes by interpolation, gridding of the point cloud into a 2D plane can

generate 2.5D rasters such as digital elevation models (DEMs) Extracted from D'Urban et al. (2020).

SfM software

The industry of SfM software has increased rapidly in line with advances in computer vision over the last 10 years (Carrivick et al., 2016). There are several options of open-source and commercial software that offer complete or specific SfM tasks. These can be separated in four groups:

- i) stand-alone software that execute the complete SfM reconstruction process: Agisoft Metashape, Pix4DMapper, AutoDesk Image Modeler, MicMac, ColMap. Although the majority of options is commercial, there is a growing number of open-source options such as Col Map, MicMac and Meshroom, or under academic licences such as Matisse.
- ii) web-services for visualisation and quick 3D model production: SketchFab, 3Dviewer (Shapr3D).
- iii) specific tasks within the reconstruction and analysis process: although the majority of options is commercial, such as Qimera, Lidar360, NaviModel, RealWorks (Trimble). Three main open source options are: CloudCompare, MeshLab, Blender which offer a wide range of tools.
- iv) Point cloud processing code libraries: Open3D, Point cloud library (PCL) which offers core processing routines in C++ and Python, and have been used to build software like CloudCompare and MeshLab.

1.3.2.2 Application of SfM in marine sciences

The widespread use of SfM in geosciences has been enhanced with the development of new methods allowing the triangulation of non-metric cameras, new feature extraction algorithms and free open source software (Carrivick et al., 2016). Underwater SfM has branched from conventional SfM given the particularities of acquiring data underwater such as light attenuation, backscatter and need for artificial light (Pizarro et al., 2009). Studies dedicated to overcome such issues whilst

taking advantage of vehicle navigation systems have optimised the application of SfM for underwater surveying (Menna et al., 2018; Pizarro, 2004; Pizarro et al., 2017, 2009).

In marine sciences, underwater SfM photogrammetry has enabled scientists to derive biophysical measures of structural complexity and carry out temporal studies that provide valuable information about ecosystem health that will also feed in information for monitoring programs (Bythell et al., 2001; Ferrari et al., 2017; Figueira et al., 2015; Lavy et al., 2015). The application of SfM in marine sciences goes from producing 3D reconstructions of corals reefs located in both tropical (Anelli et al., 2019; Burns et al., 2015a; Cocito et al., 2003; Ferrari et al., 2017; Leon et al., 2015; Pizarro et al., 2017), deep-waters (de Oliveira et al., 2021; Lim et al., 2020b; Price et al., 2019), and from vertical walls in submarine canyons (Robert et al., 2017) to hydrothermal vents (Bodenmann et al., 2017; Gerdes et al., 2019; Thornton et al., 2016), and underwater vehicle motion planning (Eustice et al., 2004; Laranjeira et al., 2020). Recently, it has gained traction as a powerful tool to aid coral reef restoration (Ferrari et al., 2021; Pascoe et al., 2021) and promote outreach (Cristobal et al., 2020; Doležal et al., 2019). It is well argued that SfM enables non-destructive, repeatable measurements of shape, volume, surface area, providing a permanent record of the 3D object, thus being a powerful tool to create legacy data and monitor changes (Capra et al., 2020; Chen and Dai, 2021; Figueira et al., 2015; Piazza et al., 2019; Westoby et al., 2012). Studies also promote SfM for its rapid sampling speed and possibility of imaging remote locations (Westoby et al., 2012).

Piazza et al. (2019) used SfM to track temporal changes in benthic habitats in Antarctica, showing a 25-49% increase in sea urchins and the complete disappearance of sponges over a period of 2 years. Figueira et al. (2015) assessed the precision and accuracy of SfM against laser reference models and concluded that the 3D geometry of coral models differed by only 1-3mm from SfM to laser reference models. The study reinforced the utility of off-the shelf photogrammetry tools to measure structural complexity of corals (Figueira et al., 2015).

1.3.3 Automated Classification Of Coral Reefs

With the advent of new technologies, scientists are acquiring vast numbers of images and video data (Beijbom et al., 2015; Stokes and Deane, 2009). Up until the last decade, the analysis of these images was conducted manually, which is time-consuming and require a large amount of resources. As consequence, valuable data from many domains are under the latency of manual analysis.

Automated analyses of benthic images have gained popularity along with the improvement of digital cameras and automatic acquisition systems (Beijbom et al., 2015; Shihavuddin et al., 2013; Stokes and Deane, 2009). There has been considerable success in automated classification of benthic images specially with the advancement of machine learning techniques (Alonso et al., 2019; Beijbom et al., 2012, 2015; Elawady, 2015; Friedman et al., 2012; Friedman, 2013; Pavoni et al., 2022; Purser et al., 2009; Shihavuddin et al., 2013; Stokes and Deane, 2009; Williams et al., 2019; Zurowietz et al., 2018). The success of these tasks is generally built upon four main pillars: i) quality of image data; ii) quality of the classification algorithm; iii) amount of training data, and; iv) the quality of training data.

Stokes and Deane (2009) utilised discrete cosine transform and k-nearest neighbours (kNNs) to do a patch wise classification of benthic substrates. Friedman et al. (2009) explored well-known algorithms such as Support Vector Machines (SVM), kNNs and decision trees to segment images based on texture colour and feature shapes. Also availing of SVMs, Beijbom et al. (2015) used SVMs to classify coral reef images and, aware of the annotation constraints, also created a benchmark dataset (Moorea Labelled Corals) with 400,00 annotations. Purser et al. (2009), being among the pioneers to use ML in CWC habitats, used an artificial neural network based on self-organising feature maps (SOMs) to estimate *Lophelia* and sponge coverages. As studies advanced, part of the efforts also went towards improving annotation schemes by creating ML assisted tools envisioning time and cost efficiency (Beijbom et al., 2015). Zurowietz et al. (2018), for example, created MAIA (Machine Learning Assisted Image Annotation), an image annotation method using a combination of autoencoder networks with mask-region based convolutional neural networks (MASK

R-CNN). Alonso et al. (2019) presented CoralSeg, a framework based on CNN semantic segmentation aiming to address sparse labelling problem which is pertinent in previous works (Beijbom et al., 2015). Recently, Pavoni et al. (2022) developed TagLab following the semantic segmentation approach which documented an increase in annotation speed assisted by semantic label automatic allocation.

Parallel to that, research has progressed towards leveraging SfM-derived datasets, object-based image analysis (OBIA) and superpixel techniques to develop semi-supervised classification of marine habitats from orthomosaics and DEMs (Argentino et al., 2022; Conti et al., 2019; Fallati et al., 2020; Lim et al., 2020b; Price et al., 2022; TERNON et al., 2022; Yuval et al., 2021). OBIA works by grouping similar pixels and building segments of pixels based on specific criteria (Blaschke, 2010; Chen et al., 2018). These segments, called image objects, become the basic unit of analysis. The use of OBIA has been widely applied in MBES bathymetric and backscatter data (Diesing et al., 2016, 2014; Lucieer et al., 2013; Summers et al., 2021). Only recently, underwater image annotation and automatic classification platforms started integrating SfM derived data such as DEMs and orthomosaics, which represents a great progress to the fine-scale analysis of benthic ecosystems (Pavoni et al., 2022, 2019)

When it comes to the classification of the 3D SfM data products such as point clouds and meshes, there is space for considerable development. Studies have created methods to automatically classify complex scenes in 3D with success. However, as a common trend, there is a focus on terrestrial and aerial classification tasks, where the region of interest are either one single 3D object (Ben-Shabat et al., 2017; Qi et al., 2017), urban scenes (Roynard et al., 2018) or terrestrial landscapes (Weidner et al., 2021). The task of classifying benthic habitats in 3D has only started recently (Hopkinson et al., 2020; King et al., 2018; Mohamed et al., 2020; Pierce et al., 2021; Young, 2018). Young et al. (2018), acknowledging that CNNs perform better in images than 3D models, used CNNs to predict fish abundance from underlying coral reef texture by converting 3D models into 2D planar grids. King et al. (2018), building up on previous semantic segmentation methods such as Beijbom et al. (2012), compared 6 patch-based CNNs with fully convolutional neural network (FCNN) and SVM based

models and then produced a 3D model with the classified images. Similarly, Hopkinson et al. (2020) applied CNNs in mesh elements extracted from the 3D models and traced back the classified elements into the 3D model. Mohamed et al. (2020) use KNNs, SVMs and bagging assembled with a fuzzy majority voting (FMV) algorithm to classify benthic images that were then used to create 3D models. Similarly, Pierce et al. (2021) used FCNN to create a semantic super pixel algorithm to classify images and project them into 3D models. What these studies have in common is that they use image-based classification techniques and then create the 3D models as an independent process, thus going through similar image annotation processes to generate labels.

There are parallel aims between automatic classification of images and then use of these images to generate 3D models (Hopkinson et al., 2020). However, automatic classification directly applied to 3D models remains less explored due to the required domain knowledge entailed on the multidimensional problem complexity (Young, 2018). One of the main challenges of segmenting and classifying point clouds is the unstructured and unordered nature of the data (Ben-Shabat et al., 2017). Image processing software such as CloudCompare have integrated automated classification schemes that have enabled binary classification of 3D dense clouds (Brodu and Lague, 2012). Although these tools were purposely built for terrestrial landscapes, their application on CWC habitats led to successful results in classifying coral and seabed features (de Oliveira et al., 2021). As research on automatic classification develops, issues related to the human induced errors and sampling sizes are also widely discussed (Durden et al., 2021, 2016; Pavoni et al., 2022).

1.4 Rationale

Despite their fundamental importance, little is known about CWCs key ecosystem functions and distribution (Freiwald et al., 1999, 2004). The global distribution of CWC and the large extent of yet unexplored areas has suited regional mapping approaches using low-resolution and wider extent proxies, i.e., metre to kilometre scales. As research advances, it is now also understood that CWC habitats have different environmental drivers and their spatial variability is not only regional but also local

(Flögel et al., 2014; Henry and Roberts, 2017; Wheeler et al., 2007). Thus, these valuable ecosystems are known to not hold ecosystem homogeneity, which is valuable knowledge that can be used to better address environmental policies (Purser et al., 2013; Roberts et al., 2006).

Before the advent of ROVs and submersibles, the investigation of benthic fauna depended on sampling methods such as cores, grabs and trawls (Christiansen, 1993). It is well acknowledged that, as the majority of sampling methods, these techniques are limited by the sampling resolution, the need for a dense sampling matrix to assure robustness of estimates whilst also being destructive techniques (Brown et al., 2011). The advent of video yielded micro-scale in-situ characterisation of ecological habitats of these mounds and ground-truthing of acoustic mapping methods (Dolan et al., 2008; Fosså et al., 2002; Guinan et al., 2009; Huvenne et al., 2005; Masson et al., 2003; Mortensen et al., 1995; Savini et al., 2014).

Wilson et al. (1979) conducted one of the first studies of CWC distribution using underwater photos and seabed sampling. The use of photos became more common in the following years, providing centimetric-scale insights on colony morphology and shape (Frederiksen et al., 1992; Freiwald et al., 1999). The equipment used in earlier investigations, however, were not suitable for providing quantitative information on the facies of these habitats (Christiansen, 1993; Mortensen et al., 1995). Mortensen et al. (1995) provided a detailed fauna quantification of *L. pertusa* from sixteen ROV video transects in the Norwegian shelf by counting different coral species from the video data. Given the extent of mapped areas, traditional quadrat counting methods in video and images may provide limited information regarding the spatial relationships among ecological communities and are restricted by time and resources being prohibitively expensive (Brown et al., 2011; Ismail et al., 2018; Mortensen et al., 1995). SfM mosaics present a larger footprint when compared to single images (Pizarro et al., 2017) and, as part of a suite of high-resolution mapping tools and methods, they enable fine-scale quantifications of structural complexity, which may support valuable ecosystem functioning traits and niche-specific evaluations (Leon et al., 2015).

Thus, the structural complexity of coral reefs can influence key species interactions at local (millimetric) and regional (metric to kilometric) scales (Buhl-mortensen et al., 2015; Donovan et al., 2022; Kazanidis et al., 2021). Its importance extends to quantifying reef fish density and biomass (Graham and Nash, 2013; McCormick, 1994). It acknowledge that the inclusion of reef structural complexity analysis should be a crucial part in CWC monitoring and research (D'Urban Jackson et al., 2020; Price et al., 2019).

However, the magnitude of influence of 3D variables such as structural complexity continues to be poorly understood (Brown et al., 2011; Kovalenko et al., 2012). Most monitoring programs reduce dimensionality when mapping and resort in quantify coral quantity as live coral cover, which is the two dimensional proportion of coral surface to the seafloor on a planar view (Fisher et al., 2007; Goatley and Bellwood, 2011). Studies reiterated that the absence of the third dimension limits the ability to characterise coral reef key health indicators (Cocito et al., 2003; Fisher et al., 2007; Goatley and Bellwood, 2011; House et al., 2018). Furthermore, the costly nature of data collection for many applications in earth sciences are escalated by the remoteness and inaccessibility of study sites (D'Urban Jackson et al., 2020; Lecours et al., 2015; Westoby et al., 2012).

Governmental institutions and the scientific community convey that there is currently a lack of information available about important marine ecosystem services around the globe and there is a need for data collection, collation and analysis of the world's marine resources to support the implementation of conservation policies and marine spatial planning (Clark, 2006; FAO, 2010, 2009; Inter-Departmental Marine Coordination Group, 2018). Therefore, a practical perspective to support decision making of stakeholders whilst representing the functional diversity of deep-water habitats is urgently needed (Baker and Harris, 2012; Davies et al., 2017; Ismail et al., 2018)

At a social-economic perspective, CWCs are valuable ecosystems but there is a lack of awareness regarding their existence and current threat status (Aanesen et al., 2015; Davies et al., 2017). This lack of awareness is less pronounced for tropical reefs. For example, a search on Google Scholar with the word "Cold-water corals" returns

173,000 results as opposed to the 503,000 results when typing “tropical corals”. In comparison to deep-sea areas, marine spatial planning and methods to understand coral habitats is more developed in shallow waters (Brown et al., 2011; Ismail et al., 2018).

As technologies to map CWCs and deep-water environments advance, there is a growing need to advance acquisition and processing techniques (Kwasnitschka et al., 2013; Singh et al., 2007). The development of new acquisition and new analyses methods that will account for the increase of data volumes are yet to be on the same pace (Beijbom et al., 2015; Kwasnitschka et al., 2013) . Hence, research is now moving to not just analyse environments as isolated studies but also to aid time-effective and high-quality analysis of large areas. Whilst several frameworks to automatic classify images have been developed, there is still a gap on frameworks that enable the automatic classification of 3D underwater data for non-experts.

1.5 Aims And Research Questions

The main aim of this PhD thesis is to advance techniques for mapping of deep-water environments. Given the limitations listed above, the research outlined here aimed to contribute towards bridging the gap between the posed challenges and possible solutions. As such, this thesis investigates how computer vision imaging techniques can be used to:

- I. develop an unprecedented 3D imaging classification workflow for CWC habitats of Ireland whilst analysing the suitability and transferability of 2D and 3D data to represent these habitats in high-resolution;
- II. quantify facies distribution and spatial variability;
- III. link image data to processes driving CWC reef development;
- IV. develop new forms of visualisation of 3D data of underwater environments;
- V. derive meaningful information from dense optical datasets.

The work presented herein documents a turning point in the analyses of underwater environments by providing novel methods to manage and analyse 3D data. Each chapter provides an overview of the work developed towards achieving these objectives, as follows:

Chapter 1, this chapter, presents an overview of the fundamental concepts in which this PhD is based upon. It starts by outlining the importance, distribution and morphological traits of CWCs and CWC mound developments, leading to addressing current issues and gaps in CWC mapping. It follows with an overview of mapping trends, equipment and the methods used herein. Finally, the aims of the thesis are outlined.

[Chapter 2](#) presents the results of the first aim of the PhD: to develop an unprecedented 3D imaging classification workflow for Irish CWC reef habitats whilst analysing the suitability and transferability of 2D and 3D data to represent these habitats in high-resolution. First, it gives an overview of the current methods to manipulate 3D data and the importance of using 3D data in CWC mapping, followed by providing a detailed description of the photogrammetric process used to reconstruct sections of a submarine canyon. A binary classification framework was developed to classify different sections of the canyon in coral and seabed. Three methods were developed based on current techniques embedded in 3D image processing software. The advantages and shortcomings of using 3D data and 2D data are outlined. [Chapter 2](#) aims to answer the following research questions:

- 1 - What software-based methods for 3D point cloud classification are available?
- 2 - What is the cost, in terms of data loss, of using 2D data for 3D objects?
- 3 - What are the main advantages and disadvantages of the 3 different 3D workflows identified within this study?

[Chapter 3](#) presents an advanced classification by integrating the use of supervised machine learning algorithms into a multiclass 3D classification framework. This study was designed upon noticing a relevant research gap in the automatic classification of deep-water habitats using machine learning. Although machine learning techniques

have become more common over the past years and advances had been made in other scientific fields, no studies outlining the use and suitability of supervised classification algorithms for 3D data of CWC habitats had been developed. In this chapter, we present a detailed assessment of six machine-learning algorithms and underline their performance with different data sample sizes. [Chapter 3](#) aims to answer the following research questions:

- 1 - Can Machine Learning be used for the classification of 3D point clouds of coral reef environments?
- 2 - Which Machine Learning classifiers produce the highest classification accuracy?
- 3 - Which parameters and variables can provide a better classification outcome?
- 4 - What is the minimum density of points required to accurately classify a point cloud model with ML?

[Chapter 4](#) focuses on detecting and analysing spatial patterns of CWC facies and understanding possible interactions among coral facies at centimetric scales. It delivers an environmental analysis of the classified data by combining geomorphometric drivers, size distribution with Euclidean distances, and point pattern analyses. This chapter brings a novel approach to point pattern distribution by using multidimensional data, integrating object sizes into the analyses and providing a 3D interpretation of a CWC habitat. To this end, [Chapter 4](#) aims to answer the four main research questions:

- 1 - What is the distribution of each facies?
- 2 - Is there a pattern in coral distribution and size of corals ?
- 3 - Do corals have a preference in habitat?
- 4 -Are coral facies clustered or dispersed?

[Chapter 5](#) explores the investigation of new techniques to visualise deep-water habitats. This chapter was designed based on the fundamental concern of CWCs: if they are “out of sight” they are “out of mind”. The study presented in this chapter aimed to contribute to raising awareness about CWC and their importance. To this

end, we integrated photogrammetry, gaming developing platforms and mobile application development to create a novel, accessible platform to visualise the seafloor in 3D from a mobile phone. The suitability of different 3D reconstructions for the mobile app was accessed to investigate the requirements for 3D resolution within the mobile app, thus [Chapter 5](#) aims to answer the following research questions:

- 1 - Can SfM and augmented reality (AR) be applied in outreach activities to promote access to deep-water environments?
- 2 - What technologies are currently available to aid visualisation of these habitats?
- 3 - What are the specificities of 3D data necessary to develop successful mobile applications?

Finally, Chapter 6 provides a summary of the findings, achievements and concluding remarks on the work carried out in this thesis. It follows by expressing the limitations of this line of work, giving alternative approaches, suggestions and future developments.

1.6 References

- Aanesen, M., Armstrong, C., Czajkowski, M., Falk-Petersen, J., Hanley, N., Navrud, S., 2015. Willingness to pay for unfamiliar public goods: Preserving cold-water coral in Norway. *Ecol. Econ.* 112, 53–67. <https://doi.org/10.1016/j.ecolecon.2015.02.007>
- Addamo, A.M., Vertino, A., Stolarski, J., García-Jiménez, R., Taviani, M., Machordom, A., 2016. Merging scleractinian genera: The overwhelming genetic similarity between solitary *Desmophyllum* and colonial *Lophelia*. *BMC Evol. Biol.* 16, 1–17. <https://doi.org/10.1186/s12862-016-0654-8>
- Agisoft, 2019. Agisoft Metashape User Manual 160.
- Alonso, I., Yuval, M., Eyal, G., Treibitz, T., Murillo, A.C., 2019. CoralSeg: Learning coral segmentation from sparse annotations. *J. F. Robot.* 36, 1456–1477. <https://doi.org/10.1002/rob.21915>
- Althaus, F., Williams, A., Schlacher, T.A., Kloser, R.J., Green, M.A., Barker, B.A., Bax, N.J., Brodie, P., Schlacher-Hoenlinger, M.A., 2009. Impacts of bottom trawling on deep-coral ecosystems of seamounts are long-lasting. *Mar. Ecol. Prog. Ser.* 397, 279–294. <https://doi.org/10.3354/meps08248>
- Anelli, M., Julitta, T., Fallati, L., Galli, P., Rossini, M., Colombo, R., 2019. Towards new applications of underwater photogrammetry for investigating coral reef morphology and habitat complexity in the Myeik Archipelago, Myanmar. *Geocarto Int.* 34, 459–472. <https://doi.org/10.1080/10106049.2017.1408703>
- Appah, J.K.M., Lim, A., Harris, K., O’Riordan, R., O’Reilly, L., Wheeler, A.J., 2020. Are Non-reef Habitats as Important to Benthic Diversity and Composition as Coral Reef and Rubble Habitats in Submarine Canyons? Analysis of Controls on Benthic Megafauna Distribution in the Porcupine Bank Canyon, NE Atlantic. *Front. Mar. Sci.* 7, 831. <https://doi.org/10.3389/fmars.2020.571820>
- Argentino, C., Savini, A., Panieri, G., 2022. Integrating Fine-Scale Habitat Mapping and Pore Water Analysis in Cold Seep Research: A Case Study from the SW Barents Sea, in: *World Atlas of Submarine Gas Hydrates in Continental Margins*. Springer International

- Publishing, Cham, pp. 505–514. https://doi.org/10.1007/978-3-030-81186-0_43
- Baker, E.K., Harris, P.T., 2012. Habitat Mapping and Marine Management. Seafloor Geomorphol. as Benthic Habitat 23–38. <https://doi.org/10.1016/B978-0-12-385140-6.00002-5>
- Barbosa, R. V, Davies, A.J., Sumida, P.Y.G., 2019. Habitat suitability and environmental niche comparison of cold-water coral species along the Brazilian continental margin. Deep. Res. Part I 103147. <https://doi.org/10.1016/j.dsr.2019.103147>
- Beijbom, O., Edmunds, P.J., Kline, D.I., Mitchell, B.G., Kriegman, D., 2012. Automated annotation of coral reef survey images, in: Proc. IEEE Comput. Soc. Conf. Comput. Vis. Pattern Recognit, pp. 1170–1177. <https://doi.org/10.1109/CVPR.2012.6247798>
- Beijbom, O., Edmunds, P.J., Roelfsema, C., Smith, J., Kline, D.I., Neal, B.P., Dunlap, M.J., Moriarty, V., Fan, T.-Y.Y., Tan, C.-J.J., Chan, S., Treibitz, T., Gamst, A., Mitchell, B.G., Kriegman, D., 2015. Towards automated annotation of benthic survey images: Variability of human experts and operational modes of automation. PLoS One 10, 1–22. <https://doi.org/10.1371/journal.pone.0130312>
- Ben-Shabat, Y., Lindenbaum, M., Fischer, A., 2017. 3D Point Cloud Classification and Segmentation using 3D Modified Fisher Vector Representation for Convolutional Neural Networks.
- Bishop, C.M., 2006. Pattern Recognition and Machine Learning, Information Science and Statistics. Springer New York.
- Blaschke, T., 2010. Object based image analysis for remote sensing. ISPRS J. Photogramm. Remote Sens. 65, 2–16. <https://doi.org/10.1016/j.isprsjprs.2009.06.004>
- Bodenmann, A., Thornton, B., Nakajima, R., Ura, T., 2017. Methods for quantitative studies of seafloor hydrothermal systems using 3D visual reconstructions. <https://doi.org/10.1186/s40648-017-0091-5>
- Boolukos, C.M., Lim, A., O’Riordan, R.M., Wheeler, A.J., O’Riordan, R.M., Wheeler, A.J., O’Riordan, R.M., Wheeler, A.J., 2019. Cold-water corals in decline – A temporal (4 year) species abundance and biodiversity appraisal of complete photomosaiced cold-

water coral reef on the Irish Margin. *Deep Sea Res. Part I Oceanogr. Res. Pap.* 146, 44–54. <https://doi.org/10.1016/j.dsr.2019.03.004>

Brandt, A., James Griffiths, H., Schiaparelli, S., Ballerini, T., Griffiths, H., Gutt, J., Linse, K., Danis, B., Pfannkuche, O., 2014. Challenges of deep-sea biodiversity assessments in the Southern Ocean. *Adv Polar Sci* 25, 204–212. <https://doi.org/10.13679/j.advps.2014.3.00204>

Breiman, L., 2001. *Random Forests* 45, 5–32.

Brodu, N., Lague, D., 2012. 3D terrestrial lidar data classification of complex natural scenes using a multi-scale dimensionality criterion: Applications in geomorphology. *ISPRS J. Photogramm. Remote Sens.* 68, 121–134. <https://doi.org/10.1016/j.isprsjprs.2012.01.006>

Brown, C.J., Smith, S.J., Lawton, P., Anderson, J.T., 2011. Benthic habitat mapping: A review of progress towards improved understanding of the spatial ecology of the seafloor using acoustic techniques. *Estuar. Coast. Shelf Sci.* 92, 502–520. <https://doi.org/10.1016/j.ecss.2011.02.007>

Buhl-Mortensen, L., Buhl-Mortensen, P., Dolan, M.F.J., Holte, B., 2015. The MAREANO programme – A full coverage mapping of the Norwegian off-shore benthic environment and fauna. *Mar. Biol. Res.* 11, 4–17. <https://doi.org/10.1080/17451000.2014.952312>

Buhl-mortensen, P., Buhl-mortensen, L., Purser, A., 2015. Trophic Ecology and Habitat Provision in Cold-Water Coral Ecosystems, in: Rossi, S., Bramanti, L., Gori, A., Orejas Saco del Valle, C. (Eds.), *Marine Animal Forests*. Springer International Publishing, Cham, pp. 1–26. <https://doi.org/10.1007/978-3-319-17001-5>

Buitinck, L., Louppe, G., Blondel, M., Pedregosa, F., Mueller, A., Grisel, O., Niculae, V., Prettenhofer, P., Gramfort, A., Grobler, J., Layton, R., Vanderplas, J., Joly, A., Holt, B., Varoquaux, G., 2013. API design for machine learning software: experiences from the scikit-learn project 1–15.

Burges, C.J.C., 1998. A Tutorial on Support Vector Machines for Pattern Recognition. *Data Min. Knowl. Discov.* 28, 121–167.

- Burke, L., Reyntar, K., Spalding, M., Perry, A., 2011. Reefs at Risk Revisited, Defenders.
- Burns, J. H. R., Delparte, D., Gates, R., Takabayashi, M., 2015a. Integrating structure-from-motion photogrammetry with geospatial software as a novel technique for quantifying 3D ecological characteristics of coral reefs. *PeerJ* 3, e1077. <https://doi.org/10.7717/peerj.1077>
- Burns, J. H. R., Delparte, D., Gates, R.D., Takabayashi, M., 2015b. Utilizing Underwater Three-Dimensional Modeling To Enhance Ecological And Biological Studies Of Coral Reefs. *Int. Arch. Photogramm. Remote Sens. Spat. Inf. Sci.* XL-5/W5, 61–66. <https://doi.org/10.5194/isprsarchives-XL-5-W5-61-2015>
- Büscher, J. V., Form, A.U., Riebesell, U., 2017. Interactive effects of ocean acidification and warming on growth, fitness and survival of the cold-water coral *Lophelia pertusa* under different food availabilities. *Front. Mar. Sci.* 4, 1–14. <https://doi.org/10.3389/fmars.2017.00101>
- Bythell, J., Pan, P., Lee, J., 2001. Three-dimensional morphometric measurements of reef corals using underwater photogrammetry techniques. *Coral Reefs* 20, 193–199. <https://doi.org/10.1007/s003380100157>
- Cairns, S.D., 2007. Deep-water corals: An overview with special reference to diversity and distribution of deep-water scleractinian corals. *Bull. Mar. Sci.* 81, 311–322.
- Cairns, S.D., 1995. The marine fauna of New Zealand: Scleractinia (Cnidaria: Anthozoa). *New Zeal. Oceanogr. Inst. Mem.*
- Capra, A., Castagnetti, C., Mancini, F., Rossi, P., Capra, A., Castagnetti, C., Mancini, F., Rossi, P., 2020. Underwater Photogrammetry for Change Detection 10–14.
- Carrivick, J.L., Smith, M.W., Quincey, D.J., 2016. Structure from Motion in the Geosciences. John Wiley & Sons, Ltd, Chichester, UK. <https://doi.org/10.1002/9781118895818>
- Cathalot, C., Van Oevelen, D., Cox, T.J.S., Kutti, T., Lavaleye, M., Duineveld, G., Meysman, F.J.R., 2015. Cold-water coral reefs and adjacent sponge grounds: hotspots of benthic respiration and organic carbon cycling in the deep sea. *Front. Mar. Sci.* 2. <https://doi.org/10.3389/fmars.2015.00037>

- Chance, T.S., Kleiner, A.A., Northcutt, J.G., 2000. The Autonomous Underwater Vehicle (AUV): A Cost-Effective Alternative to Deep-Towed Technology. *Integr. Coast. Zo. Manag. Mag.* 65–69.
- Chen, G., Weng, Q., Hay, G.J., He, Y., 2018. Geographic object-based image analysis (GEOBIA): emerging trends and future opportunities. *GIScience Remote Sens.* 55, 159–182. <https://doi.org/10.1080/15481603.2018.1426092>
- Chen, G.K., Dai, C.F., 2021. Using 3D photogrammetry to quantify the subtle differences of coral reefs under the impacts of marine activities. *Mar. Pollut. Bull.* 173, 113032. <https://doi.org/10.1016/j.marpolbul.2021.113032>
- Christiansen, B., 1993. A television and photographic survey of megafaunal abundance in Central Sognefjorden, Western Norway. *Sarsia* 78, 1–8. <https://doi.org/10.1080/00364827.1993.10413515>
- Clark, M.R., 2006. Seamounts, deep-sea corals and fisheries: vulnerability of deep-sea corals to fishing on seamounts beyond areas of national jurisdiction. *UNEP/Earthprint.*
- Cocito, S., Sgorbini, S., Peirano, A., Valle, M., 2003. 3-D reconstruction of biological objects using underwater video technique and image processing. *J. Exp. Mar. Bio. Ecol.* 297, 57–70. [https://doi.org/10.1016/S0022-0981\(03\)00369-1](https://doi.org/10.1016/S0022-0981(03)00369-1)
- Conti, L.A., Lim, A., Wheeler, A.J., 2019. High resolution mapping of a cold water coral mound. *Sci. Rep.* 9, 1016. <https://doi.org/10.1038/s41598-018-37725-x>
- Costanza, R., Costanza, R., Arge, R., Groot, R. De, Farber, S., Grasso, M., Hannon, B., 1996. The value of the world ' s ecosystem services and natural capital.
- Costello, M.J., McCrea, M., Freiwald, A., Lundälv, T., Jonsson, L., Bett, B.J., van Weering, T.C.E., de Haas, H., Roberts, J.M., Allen, D., 2005. Role of cold-water *Lophelia pertusa* coral reefs as fish habitat in the NE Atlantic, in: *Cold-Water Corals and Ecosystems*. Springer Berlin Heidelberg, pp. 771–805. https://doi.org/10.1007/3-540-27673-4_41
- Cristobal, F.R., Dodge, M., Noll, B., Rosenberg, N., Burns, J., Sanchez, J., Gotshalk, D., Pascoe, K., Runyan, A., 2020. Exploration of Coral Reefs in Hawai'i through Virtual Reality: Hawaiian Coral Reef Museum VR, in: *Practice and Experience in Advanced*

Research Computing. ACM, New York, NY, USA, NY, USA, pp. 545–546.
<https://doi.org/10.1145/3311790.3404542>

Czepiel, S.A., 2002. Maximum Likelihood Estimation of Logistic Regression Models: Theory and Implementation. *CI. Notes* 1–23.

D’Urban Jackson, T., Williams, G.J., Walker-Springett, G., Davies, A.J., 2020. Three-dimensional digital mapping of ecosystems: a new era in spatial ecology. *Proc. R. Soc. B Biol. Sci.* 287, 20192383. <https://doi.org/10.1098/rspb.2019.2383>

Danson, E., 2002. The Economics of Scale : Using Autonomous Underwater Vehicles (AUVs) for Wide-Area Hydrographic Survey and Ocean Data Acquisition The Economics of Scale : Using Autonomous Underwater Vehicles (AUVs) for Wide-Area Hydrographic Survey and Ocean Data Acq. *Proc. XXII FIG(Fédération Int. des Géomètres) Int. Congr.* 1–15.

Davies, A.J., Duineveld, G.C.A., van Weering, T.C.E., Mienis, F., Quattrini, A.M., Seim, H.E., Bane, J.M., Ross, S.W., 2010. Short-term environmental variability in cold-water coral habitat at Viosca Knoll, Gulf of Mexico. *Deep. Res. Part I Oceanogr. Res. Pap.* 57, 199–212. <https://doi.org/10.1016/j.dsr.2009.10.012>

Davies, J.S., Guillaumont, B., Tempera, F., Vertino, A., Beuck, L., Ólafsdóttir, S.H., Smith, C.J., Fosså, J.H., van den Beld, I.M.J., Savini, A., Rengstorf, A., Bayle, C., Bourillet, J.F., Arnaud-Haond, S., Grehan, A., 2017. A new classification scheme of European cold-water coral habitats: Implications for ecosystem-based management of the deep sea. *Deep. Res. Part II Top. Stud. Oceanogr.* 145, 102–109. <https://doi.org/10.1016/j.dsr2.2017.04.014>

de Haas, H., Mienis, F., Frank, N., Richter, T.O., Steinacher, R., de Stigter, H., van der Land, C., van Weering, T.C.E., 2009. Morphology and sedimentology of (clustered) cold-water coral mounds at the south Rockall Trough margins, NE Atlantic Ocean. *Facies* 55, 1–26. <https://doi.org/10.1007/s10347-008-0157-1>

De Leo, F.C., Vetter, E.W., Smith, C.R., Rowden, A.A., McGranaghan, M., 2014. Spatial scale-dependent habitat heterogeneity influences submarine canyon macrofaunal abundance and diversity off the Main and Northwest Hawaiian Islands. *Deep. Res. Part II Top. Stud. Oceanogr.* 104, 267–290. <https://doi.org/10.1016/j.dsr2.2013.06.015>

De Mol, B., Henriët, J.-P., Canals, M., 2005. Development of coral banks in Porcupine Seabight: do they have Mediterranean ancestors? *Cold-Water Corals Ecosyst.* 515–533. https://doi.org/10.1007/s10073-005-27673-4_26

De Mol, L., Van Rooij, D., Pirlet, H., Greinert, J., Frank, N., Quemmerais, F., Henriët, J.P., 2011. Cold-water coral habitats in the Penmarc'h and Guilvinec Canyons (Bay of Biscay): Deep-water versus shallow-water settings. *Mar. Geol.* 282, 40–52. <https://doi.org/10.1016/j.margeo.2010.04.011>

de Oliveira, L.M.C., Lim, A., Conti, L.A., Wheeler, A.J., 2021. 3D Classification of Cold-Water Coral Reefs: A Comparison of Classification Techniques for 3D Reconstructions of Cold-Water Coral Reefs and Seabed. *Front. Mar. Sci.* 8. <https://doi.org/10.3389/fmars.2021.640713>

Diesing, M., Green, S.L., Stephens, D., Lark, R.M., Stewart, H.A., Dove, D., 2014. Mapping seabed sediments: Comparison of manual, geostatistical, object-based image analysis and machine learning approaches. *Cont. Shelf Res.* 84, 107–119. <https://doi.org/10.1016/j.csr.2014.05.004>

Diesing, M., Mitchell, P., Stephens, D., 2016. Image-based seabed classification: what can we learn from terrestrial remote sensing? *ICES J. Mar. Sci. J. du Cons.* 73, 2425–2441. <https://doi.org/10.1093/icesjms/fsw118>

Dolan, M.F.J., Grehan, A.J., Guinan, J.C., Brown, C., 2008. Modelling the local distribution of cold-water corals in relation to bathymetric variables: Adding spatial context to deep-sea video data. *Deep. Res. Part I Oceanogr. Res. Pap.* 55, 1564–1579. <https://doi.org/10.1016/j.dsr.2008.06.010>

Doležal, M., Vlachos, M., Secci, M., Demesticha, S., Skarlatos, D., Liarokapis, F., 2019. UNDERSTANDING UNDERWATER PHOTOGRAMMETRY for MARITIME ARCHAEOLOGY THROUGH IMMERSIVE VIRTUAL REALITY. *ISPRS Ann. Photogramm. Remote Sens. Spat. Inf. Sci.* 42, 85–91. <https://doi.org/10.5194/isprs-archives-XLII-2-W10-85-2019>

Donovan, M.K., Alves, C., Burns, J., Drury, C., Meier, O.W., Ritson, R., Ross, W., Robert, C., Gretchen, P.D., Gringley, G., Henderson, L.M., Knapp, I.S.S., Levy, J., Logan, C.A., Mudge, L., Sullivan, C., Gates, R.D., Asner, G.P., 2022. From polyps to pixels : understanding coral reef resilience to local and global change across scales. *Landsc.*

Ecol. <https://doi.org/10.1007/s10980-022-01463-3>

Dorschel, B., Hebbeln, D., Foubert, A., White, M., Wheeler, A.J., 2007. Hydrodynamics and cold-water coral facies distribution related to recent sedimentary processes at Galway Mound west of Ireland. *Mar. Geol.* 244, 184–195.

Dorschel, B., Hebbeln, D., Rüggeberg, A., Dullo, W.C., Freiwald, A., 2005. Growth and erosion of a cold-water coral covered carbonate mound in the Northeast Atlantic during the Late Pleistocene and Holocene. *Earth Planet. Sci. Lett.* 233, 33–44. <https://doi.org/10.1016/j.epsl.2005.01.035>

Dorschel, B., Wheeler, A.J., Monteys, X., Verbruggen, K., 2010. Atlas of the Deep-Water Seabed, Atlas of the Deep-Water Seabed: Ireland. Springer Netherlands, Dordrecht. <https://doi.org/10.1007/978-90-481-9376-9>

Douarin, M., Sinclair, D.J., Elliot, M., Henry, L.A., Long, D., Mitchison, F., Roberts, J.M., 2014. Changes in fossil assemblage in sediment cores from Mingulay Reef Complex (NE Atlantic): Implications for coral reef build-up. *Deep. Res. Part II Top. Stud. Oceanogr.* 99, 286–296. <https://doi.org/10.1016/j.dsr2.2013.07.022>

Durden, J.M., Bett, B.J., Schoening, T., Morris, K.J., Nattkemper, T.W., Ruhl, H.A., 2016. Comparison of image annotation data generated by multiple investigators for benthic ecology. *Mar. Ecol. Prog. Ser.* 552, 61–70. <https://doi.org/10.3354/meps11775>

Durden, J.M., Hosking, B., Bett, B.J., Cline, D., Ruhl, H.A., 2021. Automated classification of fauna in seabed photographs: the impact of training and validation dataset size, with considerations for the class imbalance. *Prog. Oceanogr.* 196, 102612. <https://doi.org/10.1016/j.pocean.2021.102612>

Elawady, M., 2015. Sparse Coral Classification Using Deep Convolutional Neural Networks.

Elliott, G.M., Shannon, P.M., Haughton, P.D.W., Praeg, D., O'Reilly, B., 2006. Mid- to Late Cenozoic canyon development on the eastern margin of the Rockall Trough, offshore Ireland. *Mar. Geol.* 229, 113–132. <https://doi.org/10.1016/j.margeo.2006.03.008>

Eustice, R., Pizarro, O., Singh, H., 2004. Visually augmented navigation in an

unstructured environment using a delayed state history. Proc. - IEEE Int. Conf. Robot. Autom. 2004, 25–32. <https://doi.org/10.1109/robot.2004.1307124>

Fallati, L., Saponari, L., Savini, A., Marchese, F., Corselli, C., Galli, P., 2020. Multi-temporal UAV data and object-based image analysis (OBIA) for estimation of substrate changes in a post-bleaching scenario on a Maldivian reef. Remote Sens. 12. <https://doi.org/10.3390/rs12132093>

FAO, 2010. The state of world fisheries and aquaculture 218.

FAO, 2009. International Guidelines for the Management of Deep-sea Fisheries in the High Seas. Rome, Italy.

Fawcett, T., 2006. An introduction to ROC analysis. Pattern Recognit. Lett. 27, 861–874. <https://doi.org/10.1016/j.patrec.2005.10.010>

Ferrari, R., Figueira, W.F., Pratchett, M.S., Boube, T., Adam, A., Kobelkowsky-Vidrio, T., Doo, S.S., Atwood, T.B., Byrne, M., 2017. 3D photogrammetry quantifies growth and external erosion of individual coral colonies and skeletons. Sci. Rep. 7, 1–9. <https://doi.org/10.1038/s41598-017-16408-z>

Ferrari, R., Lachs, L., Pygas, D.R., Humanes, A., Sommer, B., Figueira, W.F., Edwards, A.J., Bythell, J.C., Guest, J.R., 2021. Photogrammetry as a tool to improve ecosystem restoration. Trends Ecol. Evol. 1–9. <https://doi.org/10.1016/j.tree.2021.07.004>

Figueira, W., Ferrari, R., Weatherby, E., Porter, A., Hawes, S., Byrne, M., 2015. Accuracy and Precision of Habitat Structural Complexity Metrics Derived from Underwater Photogrammetry. Remote Sens 7, 16883–16900.

Fischler, M.A., Bolles, R.C., 1981. Random sample consensus: A Paradigm for Model Fitting with Applications to Image Analysis and Automated Cartography. Commun. ACM 24, 381–395. <https://doi.org/10.1145/358669.358692>

Fisher, W.S., Davis, W.P., Quarles, R.L., Patrick, J., Campbell, J.G., Harris, P.S., Hemmer, B.L., Parsons, M., 2007. Characterizing coral condition using estimates of three-dimensional colony surface area. Environ. Monit. Assess. 125, 347–360. <https://doi.org/10.1007/s10661-006-9527-8>

Flögel, S., Dullo, W.C., Pfannkuche, O., Kiriakoulakis, K., Rüggeberg, A., 2014.

- Geochemical and physical constraints for the occurrence of living cold-water corals. *Deep. Res. Part II Top. Stud. Oceanogr.* 99, 19–26. <https://doi.org/10.1016/j.dsr2.2013.06.006>
- Foley, N.S., Rensburg, T.M. Van, Armstrong, C.W., 2010. Ocean & Coastal Management The ecological and economic value of cold-water coral ecosystems. *Ocean Coast. Manag.* 53, 313–326. <https://doi.org/10.1016/j.ocecoaman.2010.04.009>
- Fosså, J.H., Mortensen, P.B., Furevik, D.M., 2002. The deep-water coral *Lophelia pertusa* in Norwegian waters: Distribution and fishery impacts. *Hydrobiologia* 471, 1–12. <https://doi.org/https://doi.org/10.1023/A:1016504430684>
- Foubert, A., Huvenne, V.A.I., Wheeler, A., Kozachenko, M., Opderbecke, J., Henriët, J.-P., 2011. The Moira Mounds, small cold-water coral mounds in the Porcupine Seabight, NE Atlantic: Part B—Evaluating the impact of sediment dynamics through high-resolution ROV-borne bathymetric mapping. *Mar. Geol.* 282, 65–78. <https://doi.org/10.1016/j.margeo.2011.02.008>
- Frederiksen, R., Jensen, A., Westerberg, H., 1992. The distribution of the scleractinian coral *Lophelia pertusa* around the Faroe islands and the relation to internal tidal mixing. *Sarsia* 77, 157–171. <https://doi.org/10.1080/00364827.1992.10413502>
- Freiwald, A., Grehan, A., Fosså, J.H., Koslow, T., Roberts, J.M., 2004. Cold-Water Corals: Out of Sight – No Longer Out of Mind, Unep-Wcmc.
- Freiwald, A., Hühnerbach, V., Lindberg, B., Wilson, J.B., Campbell, J., 2002. The Sula Reef Complex, Norwegian shelf. *Facies* 47, 179–200. <https://doi.org/10.1007/BF02667712>
- Freiwald, A., Wilson, J.B., 1998. Taphonomy of modern deep, cold-temperate water coral reefs. *Hist. Biol.* 13, 37–52. <https://doi.org/10.1080/08912969809386571>
- Freiwald, A., Wilson, J.B., Henrich, R., 1999. Grounding pleistocene icebergs shape recent deep-water coral reefs. *Sediment. Geol.* 125, 1–8. [https://doi.org/10.1016/S0037-0738\(98\)00142-0](https://doi.org/10.1016/S0037-0738(98)00142-0)
- Friedman, A., 2013. Automated interpretation of benthic stereo imagery. University

of Sydney.

Friedman, A., Pizarro, O., Williams, S.B., Johnson-Roberson, M., 2012. Multi-Scale Measures of Rugosity, Slope and Aspect from Benthic Stereo Image Reconstructions. *PLoS One* 7. <https://doi.org/10.1371/journal.pone.0050440>

Fukunaga, A., Burns, J.H.R., 2020. Metrics of coral reef structural complexity extracted from 3D mesh models and digital elevation models. *Remote Sens.* 12, 2676. <https://doi.org/10.3390/RS12172676>

Fukunaga, A., Burns, J.H.R., Pascoe, K.H., Kosaki, R.K., 2020. Associations between benthic cover and habitat complexity metrics obtained from 3D reconstruction of coral reefs at different resolutions. *Remote Sens.* 12. <https://doi.org/10.3390/rs12061011>

Gass, S.E., Roberts, J.M., 2006. The occurrence of the cold-water coral *Lophelia pertusa* (Scleractinia) on oil and gas platforms in the North Sea: Colony growth, recruitment and environmental controls on distribution. *Mar. Pollut. Bull.* 52, 549–559. <https://doi.org/10.1016/j.marpolbul.2005.10.002>

GEBCO, 2017. The Nippon Foundation GEBCO Seabed 2030 Mission statement [WWW Document]. URL https://www.gebco.net/documents/seabed2030_brochure.pdf (accessed 1.26.23).

Gerdes, K., Arbizu, P.M., Schwarz-Schampera, U., Schwentner, M., Kihara, T.C., 2019. Detailed mapping of hydrothermal vent fauna: A 3d reconstruction approach based on video imagery. *Front. Mar. Sci.* 6. <https://doi.org/10.3389/fmars.2019.00096>

Goatley, C.H.R., Bellwood, D.R., 2011. The roles of dimensionality, canopies and complexity in ecosystem monitoring. *PLoS One* 6.

Graham, N.A.J., Nash, K.L., 2013. The importance of structural complexity in coral reef ecosystems. *Coral Reefs* 32, 315–326. <https://doi.org/10.1007/s00338-012-0984-y>

Graham, N.A.J., Wilson, S.K., Jennings, S., Polunin, N.V.C., Bijoux, J.P., Robinson, J., 2006. Dynamic fragility of oceanic coral reef ecosystems. *Proc. Natl. Acad. Sci. U. S. A.* 103, 8425–8429. <https://doi.org/10.1073/pnas.0600693103>

Granshaw, S.I., 1980. Bundle Adjustment Methods in Engineering Photogrammetry.

Photogramm. Rec. 10, 181–207. <https://doi.org/10.1111/j.1477-9730.1980.tb00020.x>

Guinan, J., Grehan, A., Dolan, M., Brown, C., 2009. Quantifying relationships between video observations of cold-water coral cover and seafloor features in Rockall Trough, west of Ireland. *Mar. Ecol. Prog. Ser.* 375, 125–138. <https://doi.org/10.3354/meps07739>

Hall-Spencer, J., Allain, V., Fosså, J.H., 2002. Trawling damage to Northeast Atlantic ancient coral reefs. *Proc. R. Soc. B Biol. Sci.* 269, 507–511. <https://doi.org/10.1098/rspb.2001.1910>

Hall-Spencer, J.M., Stehfest, K.M., Wheeler, A.J., 2009. Assessment of Coral Carbonate Mounds in the OSPAR area and the development of a monitoring program Background Information.

Hennige, S.J., Wolfram, U., Wickes, L., Murray, F., Roberts, J.M., Kamenos, N.A., Schofield, S., Groetsch, A., Spiesz, E.M., Aubin-Tam, M.E., Etnoyer, P.J., 2020. Crumbling Reefs and Cold-Water Coral Habitat Loss in a Future Ocean: Evidence of “Coralporosis” as an Indicator of Habitat Integrity. *Front. Mar. Sci.* 7, 1–16. <https://doi.org/10.3389/fmars.2020.00668>

Henry, L.-A., Roberts, J.M., 2017. Global Biodiversity in Cold-Water Coral Reef Ecosystems, in: Rossi, S., Bramanti, L., Gori, A., Orejas, C. (Eds.), *Marine Animal Forests*. Springer International Publishing, Cham, pp. 235–256. https://doi.org/10.1007/978-3-319-21012-4_6

Hopkinson, B.M., King, A.C., Owen, D.P., Johnson-Roberson, M., Long, M.H., Bhandarkar, S.M., 2020. Automated classification of three-dimensional reconstructions of coral reefs using convolutional neural networks. *PLoS One* 15.

House, J.E., Brambilla, V., Bidaut, L.M., Christie, A.P., Pizarro, O., Madin, J.S., Dornelas, M., 2018. Moving to 3D: relationships between coral planar area, surface area and volume. *PeerJ* 6, e4280. <https://doi.org/10.7717/peerj.4280>

Hovland, M., Croker, P.F., Martin, M., 1994. Fault-associated seabed mounds (carbonate knolls?) off western Ireland and north-west Australia. *Mar. Pet. Geol.* 11,

232–246. [https://doi.org/10.1016/0264-8172\(94\)90099-X](https://doi.org/10.1016/0264-8172(94)90099-X)

Hovland, M., Thomsen, E., 1997. Cold-water corals - Are they hydrocarbon seep related?, in: *Marine Geology*. Elsevier, pp. 159–164. [https://doi.org/10.1016/S0025-3227\(96\)00086-2](https://doi.org/10.1016/S0025-3227(96)00086-2)

Huvenne, V.A.I., Bett, B.J., Masson, D.G., Le Bas, T.P., Wheeler, A.J., 2016. Effectiveness of a deep-sea cold-water coral Marine Protected Area, following eight years of fisheries closure. *Biol. Conserv.* 200, 60–69. <https://doi.org/10.1016/j.biocon.2016.05.030>

Huvenne, V.A.I., Beyer, A., de Haas, H., Dekindt, K., Henriët, J.-P., Kozachenko, M., Olu-Le Roy, K., Wheeler, A.J., 2005. The seabed appearance of different coral bank provinces in the Porcupine Seabight, NE Atlantic: results from sidescan sonar and ROV seabed mapping. *Cold-Water Corals Ecosyst.* 535–569. https://doi.org/10.1007/3-540-27673-4_27

Huvenne, V.A.I., Blondel, P., Henriët, J.P., 2002. Textural analyses of sidescan sonar imagery from two mound provinces in the Porcupine Seabight. *Mar. Geol.* 189, 323–341. [https://doi.org/10.1016/S0025-3227\(02\)00420-6](https://doi.org/10.1016/S0025-3227(02)00420-6)

Huvenne, V.A.I., Tyler, P.A., Masson, D.G., Fisher, E.H., Hauton, C., Hühnerbach, V., Bas, T.P., Wolff, G.A., 2011. A picture on the wall: Innovative mapping reveals cold-water coral refuge in submarine canyon. *PLoS One* 6, 1–9. <https://doi.org/10.1371/journal.pone.0028755>

Inter-Departmental Marine Coordination Group, 2018. *Harnessing Our Ocean Wealth An Integrated Marine Plan for Ireland*.

Ismail, K., Huvenne, V., Robert, K., 2018. Quantifying spatial heterogeneity in submarine canyons. *Prog. Oceanogr.* 169, 181–198. <https://doi.org/10.1016/j.pocean.2018.03.006>

Jodzani, S.E., Johnson, B.A., Chen, D., 2019. Comparing Deep Neural Networks , Ensemble Classifiers , and Support Vector Machine Algorithms. *Remote Sens.* 11, 1–24.

Jones, C.G., Lawton, J.H., Shachak, M., 1994. *Organisms as Ecosystem Engineers*.

Ecosyst. Manag. 130–147. https://doi.org/10.1007/978-1-4612-4018-1_14

Jonsson, L.G., Nilsson, P.G., Floruta, F., Lundälv, T., 2004. Distributional patterns of macro- and megafauna associated with a reef of the cold-water coral *Lophelia pertusa* on the Swedish west coast. *Mar. Ecol. Prog. Ser.* 284, 163–171. <https://doi.org/10.3354/meps284163>

Kazanidis, G., Henry, L.A., Roberts, J.M., 2021. Hidden structural heterogeneity enhances marine hotspots' biodiversity. *Coral Reefs* 40, 1615–1630. <https://doi.org/10.1007/s00338-021-02114-w>

Kenyon, N.H., Akhmetzhanov, A.M., Wheeler, A.J., van Weering, T.C.E., de Haas, H., Ivanov, M.K., 2003. Giant carbonate mud mounds in the southern Rockall Trough. *Mar. Geol.* 195, 5–30. [https://doi.org/10.1016/S0025-3227\(02\)00680-1](https://doi.org/10.1016/S0025-3227(02)00680-1)

Kenyon, N.H., Ivanov, M.K., Akhmetzhanov, a M., 1998. Cold water carbonate mounds and sediment transport on the Northeast Atlantic margin. *IOC Tech. Ser.* 52.

King, A., Bhandarkar, S.M., Hopkinson, B.M., 2018. A Comparison of Deep Learning Methods for Semantic Segmentation of Coral Reef Survey Images, in: 2018 IEEE/CVF Conference on Computer Vision and Pattern Recognition Workshops (CVPRW). IEEE, pp. 1475–14758. <https://doi.org/10.1109/CVPRW.2018.00188>

Kitahara, M.V., 2007. Species richness and distribution of azooxanthellate Scleractinia in Brazil Species richness and distribution of azooxanthellate Scleractinia in Brazil. *Bull. Mar. Sci.* 81, 497–518.

Koch, A., Heipke, C., 2006. Semantically correct 2.5D GIS data - The integration of a DTM and topographic vector data. *ISPRS J. Photogramm. Remote Sens.* 61, 23–32. <https://doi.org/10.1016/j.isprsjprs.2006.07.005>

Kongsberg Gruppen, 2010. The HUGIN Family : Maximizing performance.

Kovalenko, K.E., Thomaz, S.M., Warfe, D.M., 2012. Habitat complexity: Approaches and future directions. *Hydrobiologia* 685, 1–17. <https://doi.org/10.1007/s10750-011-0974-z>

Kwasnitschka, T., Hansteen, T.H., Devey, C.W., Kutterolf, S., 2013. Doing fieldwork on the seafloor: Photogrammetric techniques to yield 3D visual models from ROV video.

Comput. Geosci. 52, 218–226. <https://doi.org/10.1016/j.cageo.2012.10.008>

Laranjeira, M., Arnaubec, A., Brignone, L., Dune, C., Opderbecke, J., 2020. 3D Perception and Augmented Reality Developments in Underwater Robotics for Ocean Sciences. *Curr. Robot. Reports* 1, 123–130. <https://doi.org/10.1007/s43154-020-00014-5>

Lavy, A., Eyal, G., Neal, B., Keren, R., Loya, Y., Ilan, M., 2015. A quick, easy and non-intrusive method for underwater volume and surface area evaluation of benthic organisms by 3D computer modelling. *Methods Ecol. Evol.* 6, 521–531. <https://doi.org/10.1111/2041-210X.12331>

Le Danois, E. 1887-, 1948. Les profondeurs de la mer; trente ans de recherches sur la faune sous-marine au large des côtes de France. LK -, Bibliothèque scientifique TA - TT -. Payot, Paris SE - 303 pages illustrations, maps 23 cm.

Lecours, V., Devillers, R., Schneider, D., Lucieer, V., Brown, C., Edinger, E., 2015. Spatial scale and geographic context in benthic habitat mapping: review and future directions. *Mar. Ecol. Prog. Ser.* 535, 259–284. <https://doi.org/10.3354/meps11378>

Leon, J.X., Roelfsema, C.M., Saunders, M.I., Phinn, S.R., 2015. Measuring coral reef terrain roughness using ‘Structure-from-Motion’ close-range photogrammetry. *Geomorphology* 242, 21–28. <https://doi.org/10.1016/j.geomorph.2015.01.030>

Leverette, T.L., Metaxas, A., 2006. Predicting habitat for two species of deep-water coral on the Canadian Atlantic continental shelf and slope, in: *Cold-Water Corals and Ecosystems*. Springer-Verlag, pp. 467–479. https://doi.org/10.1007/3-540-27673-4_23

Lim, A., 2017. Spatio – temporal Patterns and Controls on Cold-water Coral Reef Development : The Moira Mounds , Porcupine Seabight , Offshore Ireland. Porcupine Seabight, Offshore Ireland.

Lim, A., Wheeler, A.J., Arnaubec, A., 2017. High-resolution facies zonation within a cold-water coral mound: The case of the Piddington Mound, Porcupine Seabight, NE Atlantic. *Mar. Geol.* 390, 120–130. <https://doi.org/10.1016/j.margeo.2017.06.009>

Lim,A. Wheeler, A.J., Conti, L., 2020a. Cold-Water Coral Habitat Mapping: Trends and

Developments in Acquisition and Processing Methods. *Geosciences* 11, 9. <https://doi.org/10.3390/geosciences11010009>

Lim, A., Wheeler, A.J., Price, D.M., O'Reilly, L., Harris, K., Conti, L., 2020b. Influence of benthic currents on cold-water coral habitats: a combined benthic monitoring and 3D photogrammetric investigation. *Sci. Rep.* 10, 19433. <https://doi.org/10.1038/s41598-020-76446-y>

Liu, P., Choo, K.-K.R., Wang, L., Huang, F., 2017. SVM or deep learning? A comparative study on remote sensing image classification. *Soft Comput.* 21, 7053–7065. <https://doi.org/10.1007/s00500-016-2247-2>

Long, D., Roberts, J.M., Gillespie, E.J., 1999. Occurrences of *Lophelia pertusa* on the Atlantic margin. Tech. Rep. WB/99/24 44.

Lowe, D.G., 1999. Object recognition from local scale-invariant features, in: *Proceedings of the Seventh IEEE International Conference on Computer Vision*. IEEE, pp. 1150–1157 vol.2. <https://doi.org/10.1109/ICCV.1999.790410>

Lowe, G., 2004. Sift-the scale invariant feature transform. *Int. J.* 2, 2.

Lucieer, V., Hill, N.A., Barrett, N.S., Nichol, S., 2013. Do marine substrates 'look' and 'sound' the same? Supervised classification of multibeam acoustic data using autonomous underwater vehicle images. *Estuar. Coast. Shelf Sci.* 117, 94–106. <https://doi.org/10.1016/J.ECSS.2012.11.001>

Mangini, A., Lomitschka, M., Eichstädter, R., Frank, N., Vogler, S., Bonani, G., Hajdas, I., Patzold, J., 1998. Coral provides way to age deep water. *Nature* 392, 347–348. <https://doi.org/10.1038/32804>

Masson, D., Bett, B., Billett, D.S., Jacobs, C., Wheeler, A., Wynn, R., 2003. The origin of deep-water, coral-topped mounds in the northern Rockall Trough, Northeast Atlantic. *Mar. Geol.* 194, 159–180. [https://doi.org/10.1016/S0025-3227\(02\)00704-1](https://doi.org/10.1016/S0025-3227(02)00704-1)

Mazzini, A., Akhmetzhanov, A., Monteys, X., Ivanov, M., 2012. The Porcupine Bank Canyon coral mounds: oceanographic and topographic steering of deep-water carbonate mound development and associated phosphatic deposition. *Geo-Marine Lett.* 32, 205–225. <https://doi.org/10.1007/s00367-011-0257-8>

- McCormick, M.I., 1994. Comparison of field methods for measuring surface tomography and their associations with a tropical reef fish assemblage. *Mar. Ecol. Prog. Ser.* 112, 87–96. <https://doi.org/10.3354/meps112087>
- Menna, F., Nocerino, E., Remondino, F., 2018. Photogrammetric Modelling of Submerged Structures: Influence of Underwater Environment and Lens Ports on Three-Dimensional (3D) Measurements, in: *Latest Developments in Reality-Based 3D Surveying and Modelling*. MDPI, pp. 279–303. <https://doi.org/10.3390/books978-3-03842-685-1-13>
- Mienis, F., van Weering, T., de Haas, H., de Stigter, H., Huvenne, V., Wheeler, A., 2006. Carbonate mound development at the SW Rockall Trough margin based on high resolution TOBI and seismic recording. *Mar. Geol.* 233, 1–19. <https://doi.org/10.1016/j.margeo.2006.08.003>
- Moberg, F., Folke, C., 1999. Ecological goods and services of coral reef ecosystems. *Ecol. Econ.* 29, 215–233. [https://doi.org/10.1016/S0921-8009\(99\)00009-9](https://doi.org/10.1016/S0921-8009(99)00009-9)
- Mohamed, H., Nadaoka, K., Nakamura, T., 2020. Towards Benthic Habitat 3D Mapping Using Machine Learning Algorithms and Structures from Motion Photogrammetry. *Remote Sens* 12, 127.
- Mortensen, P.B., Hovland, M., Brattegard, T., Farestveit, R., 1995. Deep water bioherms of the scleractinian coral *Lophelia pertusa* (L.) at 64° n on the Norwegian shelf: Structure and associated megafauna. *Sarsia* 80, 145–158. <https://doi.org/10.1080/00364827.1995.10413586>
- Mortensen, P.B., Hovland, T., Fosså, J.H., Furevik, D.M., 2001. Distribution, abundance and size of *Lophelia pertusa* coral reefs in mid-Norway in relation to seabed characteristics. *J. Mar. Biol. Assoc. United Kingdom* 81, 581–597. <https://doi.org/10.1017/S002531540100426X>
- Negahdaripour, S., Madjidi, H., 2003. Stereovision imaging on submersible platforms for 3-D mapping of benthic habitats and sea-floor structures. *IEEE J. Ocean. Eng.* 28, 625–650. <https://doi.org/10.1109/JOE.2003.819313>
- Nyimbili, P.H., Demirel, H., Seker, D.Z., Erden, T., 2016. Structure from Motion (SfM)

- Approaches and Applications. Int. Sci. Conf. Appl. Sci.

O'Reilly, L., Fentimen, R., Butschek, F., Titschack, J., Lim, A., Moore, N., O'Connor, O.J., Appah, J., Harris, K., Vennemann, T., Wheeler, A.J., 2022. Environmental forcing by submarine canyons: Evidence between two closely situated cold-water coral mounds (Porcupine Bank Canyon and Western Porcupine Bank, NE Atlantic). *Mar. Geol.* 106930. <https://doi.org/10.1016/j.margeo.2022.106930>

Oevelen, D. van, Duineveld, G., Lavaleye, M., Mienis, F., Soetaert, K., Heip, C.H.R., 2009. The cold-water coral community as hotspot of carbon cycling on continental margins: A food-web analysis from Rockall Bank (northeast Atlantic). *Limnol. Oceanogr.* 54, 1829–1844. <https://doi.org/10.4319/lo.2009.54.6.1829>

Orejas, C., Gori, A., Lo Iacono, C., Puig, P., Gili, J.M., Dale, M.R.T.T., 2009. Cold-water corals in the Cap de Creus canyon, northwestern Mediterranean: Spatial distribution, density and anthropogenic impact. *Mar. Ecol. Prog. Ser.* 397, 37–51. <https://doi.org/10.3354/meps08314>

Paradis, S., Puig, P., Masqué, P., Juan-Díaz, X., Martín, J., Palanques, A., 2017. Bottom-trawling along submarine canyons impacts deep sedimentary regimes. *Sci. Rep.* 7, 1–12. <https://doi.org/10.1038/srep43332>

Pascoe, K.H., Fukunaga, A., Kosaki, R.K., Burns, J.H.R., 2021. 3D assessment of a coral reef at Lalo Atoll reveals varying responses of habitat metrics following a catastrophic hurricane. *Sci. Rep.* 11, 12050. <https://doi.org/10.1038/s41598-021-91509-4>

Pavoni, G., Corsini, M., Callieri, M., Palma, M., Scopigno, R., 2019. SEMANTIC SEGMENTATION of BENTHIC COMMUNITIES from ORTHO-MOSAIC MAPS. *ISPRS Ann. Photogramm. Remote Sens. Spat. Inf. Sci.* 42, 151–158. <https://doi.org/10.5194/isprs-archives-XLII-2-W10-151-2019>

Pavoni, G., Corsini, M., Ponchio, F., Muntoni, A., Edwards, C., Pedersen, N., Sandin, S., Cignoni, P., 2022. TagLab: AI-assisted annotation for the fast and accurate semantic segmentation of coral reef orthoimages. *J. F. Robot.* 39, 246–262. <https://doi.org/10.1002/rob.22049>

Pedregosa, F., Varoquaux, G., Gramfort, A., Michel, V., Thirion, B., Grisel, O., Blondel,

M., Prettenhofer, P., Weiss, R., Dubourg, V., others, 2011. Scikit-learn: Machine learning in Python. *J. Mach. Learn. Res.* 12, 2825–2830.

Piazza, P., Cummings, V., Guzzi, A., Hawes, I., Lohrer, A., Marini, S., Marriott, P., Menna, F., Nocerino, E., Peirano, A., Kim, S., Schiaparelli, S., 2019. Underwater photogrammetry in Antarctica: long-term observations in benthic ecosystems and legacy data rescue. *Polar Biol.* 42, 1061–1079. <https://doi.org/10.1007/s00300-019-02480-w>

Pierce, J., Butler, M.J.I., Rzhhanov, Y., Lowell, K., Dijkstra, J.A., 2021. Classifying 3-D Models of Coral Reefs Using Structure-From-Motion and Multi-View Semantic Segmentation. *Front. Mar. Sci.* 0, 1623. <https://doi.org/10.3389/FMARS.2021.706674>

Pizarro, O., 2004. Large Scale Structure from Motion for Autonomous Underwater Vehicle Surveys. Massachusetts Institute of Technology.

Pizarro, O., Eustice, R.M., Singh, H., 2009. Large area 3-D reconstructions from underwater optical surveys. *IEEE J. Ocean. Eng.* 34, 150–169. <https://doi.org/10.1109/JOE.2009.2016071>

Pizarro, O., Friedman, A., Bryson, M., Williams, S.B., Madin, J., 2017. A simple, fast, and repeatable survey method for underwater visual 3D benthic mapping and monitoring. *Ecol. Evol.* 7, 1770–1782. <https://doi.org/10.1002/ece3.2701>

Pontoppidan, E., 1755. The Natural History of Norway. A. Linde, Bookseller to Her Royal Highness the Princess Dowager of Wales, in Catherine-Street in the Strand.

Price, D.M., Felgate, S.L., Huvenne, V.A.I., Strong, J., Carpenter, S., Barry, C., Lichtschlag, A., Sanders, R., Carrias, A., Young, A., Andrade, V., Cobb, E., Le Bas, T., Brittain, H., Evans, C., 2022. Quantifying the Intra-Habitat Variation of Seagrass Beds with Unoccupied Aerial Vehicles (UAVs). *Remote Sens.* 14, 480. <https://doi.org/10.3390/rs14030480>

Price, D.M., Robert, K., Callaway, A., Lo Iacono, C., Hall, R.A., Huvenne, V.A.I., 2019. Using 3D photogrammetry from ROV video to quantify cold-water coral reef structural complexity and investigate its influence on biodiversity and community assemblage. *Coral Reefs* 38, 1007–1021. <https://doi.org/10.1007/s00338-019-01827-3>

- Puig, P., Canals, M., Company, J.B., Martín, J., Amblas, D., Lastras, G., Palanques, A., Calafat, A.M., 2012. Ploughing the deep sea floor. *Nature* 489, 286–289. <https://doi.org/10.1038/nature11410>
- Purser, A., Bergmann, M., Lundälv, T., Ontrup, J., Nattkemper, T.W., 2009. Use of machine-learning algorithms for the automated detection of cold-water coral habitats: A pilot study. *Mar. Ecol. Prog. Ser.* 397, 241–251. <https://doi.org/10.3354/meps08154>
- Purser, A., Orejas, C., Gori, A., Tong, R., Unnithan, V., Thomsen, L., 2013. Local variation in the distribution of benthic megafauna species associated with cold-water coral reefs on the Norwegian margin. *Cont. Shelf Res.* 54, 37–51. <https://doi.org/10.1016/j.csr.2012.12.013>
- Qi, C.R., Su, H., Mo, K., Guibas, L.J., 2017. PointNet: Deep learning on point sets for 3D classification and segmentation. *Proc. - 30th IEEE Conf. Comput. Vis. Pattern Recognition, CVPR 2017 2017-Janua*, 77–85. <https://doi.org/10.1109/CVPR.2017.16>
- Quincey, D.J., Bishop, M.P., Kääh, A., Berthier, E., Flach, B., Bolch, T., Buchroithner, M., Kamp, U., Khalsa, S.J.S., Toutin, T., Haritashya, U.K., Racoviteanu, A., Shroder, J.F., Raup, B.H., 2014. Digital Terrain Modeling and Glacier Topographic Characterization, in: *Global Land Ice Measurements from Space*. Springer Berlin Heidelberg, Berlin, Heidelberg, pp. 113–144. https://doi.org/10.1007/978-3-540-79818-7_5
- Ragey, L., 1952. The work of Laussedat and education in photogrammetry at the National School of Arts and Crafts, Paris. *Photogramm. Eng.* 1, 21–26.
- Reaka-Kudla, M.L., 1997. The Global Biodiversity of Coral Reefs: A comparison with Rain Forests. *Biodivers. II Underst. Prot. Our Biol. Resour.* 83–108.
- Robert, K., Huvenne, V.A.I.I., Georgiopoulou, A., Jones, D.O.B.B., Marsh, L., Carter, D.O.G., Chaumillon, L., 2017. New approaches to high-resolution mapping of marine vertical structures. *Sci. Rep.* 7, 1–14. <https://doi.org/10.1038/s41598-017-09382-z>
- Roberts, J.M., Harvey, S.M., Lamont, P.A., Gage, J.D., Humphery, J.D., 2000. Seabed photography, environmental assessment and evidence for deep-water trawling on the continental margin west of the Hebrides. *Hydrobiologia* 441, 173–183.

<https://doi.org/10.1023/A:1017550612340>

Roberts, J.M., Long, D., Wilson, J.B., Mortensen, P.B., Gage, J.D., 2003. The cold-water coral *Lophelia pertusa* (Scleractinia) and enigmatic seabed mounds along the north-east Atlantic margin: Are they related? *Mar. Pollut. Bull.* 46, 7–20. [https://doi.org/10.1016/S0025-326X\(02\)00259-X](https://doi.org/10.1016/S0025-326X(02)00259-X)

Roberts, J.M., Peppe, O.C., Dodds, L.A., Mercer, D.J., Thomson, W.T., Gage, J.D., Meldrum, D.T., 2006. Monitoring environmental variability around cold-water coral reefs: the use of a benthic photolander and the potential of seafloor observatories, in: *Cold-Water Corals and Ecosystems*. Springer-Verlag, pp. 483–502. https://doi.org/10.1007/3-540-27673-4_24

Roberts, J.M., Wheeler, A., Freiwald, A., Cairns, S., 2009. *Cold-Water Corals, Cold-Water Corals: The Biology and Geology of Deep-Sea Coral Habitats*. Cambridge University Press. <https://doi.org/10.1017/CBO9780511581588>

Roberts, M., 1997. Coral in deep water | New Scientist [WWW Document]. URL <https://www.newscientist.com/article/mg15521005-500-coral-in-deep-water/> (accessed 1.25.23).

Roberts, Wheeler, A.J., Freiwald, A., 2006. Reefs of the Deep: The Biology and Geology of Cold-Water Coral Ecosystems. *Science* (80-.). 312, 543–547. <https://doi.org/10.1126/science.1119861>

Rogers, A.D., 1999. The Biology of *Lophelia pertusa* (Linnaeus 1758) and Other Deep-Water Reef-Forming Corals and Impacts from Human Activities. *Int. Rev. Hydrobiol.* 84, 315–406. <https://doi.org/10.1002/iroh.199900032>

Roynard, X., Deschaud, J.E., Goulette, F., 2018. Classification of point cloud scenes with multiscale voxel deep network. *arXiv*.

Rudall, B.H., 1978. Lecture notes in computer science. Vol. 15—L-systems. *Int. J. Biomed. Comput.* 9, 242. [https://doi.org/10.1016/0020-7101\(78\)90038-7](https://doi.org/10.1016/0020-7101(78)90038-7)

Rüggeberg, A., Flögel, S., Dullo, W.C., Hissmann, K., Freiwald, A., 2011. Water mass characteristics and sill dynamics in a subpolar cold-water coral reef setting at Stjernsund, northern Norway. *Mar. Geol.* 282, 5–12.

<https://doi.org/10.1016/j.margeo.2010.05.009>

Russell, S.J., Norvig, P., 2010. *Artificial Intelligence: A modern Approach*, 3rd ed. Upper Saddle River, NJ: Prentice Hall.

Savini, A., Corselli, C., 2010. High-resolution bathymetry and acoustic geophysical data from Santa Maria di Leuca Cold Water Coral province (Northern Ionian Sea-Apulian continental slope). *Deep. Res. Part II Top. Stud. Oceanogr.* 57, 326–344. <https://doi.org/10.1016/j.dsr2.2009.08.014>

Savini, A., Marchese, F., Fallati, L., Corselli, C., Galli, P., 2020. Integrating acoustics and photogrammetry-based 3D point clouds for the generation of a continuous bathymetric model in coral reef environment. EGU2020. <https://doi.org/10.5194/EGUSPHERE-EGU2020-22054>

Savini, A., Vertino, A., Marchese, F., Beuck, L., Freiwald, A., 2014. Mapping cold-water coral habitats at different scales within the Northern Ionian Sea (central Mediterranean): An assessment of coral coverage and associated vulnerability. *PLoS One* 9, 2002–2005. <https://doi.org/10.1371/journal.pone.0087108>

Schenk, T., 2005. *Introduction to Photogrammetry*. Dep. Civ. Environ. Eng. Geod. Sci. Ohio State Univ. 79–95.

Schlacher, T.A., Williams, A., Althaus, F., Schlacher-Hoenlinger, M.A., 2010. High-resolution seabed imagery as a tool for biodiversity conservation planning on continental margins. *Mar. Ecol.* 31, 200–221. <https://doi.org/10.1111/j.1439-0485.2009.00286.x>

Schoening, T., Osterloff, J., Nattkemper, T.W., 2016. RecoMIA—Recommendations for Marine Image Annotation: Lessons Learned and Future Directions. *Front. Mar. Sci.* 3. <https://doi.org/10.3389/fmars.2016.00059>

Shannon, P.M., 1991. The development of Irish offshore sedimentary basins. *J. Geol. Soc. London.* 148, 181–189. <https://doi.org/10.1144/gsjgs.148.1.0181>

Shewchuk, J.R., 2002. Delaunay refinement algorithms for triangular mesh generation. *Comput. Geom.* 22, 21–74. [https://doi.org/10.1016/S0925-7721\(01\)00047-5](https://doi.org/10.1016/S0925-7721(01)00047-5)

Shihavuddin, A.S.M., Gracias, N., Garcia, R., Gleason, A., Gintert, B., 2013. Image-Based

Coral Reef Classification and Thematic Mapping. *Remote Sens.* 5, 1809–1841. <https://doi.org/10.3390/rs5041809>

Singh, H., Roman, C., Pizarro, O., Eustice, R., Can, A., 2007. Towards high-resolution imaging from underwater vehicles. *Int. J. Rob. Res.* 26, 55–74. <https://doi.org/10.1177/0278364907074473>

Smith, M.W., Carrivick, J.L., Quincey, D.J., 2016. Structure from motion photogrammetry in physical geography. *Prog. Phys. Geogr.* 40, 247–275. <https://doi.org/10.1177/0309133315615805>

Spetsakis, M., Aloimonos, J.Y., 1991. A multi-frame approach to visual motion perception. *Int. J. Comput. Vis.* 6, 245–255. <https://doi.org/10.1007/BF00115698>

Spezzaferri, S., Vertino, A., Party, and the E.-C.M. cruise scientific, 2012. Cold-water coral ecosystems from the Moira Mounds (NE Atlantic): affinities and differences with modern and Pleistocene Mediterranean counterparts. *RV Belgica, Cruise No. 2012/16, EUROFLEE.*

Squires, D.F., 1964. Fossil Coral Thickets in Wairarapa, New Zealand. *J. Paleontol.* 38, 904–915.

Stokes, M.D., Deane, G.B., 2009. Automated processing of coral reef benthic images. *Limnol. Oceanogr. Methods* 7, 157–168. <https://doi.org/10.4319/lom.2009.7.157>

Storlazzi, C.D., Dartnell, P., Hatcher, G.A., Gibbs, A.E., 2016. End of the chain? Rugosity and fine-scale bathymetry from existing underwater digital imagery using structure-from-motion (SfM) technology. *Coral Reefs* 35, 889–894. <https://doi.org/10.1007/s00338-016-1462-8>

Summers, G., Lim, A., Wheeler, A.J., 2021. A Scalable, Supervised Classification of Seabed Sediment Waves Using an Object-Based Image Analysis Approach. *Remote Sens.* 13, 2317. <https://doi.org/10.3390/rs13122317>

Ternon, Q., Danet, V., Thiriet, P., Ysnel, F., Feunteun, E., Collin, A., 2022. Classification of underwater photogrammetry data for temperate benthic rocky reef mapping. *Estuar. Coast. Shelf Sci.* 270, 107833. <https://doi.org/10.1016/j.ecss.2022.107833>

Theodoridis, S., Koutroumbas, K., 2009. *Pattern Recognition - minder good.*

Thornton, B., Bodenmann, A., Pizarro, O., Williams, S.B., Friedman, A., Nakajima, R., Takai, K., Motoki, K., Watsuji, T. o., Hirayama, H., Matsui, Y., Watanabe, H., Ura, T., 2016. Biometric assessment of deep-sea vent megabenthic communities using multi-resolution 3D image reconstructions. *Deep. Res. Part I Oceanogr. Res. Pap.* 116, 200–219. <https://doi.org/10.1016/j.dsr.2016.08.009>

Titschack, J., Thierens, M., Dorschel, B., Schulbert, C., Freiwald, A., Kano, A., Takashima, C., Kawagoe, N., Li, X., 2009. Carbonate budget of a cold-water coral mound (Challenger Mound, IODP Exp. 307). *Mar. Geol.* 259, 36–46. <https://doi.org/10.1016/j.margeo.2008.12.007>

Turner, A.K., 1997. What's the difference among 2D, 2.5D, 3D and 4D? *Appl. Geosci. Forum.*

Urbina-barreto, I., Pinel, R., Fr, L., Mahamadaly, V., Elise, S., Kulbicki, M., Quod, J., Dutrieux, E., 2020. Quantifying the shelter capacity of coral reefs using photogrammetric 3D modeling : From colonies to reefscales. *Ecol. Indic.* 107151. <https://doi.org/10.1016/j.ecolind.2020.107151>

Van Audenhaege, L., Broad, E., Hendry, K.R., Huvenne, V.A.I., 2021. High-Resolution Vertical Habitat Mapping of a Deep-Sea Cliff Offshore Greenland. *Front. Mar. Sci.* 8. <https://doi.org/10.3389/fmars.2021.669372>

Wakita, N., Hirokawa, K., Ichikawa, T., Yamauchi, Y., 2010. Development of Autonomous Underwater Vehicle (AUV) for Exploring Deep Sea Marine Mineral Resources. *Mitsubishi Heavy Ind. Tech. Rev.* 47, 73–80.

Weidner, L., Walton, G., Krajnovich, A., 2021. Classifying rock slope materials in photogrammetric point clouds using robust color and geometric features. <https://doi.org/10.13140/RG.2.2.35632.89604>

Weinmann, M., Jutzi, B., Hinz, S., Mallet, C., 2015. Semantic point cloud interpretation based on optimal neighborhoods, relevant features and efficient classifiers. *ISPRS J. Photogramm. Remote Sens.* 105, 286–304. <https://doi.org/10.1016/j.isprsjprs.2015.01.016>

Westoby, M.J., Brasington, J., Glasser, N.F., Hambrey, M.J., Reynolds, J.M., 2012.

'Structure-from-Motion' photogrammetry: A low-cost, effective tool for geoscience applications. *Geomorphology* 179, 300–314. <https://doi.org/10.1016/J.GEOMORPH.2012.08.021>

Wheeler, A.J., Beyer, A., Freiwald, A., de Haas, H., Huvenne, V.A.I.I., Kozachenko, M., Olu-Le Roy, K., Opderbecke, J., 2007. Morphology and environment of cold-water coral carbonate mounds on the NW European margin. *Int. J. Earth Sci.* 96, 37–56. <https://doi.org/10.1007/s00531-006-0130-6>

Wheeler, A.J., Kozachenko, M., Henry, L.-A., Foubert, A., de Haas, H., Huvenne, V.A.I.A.I., Masson, D.G.G., Olu, K., 2011. The Moira Mounds, small cold-water coral banks in the Porcupine Seabight, NE Atlantic: Part A—an early stage growth phase for future coral carbonate mounds? *Mar. Geol.* 282, 53–64. <https://doi.org/10.1016/j.margeo.2010.08.006>

Wheeler, A.J., Kozachenko, M., Masson, D.G., Huvenne, V.A.I., 2008. Influence of benthic sediment transport on cold-water coral bank morphology and growth: the example of the Darwin Mounds, north-east Atlantic. *Sedimentology* 55, 1875–1887. <https://doi.org/10.1111/j.1365-3091.2008.00970.x>

Wheeler, A.J., Beck, T., Thiede, J., Klages, M., Grehan, A., Monteys, F.X., 2005a. Deep-water coral mounds on the Porcupine Bank, Irish Margin: preliminary results from the Polarstern ARK-XIX/3a ROV cruise, in: Freiwald, A., Roberts, J.M. (Eds.), *Cold-Water Corals and Ecosystems*. Springer Berlin Heidelberg, Berlin, Heidelberg, pp. 393–402. https://doi.org/10.1007/3-540-27673-4_19

Wheeler, A.J., Bett, B., Billett, D.S., Masson, D.G., Mayor, D.J., 2005b. The Impact of Demersal Trawling on Northeast Atlantic Deepwater Coral Habitats: The Case of the Darwin Mounds, United Kingdom. *Am. Fish. Soc. Symp.* 41, 807–817.

White, M., 2007. Benthic dynamics at the carbonate mound regions of the Porcupine Sea Bight continental margin. *Int. J. Earth Sci.* 96, 1–9. <https://doi.org/10.1007/s00531-006-0099-1>

Williams, I.D., Couch, C., Beijbom, O., Oliver, T., Vargas-Angel, B., Schumacher, B., Brainard, R., 2019. Leveraging automated image analysis tools to transform our capacity to assess status and trends on coral reefs. *Front. Mar. Sci.* 6.

<https://doi.org/10.3389/fmars.2019.00222>

Wilson, J.B., 1979a. 'Patch' development of the deep-water coral *Lophelia pertusa* (L.) on Rockall Bank. *J. Mar. Biol. Assoc. United Kingdom* 59, 165–177. <https://doi.org/10.1017/S0025315400046257>

Wilson, J.B., 1979b. The distribution of the coral *Lophelia pertusa* (L.) [*L. prolifera* (Pallas)] in the north-east Atlantic. *J. Mar. Biol. Assoc. United Kingdom* 59, 149–164. <https://doi.org/10.1017/S0025315400046245>

Wolf, P.R., Dewitt, B.A., Wilkinson, B.E., 2014. *Elements of Photogrammetry with Applications in GIS*, 4th ed. 696 pp.

Young, G.C., 2018. Convolutional Neural Networks Predict Fish Abundance from Underlying Coral Reef Texture.

Young, G.C., 2017. Three-Dimensional Modelling of Coral Reefs for Structural Complexity Analysis. Thesis 184.

Young, G.C., Dey, S., Rogers, A.D., Exton, D., 2018. Cost and time-effective method for multi-scale measures of rugosity, fractal dimension, and vector dispersion from coral reef 3D models. *PLoS One* 13, 1–18. <https://doi.org/10.1371/journal.pone.0201847>

Yuval, M., Alonso, I., Eyal, G., Tchernov, D., Loya, Y., Murillo, A.C., Treibitz, T., 2021. Repeatable Semantic Reef-Mapping through Photogrammetry and Label-Augmentation. *Remote Sens.* 13, 659. <https://doi.org/10.3390/rs13040659>

Zurowietz, M., Langenk"amper, D., Hosking, B., Ruhl, H.A., Nattkemper, T.W., 2018. MAIA-A machine learning assisted image annotation method for environmental monitoring and exploration. *PLoS One* 13.

2. 3D Classification of Cold-Water Coral Reefs: A Comparison of Classification Techniques for 3D Reconstructions of Cold-Water Coral Reefs and Seabed

Larissa Macedo Cruz de Oliveira, Aaron Lim, Luis A. Conti and Andrew J. Wheeler

(Current status: Published, *Frontiers in Marine Science*)

DOI: <https://doi.org/10.3389/fmars.2021.64071>

This chapter comprises a paper that is published in the journal *Frontiers in Marine Sciences*:

de Oliveira, L.M.C., Lim, A., Conti, L.A., Wheeler, A.J., 2021. 3D Classification of Cold-Water Coral Reefs: A Comparison of Classification Techniques for 3D Reconstructions of Cold-Water Coral Reefs and Seabed. *Front. Mar. Sci.* 8. <https://doi.org/10.3389/fmars.2021.640713>

This chapter is organised as follows: introduction, materials and methods, results, discussion and references. Author contributions are outlined according to the [Contributor Roles Taxonomy \(CRediT\)](#) author statement.

This chapter presents the results of the first aim of the PhD: to develop an unprecedented 3D imaging classification workflow for Irish CWC reef habitats whilst analysing the suitability and transferability of 2D and 3D data to represent these habitats in high-resolution. Motivated by the absence of methods for semi-automated classification of 3D data, we explore the capabilities of current technologies to perform a 3D classification task on the Porcupine Bank Canyon and identify the aspects that need to be further investigated.

Candidate contributions to the study: Larissa de Oliveira conceptualised the study, developed the methodology, data curation, software, carried out the investigation, formal analyses, data visualisation, writing of the original draft, review, submission and editing.

The project which lead to the work developed in this chapter was funded through the Science Foundation of Ireland's Investigator Programme to Prof. Andy Wheeler: Mapping, Modelling and Monitoring Key Processes and Controls on Cold-water Coral Habitats in Submarine Canyons (MMMonKey_Pro) - 16/IA/4528. Larissa Oliveira conceptualised the study, developed the methodology and data curation with support of Dr Aaron Lim. Dr Lim was the chief scientist responsible for the data collected for the study during the research cruises CE19008 and CE19014. Dr Lim conceptualised the initial project that led to this chapter (and subsequent publication) and generated the 3D reconstructions of the Porcupine Bank Canyon used in the study. The project was supervised by Prof Andy Wheeler, Dr Aaron Lim and Prof Luis Conti. These co-authors also contributed with editing and proof-reading of the manuscript.

Abstract

Cold-water coral (CWC) reefs are complex structural habitats that are considered biodiversity “hotspots” in deep-sea environments and are subject to several climate and anthropogenic threats. As three-dimensional structural habitats, there is a need for robust and accessible technologies to enable more accurate reef assessments. Photogrammetry derived from remotely operated vehicle video data is an effective and non-destructive method that creates high-resolution reconstructions of CWC habitats. Here, three classification workflows [Multiscale Geometrical Classification (MGC), Colour and Geometrical Classification (CGC) and Object-Based Image Classification(OBIA)] are presented and applied to photogrammetric reconstructions of CWC habitats in the Porcupine Bank Canyon, NE Atlantic. In total, six point clouds, orthomosaics, and digital elevation models, generated from structure-from-motion photogrammetry, are used to evaluate each classification workflow. Our results show that 3D Multiscale Geometrical Classification outperforms the Colour and Geometrical Classification method. However, each method has advantages for specific applications pertinent to the wider marine scientific community. Results suggest that advancing from commonly employed 2D image analysis techniques to 3D photogrammetric classification methods is advantageous and provides a more realistic representation of CWC habitat composition.

2.1 Introduction

Azooxanthallate scleractinian corals, such as *Lophelia pertusa* (synonymised to *Desmophyllum pertusum* in Addamo et al., 2016) and *Madrepora oculata*, are recognised by their three-dimensional branching morphology and framework building capacity (Mortensen et al., 1995; Roberts, 2002; Jonsson et al., 2004; Costello et al., 2005; Wheeler et al., 2005a, 2007b; Gass and Roberts, 2006; Guinan et al., 2009). In suitable environmental conditions, these cold-water coral (CWC) species can form structural habitats such as small coral patches (Wilson, 1979a), reefs (Masson et al., 2003; Roberts et al., 2006b; Victorero et al., 2016; Lim et al., 2018), and giant carbonate mounds (Hovland and Thomsen, 1997; Mienis et al., 2006; Wheeler et al., 2007a; Freiwald et al., 2011; Huvenne et al., 2011) that can reach up to 400 m above the seabed. The presence of reef-forming CWC colonies has been documented in a range of settings from fjords (Fosså et al., 2006) to continental shelves, slopes (Wilson, 1979b; Mortensen et al., 1995; Wheeler et al., 2005c; Leverette and Metaxas, 2006; Mienis et al., 2006) to seamounts and submarine canyons (Huvenne et al., 2011; Appah et al., 2020) throughout the North Atlantic, Indian, and Pacific oceans and the Mediterranean Sea (de Mol et al., 2005; Freiwald and Roberts, 2005; Wheeler et al., 2007a, b; Roberts et al., 2009; Freiwald et al., 2011; Lim et al., 2018).

Cold-water coral environments are commonly considered marine biodiversity “hotspots” as they can harbour increased biodiversity and biomass relative to their surrounding areas (Jonsson et al., 2004; Wheeler et al., 2007a; Fanelli et al., 2017). Despite being among the world’s most important reservoirs of marine biodiversity (Freiwald et al., 2011), CWC reefs are also susceptible to environmental changes and threats such as temperature and salinity changes, as well as anthropogenic activities (Roberts et al., 2006a; Wheeler et al., 2007a; Orejas et al., 2009; Huvenne et al., 2016), e.g., bottom trawling (Wheeler et al., 2005b), mining (Savini et al., 2014), and oil and gas exploration (Roberts, 2002; Gass and Roberts, 2006; Barbosa et al., 2019). Several studies have affirmed that CWC reefs are declining rapidly in response to high rates of environmental change (Lim et al., 2018; Boolukos et al., 2019) and ocean acidification (Turley et al., 2007; Findlay et al., 2013). Consequently, there is a need for CWC reef

assessments that quantify variations in temperature, salinity, food supply, and growth rates combined with measurements of structural complexity and biodiversity. It is therefore essential to understand these environments and to assign priority areas for protection (Ferrari et al., 2018; Appah et al., 2020).

Three-dimensional structures enhance small-scale spatial variability and play a major role in species **biodiversity** and nutrient cycling (Graham and Nash, 2013; Pizarro et al., 2017; Lim et al., 2018). The use of multibeam echosounders (MBES) can provide sub-metre pixel resolution bathymetric coverages of submarine canyons (Huvenne et al., 2011; Robert et al., 2017) and CWC environments (De Clippele et al., 2017; Lim et al., 2017). However, there is a lack of studies at a centimetric resolution (King et al., 2018; Anelli et al., 2019; Price et al., 2019) that reveal the complexity of coral frameworks. The analysis of these environments usually relies on 1D or 2D estimates of coral cover and distribution that can potentially disregard important changes in reef habitats as they may not integrate accurate vertical or volumetric information (Courtney et al., 2007; Goatley and Bellwood, 2011; House et al., 2018). Therefore, there is an increasing demand for the development of novel techniques for measuring coral reef environments in 3D (Burns et al., 2015a, b; House et al., 2018; Fukunaga et al., 2019). This demand has been mitigated with the use of novel mapping techniques such as structure-from-motion (SfM) photogrammetry (Cocito et al., 2003; Burns et al., 2015b; Storlazzi et al., 2016; Robert et al., 2017; Price et al., 2019) which is becoming progressively more common since the introduction of remotely operated vehicles (ROVs) (Kwasnitschka et al., 2013; Lim et al., 2020). Increasing access to computer processing power, high-resolution digital imagery, and recent developments in image processing software has led to a considerably higher number of studies utilising photogrammetry for seabed habitat mapping (Storlazzi et al., 2016; Pizarro et al., 2017; Hopkinson et al., 2020). SfM photogrammetry is considered a time- and cost-effective method for seabed mapping that allows high-resolution environment reconstruction (Burns et al., 2015a, b; Storlazzi et al., 2016; Robert et al., 2017; House et al., 2018). SfM utilises multiple overlapping images at various angles to reconstruct 3D models of complex scenes. To this end, SfM uses a scale-invariant feature transform (SIFT) algorithm to extract corresponding image features from an

offset of images captured sequentially along the camera transect (Lowe, 1999). These calculations of overlapping imagery can be used to reconstruct 3D point cloud models of the photographed surface or scene (Carrivick et al., 2016). Moreover, the use of ROV video data has a number of benefits when compared to traditional sampling methods given that it is non-destructive and can have a wide spatial coverage (Guinan et al., 2009; Bennecke et al., 2016; De Clippele et al., 2017; Young, 2017).

The increase of data derived from SfM mapping has led to the necessity for new tools and techniques to aid time-effective and high-quality analysis of large areas (Storlazzi et al., 2016; Pizarro et al., 2017; Young et al., 2018; Marre et al., 2019). As technology advances, datasets are also becoming larger which, in turn, leads to a need for automated processing with faster, more precise, and accurate classification outputs (Brodu and Lague, 2012; Weinmann et al., 2015). Currently, this need has been achieved by integrating machine learning (ML) with mapping techniques to achieve automated meaningful pattern detection from multi-thematic datasets. ML has been widely used in remote sensing (Pal, 2005; Mountrakis et al., 2011), archaeology (Menna et al., 2018; Lambers et al., 2019), and to predict fish abundances (Young, 2018). Studies have shown optimal results on the application of ML for satellite, aerial, and terrestrial imagery (Wang et al., 2015; Pirotti and Tonion, 2019). Classification studies using LiDAR data performed in Walton et al. (2016) and Weidner et al. (2019) are also good examples. However, there is still a scientific gap between ML and marine surveying for seabed classification due to the costly computational nature of ML methods and the time-intensive annotation of marine datasets which usually requires expert knowledge (Shihavuddin et al., 2013; Marburg and Bigham, 2016; Hopkinson et al., 2020). This gap is emphasised when we consider the use of 3D data. Even though existing ML models such as neural networks (NNs) have shown promising results on 3D reconstructions of single objects, there is still room for improvement for the classification of complex 3D scenes (Weinmann et al., 2015; Roynard et al., 2018), especially in the case of marine habitats (Gómez-ríos et al., 2018; Hopkinson et al., 2020). Challenges related to the complexity derived from variability of point density, non-uniform point structure, and size of the dataset still cause difficulties when developing and applying new methodologies for 3D point cloud classification

(Weinmann et al., 2013). In the specific case of coral reefs, difficulties in detecting coral shape, colour, and texture have also been reported (Gómez-ríos et al., 2018; King et al., 2018; Hopkinson et al., 2020) especially as corals tend to occur in colonies and can have similar features.

In this study, we assess three different image classification techniques embedded in image analysis software and evaluate both the performance and results when using 3D data. We also compare their resource requirements and information outputs. The usability and the computing power required to process and analyse data were also taken into account. In a wider scenario, this study aims to show novel applications of ML for seabed mapping of submarine canyons and CWC reefs. Furthermore, we provide a classification workflow created for these environments and evaluate the limitations and advantages of using 3D data in comparison to 2D. For the first time, the techniques were applied to the CWC reefs in the Porcupine Bank Canyon (PBC), NE Atlantic. As such, this paper contributes to the wider scientific community using existing image processing software for 3D classification of deep-sea environments.

2.2 Materials and Methods

Three classification workflows applied to underwater photogrammetric reconstructions of CWC habitats in the PBC are analysed. The methods range from a relatively straight-forward appraisal to ones of increased complexity in terms of computational requirements and user knowledge. Herein, we describe data acquisition, processing, and the workflow of the applied methods.

2.2.1 Study Area

Submarine canyons offer a variety of CWC habitats including vertical habitats (Huvenne et al., 2011; De Clippele et al., 2017; Robert et al., 2017). The three methodologies presented herein were applied to CWC habitats in the PBC, located approximately 300 km southwest of Ireland (Figure 2.1). The canyon is located

between the Porcupine Seabight to the southeast and the Rockall Trough to the west (Wheeler et al., 2005a). Measuring 63 km in length, the PBC is one of the largest submarine canyons on Ireland's western margin. Since 2016, the PBC has been designated as a special area of conservation (SAC) (n°003001) by the European Union Habitats Directive (2016), and therefore no fishing or other exploratory activities are allowed in the area.

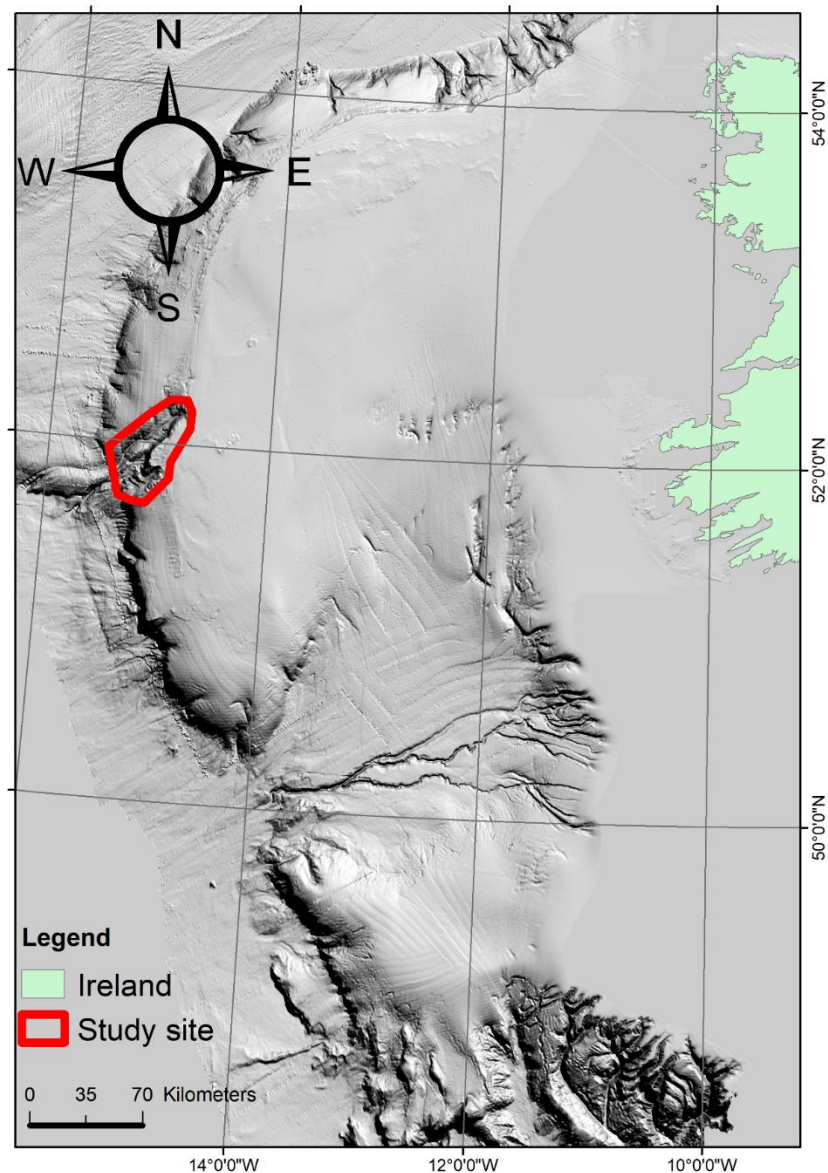


Figure 2.1: Study site (in red)—The Porcupine Bank Canyon study area on the Irish continental margin west of Ireland

The PBC is a tectonically controlled (Shannon, 1991), asymmetrical canyon with two branching heads separated by a ridge and exiting separately into the Rockall Trough

(Appah et al., 2020; Lim et al., 2020). A steep, ~700 m high, cliff face exists at the southeast margin of the canyon with exposed bedrock. This bedrock contrasts with the sediment-dominant slope on the northwest margin that extends to the canyon base (Dorschel et al., 2010; Appah et al., 2020; Lim et al., 2020). Giant carbonate mounds of up to 100 m high (Wheeler et al., 2005a) are concentrated along the edges of the canyons or associated with fault systems existing around the canyon head, leading to escarpments of up to 60 m high (Mazzini et al., 2012).

The PBC is influenced by strong currents along the mound tops and flanks, water column stratification, enhanced bottom currents, and upwelling (Mazzini et al., 2012). Unprecedented current speeds of 114 cm s^{-1} have been recorded within the PBC, which is the highest current speed ever recorded in a CWC habitat (Lim et al., 2020). Data from conductivity-temperature-depth (CTD) measurements show that the region is mainly influenced by the eastern north atlantic water (ENAW) down to 800 m water depth flowing northerly (Lim et al., 2020) with the labrador sea water (LSW) below 1100 m depth (Appah et al., 2020). Mediterranean outflow water (MOW) also flows through the canyon between 800 and 1100 m water depth (Appah et al., 2020; Lim et al., 2020). It is suggested that current regimes influence the distribution of benthic fauna throughout the canyon and that CWC habitats in the PBC can tolerate considerably high current speeds (Lim et al., 2020). High biodiversity including actively growing and well-developed coral colonies is found at depths of 600–1000 m where the ENAW and MOW occur, while poorly developed coral colonies were related to the LSW (Appah et al., 2020). The main framework forming CWC in the canyon is *L. pertusa* (syn. *D. pertusum*), and the other most common coral species were black corals *Stichopathes cf. abyssicola* and *Leiopathes glaberrima* and sponges *Aphrocallistes beatrix* and *Hexadella dedritifera* (Appah et al., 2020).

2.2.2 Video Survey and Data Collection

The video data used in this survey were acquired during research cruises CE19008 (Lim et al., 2019b) and CE19014 (Lim et al., 2019a) from 13rd to 23rd of May of 2019 and 25th to 31st of July of 2019, respectively. Video data were collected using the

Holland 1 ROV, although the methodologies compared in this paper could be applied to towed-camera or diver surveys. The ROV is equipped with 11 camera systems of which two were used as data sources for analysis in this paper: an HDTV camera (HD Insite mini-Zeus with HD SDI fibre output), and a Kongsberg OE 14–208 digital stills camera. Two deep-sea power lasers spaced at 10 cm were used for scaling. Positioning data were recorded with a Sonardyne Ranger 2 ultra-short baseline (USBL) beacon and corrected by an IXBlue doppler velocity logger (DVL) (Lim et al., 2020). ROV video data were acquired at a height of ~2 m above the seabed with a survey speed of <0.2 knots at locations in the PBC. High-definition video data (1080p) were acquired at 50 fps and stored as *.mov files. The areas selected for reconstruction were based on the distribution and variety of CWC habitats such as small individual coral colonies, coral colonies on rock outcrops, coral gardens, and mounds.

2.2.3 3D Reconstruction Using Structure-From-Motion (SfM) Photogrammetry

ROV video data, digital stills, and camera positioning information were used to produce the 3D reconstructions in this study. One frame per second was extracted from the raw video data with Blender (version 2.78). The frames were imported into Agisoft Metashape Professional v1.6, and each frame was georeferenced with its relative USBL positioning data. The lasers from the HD camera were utilised to scale features during the reconstruction process. The workflow for model rendering was carried out as detailed in Agisoft (2019) using an Intel i7 hexa core, 16 GB of RAM, and NVIDIA GTX1070 (8 GB) graphics card. The overall workflow and data outputs are shown in Figure 2.2. Dense clouds were used in method 1–MGC [section “Method 1–Multiscale Geometrical Classification (MGC)”] and method 2–CGC [section “Method 2–Colour and Geometrical Classification (CGC)”], while the orthomosaics were used for method 3–OBIA [section “Method 3–2D Object-Based Image Analysis (OBIA)”].

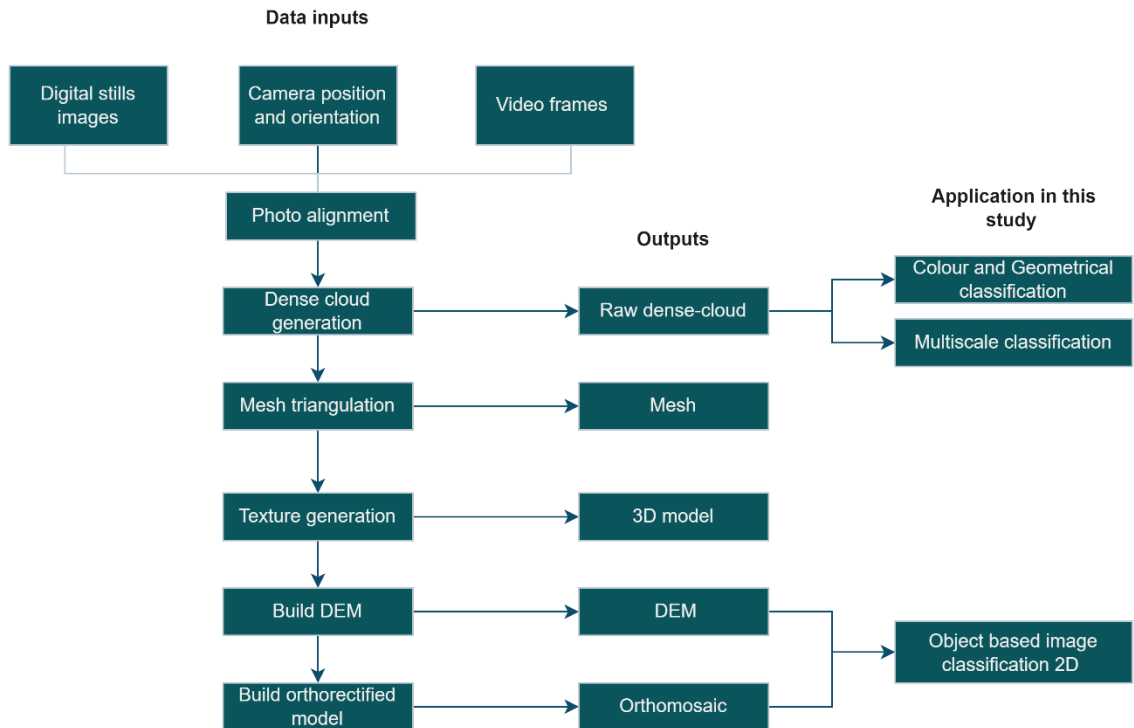


Figure 2.2: Workflow for 3D model reconstruction and applications of each output data within this study.

2.2.4 Classification Methods

2.2.4.1 Method 1–Multiscale Geometrical Classification (MGC)

An MGC approach was utilised in this study to perform a binary classification of our 3D CWC reef reconstructions. We utilised Canupo (Brodu and Lague, 2012), a support vector machine (SVM) classification algorithm implemented in the open-source software CloudCompare (Girardeau-Montaut, 2011). This method was chosen due to its solid workflow for classification of point clouds applicable to natural environments (Brodu and Lague, 2012). As this technique uses dimensionality (computation of vector dispersion for each point relative to a neighbourhood of points) as a parameter for classification, it provides flexibility when applied to data derived from different sources as geometrical measurements are not dependent on the instrument used (Brodu and Lague, 2012). Therefore, these SVM-based classifiers can be reutilised by other users with point cloud data derived from different sources, e.g., terrestrial or airborne laser scanning. Another reason for choosing a dimensionality-based classifier

is the limited separability of RGB component spectral signatures in underwater photogrammetry.

The multiscale classification technique used here computes the degree to which each neighbourhood of points can be examined as single-, two-, or three-dimensional aspects by identifying the principal components of the point coordinates in the given neighbourhood (Brodu and Lague, 2012). This method is defined as a multiscale classification because it calculates these statistics for each core point in the scene at a spherical neighbourhood of different sizes, referred to as scales parameters. As such, this method generates a feature vector that can distinguish between semantic objects (Maxwell et al., 2018; Weidner et al., 2019), such as coral and bedrock. The computation of neighbourhoods defined by each scale gives the classifier a multi-scale refining property (Brodu and Lague, 2012; Weidner et al., 2019). The final product of this process is defined herein as a multiscale classifier that is applied to the test dataset. Here, the neighbourhood sizes were chosen to include a range from coral frameworks to differing rock sizes so that small-scale objects would also be captured in large-scale sizes.

As this technique is a semi-automated classification that employs a probabilistic approach, it is essential to build classifiers based on samples of features of interest from a training dataset, i.e., live and dead corals. Entire dense clouds were manually segmented into objects of interest and divided in two classes: “coral” and “seabed.” The class “coral” consisted of hard and soft coral colonies and frameworks. The class seabed consisted of the remainder, i.e., seafloor and other benthic organisms (e.g., coral rubble, echinoderms, sponges, etc.). The segmentation process was repeated on each axis (X, Y, and Z) to avoid single view bias.

Scale parameters used for the multiscale descriptors were based on the variance of object size within the scene. Ten initial scales with steps of 0.1 or 0.005 were chosen based on an empirical analysis of the data, combining the evaluation of features to be identified with a trial-and-error approach. The maximum number of core points (MNCPs) value is the number of randomly sub-sampled points that will be used for computations on the scene data. The higher the MNCP value, the greater the number of computations. Thus, an increase in the number of scales and core points was

directly related to the ability to discriminate and the processing power required to train the classifier. The performance of each classifier was quantified by the Balanced Accuracy (ba) value which is defined by the equation:

$$ba = \frac{1}{2}(a_{c1} + a_{c2})$$

Where each class accuracy (a_{c1} and a_{c2}) is defined as $a_{c1} = \frac{tc_{c1}}{(tc_{c1} + fc_{c2})}$ and $a_{c2} = \frac{tc_{c2}}{(tc_{c2} + fc_{c1})}$ (tc_{c1} - truly classified class 1, tc_{c2} - truly classified class 2, fc_{c1} – falsely classified class 1, fc_{c2} – falsely classified class 2). For each sample, the classifier assigns a distance, d , from the separation line of the classifier and the measure of separability is calculated by the Fisher Discriminant Ratio (fdr) described in (Sergios Theodoridis and Konstantinos Koutroumbas, 2008) which is defined as:

$$fdr = \frac{(\mu_2 - \mu_1)^2}{v_1 + v_2}$$

where μ_2 and μ_1 and v_1 and v_2 are the mean and the variance of the aforementioned distance d for each class 1 and 2. The fdr is used to assess the class separability, i.e., how well the classes are separated. Therefore, a high ba value indicates that the trained classifier has a good recognition performance whereas a high fdr indicates that the classes are well separated in a plane of maximal separability. The classifier quality is directly proportional to ba and fdr values. The higher the values, the better the classifier can identify and classify objects into two classes. Further details can be found in Brodu and Lague (2012).

The dataset consisted of eight dense clouds that were split into training and testing sets. The training set was used for training the classifier, which was then applied onto the unseen testing set. Each classifier was trained with a combination of segments from a single dense-cloud or two different dense-clouds, referred to here as source-clouds. The testing dataset composed by the remainder of the dataset after excluding the dense clouds was used to train the classifier. The classifiers with the highest ba and fdr values were applied to the testing dataset to evaluate their robustness and reproducibility, i.e., their ability to be applied to analogous environments. Initially, no

confidence threshold was set for the classification. Therefore, all points were classified as either coral or seabed. After a visual inspection of preliminary results, a confidence threshold was set to arbitrary values 0.5 or 0.9 and the classifier was executed again. The confidence threshold allows class labels to be assigned only if the results exceed that value; otherwise, the point is left unclassified. If more than 30% of the points were left unclassified, the classifier was retrained with a different number of scales and core points (Supplementary Figure 2.10). This threshold was set to reassure classification quality in a trial-and-error approach (Weidner et al., 2019). Hence, higher values will result in less generalisation and more complex decision boundaries (Maxwell et al., 2018). Studies in terrestrial point clouds for rock slope classification have chosen the confidence threshold based on up to 15% of unclassified points (Weidner et al., 2019). A 30% confidence threshold was chosen for this study due to the point cloud density differences and the classes of objects to be addressed.

2.2.4.2 Method 2–Colour and Geometrical Classification (CGC)

The second classification workflow is based on the use of colour and geometrical feature information following the work of Becker et al. (2018) which has shown satisfactory results for ground classification point clouds surveys using unmanned aerial vehicles (UAVs) (Klápště et al., 2018).

The use of geometrical features for semantic classification has brought positive results in several terrestrial data studies (Weinmann et al., 2015; Hackel et al., 2016). In addition to geometrical features, the use of colour information in the classification process of point clouds provides a significant increase in prediction accuracy (Lichti, 2005; Becker et al., 2018). For underwater photogrammetry, the use of colour has been advised as a way to include important image spectral information (Beijbom et al., 2012; Bryson et al., 2013, 2015, 2016). However, its importance is questionable as there are interactions between the colour spectrum and water column, e.g., the red colour channel is attenuated with distance from camera (Carlevaris-Bianco et al., 2010; Beijbom et al., 2012; Bryson et al., 2013).

Here, the same training set of dense point clouds was classified using the supervised multiclass classification algorithm implemented in Agisoft Metashape (Supplementary Figure 2.11). This automatic multiclass classification approach associates geometric and colour features that are fed into the Gradient Boosted Tree (GBT) algorithm to predict the class of each point in the point cloud. GBT utilises colour features computed from the colour values of each point and the average colour values of its neighbouring points.

Geometrical features used in the algorithm were previously presented in Becker et al. (2018). For each point, its neighbouring points are computed, and the set is used to build a local 3D structure covariance tensor which summarises the predominant direction of the slope gradients in the neighbourhood of a point. The eigenvalues and corresponding eigenvectors are used to compute the local geometric features, for instance, omnivariance, eigentropy, anisotropy, planarity, linearity, surface variation, verticality, and scatter. These features, which originate from the 3D covariance matrix of nearest neighbours of each point, can be used to describe the local 3D structure and dimensionality (Weinmann et al., 2013). Further information about the algorithm can be found in Becker et al. (2018). This technique provides a supervised classification which is pre-trained using terrestrial datasets. The dense clouds were classified with the GBT classifier into ground (seabed) and low vegetation (corals).

2.2.4.3 Method 3—2D Object-Based Image Analysis (OBIA)

As a baseline method, object image classification was utilised to analyse the range of information that 2D data classification can provide in comparison to the 3D data. Object-based analysis techniques have been widely applied across different remote sensing areas, especially for marine studies (Conti et al., 2019; Lim et al., 2020), aerial imagery (Zhang et al., 2010), and land cover mapping (Benz et al., 2004).

For this classification method, the georeferenced orthomosaics, DEM, and slope from the training set were used. Slope was derived from the DEM in ArcGIS Spatial Analyst toolbox. Slope, DEM, and the orthomosaics derived from the point cloud processing were imported into eCognition Developer (Trimble Germany GmbH, 2019) and

segmented using the multi-resolution segmentation algorithm (Benz et al., 2004) at a pixel level using different layer weights for RGB, DEM, and slope layers. This segmentation approach merges pixels of similar values into objects based on relative homogeneity criterion. The homogeneity criterion measures how homogeneous an image object is in relation to itself and it is calculated as a combination of spectral and shape criteria (Trimble, 2018). The shape ratio determines to what extent the shape influences the segmentation compared to colour. The compactness is a weighting value that affects the compactness of the objects in relation to smoothness created during the segmentation. These ratios are obtained by calculating primary object features, shape, and colour, with heterogeneity calculations, i.e., standard deviation (Benz et al., 2004). Layer weight values control the emphasis given to colour and shape during the heterogeneity calculation (Koop et al., 2021) as it increases the weight of a layer based on the heterogeneity. The weight parameters adapt the heterogeneity definition to the application in order to get suitable segmentation output for image data (Benz et al., 2004). The layer weight values used were chosen following Lim et al. (2020). The scale parameter is considered the most effective parameter (Benz et al., 2004; Kavzoglu and Yildiz, 2014) and is used to control the average image object size in relation to the whole scene, the higher the value, the larger the objects will be. Scale parameters, shape, and compactness thresholds were set for each model individually, following a trial-and-error approach.

After the segmentation, each model was manually classified by an expert. The simplified process is defined in the workflow in Supplementary Figure 2.12.

2.2.4.4 Ground Truthing

To assess classification performance, dense cloud datasets were manually annotated. These points were then compared to the classification outputs from the MGC and CGC methods. Classification accuracy was calculated in Python with the ML library Scikit-learn (Pedregosa et al., 2011).

The accuracy score was calculated by summing the true positives and true negatives of all classes and dividing by the total number of annotated points (true positives, false positives, true negatives, and false negatives). The balanced accuracy was calculated as the arithmetic mean of sensitivity (true positive rate) and specificity (true negative rate) of each class. These metrics were chosen because they take into account the class imbalance, i.e., classes do not have the same number of samples, which is typical of seabed imagery datasets. Failure to do so would accidentally inflate the performance of classifiers (Akbari et al., 2004; Brodersen et al., 2010).

2.3 Results

A total of eight 3D reconstructions were produced using 3681 images. Dense clouds were composed of a total of 165,356,594 points. The average reconstruction length was 19.73 m and depths ranged from 595 to 1001 m, with average depth of 732.57 m. Mean total error (i.e., root-mean-square error for X, Y, and Z coordinates for all the cameras) was 13.015. Continuous video acquisition along the ROV transects was not regularly possible because of variations in ROV height and speed. High current speeds at the PBC and the presence of particles in suspension in water column (marine snow) also impacted the ROV video transect and consequently the video quality in some areas. Low-quality data were rejected prior to reconstruction. Despite the presence of a few gaps in the surface, the reconstructions showed medium scale features (>10 cm) such as coral branches, coral rubble, and some benthic species with distinction. However, fine scale features (<5 cm) such as individual coral polyps and encrusted algae were not easily visible.

2.3.1 Coral and Seabed Distribution in the Porcupine Bank Canyon

The dense clouds were manually annotated by an expert and segmented into classes: coral and seabed. The percentage distribution of the coral and seabed samples from the annotated test set showed an average of 7.19% coral and 92.81% seabed. Models A, B, and C, located on the upper part of the PBC, showed higher percentages of coral

(>10%) and sediment-dominated facies with dropstones (Figure 2.3). Models D, E, and F, located on the canyon flank ridge, showed lower percentages of coral (<5%), predominance of bedrock with occasional sediment-dominated facies in areas proximal to the eastern side of the flank (Model F; Figure 2.3).

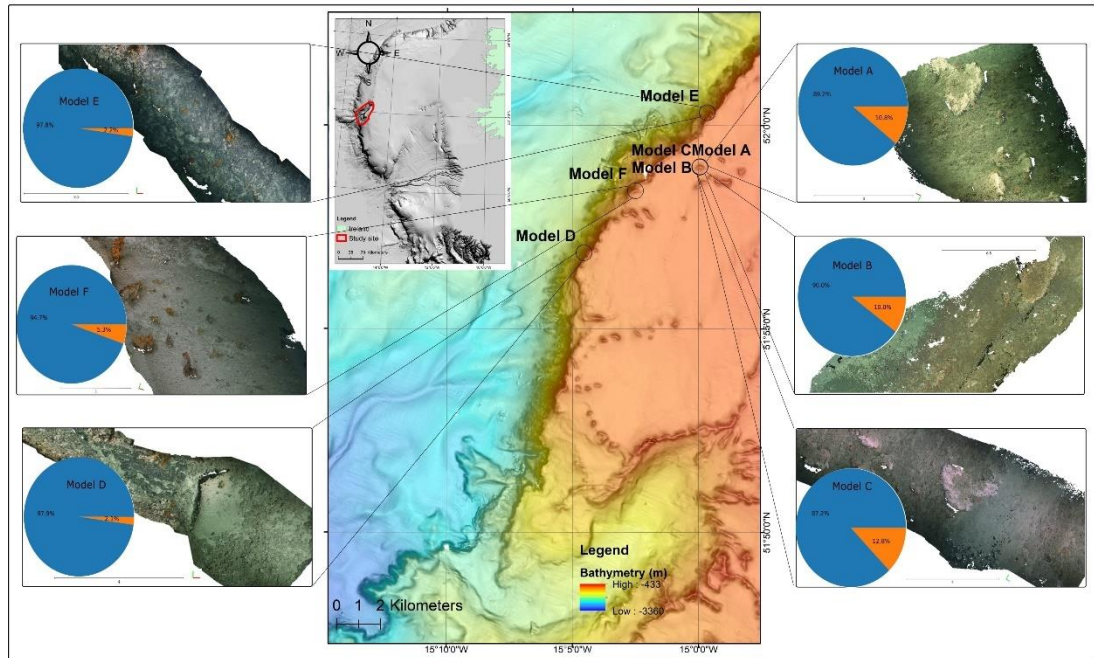


Figure 2.3: Map showing the location of the Porcupine Bank Canyon on the Irish continental shelf and the location of each SfM reconstructed dense cloud produced in this study and its respective class distribution with manual annotation. Blue represents seabed and orange represents coral.

2.3.2 Multiscale Geometrical Classification (MGC)

A total of 11 SVM classifiers were built based on different combinations of annotated samples from the training dataset (Part 1 of Supplementary Figure 2.10). Overall classifier training results had an average *ba* of 89.85%, and *fdr* ratio of 4.27. Classifier 6 presented the best *ba* and *fdr* with values of 99.8 and 8.98%, respectively (Figure 2.4). The training was performed with 20,000 core points and 10 scales with a minimum of 0.1, maximum of 1, and step of 0.2. Classifiers trained with classes from two different source clouds hence, different environments, presented higher *ba* and *fdr* ratios than classifiers trained with one single cloud source.

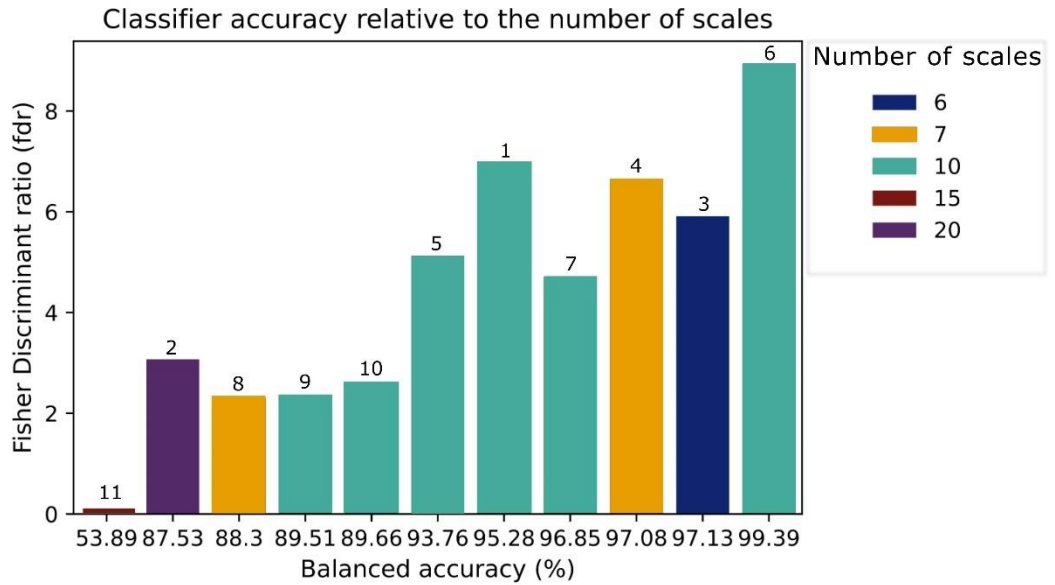


Figure 2.4: Classifier accuracy in relation to the number of scales. The classifier ID is placed on the top of each bar. In the MGC method, scale is defined as the neighbourhood size of pixels to which the classifiers compute each metrics.

The classifier that presented the best performance (classifier 6 on Figure 2.4) was applied to the testing dataset (see Part 2 of Supplementary Figure 2.10). As this classifier was trained with two different source clouds, these were excluded from the test set, which was composed of the remainder of the dataset, i.e., six manually annotated dense clouds. Average accuracy and balanced accuracy scores were 68.2 and 74.7%, respectively. Two models presented accuracy scores above 80% and two models above 60% (Figure 2.5).

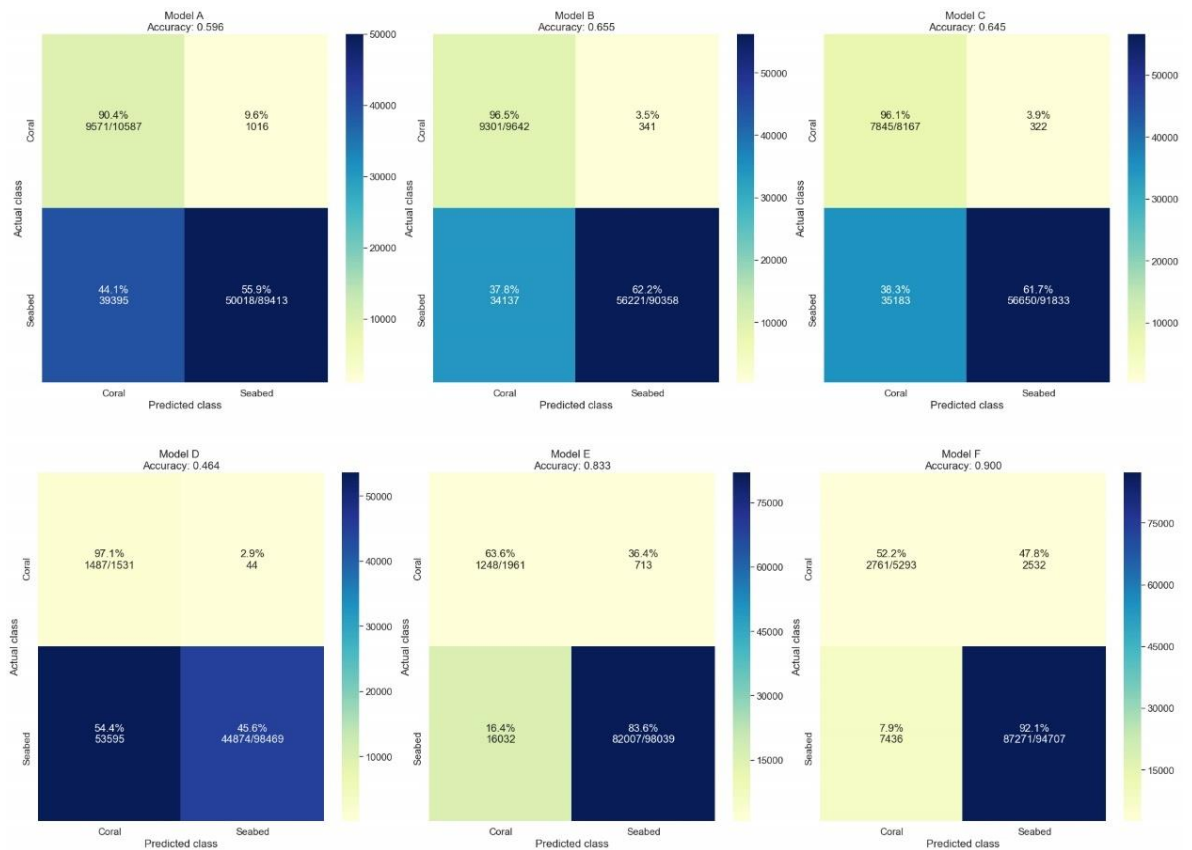


Figure 2.5: Confusion matrices representing the MGC classification results for each dense cloud reconstruction. Confusion matrices show the accuracy score and the relationship between the referenced data and the classification. The “Actual class” on the y-axis refers to the manually annotated data, whereas the “Predicted class” on the x-axis relates to the classification output. The main diagonal of the matrices lists the correctly classified percentage of points per class. The colour scale bar on the right of each confusion matrix represents the number of points.

Models which presented an accuracy score above 80% shared a similar coral distribution pattern. This pattern is represented by the vertical elongation of the coral branches through the Z-axis, i.e., height information, which can be accurately determined using 3D information (Figure 2.6, Model F).

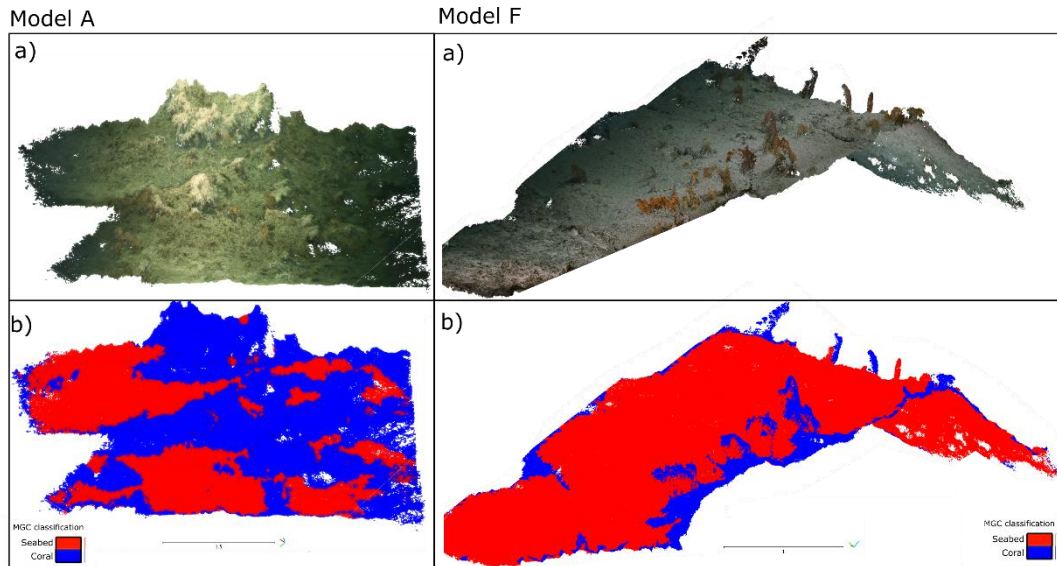


Figure 2.6: Model F - Results of classification using the MGC method – (A) Dense cloud (B) Classification output. Model with predominance of black corals (*Leiopathes sp.*). Red is seabed and blue is coral. Model A – Results of classification using the MGC method – (A) Dense cloud (B) Classification output. Model with predominance of coral rubble patterns. Red is seabed and blue is coral.

2.3.3 Colour and Geometrical Classification (CGC)

The average classification accuracy score using the colour and geometrical classification method was approximately 67.9% with an average balanced accuracy of 58.1%. The classification output resulting from this method is shown in Figure 2.7. From the six models analysed on our testing dataset, two models presented accuracy scores below 60%. The remainder presented accuracy scores above 70%, ranging from 75 to 95% (Figure 2.8).

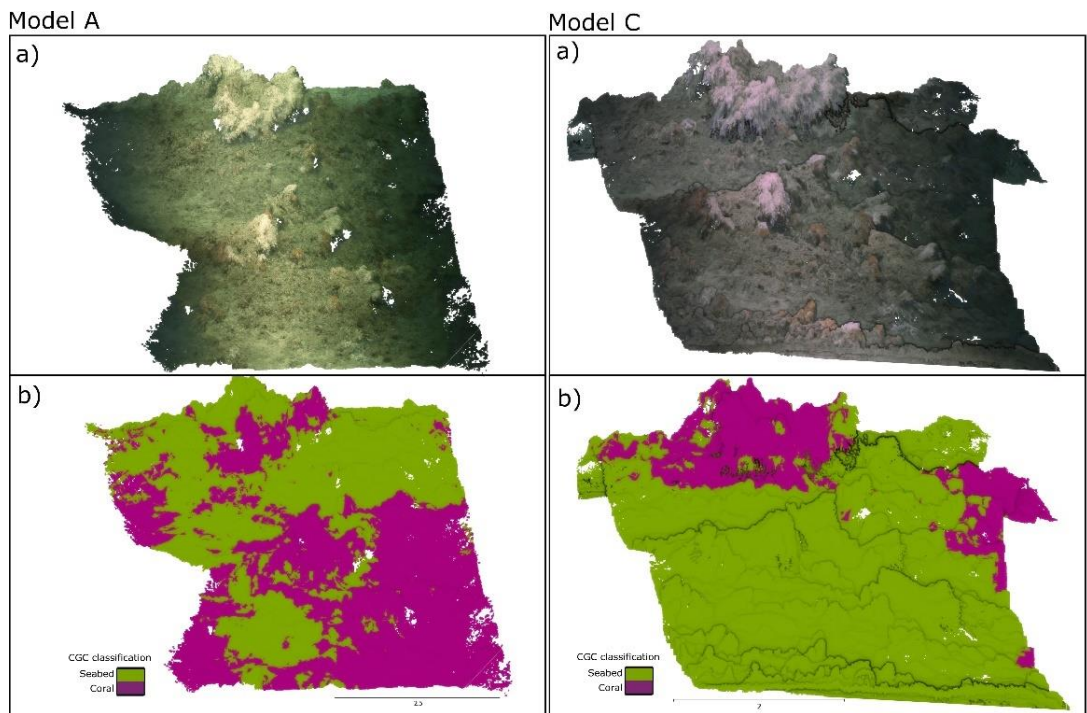


Figure 2.7: Results of classification using CGC method—(A) Dense cloud and (B) classification output with CGC method.

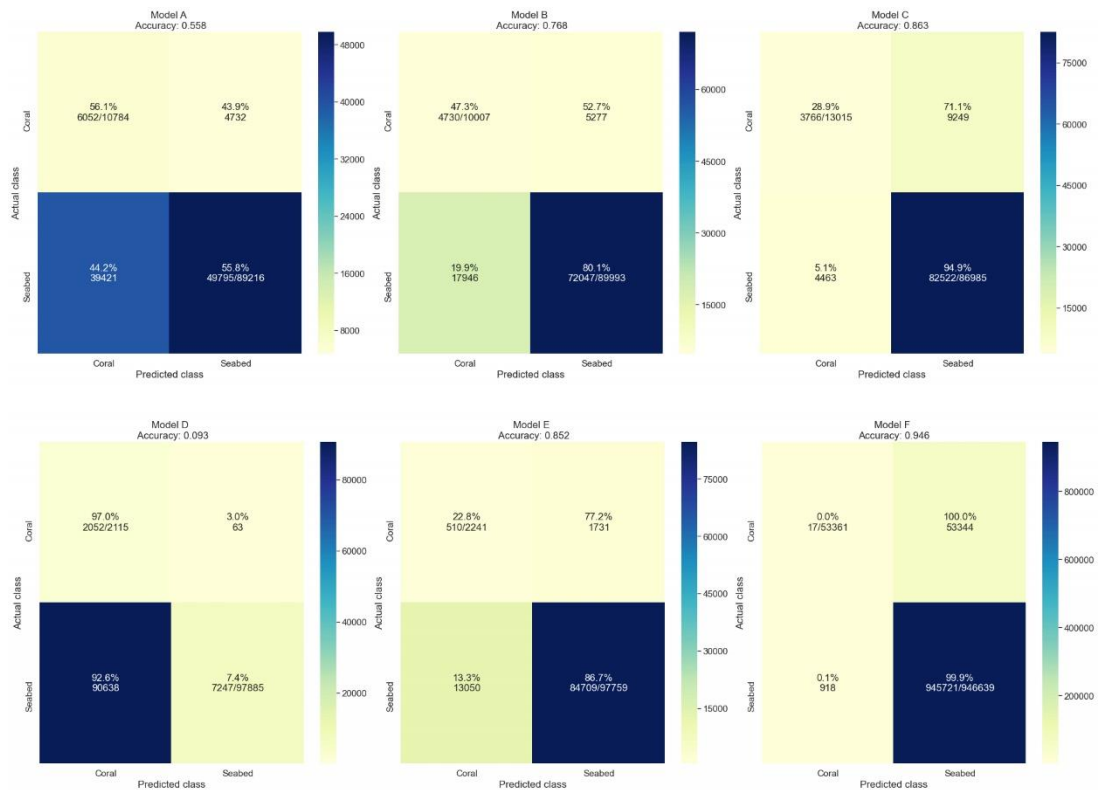


Figure 2.8: Confusion matrices representing the CGC classification results for each dense cloud reconstruction. The “Actual class” on the y-axis refers to the manually annotated data, whereas the “Predicted class” on the x-axis relates to the classification output. The main diagonal of the matrices lists the correctly classified percentage of points per class. The colour scale bar on the right of each confusion matrix represents the number of points.

2.3.4 Object-Based Image Classification (OBIA)

The OBIA method was performed on the orthomosaics, respective DEMs, and calculated slopes of the same dataset. The average classification accuracy was approximately 100%. This result is to be expected because all orthomosaics were manually classified (Figure 2.9) and an adequate manual classification, when repeated by an expert, is expected to have the same outcome.

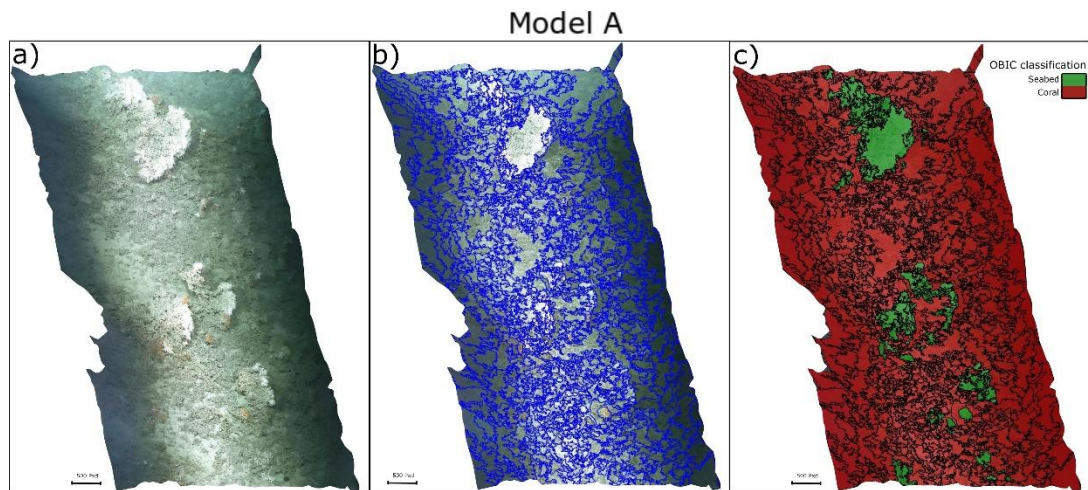


Figure 2.9: Results of classification using OBIA method—(A) Orthomosaic, (B) output of the multi-resolution automated segmentation, and (C) manual classification.

2.4 Discussion

This study compares classification methods of 3D point clouds and 2D images. The workflow involved annotation of datasets, training of classifiers (MGC method), evaluation of the classification output, and the analysis of 3D and 2D-derived information from CWC environments. Studies have shown that overall accuracy is widely used for both OBIA and pixel-based classification accuracy assessments (Ye et al., 2018). Recent developments in accuracy assessment techniques have indicated redundancies in metrics such as standard Kappa indices (Foody, 1992; Pontius and Millones, 2011; Ye et al., 2018; Verma et al., 2020). The use of a Kappa score (Cohen, 1960) as a metric compares the observed accuracy to random accuracy; therefore, it is considered questionable to create a classification map (Foody, 2008; Pontius and Millones, 2011). Although there is substantial discussion on the appropriate metrics for image classification (Congalton, 1991; Banko, 1998; Foody, 2008; Ye et al., 2018), the confusion matrices presented here are a neutral representation of the true positives and true negatives of the classification.

The class distribution of the test data showed more abundance of corals on areas located on the eastern canyon flank. Reconstructions from sites located proximal to the canyon axis, towards the west, presented fewer coral features than sites located on the eastern canyon flank, as also described in previous studies (Appah et al., 2020;

Lim et al., 2020). Appah et al. (2020) show that benthic taxa mean percentage coverage is twice as high in the flank as in adjacent areas, such as north towards the canyon head and the southern part of the canyon. Lim et al. (2020) provide a high-resolution habitat suitability correlation with current speeds, photogrammetry, and coral distribution in the PBC, showing that the variation in coral habitats does not follow a specific pattern, for example, from south to north. This result was also observed in reconstructions from areas located proximal to the canyon flank ridge (models D, E, and F), where the percentage of coral did not present any major increase or decrease following the north–south trend.

2.4.1 Classification results

The *ba* and *fdr* ratios obtained for method MGC indicate that classifiers were influenced by the diversity of point sources used during the training process. Classifiers that were trained with two different dense clouds showed higher *ba* and *fdr* than classifiers trained with a single dense cloud. This suggests that training data with different datasets including those with habitat variability, e.g., different ratios of coral, seabed, and seabed facies, have a positive impact on the classifier performance, as also seen by Mountrakis et al. (2011), Brodu and Lague (2012), and Weidner et al. (2019) in terrestrial data studies. Interestingly, classifier accuracy results (*ba* and *fdr* ratios) showed that increasing the number of scales did not directly impact the quality of the classifier, as increasing the scale past a certain number did not necessarily lead to an increase in accuracy (see Figure 2.4). Thus, incorporating a great number of scales to build a classifier aiming to address a variety of seabed features in the classification computation did not show an improvement on the classifier performance and it can increase the computational complexity required to train the classifier. The process of incorporating multiple scales to acquire the best combination of scales thereby allowing the maximum separability between two classes is constructed automatically and as such, it can tend to overfit. SVM model overfitting can happen by maximising the margin and minimising the training error, which is

typical of not only SVMs but also general kernel-based functions (Mountrakis et al., 2011).

Dense clouds that shared a similar coral distribution pattern, such as individual coral colonies with high vertical elongation and low presence of coral rubble as shown in Model F (Figure 2.6), had high accuracy scores (>80%). In contrast, models with lower accuracy results (<60%) (Figure 2.6-Model A) originated from areas with less defined feature boundaries such as coral rubble.

The colour and geometrical classification algorithm applied in the CGC method did not show any definite patterns concerning the structural complexity of the environment. Even though the classification outputs showed that coral colonies and patches tended to be misclassified in non-flat areas, the classifier resulted in different behaviours when applied to dense-cloud reconstructions of similar environments (Figure 2.7). In previous studies, the algorithm performed well for the detection of buildings and roads, but it misclassified vegetation and ground, especially in datasets containing hills and non-flat surfaces (Becker et al., 2018) meaning that terrain variations could have influenced object detection. Performance results showed that, although accuracy scores were > 60% for the majority of the models, the visual assessment of the predicted output was not in accordance with the high values, as the classification results did not reflect the real objects clearly. Therefore, this result suggests that the high accuracy score may have been derived from the class imbalance in the test dataset, given that the seabed is more dominant than the coral class. Thus, the balanced accuracy provided a better representation of the overall performance. These results may also reflect the similarity of RGB spectral signatures as previously mentioned here and discussed in Lichti (2005), Beijbom et al. (2012), and Hopkinson et al. (2020). It is also possible that the performance of the CGC classifier may improve if there was an intermediary step that allowed training with seafloor and coral data within Agisoft Metashape. Nevertheless, the minimal user input required for this method, since pre-training is not necessary, makes it suitable for fast identification of seabed distribution.

In relation to the OBIA method, the automated segmentation performed better in small-scale orthomosaics (<4 m) where corals and rubble were easily distinguishable.

In large-scale models (>8 m), the segmentation tended to under or over-segment, resulting in a poor differentiation in coral and seabed classes, specifically between coral patches and coral rubble (Figure 2.9). A benefit of utilising object-based techniques applied to classification tasks is the automatic segmentation process, which in the workflow shown herein (Supplementary Figure 2.12) can be faster and more accurate than manual segmentation for annotation of datasets. However, although orthomosaics and DEMs provide height information that is useful for larger scale models, they can be limiting for high-resolution analyses. Conversely, 3D metrics derived from vector dispersion and triangulation in dense clouds provide more detailed information for characterising individual coral colonies and benthic species (Fukunaga and Burns, 2020). Thus, the use of 2D metrics for detailed habitat analysis can lead to lack of discernment when detecting seabed features, e.g., coral branches, coral rubble, and sand ripples as also noted by Hopkinson et al. (2020).

2.4.2 Comparison Within 3D Classifications

Accuracy results (Table 2.1) suggest that models behaved similarly when 3D methods are used (MGC and CGC). Models that obtained an accuracy score of >60% with the MGC method also obtained a comparable result for the CGC method. Occasionally, MGC tended to ignore coral, while CGC tended to overclassify such objects. Both CGC and MGC appeared to be susceptible to object occlusion and canopy effects created by objects. This occlusion was recognised by a classification pattern occurring not only on the object itself (e.g., coral) but also on the shade it created, producing an elongated pattern behind the object consistent with its shadow (Figure 2.6 and Figure 2.7).

Table 2.1: Accuracy metrics for Method 1 – Multiscale Geometrical Classification (MGC), Method 2 - Colour and Geometrical Classification (CGC) and Method 3 – Object-based Image Classification (OBIA)

Accuracy/Method	MGC	CGC	OBIA
Balanced accuracy	0.74	0.66	1
Accuracy score	0.68	0.56	1

In support of this observation, challenges related to the partial occlusion of objects and lighting artefacts have been addressed in other studies (Singh et al., 2004; Gracias and Negahdaripour, 2005). Lighting artefacts such as light scattering, colour shifts, and blurring related to the data acquisition can be considered a bottleneck which impacts the overall model resolution and hence the classification output (Bryson et al., 2015, 2016, 2017). This difficulty can be addressed with the use of image enhancement methods, e.g., texture delighting and colour filtering that can diminish object occlusion artefacts (Bryson et al., 2015). In the overall outputs, the canopy effect pattern was more evident in the CGC method. Furthermore, dense cloud models with a low RGB variability hence, similar RGB values for coral and seabed, resulted in slightly different classification outputs with the CGC method not being able to recognise seabed as compared to the method MGC. As previously mentioned, the classifier in the CGC method also seemed to take into consideration terrain surface variations. Conversely, the geometrical approach and the resistance to shadow effects of the MGC provided a degree of variability and heterogeneity in the class characteristics. As such, MGC appears more suitable for the classification of CWC because (a) it addressed coral colonies and coral patches more accurately, (b) it was able to identify seabed coverage in all 3D reconstructions, and (c) it can be reapplied to classify similar coral reef environments. As a preliminary study, the results showed herein provide important insights towards the advancement on the venue of 3D classification as an accessible and informative approach.

2.4.3 Cost and Data Loss Related to Representing 3D Objects as 2D

With the exception of the CGC method, all methods required similar amounts of data processing, which was mainly allocated to segmentation, labelling, and parameter-tuning, e.g., manual segmentation and labelling in MGC and manual classification in the OBIA method. Even though visual classification output did not fully delineate areas where coral rubble and gradational boundaries were present, the CGC method provided more accurate results when applied to models where objects have well-defined boundaries and sharp edges such as man-made objects (Becker et al., 2018). Conversely, the MGC method is more appropriate for complex scenes with high environmental variability (Brodu and Lague, 2012). One important aspect that should be considered in the MGC application is the amount of training data required to train the classifier. As for most of the classification methods, training data size and availability should be evaluated prior to choosing the methodology to be followed as it directly impacts the performance of the classifier (Lu and Weng, 2007; Maxwell et al., 2018; Zurowietz et al., 2018).

Similarly, the abundance of coral rubble and octocorals must be considered when choosing the classification method as they are subject to underwater colour and intensity distortions (Beijbom et al., 2012; Bryson et al., 2013). Such features present similar values within the intensity range and tend to exhibit wave-length attenuation when reconstructed (Bryson et al., 2013). Attention is drawn to coral rubble features as they present undefined boundary features which hinders their detection. Previous studies have also highlighted the difficulties of automatically classifying coral rubble in images (Beijbom et al., 2012) and 3D models (Hopkinson et al., 2020). Coral rubble occurs due to the coral exposure for extensive periods which lead to abrasion and bioerosion of coral framework (Titschack et al., 2015). High proportions of coral rubble may be indicative of high current speeds in the area (Lim et al., 2020). In contrast, the segmentation utilised in the OBIA method successfully distinguished coral rubble from sediment. This observation agrees with previous studies that have shown that orthomosaics can be useful for high-resolution habitat mapping of large areas (Lim et

al., 2017; Conti et al., 2019). Although coral rubble was not included as a class on our framework, this observation can be useful for future studies.

Representing 3D objects in a 2D space may potentially lead to data bias due to misrepresentation of the object in the feature space and the use of metrics that disregard its multidimensionality factors. In this study, two manual annotation schemes were used to provide a baseline and ground-truth for accuracy calculation. Annotations were performed by an expert in dense-clouds (3D) and orthomosaics for each 3D reconstruction. Table 2.2 shows the percentage distribution of classes of each model in each manual annotation schemes: 3D dense cloud annotation and OBIA manual classification.

Table 2.2: Percentage of class distribution results for each habitat and each class in 2D and 3D

	3D dense cloud		OBIA	
	Coral	Seabed	Coral	Seabed
Model A	10.8%	89.2%	9.3%	90.7%
Model B	10.0%	90.0%	6.9%	93.1%
Model C	12.8%	87.2%	8.4%	91.6%
Model D	2.1%	97.9%	5.5%	94.5%
Model E	2.2%	97.8%	4.5%	95.5%
Model F	5.3%	94.7%	7.7%	92.3%
Average:	7.2%	92.8%	7.1%	92.9%

Class distribution results for each method (Table 2.2) show that there is a higher distribution of coral class within the 3D dense-cloud annotation in comparison to the OBIA method in 50% of the models. When such variation happens, there is a difference of up to 4.45% in the percentage of coral with a mean of 3.02%. Conversely, in models where the distribution of coral class is higher in the OBIA methods, the difference is only up to 3.39%, with a mean of 2.75%.

The average class distribution for the 3D dense cloud was 7.2% coral and 92.8% seabed as opposed to 7.1% coral and 92.9% seabed in the OBIA method. The average of the difference between class distributions was 0.2%. These results show that there is potentially an impact of at least a magnitude order of a tenth of the value in using 2D methods to represent objects that are naturally 3D structures. Although these values may not appear significant in the overall scheme, they have the potential to impact studies whose aims are derived from habitat mapping at a sub-centimetre resolution and a more significant impact when applied over large areas.

Scleractinian corals are naturally vertical-orientated features that, when mapped using 2D metrics, may give a small contribution in the percentage coverage. The 3D branching framework of CWC can increase sediment baffling with reefs or around colonies by offering a resistance to currents, for example (Mienis et al., 2019; Lim et al., 2020). However, the vertical structure of corals would be taken into account in overall biomass estimates if mapped in 3D. Furthermore, calculation of biomass considering all aspects of the environment is extremely relevant to understanding coral reef metabolism and overall environmental dynamics (McKinnon et al., 2011; Burns et al., 2015a, 2019; Price et al., 2019; Hopkinson et al., 2020). In comparison to 2D metrics, the use of multiscale dimensionality features that describe the local geometry of each point in relation to the entire scene makes 3D classification more suitable for the analysis of real complex scenarios at higher resolutions. Thus, advancing from commonly employed 2D image analysis techniques to 3D methods could provide more realistic representations of coral reefs and submarine environments (Fisher et al., 2007; Anelli et al., 2019).

2.4.4 Main Advantages and Disadvantages of the 3D Workflows Identified Within This Study

Three-dimensional reconstructions provide rich, non-destructive ecological and structural habitat information (Burns et al., 2015b; Figueira et al., 2015; Pizarro et al., 2017; Price et al., 2019), serving as a valuable tool for monitoring growth rates and assessing impacts of environmental disturbances (Bennecke et al., 2016; Marre et al.,

2019). The use of SfM can also increase versatility and repeatability of reef surveys (Storlazzi et al., 2016; Bayley et al., 2019; Lim et al., 2020) as it can provide accurate quantifications for habitat coverage as well as coral orientation analyses (Lim et al., 2020). The 3D reconstructions produced in this study can complement recent studies (e.g., Appah et al., 2020; Lim et al., 2020) by providing an object of comparison for spatio-temporal changes in the PBC. The workflows applied herein yield the identification and quantification of CWC distribution at high resolutions.

In contrast, monitoring seabed habitats through 3D reconstruction require centimetric to millimetric resolutions and corresponding accuracies (Marre et al., 2019). High-resolution 3D models require significant data resources (storage and processing power) (Bayley and Mogg, 2020; Hopkinson et al., 2020; Mohamed et al., 2020). Therefore, it is important to highlight the constraints associated with manipulating 3D data. In many cases, it is necessary to develop sub-sampling processes to analyse large batches of data without compromising data resolution. The computer resources and methods available to manipulate and analyse 3D data from marine environments at larger scales could be further improved (Bryson et al., 2017; Robert et al., 2017). The 3D-based workflows described herein demonstrate that most off-the-shelf algorithms need to be adapted for seabed classification and mapping.

The use of SfM for seabed mapping requires consideration of a number of variables to determine the feasibility and accuracy of each study (Burns et al., 2015a; Bayley and Mogg, 2020). For example, environmental conditions such as visibility, swell variations, changes in camera altitude, and ROV speed can impact the survey design, hence, the video quality (Mohamed et al., 2018; Anelli et al., 2019; Marre et al., 2019). Factors related to HD video acquisition and processing such as camera position, lens, light attenuation, calibration, image overlap, and software options can affect the results of 3D reconstructions (Marre et al., 2019; Rossi et al., 2020). Furthermore, high-resolution reconstruction of models can take up to 12 h of processing and a considerable amount of HD video footage (Robert et al., 2017). A regular laptop computer may face limitations to process the resulting models, which can be over 10 GB in size (Robert et al., 2017).

2.5 Conclusions

Cold-water corals significantly contribute to deep-sea biodiversity due to their 3D structure and reef-building capacity. Submarine canyons act as conduits for sediments, nutrients, and organic matter supporting high biomass communities (Nittrouer and Wright, 1994; Puig and Palanques, 1998; Harris and Whiteway, 2011). There is an increasing demand for new methods able to efficiently capture fine-scale changes in these environments. SfM can contribute to more precise structural analysis of CWC habitats while also providing grounds for temporal and volumetric change detection in CWC reefs. This study describes three classification methods applied to CWC reefs within the PBC SAC in the North East Atlantic. The workflows described provide an original and not yet applied methodology for the classification of 3D reconstructed marine environments at the PBC. The dataset consisted of 3D reconstructed point clouds, respective orthomosaics, DEMs, and associated terrain variables of CWC environments. The classification workflows designed for 3D point clouds showed a similar accuracy, even though visual results had different outputs and had a different level of robustness. The balanced accuracy and accuracy scores averaged 67.2% for the 3D methods. The study defines methodologies that are compatible with off-the-shelf commercial software with high-resolution data. Furthermore, the execution of the methods was fast and appeared suitable for the wider deep-sea research community who have access to the SfM point cloud data. Executing more complex frameworks is possible at the expense of computation power and time resources. Future research should involve the application of unsupervised learning with use of geometrical features and application of other ML algorithms for supervised learning. The use of more robust classification methods and higher resolution 3D reconstructions will aid the inclusion of more classes, especially of objects with irregular contour boundaries.

2.6 References

- Addamo, A. M., Vertino, A., Stolarski, J., García-Jiménez, R., Taviani, M., and Machordom, A. (2016). Merging scleractinian genera: The overwhelming genetic similarity between solitary *Desmophyllum* and colonial *Lophelia*. *BMC Evolutionary Biology* 16, 1–17. doi:10.1186/s12862-016-0654-8.
- Agisoft (2019). Agisoft Metashape User Manual. 160. Available at: https://www.agisoft.com/pdf/metashape-pro_1_5_en.pdf.
- Akbani, R., Kwek, S., & Japkowicz, N. (2004). Applying Support Vector Machines to Imbalanced Datasets. *European Conference on Machine Learning*, 39–50
- Anelli, M., Julitta, T., Fallati, L., Galli, P., Rossini, M., and Colombo, R. (2019). Towards new applications of underwater photogrammetry for investigating coral reef morphology and habitat complexity in the Myeik Archipelago, Myanmar. *Geocarto International* 34, 459–472. doi:10.1080/10106049.2017.1408703.
- Appah, J. K. M., Lim, A., Harris, K., O’Riordan, R., O’Reilly, L., and Wheeler, A. J. (2020). Are Non-reef Habitats as Important to Benthic Diversity and Composition as Coral Reef and Rubble Habitats in Submarine Canyons? Analysis of Controls on Benthic Megafauna Distribution in the Porcupine Bank Canyon, NE Atlantic. *Frontiers in Marine Science* 7, 831. doi:10.3389/fmars.2020.571820.
- Banko, G. (1998). A review of assessing the accuracy of and of methods including remote sensing data in forest inventory. *International Institute for Applied Systems Analysis, Interim Report IT-98-081, Laxenburg, Austria.*
- Barbosa, R. v, Davies, A. J., and Sumida, P. Y. G. (2019). Habitat suitability and environmental niche comparison of cold-water coral species along the Brazilian continental margin. *Deep-Sea Research Part I*, 103147. doi:10.1016/j.dsr.2019.103147.
- Bayley, D. T. I., and Mogg, A. O. M. (2020). A protocol for the large-scale analysis of reefs using Structure from Motion photogrammetry. *Methods in Ecology and Evolution*. doi:10.1111/2041-210x.13476.

Bayley, D. T. I., Mogg, A. O. M., Koldewey, H., and Purvis, A. (2019). Capturing complexity: Field-testing the use of “structure from motion” derived virtual models to replicate standard measures of reef physical structure. *PeerJ* 2019. doi:10.7717/peerj.6540.

Becker, C., Rosinskaya, E., Häni, N., d’Angelo, E., and Strecha, C. (2018). Classification of aerial photogrammetric 3D point clouds. *Photogrammetric Engineering and Remote Sensing* 84, 287–295. doi:10.14358/PERS.84.5.287.

Beijbom, O., Edmunds, P. J., Kline, D. I., Mitchell, B. G., and Kriegman, D. (2012). Automated annotation of coral reef survey images. *Proceedings of the IEEE Computer Society Conference on Computer Vision and Pattern Recognition*, 1170–1177. doi:10.1109/CVPR.2012.6247798.

Bennecke, S., Kwasnitschka, T., Metaxas, A., and Dullo, W. C. (2016). In situ growth rates of deep-water octocorals determined from 3D photogrammetric reconstructions. *Coral Reefs* 35, 1227–1239. doi:10.1007/s00338-016-1471-7.

Benz, U. C., Hofmann, P., Willhauck, G., Lingenfelder, I., and Heynen, M. (2004). Multi-resolution, object-oriented fuzzy analysis of remote sensing data for GIS-ready information. *ISPRS Journal of Photogrammetry and Remote Sensing* 58, 239–258. doi:10.1016/j.isprsjprs.2003.10.002.

Boolukos, C. M., Lim, A., O’Riordan, R. M., & Wheeler, A. J. (2019). Cold-water corals in decline – A temporal (4 year) species abundance and biodiversity appraisal of complete photomosaiced cold-water coral reef on the Irish Margin. *Deep-Sea Research Part I: Oceanographic Research Papers*, 146(June), 44–54. <https://doi.org/10.1016/j.dsr.2019.03.004>

Brodersen, K. H., Ong, C. S., Stephan, K. E., & Buhmann, J. M. (2010). The balanced accuracy and its posterior distribution. *Proceedings - International Conference on Pattern Recognition*, 3121–3124. <https://doi.org/10.1109/ICPR.2010.764>

Brodu, N., and Lague, D. (2012). 3D terrestrial LiDAR data classification of complex natural scenes using a multi-scale dimensionality criterion: Applications in geomorphology. *ISPRS Journal of Photogrammetry and Remote Sensing* 68, 121–134. doi:10.1016/j.isprsjprs.2012.01.006. Bryson, M., Ferrari, R., Figueira, W., Pizarro, O.,

Madin, J., Williams, S., et al. (2017). Characterization of measurement errors using structure-from-motion and photogrammetry to measure marine habitat structural complexity. *Ecology and Evolution* 7, 5669–5681. doi:10.1002/ece3.3127.

Bryson, M., Johnson-Roberson, M., Pizarro, O., and Williams, S. (2016). Colour-Consistent Structure-from-Motion Models using Underwater Imagery. doi:10.15607/rss.2012.viii.005.

Bryson, M., Johnson-Roberson, M., Pizarro, O., and Williams, S. B. (2013). Colour-consistent structure-from-motion models using underwater imagery. *Robotics: Science and Systems* 8, 33–40. doi:10.7551/mitpress/9816.003.0010.

Bryson, M., Johnson-Roberson, M., Pizarro, O., and Williams, S. B. (2015). True Color Correction of Autonomous Underwater Vehicle Imagery. *Journal of Field Robotics* 33, 1–17. doi:10.1002/rob.21638.

Burns, Delparte, D., Gates, R. D., and Takabayashi, M. (2015a). Integrating structure-from-motion photogrammetry with geospatial software as a novel technique for quantifying 3D ecological characteristics of coral reefs. *PeerJ* 2015. doi:10.7717/peerj.1077.

Burns, Delparte, D., Gates, R. D., and Takabayashi, M. (2015b). Utilizing underwater three-dimensional modeling to enhance ecological and biological studies of coral reefs. *International Archives of the Photogrammetry, Remote Sensing and Spatial Information Sciences - ISPRS Archives* 40, 61–66. doi:10.5194/isprsarchives-XL-5-W5-61-2015.

Burns, Fukunaga, A., Pascoe, K. H., Runyan, A., Craig, B. K., Talbot, J., et al. (2019). 3D habitat complexity of coral reefs in the northwestern hawaiian islands is driven by coral assemblage structure. *ISPRS Annals of the Photogrammetry, Remote Sensing and Spatial Information Sciences* 42, 61–67. doi:10.5194/isprs-archives-XLII-2-W10-61-2019.

Carlevaris-Bianco, N., Mohan, A., and Eustice, R. M. (2010). Initial results in underwater single image dehazing. *MTS/IEEE Seattle, OCEANS* 2010. doi:10.1109/OCEANS.2010.5664428.

- Carrivick, J. L., Smith, M. W., and Quincey, D. J. (2016). *Structure from Motion in the Geosciences*. Wiley Blackwell.
- Cocito, S., Sgorbini, S., Peirano, A., and Valle, M. (2003). 3-D reconstruction of biological objects using underwater video technique and image processing. *Journal of Experimental Marine Biology and Ecology* 297, 57–70. doi:10.1016/S0022-0981(03)00369-1.
- Cohen, J. (1960). A Coefficient of Agreement for Nominal Scales. *Educational and Psychological Measurement* 20, 37–46. doi:10.1177/001316446002000104.
- Congalton, R. G. (1991). A review of assessing the accuracy of classifications of remotely sensed data. *Remote Sensing of Environment* 37, 35–46. doi:10.1016/0034-4257(91)90048-B.
- Conti, L. A., Lim, A., and Wheeler, A. J. (2019). High resolution mapping of a cold water coral mound. *Scientific Reports* 9. doi:10.1038/s41598-018-37725-x.
- Costello, M. J., McCrea, M., Freiwald, A., Lundälv, T., Jonsson, L., Bett, B. J., et al. (2005). "Role of cold-water *Lophelia pertusa* coral reefs as fish habitat in the NE Atlantic," in *Cold-Water Corals and Ecosystems* (Springer Berlin Heidelberg), 771–805. doi:10.1007/3-540-27673-4_41.
- Courtney, L. A., Fisher, W. S., Raimondo, S., Oliver, L. M., and Davis, W. P. (2007). Estimating 3-dimensional colony surface area of field corals. *Journal of Experimental Marine Biology and Ecology* 351, 234–242. doi:10.1016/j.jembe.2007.06.021.
- de Clippele, L. H., Gafeira, J., Robert, K., Hennige, S., Lavaleye, M. S., Duineveld, G. C. A., et al. (2017). Using novel acoustic and visual mapping tools to predict the small-scale spatial distribution of live biogenic reef framework in cold-water coral habitats. *Coral Reefs* 36, 255–268. doi:10.1007/s00338-016-1519-8.
- de Mol, B., Henriët, J.-P., and Canals, M. (2005). Development of coral banks in Porcupine Seabight: do they have Mediterranean ancestors? *Cold-Water Corals and Ecosystems*, 515–533. doi:10.1007/3-540-27673-4_26.
- Dorschel, B., Wheeler, A. J., Monteys, X., and Verbruggen, K. (2010). *Atlas of the deep-water seabed: Ireland*. Springer Netherlands doi:10.1007/978-90-481-9376-9.

European Union Habitats Directive (2016). European Union Habitats (Porcupine Bank Canyon Special Area of Conservation 003001) Regulations 2016. Ireland Available at: <http://www.irishstatutebook.ie/eli/2016/si/106/made/en/pdf> [Accessed October 25, 2020].

Fanelli, E., Delbono, I., Ivaldi, R., Pratellesi, M., Cocito, S., and Peirano, A. (2017). Cold-water coral *Madrepora oculata* in the eastern Ligurian Sea (NW Mediterranean): Historical and recent findings. *Aquatic Conservation: Marine and Freshwater Ecosystems* 27, 965–975. doi:10.1002/aqc.2751.

Ferrari, R., Marzinelli, E. M., Ayroza, C. R., Jordan, A., Figueira, W. F., Byrne, M., et al. (2018). Large-scale assessment of benthic communities across multiple marine protected areas using an autonomous underwater vehicle. *PLoS ONE* 13, 1–20. doi:10.1371/journal.pone.0193711.

Figueira, W., Ferrari, R., Weatherby, E., Porter, A., Hawes, S., and Byrne, M. (2015). Accuracy and Precision of Habitat Structural Complexity Metrics Derived from Underwater Photogrammetry. *Remote Sensing* 7, 16883–16900. doi:10.3390/rs71215859.

Findlay, H. S., Artioli, Y., Moreno Navas, J., Hennige, S. J., Wicks, L. C., Huvenne, V. A. I., et al. (2013). Tidal downwelling and implications for the carbon biogeochemistry of cold-water corals in relation to future ocean acidification and warming. *Global Change Biology* 19, 2708–2719. doi:10.1111/gcb.12256.

Fisher, W. S., Davis, W. P., Quarles, R. L., Patrick, J., Campbell, J. G., Harris, P. S., et al. (2007). Characterizing coral condition using estimates of three-dimensional colony surface area. *Environmental Monitoring and Assessment* 125, 347–360. doi:10.1007/s10661-006-9527-8.

Foody, G. M. (1992). On the Compensation for Chance Agreement in Image Classification Accuracy Assessment. *Photogrammetric Engineering & Remote Sensing*, 58.

Foody, G. M. (2008). Harshness in image classification accuracy assessment. *International Journal of Remote Sensing* 29, 3137–3158. doi:10.1080/01431160701442120.

- Fosså, J. H., Lindberg, B., Christensen, O., Lundälv, T., Svellingen, I., Mortensen, P. B., et al. (2006). "Mapping of *Lophelia* reefs in Norway: experiences and survey methods," in *Cold-Water Corals and Ecosystems* (Springer-Verlag), 359–391. doi:10.1007/3-540-27673-4_18.
- Freiwald, A., Fosså, J. H., Grehan, A., Koslow, T., and Roberts, J. M. (2011). *Cold-water Coral Reefs: out of sight - no longer out of mind*. UNEP-WCMC Biodiversity Series, 2002–2005. doi:10.5962/bhl.title.45025.
- Freiwald, A., and Roberts, J. M. (2005). *Cold-Water Corals and Ecosystems*. Springer Berlin Heidelberg doi:10.1007/3-540-27673-4.
- Fukunaga, A., and Burns, J. H. R. (2020). Metrics of coral reef structural complexity extracted from 3D mesh models and digital elevation models. *Remote Sensing* 12, 2676. doi:10.3390/RS12172676.
- Fukunaga, A., Burns, J. H. R., Craig, B. K., and Kosaki, R. K. (2019). Integrating three-dimensional benthic habitat characterization techniques into ecological monitoring of coral reefs. *Journal of Marine Science and Engineering* 7. doi:10.3390/jmse7020027.
- Gass, S. E., and Roberts, J. M. (2006). The occurrence of the cold-water coral *Lophelia pertusa* (Scleractinia) on oil and gas platforms in the North Sea: Colony growth, recruitment and environmental controls on distribution. *Marine Pollution Bulletin* 52, 549–559. doi:10.1016/j.marpolbul.2005.10.002.
- Girardeau-Montaut, D. (2011). CloudCompare-open source project. OpenSource Project.
- Goatley, C. H. R., and Bellwood, D. R. (2011). The roles of dimensionality, canopies and complexity in ecosystem monitoring. *PLoS ONE* 6. doi:10.1371/journal.pone.0027307.
- Gómez-ríos, A., Tabik, S., Luengo, J., and Shihavuddin, A. S. M. (2018). Towards Highly Accurate Coral Texture Images Classification Using Deep Convolutional Neural Networks and Data Augmentation Towards highly accurate coral texture images classification using deep convolutional neural networks and data augmentation. doi:10.1016/j.eswa.2018.10.010.

- Gracias, N., and Negahdaripour, S. (2005). Underwater mosaic creation using video sequences from different altitudes. *Proceedings of MTS/IEEE OCEANS, 2005* 2005. doi:10.1109/OCEANS.2005.1639933.
- Graham, N. A. J., and Nash, K. L. (2013). The importance of structural complexity in coral reef ecosystems. *Coral Reefs* 32, 315–326. doi:10.1007/s00338-012-0984-y.
- Guinan, J., Grehan, A. J., Dolan, M. F. J., and Brown, C. (2009). Quantifying relationships between video observations of cold-water coral cover and seafloor features in rockall trough, west of Ireland. *Marine Ecology Progress Series* 375, 125–138. doi:10.3354/meps07739.
- Hackel, T., Wegner, J. D., and Schindler, K. (2016). Fast semantic segmentation of 3d point clouds with strongly varying density. in *ISPRS Annals of the Photogrammetry, Remote Sensing and Spatial Information Sciences (Copernicus GmbH)*, 177–184. doi:10.5194/isprs-annals-III-3-177-2016.
- Harris, P. T., & Whiteway, T. (2011). Global distribution of large submarine canyons: Geomorphic differences between active and passive continental margins. *Marine Geology*, 285(1–4), 69–86. <https://doi.org/10.1016/j.margeo.2011.05.008>
- Hopkinson, B. M., King, A. C., Owen, D. P., Johnson-Roberson, M., Long, M. H., and Bhandarkar, S. M. (2020). Automated classification of three-dimensional reconstructions of coral reefs using convolutional neural networks. *PLoS ONE* 15, 1–20. doi:10.1371/journal.pone.0230671.
- House, J. E., Brambilla, V., Bidaut, L. M., Christie, A. P., Pizarro, O., Madin, J. S., et al. (2018). Moving to 3D: Relationships between coral planar area, surface area and volume. *PeerJ* 2018. doi:10.7717/peerj.4280.
- Hovland, M., and Thomsen, E. (1997). Cold-water corals - Are they hydrocarbon seep related? in *Marine Geology (Elsevier)*, 159–164. doi:10.1016/S0025-3227(96)00086-2.
- Huvenne, V. A. I., Bett, B. J., Masson, D. G., le Bas, T. P., and Wheeler, A. J. (2016). Effectiveness of a deep-sea cold-water coral Marine Protected Area, following eight

years of fisheries closure. *Biological Conservation* 200, 60–69. doi:10.1016/j.biocon.2016.05.030.

Huvenne, V. A. I., Tyler, P. A., Masson, D. G., Fisher, E. H., Hauton, C., Hühnerbach, V., et al. (2011). A picture on the wall: Innovative mapping reveals cold-water coral refuge in submarine canyon. *PLoS ONE* 6, 1–9. doi:10.1371/journal.pone.0028755.

Jonsson, L. G., Nilsson, P. G., Floruta, F., and Lundälv, T. (2004). Distributional patterns of macro- and megafauna associated with a reef of the cold-water coral *Lophelia pertusa* on the Swedish west coast. *Marine Ecology Progress Series* 284, 163–171. doi:10.3354/meps284163.

Kavzoglu, T., and Yildiz, M. (2014). Parameter-Based Performance Analysis of Object-Based Image Analysis Using Aerial and Quikbird-2 Images. *ISPRS Annals of Photogrammetry, Remote Sensing and Spatial Information Sciences II-7*, 31–37. doi:10.5194/isprsannals-ii-7-31-2014.

King, A., Bhandarkar, S. M., and Hopkinson, B. M. (2018). A Comparison of Deep Learning Methods for Semantic Segmentation of Coral Reef Survey Images. in 2018 IEEE/CVF Conference on Computer Vision and Pattern Recognition Workshops (CVPRW) (IEEE), 1475–14758. doi:10.1109/CVPRW.2018.00188.

Klápště, P., Urban, R., and Moudrý, V. (2018). Ground Classification of UAV Image-based Point Clouds through Different Algorithms: Open Source vs . Commercial Software. 6th International Conference on “Small Unmanned Aerial Systems for Environmental Research,” 15–18.

Koop, L., Snellen, M., & Simons, D. G. (2021). An Object-Based Image Analysis Approach Using Bathymetry and Bathymetric Derivatives to Classify the Seafloor. *Geosciences*, 11(2), 45. <https://doi.org/10.3390/geosciences11020045>

Kwasnitschka, T., Hansteen, T. H., Devey, C. W., and Kutterolf, S. (2013). Doing fieldwork on the seafloor: Photogrammetric techniques to yield 3D visual models from ROV video. *Computers and Geosciences* 52, 218–226. doi:10.1016/j.cageo.2012.10.008.

Lambers, K., Verschoof-van der Vaart, W. B., and Bourgeois, Q. P. J. (2019). Integrating remote sensing, machine learning, and citizen science in dutch archaeological prospection. *Remote Sensing* 11, 1–20. doi:10.3390/rs11070794.

Leverette, T. L., and Metaxas, A. (2006). “Predicting habitat for two species of deep-water coral on the Canadian Atlantic continental shelf and slope,” in *Cold-Water Corals and Ecosystems* (Springer-Verlag), 467–479. doi:10.1007/3-540-27673-4_23.

Lichti, D. D. (2005). Spectral filtering and classification of terrestrial laser scanner point clouds. *Photogrammetric Record* 20, 218–240. doi:10.1111/j.1477-9730.2005.00321.x.

Lim, A., Huvenne, V. A. I., Vertino, A., Spezzaferri, S., and Wheeler, A. J. (2018). New insights on coral mound development from groundtruthed high-resolution ROV-mounted multibeam imaging. *Marine Geology* 403, 225–237. doi:10.1016/j.margeo.2018.06.006.

Lim, A., O’Reilly, L., Summer, G., Harris, K., Oliveira, L., O’Hanlon, Z., et al. (2019a). CE19014 - Monitoring Changes in Submarine Canyon Coral Habitats - Leg 2 (MoCha _ Scan II). Cork, Ireland.

Lim, A., O’Reilly, L., Summer, G., Harris, K., Shine, A., Harman, L., et al. (2019b). Monitoring Changes in Submarine Canyon Coral Habitats - Leg 1 (MoCha_SCan).

Lim, A., Wheeler, A. J., and Arnaubec, A. (2017). High-resolution facies zonation within a cold-water coral mound: The case of the Piddington Mound, Porcupine Seabight, NE Atlantic. *Marine Geology* 390, 120–130. doi:10.1016/j.margeo.2017.06.009.

Lim, A., Wheeler, A. J., Price, D. M., O’Reilly, L., Harris, K., and Conti, L. (2020). Influence of benthic currents on cold-water coral habitats: a combined benthic monitoring and 3D photogrammetric investigation. *Scientific Reports* 10, 19433. doi:10.1038/s41598-020-76446-y.

Lu, D., and Weng, Q. (2007). A survey of image classification methods and techniques for improving classification performance. *International Journal of Remote Sensing* 28, 823–870. doi:10.1080/01431160600746456.

- Marburg, A., and Bigham, K. (2016). Deep learning for benthic fauna identification. *OCEANS 2016 MTS/IEEE Monterey*, OCE 2016. doi:10.1109/OCEANS.2016.7761146.
- Marre, G., Holon, F., Luque, S., Boissery, P., and Deter, J. (2019). Monitoring marine habitats with photogrammetry: A cost-effective, accurate, precise and high-resolution reconstruction method. *Frontiers in Marine Science* 6. doi:10.3389/fmars.2019.276.
- Masson, D. G., Bett, B. J., Billett, D. S. M., Jacobs, C. L., Wheeler, A. J., and Wynn, R. B. (2003). The origin of deep-water, coral-topped mounds in the northern Rockall Trough, Northeast Atlantic. *Marine Geology* 194, 159–180. doi:10.1016/S0025-3227(02)00704-1.
- Maxwell, A. E., Warner, T. A., and Fang, F. (2018). Implementation of machine-learning classification in remote sensing: an applied review. *International Journal of Remote Sensing*. doi:10.1080/01431161.2018.1433343.
- Mazzini, A., Akhmetzhanov, A., Monteys, X., and Ivanov, M. (2012). The Porcupine Bank Canyon coral mounds: Oceanographic and topographic steering of deep-water carbonate mound development and associated phosphatic deposition. *Geo-Marine Letters* 32, 205–225. doi:10.1007/s00367-011-0257-8.
- McKinnon, D., He, H., Upcroft, B., and Smith, R. N. (2011). Towards Automated and In-Situ, Near-Real Time 3-D Reconstruction of Coral Reef Environments.
- Menna, F., Agrafiotis, P., and Georgopoulos, A. (2018). State of the art and applications in archaeological underwater 3D recording and mapping. *Journal of Cultural Heritage* 33, 231–248. doi:10.1016/j.culher.2018.02.017.
- Mienis, F., Bouma, T., Witbaard, R., van Oevelen, D., and Duineveld, G. (2019). Experimental assessment of the effects of coldwater coral patches on water flow. *Marine Ecology Progress Series* 609, 101–117. doi:10.3354/meps12815.
- Mienis, F., van Weering, T., de Haas, H., de Stigter, H., Huvenne, V., and Wheeler, A. (2006). Carbonate mound development at the SW Rockall Trough margin based on high resolution TOBI and seismic recording. *Marine Geology* 233, 1–19. doi:10.1016/j.margeo.2006.08.003.

Mohamed, H., Nadaoka, K., and Nakamura, T. (2018). Assessment of machine learning algorithms for automatic benthic cover monitoring and mapping using towed underwater video camera and high-resolution satellite images. *Remote Sensing* 10. doi:10.3390/rs10050773.

Mohamed, H., Nadaoka, K., and Nakamura, T. (2020). Towards Benthic Habitat 3D Mapping Using Machine Learning Algorithms and Structures from Motion Photogrammetry. *Remote Sensing* 12, 127. doi:10.3390/rs12010127.

Mortensen, P. B., Hovland, M., Brattegard, T., and Farestveit, R. (1995). Deep water bioherms of the scleractinian coral *Lophelia pertusa* (L.) at 64° n on the norwegian shelf: Structure and associated megafauna. *Sarsia* 80, 145–158. doi:10.1080/00364827.1995.10413586.

Mountrakis, G., Im, J., and Ogole, C. (2011). Support vector machines in remote sensing: A review. *ISPRS Journal of Photogrammetry and Remote Sensing* 66, 247–259. doi:10.1016/j.isprsjprs.2010.11.001.

Orejas, C., Gori, A., lo Iacono, C., Puig, P., Gili, J. M., and Dale, M. R. T. (2009). Cold-water corals in the Cap de Creus canyon, northwestern Mediterranean: Spatial distribution, density and anthropogenic impact. *Marine Ecology Progress Series* 397, 37–51. doi:10.3354/meps08314.

Nittrouer, C. A., & Wright, L. D. (1994). Transport of particles across continental shelves. *Reviews of Geophysics*, 32(1), 85–113. <https://doi.org/10.1029/93RG02603>

Pal, M. (2005). Random forest classifier for remote sensing classification. *International Journal of Remote Sensing* 26, 217–222. doi:10.1080/01431160412331269698.

Pedregosa, F., Varoquaux, G., Gramfort, A., Michel, V., Thirion, B., Grisel, O., et al. (2011). Scikit-learn: Machine learning in Python. *the Journal of machine Learning research* 12, 2825–2830.

Pirotti, F., and Tonion, F. (2019). Classification of aerial laser scanning point clouds using machine learning: A comparison between random forest and tensorflow. *International Archives of the Photogrammetry, Remote Sensing and Spatial Information Sciences - ISPRS Archives* 42, 1105–1111. doi:10.5194/isprs-archives-XLII-2-W13-1105-2019.

Pizarro, O., Friedman, A., Bryson, M., Williams, S. B., and Madin, J. (2017). A simple, fast, and repeatable survey method for underwater visual 3D benthic mapping and monitoring. *Ecology and Evolution* 7, 1770–1782. doi:10.1002/ece3.2701.

Pontius, R. G., and Millones, M. (2011). Death to Kappa: Birth of quantity disagreement and allocation disagreement for accuracy assessment. *International Journal of Remote Sensing* 32, 4407–4429. doi:10.1080/01431161.2011.552923.

Price, Robert, K., Callaway, A., lo lacono, C., Hall, R. A., and Huvenne, V. A. I. (2019). Using 3D photogrammetry from ROV video to quantify cold-water coral reef structural complexity and investigate its influence on biodiversity and community assemblage. *Coral Reefs* 38, 1007–1021. doi:10.1007/s00338-019-01827-3.

Puig, P., & Palanques, A. (1998). Temporal variability and composition of settling particle fluxes on the Barcelona continental margin (Northwestern Mediterranean). *Journal of Marine Research*, 56(3), 639–654. <https://doi.org/10.1357/002224098765213612>

Robert, K., Huvenne, V. A. I., Georgiopoulou, A., Jones, D. O. B., Marsh, L., Carter, D. O. G., et al. (2017). New approaches to high-resolution mapping of marine vertical structures. *Scientific Reports* 7, 1–14. doi:10.1038/s41598-017-09382-z.

Roberts, J. M. (2002). The occurrence of the coral *Lophelia pertusa* and other conspicuous epifauna around an oil platform in the North Sea. *Underwater Technology* 25, 83–91. doi:10.3723/175605402783219163.

Roberts, J. M., Peppe, O. C., Dodds, L. A., Mercer, D. J., Thomson, W. T., Gage, J. D., et al. (2006a). “Monitoring environmental variability around cold-water coral reefs: the use of a benthic photolander and the potential of seafloor observatories,” in *Cold-Water Corals and Ecosystems* (Springer-Verlag), 483–502. doi:10.1007/3-540-27673-4_24.

Roberts, J. M., Wheeler, A., Freiwald, A., and Stephen Cairns (2009). *Cold-Water Corals: The Biology and Geology of Deep-Sea Coral Habitats*. Available at: <https://books.google.ie/books?id=L6X6UW7ZszlC&pg=PA310&lpg=PA310&dq=Rober%20ts,+J.M.,+2002.+The+occurrence+of+the+coral+Lophelia+pertusa+and+other+conspicuous+epifauna+around+an+oil+platform+in+the+North+Sea.+Journal+of+the+Socie>

ty+for+Underwater+Technology+25,+83%E2%80%9391&source=bl&ots=i5-YhZ3N-
v&sig=ACfU3U0Deub73vpl53Hu_Mo_t33_YOLrkg&hl=en&sa=X&ved=2ahUKEwixt6u
c38rsAhXRqHEKHTZkCg0Q6AEwB3oECACQAg#v=onepage&q&f=false [Accessed
October 23, 2020].

Roberts, J. M., Wheeler, A. J., and Freiwald, A. (2006b). *Reefs of the Deep: The Biology and Geology of Cold-Water Coral Ecosystems*.

Rossi, P., Castagnetti, C., Capra, A., Brooks, A. J., and Mancini, F. (2020). Detecting change in coral reef 3D structure using underwater photogrammetry: critical issues and performance metrics. *Applied Geomatics* 12, 3–17. doi:10.1007/s12518-019-00263-w.

Roynard, X., Deschaud, J.-E., and Goulette, F. (2018). Classification of Point Cloud Scenes with Multiscale Voxel Deep Network. Available at: <http://arxiv.org/abs/1804.03583>.

Savini, A., Vertino, A., Marchese, F., Beuck, L., and Freiwald, A. (2014). Mapping cold-water coral habitats at different scales within the Northern Ionian Sea (central Mediterranean): An assessment of coral coverage and associated vulnerability. *PLoS ONE* 9, 2002–2005. doi:10.1371/journal.pone.0087108.

Sergios Theodoridis, and Konstantinos Koutroumbas (2008). “Chapter 5 - Feature Selection,” in *Pattern Recognition (Elsevier Science & Technology)*, 280–282.

Shannon, P. M. (1991). The development of Irish offshore sedimentary basins. *Journal of the Geological Society* 148, 181–189. doi:10.1144/gsjgs.148.1.0181.

Shihavuddin, A. S. M., Gracias, N., Garcia, R., Gleason, A., and Gintert, B. (2013). Image-Based Coral Reef Classification and Thematic Mapping. *Remote Sensing* 5, 1809–1841. doi:10.3390/rs5041809.

Singh, H., Howland, J., and Pizarro, O. (2004). Advances in Large-Area Photomosaicking. *Journal of Oceanic Engineering* 29, 872–886.

Storlazzi, C. D., Dartnell, P., Hatcher, G. A., and Gibbs, A. E. (2016). End of the chain? Rugosity and fine-scale bathymetry from existing underwater digital imagery using

structure-from-motion (SfM) technology. *Coral Reefs* 35, 889–894. doi:10.1007/s00338-016-1462-8.

Titschack, J., Baum, D., de Pol-Holz, R., López Correa, M., Forster, N., Flögel, S., et al. (2015). Aggradation and carbonate accumulation of Holocene Norwegian cold-water coral reefs. *Sedimentology* 62, 1873–1898. doi:10.1111/sed.12206.

Trimble. (2018). Trimble Documentation: eCognition® Developer User Guide. March, 1–272.

Trimble Germany GmbH (2019). Trimble eCognition Developer - for Windows operating system - Reference Book. 9.5.1. Munich: Trimble Germany GmbH.

Turley, C. M., Roberts, A. J. M., and Guinotte, A. J. M. (2007). Corals in deep-water: will the unseen hand of ocean acidification destroy cold-water ecosystems? *Coral Reefs*. doi:10.1007/s00338-007-0247-5.

Verma, P., Raghubanshi, A., Srivastava, P. K., and Raghubanshi, A. S. (2020). Appraisal of kappa-based metrics and disagreement indices of accuracy assessment for parametric and nonparametric techniques used in LULC classification and change detection. *Modeling Earth Systems and Environment* 6, 1045–1059. doi:10.1007/s40808-020-00740-x.

Victorero, L., Blamart, D., Pons-Branchu, E., Mavrogordato, M. N., and Huvenne, V. A. I. (2016). Reconstruction of the formation history of the Darwin Mounds, N Rockall Trough: How the dynamics of a sandy contourite affected cold-water coral growth. *Marine Geology* 378, 186–195. doi:10.1016/j.margeo.2015.12.001.

Walton, G., Mills, G., Fotopoulos, G., Radovanovic, R., and Stancliffe, R. P. W. (2016). An approach for automated lithological classification of point clouds. *Geosphere* 12, 1833–1841. doi:10.1130/GES01326.1.

Wang, Z., Zhang, L., Fang, T., Mathiopoulos, P. T., Tong, X., Qu, H., et al. (2015). A multiscale and hierarchical feature extraction method for terrestrial laser scanning point cloud classification. *IEEE Transactions on Geoscience and Remote Sensing* 53, 2409–2425. doi:10.1109/TGRS.2014.2359951.

Weidner, L., Walton, G., and Kromer, R. (2019). Classification methods for point clouds in rock slope monitoring: A novel machine learning approach and comparative analysis. *Engineering Geology* 263, 105326. doi:10.1016/j.enggeo.2019.105326.

Weinmann, M., Jutzi, B., Hinz, S., and Mallet, C. (2015). Semantic point cloud interpretation based on optimal neighborhoods , relevant features and efficient classifiers. *ISPRS Journal of Photogrammetry and Remote Sensing* 105, 286–304. doi:10.1016/j.isprsjprs.2015.01.016.

Weinmann, M., Jutzi, B., and Mallet, C. (2013). Feature relevance assessment for the semantic interpretation of 3D point cloud data. *ISPRS Annals of the Photogrammetry, Remote Sensing and Spatial Information Sciences* 2, 313–318. doi:10.5194/isprsannals-II-5-W2-313-2013.

Wheeler, Beck, T., Thiede, J., Klages, M., Grehan, A., and Monteys, F. X. (2005a). “Deep-water coral mounds on the Porcupine Bank, Irish Margin: preliminary results from the Polarstern ARK-XIX/3a ROV cruise,” in *Cold-Water Corals and Ecosystems* (Springer Berlin Heidelberg), 393–402. doi:10.1007/3-540-27673-4_19.

Wheeler, Bett, B. J., Billett, D. S. M., Masson, D. G., and Mayor, D. J. (2005b). The impact of demersal trawling on northeast Atlantic deepwater coral habitats: The case of the Darwin mounds, United Kingdom. *American Fisheries Society Symposium* 41, 807–818.

Wheeler, Beyer, A., Freiwald, A., de Haas, H., Huvenne, V. A. I., Kozachenko, M., et al. (2007a). Morphology and environment of cold-water coral carbonate mounds on the NW European margin. *International Journal of Earth Sciences* 96, 37–56. doi:10.1007/s00531-006-0130-6.

Wheeler, Ferdelman, T., Freiwald, a, Hebbeln, D., and Henriët, J. P. (2007b). Cold-Water Coral Ecosystem Functioning through Time in the Deep Sea : The example of cold-water coral carbonate mounds in the northeast Atlantic (from IODP307 to EuroMARC - CARBONATE). 9.

Wheeler, Kozachenko, M., Beyer, A., Foubert, A., Huvenne, V. A. I., Klages, M., et al. (2005c). “Sedimentary processes and carbonate mounds in the Belgica Mound

province, Porcupine Seabight, NE Atlantic,” in *Cold-Water Corals and Ecosystems* (Springer Berlin Heidelberg), 571–603. doi:10.1007/3-540-27673-4_28.

Wilson, J. B. (1979a). Patch Development of the Deep-Water Coral *Lophelia pertusa* (L.) on Rockall Bank. *Journal of the Marine Biological Association of the United Kingdom* 59, 165–177. doi:10.1017/S0025315400046257.

Wilson, J. B. (1979b). The Distribution of the Coral *Lophelia pertusa* (L.) [L.Prolifera (Pallas)] in the North-East Atlantic. *Journal of the Marine Biological Association of the United Kingdom* 59, 149–164. doi:10.1017/S0025315400046245.

Ye, S., Pontius, R. G., and Rakshit, R. (2018). A review of accuracy assessment for object-based image analysis: From per-pixel to per-polygon approaches. *ISPRS Journal of Photogrammetry and Remote Sensing* 141, 137–147. doi:10.1016/j.isprsjprs.2018.04.002.

Young, G. C. (2017). Three-Dimensional Modelling of Coral Reefs for Structural Complexity Analysis. Thesis, 184.

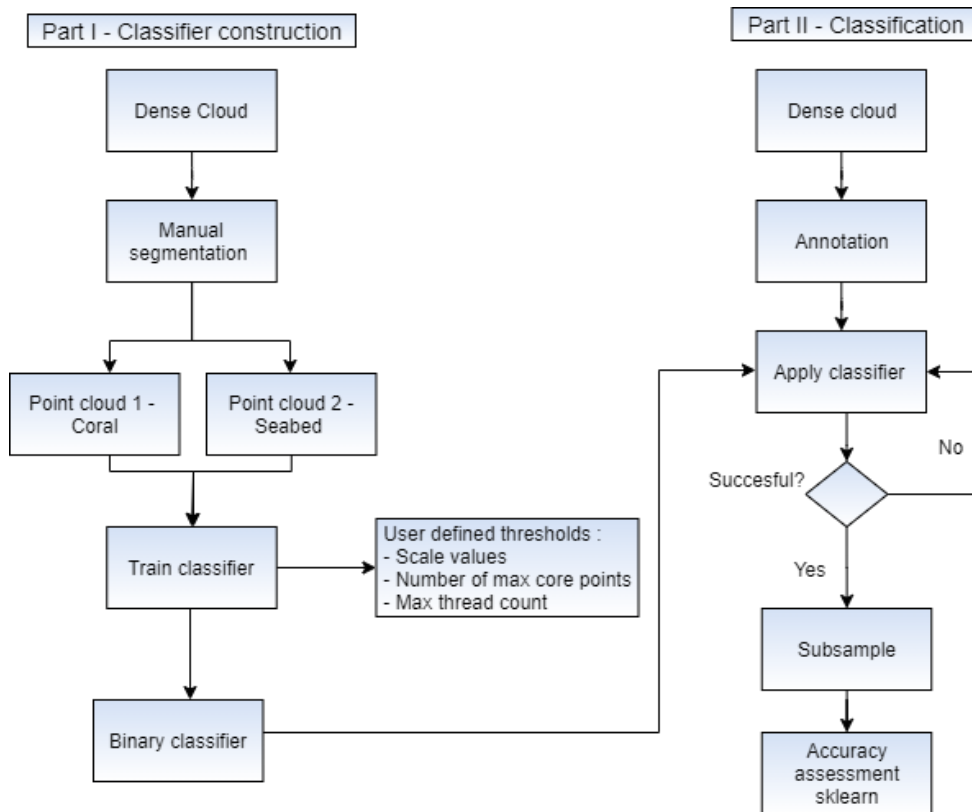
Young, G. C. (2018). Convolutional Neural Networks Predict Fish Abundance from Underlying Coral Reef Texture. 41, 345–362.

Young, G. C., Dey, S., Rogers, A. D., and Exton, D. (2018). Cost and time-effective method for multi-scale measures of rugosity, fractal dimension, and vector dispersion from coral reef 3D models. *PLoS ONE* 13, 1–18. doi:10.1371/journal.pone.0201847.

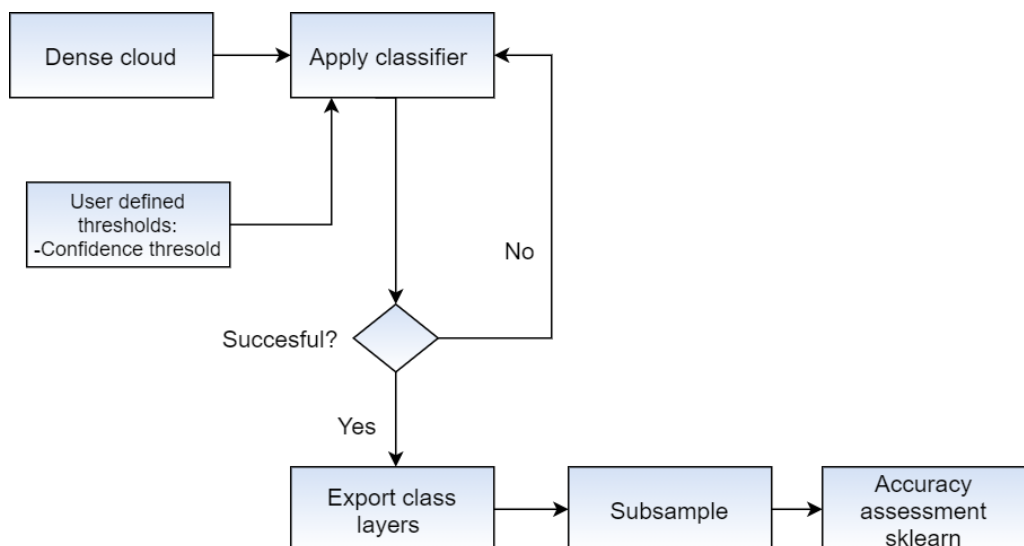
Zhang, Y., Maxwell, T., Tong, H., and Dey, V. (2010). Development of a supervised software tool for automated determination of optimal segmentation parameters for ecognition. *ISPRS TC VII Symposium XXXVIII*, 690–696. Available at: http://www.isprs.org/proceedings/Xxxviii/part7/b/pdf/690_XXXVIII-part7B.pdf.

Zurowietz, M., Langenkämper, D., Hosking, B., Ruhl, H. A., and Nattkemper, T. W. (2018). MAIA-A machine learning assisted image annotation method for environmental monitoring and exploration. *Plos One* 13. doi:10.1371/journal.pone.0207498.

2.7 Supplementary materials

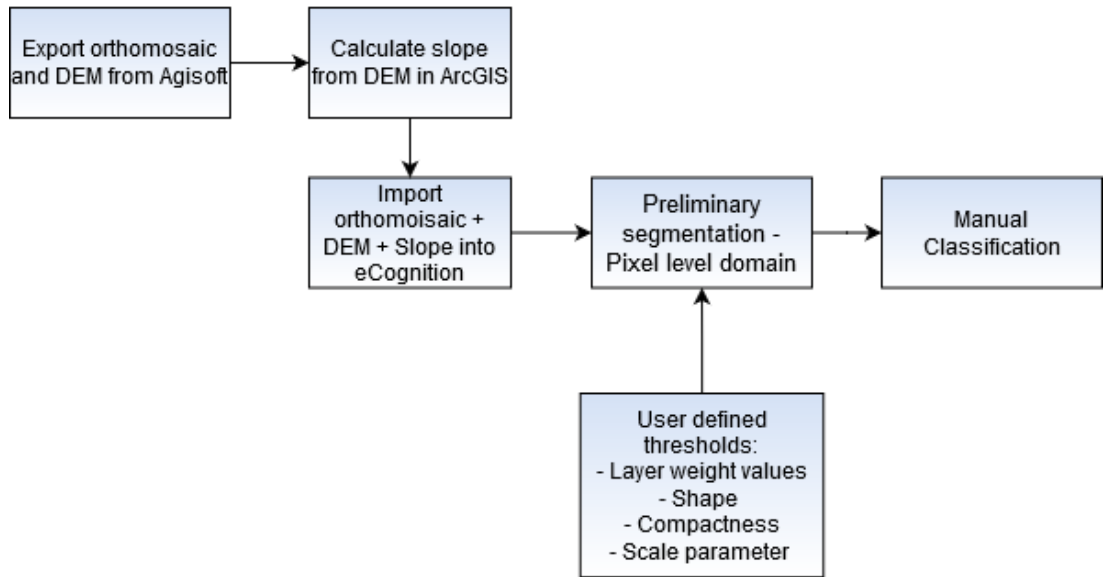


Supplementary Figure 2.10. Workflow for the Multiscale Geometrical Classification (MGC).



Supplementary Figure 2.11: Workflow for the Colour and Geometrical Classification method (CGC)

OBIA workflow



Supplementary Figure 2.12: Workflow for the method 2D Object-based Image classification (OBIA)

3. High-resolution 3D Mapping Of Cold-Water Coral Reefs Using Machine Learning

Larissa Macedo Cruz de Oliveira, Aaron Lim, Luis A. Conti and Andrew J. Wheeler

(Current status: Published, *Frontiers in Environmental Science*)

DOI: <https://doi.org/10.3389/fenvs.2022.1044706>

This chapter comprises a paper that is published in the journal *Frontiers in Environmental Science*:

de Oliveira, L.M.C., Lim, A., Conti, L.A., Wheeler, A.J., 2022. High-resolution 3D mapping of cold-water coral reefs using machine learning. *Front. Environ. Sci.* 10, 1–20. <https://doi.org/10.3389/fenvs.2022.1044706>

This chapter is organised as follows: introduction, materials and methods, results, discussion and references.

This chapter presents a multiclass 3D classification framework classification study developed with SfM and supervised machine learning algorithms. This study was designed upon identifying the paucity in research related to the automatic classification of deep-water habitats using machine learning and the need for new methods for 3D data which was previously identified in [Chapter 2](#). Building upon the identified challenges outlined the previous chapter, a multiclass 3D classification framework was developed and tested in datasets of different sample sizes to evaluate the performance of different ML algorithms in relation to the amount of training data. A section of the Piddington Mound was classified into four classes based on previous facies distribution studies, in this case, live coral framework (LCF), dead coral framework (DCF) and coral rubble (CR), apart from sediments and drop stones (SD). To the first author's knowledge, this is the first study to develop a classification of CWC reef habitats in 3D and provide a detailed comparison of ML algorithms, thus creating a benchmark for the development of future studies.

Candidate contributions to the study: Larissa de Oliveira conceptualised the study, developed the methodology, carried out the funding acquisition, data curation, investigation, formal analyses, software programming, data visualisation, validation, writing of the original draft, review, submission and editing.

The project which lead to the work developed in this chapter was developed by Larissa de Oliveira and funded through the Irish Research Council Postgraduate Scholarship awarded to Larissa Oliveira: Advancing Seabed Mapping Techniques for Deep-water Habitat Classification in Submarine Canyons (ASMaT) - GOIPG/2020/1659. Dr Aaron Lim was the chief scientist responsible for the data collected for the study during the research cruise CE20011, in which Larissa Oliveira was data manager. Dr Aaron Lim contributed to the conceptualisation, methodology and validation. The project was supervised by Prof Andy Wheeler, Dr Aaron Lim and Prof Luis Conti. These co-authors also contributed with editing and proof-reading of the manuscript and funding acquisition.

Abstract

Structure-from-Motion (SfM) photogrammetry is a time and cost effective method for high resolution 3D mapping of cold-water corals (CWC) reefs and deep-water environments. The accurate classification and analysis of marine habitats in 3D provide valuable information for the development of management strategies for large areas at various spatial and temporal scales. Given the amount of data derived from SfM data sources such as Remotely-Operated Vehicles (ROV), there is an increasing need to advance towards automatic and semiautomatic classification approaches. However, the lack of training data, benchmark datasets for CWC environments and processing resources are a bottleneck for the development of classification frameworks. In this study, machine learning (ML) methods and SfM-derived 3D data were combined to develop a novel multiclass classification workflow for CWC reefs in deep-water environments. The Piddington Mound area, southwest of Ireland, was selected for 3D reconstruction from high-definition video data acquired with an ROV. Six ML algorithms, namely: Support Vector Machines, Random Forests, Gradient Boosting Trees, k-Nearest Neighbours, Logistic Regression and Multilayer Perceptron, were trained in two datasets of different sizes (1,000 samples and 10,000 samples) in order to evaluate accuracy variation between approaches in relation to the number of samples. The Piddington Mound was classified into four classes: live coral framework, dead coral framework, coral rubble and sediment and dropstones. Parameter optimisation was performed with grid search and cross-validation. Run times were measured to evaluate the trade-off between processing time and accuracy. In total, eighteen variations of ML algorithms were created and tested. The results show that four algorithms yielded $f1$ -scores >90% and were able to discern between the four classes, especially those with usually similar characteristics, e.g., coral rubble and dead coral. The accuracy variation among them was 3.6% which suggests that they can be used interchangeably depending on the classification task. Furthermore, results on sample size variations show that certain algorithms benefit more from larger datasets whilst others showed discrete accuracy variations (<5%) when trained in datasets of different sizes.

3.1 Introduction

Cold-water corals (CWC) play an important role in deep-sea ecosystems (Rogers, 1999; Costello et al., 2005). Species such as *Lophelia pertusa* (synonymized to *Desmophyllum pertusum*) (Addamo et al., 2016) and *Madrepora oculata* are formed by three-dimensional (3D) calcareous frameworks that can baffle bypassing sediments (Dorschel, 2003; Titschack et al., 2015; Lim et al., 2020a), and given favourable environmental conditions (e.g., hydrodynamic regime, temperature and nutrient supply), they can form positive topographic features such as coral patches, mounds, reefs and giant carbonate mounds (Mortensen et al., 1995; Freiwald, 2002; Wheeler et al., 2005a; Freiwald et al., 2005; Wheeler et al., 2007; Guinan et al., 2009; Roberts et al., 2009; Lim et al., 2017; 2020b). CWC reefs are associated with highly diverse faunal assemblages (Rogers, 1999) being often considered “biodiversity hotspots” of deep-sea environments (Turley et al., 2007; Lim et al., 2018a; Boolukos et al., 2019; Dorey et al., 2020) as they act as a refuge and nursery for deep-sea species, including commercial fish (Fosså et al., 2002; Turley et al., 2007). The association of not only live coral frameworks but also dead corals and coral rubbles is also considered key for the development of microhabitats that promote enhanced biodiversity (Luckhurst et al., 1978; Buhl-Mortensen et al., 2010; Henry et al., 2017; Lim et al., 2020b; Clippele et al., 2021). However, these vital ecosystems are impacted by anthropogenic activities such as bottom trawling, deep sea mining and oil and gas exploration (Rogers, 1999; Wheeler et al., 2005a; Turley et al., 2007; Boolukos et al., 2019). Studies evidence the impact of fishery-related activities and climate change in CWCs, suggesting that coral health is affected by trawling and/or dredging (Rogers, 1999; Roberts et al., 2000; Wheeler et al., 2005b; Althaus et al., 2009), ocean acidification, CO² emission and ocean uptake leading to a decrease of ocean pH (Turley et al., 2007) and rising temperatures (Gori et al., 2016).

As 3D structures, CWCs enhance small scale spatial variability and influence species biodiversity and nutrient cycling (Graham and Nash 2013; Pizarro et al., 2017; Lim et al., 2018b). However, the analysis of these environments often rely on planar derivatives from 1D or 2D estimates of coral reef coverage, rugosity and distribution

that may disregard key variations on coral habitats, as accurate vertical and volumetric information may not be integrated into the analysis (Cocito et al., 2003; Courtney et al., 2007; Goatley and Bellwood 2011; House et al., 2018). Whilst 2D approaches are useful to produce rapid estimates of coral reef health (Kornder et al., 2021), they may overlook the naturally complex 3D morphology of corals reefs and maximise the tendency of large coral colonies to obscuring understory biota (Goatley and Bellwood 2011; Bergh et al., 2021; Kornder et al., 2021) represented by the so-called 'canopy' effect. Therefore, there is a demand for novel mapping methods that will take into account the 3D morphological structure of CWC in order to better understand the key drivers and controls of CWC environments.

Structure from Motion (SfM) is a relatively new branch of photogrammetry that can be applied to geospatially reconstruct seabed habitats whilst providing detailed descriptors regarding coral reef conditions and microhabitats (Ferrari et al., 2017; Pizarro et al., 2017; Conti et al., 2019; Price et al., 2019, 2021; Calders et al., 2020; Lim et al., 2020c; Urbina-barreto et al., 2021, 2022). In contrast to traditional photogrammetry, SfM uses algorithms such as Scale Invariant Feature Transform (SIFT) (Lowe, 1999) to identify matching features in a set of overlapping images whilst calculating the variations in camera orientation and position of the matched features (Carrivick et al., 2016). The process yields high-resolution 3D reconstructions of different landscapes in the form of 3D point clouds, meshes, digital elevation models (DEMs) and orthomosaics (geometrically- corrected, scaled and georeferenced mosaic of images containing RGB information) (Carrivick et al., 2016). Besides requiring less time and cost resources when compared to traditional seabed mapping techniques such as the 'chain-and-tape' method (Storlazzi et al., 2016), SfM and 3D photogrammetry enables non-destructive quantitative monitoring of: 1) biological estimates, e.g., benthic cover, coral colony health, abundance and size (Burns et al., 2015; Lange and Perry 2020; Pascoe et al., 2021); 2) physical estimates of reef terrain features such as slope, fractal dimension, surface and structural complexity (Burns et al., 2015; Figueira et al., 2015; Leon et al., 2015; Storlazzi et al., 2016; Fukunaga and Burns 2020; Urbina-barreto et al., 2021) up to very high- resolution analysis at colony

scale such as 3) sub-centimetre reconstructions of individual branches and polyps (Cocito et al., 2003; Gutierrez-Heredia et al., 2016; Lange and Perry 2020).

The application of computer vision and machine learning (ML) methods in remote sensing has contributed to unprecedented progress in automated spatial (Gilardi 1995; Pal 2005; Mountrakis et al., 2011; Belgiu and Drăgu 2016; Durden et al., 2021) and marine data analyses (Beijbom et al., 2012; Beijbom et al., 2015; Williams et al., 2019; Summers et al., 2021). The use of supervised and unsupervised ML classification methods has rapidly grown, especially in the context of underwater image analysis (Huang et al., 2011; Shihavuddin et al., 2013; Young 2018; Conti et al., 2019; Yu et al., 2019; Lim et al., 2020c; González-Rivero et al., 2020). Advancements have been made with the application of assembled ML algorithms and deep-learning such as convolutional neural networks (CNNs) to automate the annotation process by applying path-based image classification techniques to assign labels automatically to unseen images (Shihavuddin et al., 2013; Modasshir et al., 2018; Mahmood et al., 2019) and alternatively using the classified images to produce 3D models (Mohamed et al., 2020). Recent studies used CNNs such as ResNET152 to generate dense labels from sparse label annotation by extracting patches of the 3D models (Hopkinson et al., 2020). Other studies have created a combined approach by using CNN for sparse label annotation through patch extraction and using the resulting classified images to produce 3D models of the environment (Pierce et al., 2021). Point clouds are composed by a set of points containing coordinates (X, Y, Z) oriented in a cartographic space. 3D models derived from point clouds are useful to optimise the trade-off between precision and geometric complexity (Poux et al., 2018). However, the semantic segmentation of point clouds, while having numerous real world applications, has been considered a challenge (Poux et al., 2018; Xu et al., 2018; Yuval et al., 2021). Deep learning has advanced in favour of image segmentation and classification tasks, but its use towards semantic point cloud segmentation needs to be further explored (Karara et al., 2021). Representation models such as PointNET which learn features directly from unstructured point data, i.e., dense clouds/point clouds are considered state-of-the-art techniques for dense cloud classification (Qi et al., 2017). However, these frameworks require large annotated datasets and

computational requirements for producing meaningful results (Gilardi 1995; Yuval et al., 2021). In the context of deep-water environments, the lack of training data available has reportedly been the bottleneck for advances of ML algorithms (Roelfsema et al., 2021; Walker et al., 2021; Mohamed et al., 2022). Although annotation frameworks to gather specific data from underwater environments have been developed (Beijbom et al., 2012; Beijbom et al., 2015; Zurowietz et al., 2018), there is still a need for specifically designed dataset benchmarks for the application of robust ML methods for 3D points clouds of deep-water environments. Additionally, researchers are continuously working towards minimising the effects of the “black box issue” to properly understand the machine decision process in the classification and how parameters and data affect the output (Gilardi 1995; Castelvechi, 2016).

In this study, we intend to tackle the automatic classification problem with a different approach. Instead of classifying the images to produce the 3D models, we created a classification framework to classify the 3D models directly, minimizing the need to provide extensive manual image annotations. As of this moment, this study is the first of the field to provide a comparison and performance analyses of six ML algorithms applied in 3D point clouds of CWC reefs. A number of studies have performed comparison analyses using widely used ML algorithms such as Support Vector Machines (SVMs), Neural Networks (NNs) and common ensemble methods, e.g., Random Forests (RFs) and Gradient Boosting Trees (GBTs) in multispectral imagery (Dixon et al., 2008; Liu et al., 2017; Zhang et al., 2017; Fu et al., 2018; Jodzani et al., 2019). Although insightful contributions can be drawn from such analyses, these studies focused on land use and classification of urban areas. Therefore, the fundamental properties of these algorithms for marine mapping applications are not well understood and advancements are required in order to progress on seabed habitat mapping of larger areas. To this end, this research bridges the knowledge gap between ML and CWC classification in 3D by providing a comparison of ML algorithms, performance analyses whilst delivering an optimised workflow for classification of photogrammetry derived data.

This study applies ML classification to 3D photogrammetric reconstructions of coral reef habitats to analyse the outputs, data requirements and constraints of the coupled

application of both methods. We aim to develop a novel classification method using SVM, RF, k-Nearest Neighbours (kNN), Logistic Regression (LR), GBT and Multilayer Perceptron (MLP) algorithms. Furthermore, this paper presents the results of an empirical comparison of seven supervised learning algorithms and evaluated by four performance criteria (*f1* score, receiver operating characteristic (ROC) curves, area under the curve (AUC) scores and *f1* scores of k-fold cross- validations). Each algorithm was analysed based on: 1) its suitability to the given classification task 2) their hyperparameters and processing times, and; 3) its performance with two datasets of different sample sizes (1,000 and 10,000 samples) to analyse the trade-off between accuracy, processing times and sample size.

3.2 Study Area

The Piddington Mound is a CWC mound located in the Belgica Mound Province (BMP), Porcupine Seabight, NE Atlantic. The mound was selected to develop this study given the existence of high-definition (HD) video data and bathymetric surveys covering a large extent of the area (Lim et al., 2017), the evidence of temporal changes in coral cover (Bohlukos et al., 2019) and dynamic sediment facies (Lim et al., 2018a; Conti et al., 2019). The BMP is a designated Special Area of Conservation (SAC) under the EU Habitats Directive located on the eastern margin of the Porcupine Seabight, southwest of Ireland (Figure 3.1 A, B).

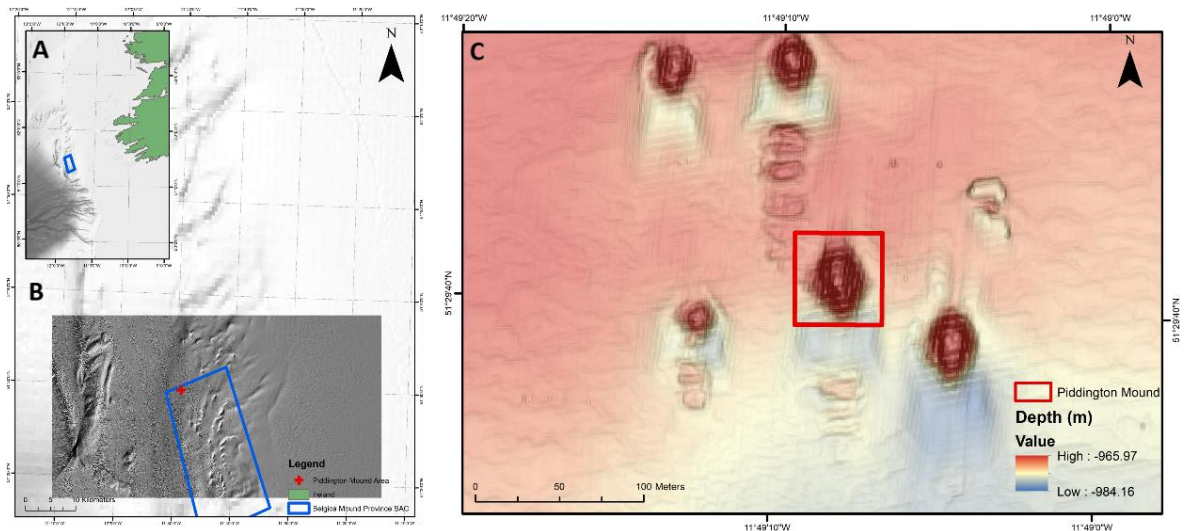


Figure 3.1: Map of the study site (A): Porcupine Seabight location relative to Ireland. The blue box indicates the location of the Belgica Mound Province (BMP) Special Area of Conservation (SAC) (B) Close view of the Porcupine Seabight and BMP with the Piddington Mound. (C) Bathymetric map of the Moira Mounds and location of the Piddington Mound Area (red box) within adjacent mounds.

The province hosts numerous CWC carbonate mounds and reefs dominated by framework-building scleractinian species *Lophelia pertusa* and *Madrepora oculata* (Huvenne et al., 2002; Wheeler et al., 2005b; Mol et al., 2007). Coral mounds in the BMP range from 3 to 10 m in height, e.g., the Moira Mounds (Wheeler et al., 2005b; Foubert et al., 2011; Wheeler et al., 2011), of which the Piddington Mound is one of the largest (Lim et al., 2017), to giant carbonate mounds that are up to 150 m high, e.g., the Challenger (Thierens et al., 2013), Therese Mound (Mol et al., 2007) and Galway Mound (Foubert et al., 2006; Dorschel et al., 2007). The Moira Mounds occur between 800 and 1,100 m water depth (Wheeler et al., 2005b) and have a semi-circular to ridge-shaped morphology with predominant alignment to the current direction (Wheeler et al., 2011). Comprising a small extent of 60 × 40 m in area (Foubert et al., 2006), the Moira Mounds are divided into a northern area, upslope area, midslope area and downslope area, where the Piddington Mound is located (Wheeler et al., 2011; Lim et al., 2018a). The Piddington Mound has documented current speeds of 40 cm s⁻¹ (Lim, 2017). Previous work carried out by Lim et al. (2017) have identified four distinct facies in the Piddington Mound area namely: live coral framework, dead coral framework, coral rubble and hemipelagic sediment with dropstones. These facies occur in a ring-like distribution, with coral rubble, live coral and dead coral frameworks distributed around the mound summit, forming an ‘on

mound' setting with high presence of corals, whilst sediments and drop stones occur where seabed becomes flat (Lim et al., 2017). These facies have also been adopted herein.

3.3 Materials and Methods

This study is divided into a photogrammetry workflow to produce the 3D reconstructions of the Piddington Mound area and the development of multiclass classifications for these 3D point clouds. The photogrammetry process is outlined below followed by a description of the ML workflow. An overview of the classification algorithms, the model selection and the accuracy assessment is then further outlined. The ML workflow was executed in Python 3.8. Processing was executed with an Intel Core i7 CPU, 32 Gb RAM with NVIDIA Geforce RTX 2070 (8 Gb) graphics card (GPU). Here, the terms classification model, classifier and estimator are used interchangeably.

3.3.1 Photogrammetry

The data used in this study were acquired during the research cruise CE20011 (Lim et al., 2020b). The video data were collected with the ROV *Holland 1* which is equipped with 11 camera systems. For this survey, two of these camera systems were used, namely: the HDTV camera (HD Insite mini-Zeus with HD SDI fibre output), and a Kongsberg OE 14–208 digital stills camera. The ROV is also mounted with two deep-sea lasers spaced at 10 cm for scaling. Positioning data were acquired with a Sonardyne Ranger 2 ultra- short baseline (USBL) beacon with accuracy of 1.3% of slant range (measurement of relative position from time of return signal from ROV transponder to the USBL in relation to the Turnaround Travel Time (TAT) and underwater sound velocity) similar to (Lim et al., 2020a; Oliveira et al., 2021). The ROV was kept at a height of approximately 2 m above the seabed with a survey speed of <0.2 knots during the video data collection. HD videos (1080p) were acquired at a rate

of 50 frames per second (FPS) and stored as *.mov files. The section of the survey used herein was derived from one ROV dive performed as a grid with 35 lines spaced at 5 m from each other in a N-S direction. Previous seabed imaged acquisition studies showed that video mosaicking of a mound or grid of spaced lines yield more representative mosaics of CWC mounds (Lim et al., 2018a). In total, 4 h and 49 min of HD videos were recorded, summing 241.7 gigabytes (GB) of video data collected in one ROV dive.

The ROV video and navigation data were used to produce and georeference the 3D reconstructions. Video frames were extracted at a rate of 1 FPS from the raw video data with Blender (version 2.78). For the 3D point cloud reconstruction, frames were extracted and imported into Agisoft Metashape Professional version 1.7.2 (Agisoft-LLC 2020). Key point limit and tie point limits were chosen based on an empirical approach. Camera optimisation was performed after the camera alignment to refine the exterior and interior camera orientation parameters and triangulated tie point coordinates (Agisoft LLC, 2020). The dense point cloud was georeferenced with frame-relative USBL positioning data with X and Y coordinates, depth, yaw, pitch, roll and accuracy (°). The constant 10 cm distance from the parallel lasers of the ROV was used for scaling the model. The laser distance provides a measurement to scale and validate geometric uncertainties in the reconstruction process. The site was separated into an on-mound and off-mound areas based on the depth difference between grid areas. The dense point cloud generated in the process was used for training and validation of the methodology.

A total of 7,301 images (1920 × 1,080 pixel resolution) were used in the point cloud reconstruction process. Camera optimization was applied using the focal length (f), radial distortion coefficients (K1- K3), and tangential distortion coefficients (P1- P2). The photo alignment process was performed with a key point limit of 20,000 and a tie point limit of 2,000. The yaw, pitch, roll and accuracy values were set to 135°, 0°, 0°, and 2 m, respectively.

3.3.2 Multiclass Classification Of 3D Point Clouds

3.3.2.1 Pre-processing

In this study, the point cloud created during the photogrammetry stage was used for the development of the ML workflow. The labelled dataset was created from the manual segmentation of point cloud objects into four classes. The classes were chosen to best represent the environmental variability of the specific area. The on-mound section of the Piddington Mound was chosen for reconstruction as it contained the largest volume of CWC and coral rubbles. The classes were outlined based on the analysis distribution of the regions of interest (ROIs), in this case, live coral framework (LCF), dead coral framework (DCF) and coral rubble (CR), apart from sediments and drop stones (SD).

Previous studies carried out in the Piddington Mound area have also adopted this classification scheme as it best represents the location (Lim et al., 2017). This potentially allows further comparisons over the temporal changes over the mound. A detailed class description was carried out for each class based on spatial distribution studies of the Piddington Mound and the Porcupine Bank Canyon (Lim et al., 2017; Appah et al., 2020). Table 3.1 provides a description of each class. The annotation process was performed in CloudCompare using the high- resolution orthomosaic as a visual aid.

Table 3.1: Class label definitions used in the study

CLASS	DESCRIPTION
1. Live Coral Framework (LCF)	Coral presenting any signs of identifiable living parts (polyps or mucus-covered frameworks evident) although major proportions of the coral framework may be dead. Coral polyps, skeletal casing are usually bright, white or orange in colour (Appah et al., 2020)
2. Sediments And Dropstones (SD)	Sediment (sand or mud) and dropstones, includes sediment waves, ripples and scour marks.
3. Dead Coral Framework (DCF)	Coral framework which has no identifiable living parts. Identified by darker gray or brown skeleton (Appah et al., 2020)

4. Coral Rubble (CR)	Coral rubble is recognisable by biogenic material where >50% of detached dead coral fragments, shell fragments and sediment is observed (Lim et al., 2017).
-----------------------------	---

The point cloud was composed of a set of points and their relative feature values. Each point contained information of 7 features (X, Y, Z, R, G, B and Normal_y) and its ground truth label. Following the feature selection and labelling, the point cloud was separated into two datasets, namely dataset 1, composed of 1,000 samples and dataset 2, consisting of 10,000 samples. Each dataset was split into training and validation sets at a ratio of 75%/25%. In addition, a test set composed of 10,000 random samples was created from the points that remained from the initial point cloud after the train and test set were extracted. Therefore, the model evaluation was performed on the validation set and an additional cross-validation was performed on the test set.

After the training and testing splits were performed, datasets were scaled with a MinMax scaler, which was fitted on the training set of dataset 2 and applied to the remainder datasets (validation set of dataset 2 and training and validation sets of dataset 1). Synthetic Minority Oversampling Technique (SMOTE) (Chawla et al., 2002) was applied to balance the training set. SMOTE works by making a linear interpolation of a randomly selected observation from the minority class with another k-nearest neighbour of the same minority class. The new sample is created from the interpolation of those two samples. Previous studies have considered the oversampling approach to be beneficial for classification results in commonly used classifiers (Last et al., 2017) and CNNs (Buda et al., 2018).

3.3.2.2 Classification algorithms

3.3.2.2.1 *Random Forest*

The RF algorithm is a tree-based ensemble classifier where each classifier is created using a random vector sampled from the input vector. Each tree provides a unit vote for the most popular class to classify the input vector (Pal 2005). Predictions are

generated as an ensemble estimate from a number of decision trees from bootstrap samples (termed bagging) (Hengl et al., 2018). RF classifications have been successfully applied in a number of marine (Robert et al., 2016; Misiuk et al., 2019; Shang et al., 2021; Price et al., 2022) and terrestrial studies (Schratz et al., 2019). Comparison performance studies in land cover suggest that RF has provided the best performance in object-based classification tasks (Ma et al., 2017).

In this study, the grid search and cross-validation was performed to find the best number of estimators, i.e., number of trees, and the number of maximum features to be considered for the best split. The number of estimators was set with options of ranging from 10 to 1,000 and the number of features was set to a range of 1–7 for the first sets of RFs. The Scikit-learn options 'auto' and 'log2' were also considered. The best-performance RF model was selected based on the accuracy considering the permutation of the grid search parameters. The other parameters were set to the default of Scikit-learn class. The full list of parameters can be found on the Scikit-learn webpage. In the case of RFs, four classifiers were trained with four different options of parameter grids. Each of these four variations of RFs was trained with datasets 1 and 2, resulting in 8 trained RF models.

3.3.2.2.2 *Gradient Boosting Trees*

GBT is another popular ensemble method closely related to RFs. The method trains an ensemble of trees based on minimising the loss function i.e., the measure of fit between the actual data and the modelled data, in each interaction. Each tree is improved by attempting to minimise the error of the previous tree (Jodzani et al., 2019). Boosting refers to combining these weak learners, i.e., single decision trees so that the following tree model corrects the errors of the previous one (Friedman, 2001). The learning rate is also introduced to control the robustness of the classifier. Empirical studies have attested to the efficiency of GBTs over other supervised learning algorithms (Caruana and Niculescu-Mizil 2006). The decision trees in the GBT tend to be robust with respect to the addition of irrelevant features (Friedman, 2001). Here, the parameter grid defined to find the optimal GBT parameters with the grid search were: learning rate, number of estimators, the maximum depth of estimators

and the subsample rate. The learning rate was set to options of 0.0001, 0.001, 0.01, 0.1, 1. The number of estimators was defined to 10, 50, 100, 500 and 1,000. The subsample rate was set to a range of 0.5, 0.7 and 1. Although the default subsampling value in Scikit-learn is set to 1, the range of values was expanded to include other two values, 0.7 and 0.5, which is the suggested value of subsampling according to Buitinck et al. (2013). It is noteworthy that, if subsampling is set to a value >1 , the classifier changes to Stochastic Gradient Boosting (Buitinck et al., 2013). In this study, two GBT classifiers were trained with one set of parameter grids.

3.3.2.2.3 *Support Vector Machines*

The SVM concept is based on the construction of optimal hyperplanes in a high dimensional space between a proximal training sample and the separating hyperplane (Pedregosa et al., 2011). SVMs have a regularization parameter 'C' and gamma (γ) that allow the control of the decision function complexity and the level of influence of each sample towards it. The main advantages of the SVMs are the regularization parameter, which allows the user to control over-fitting, the kernel trick and the convex optimization problem (no local minima) (Liu et al., 2017). Other studies suggested that one advantage of SVMs is that the objective function is convex which reflects on a relatively straightforward solution for the optimization problem even though the training involves nonlinear optimization (Bishop, 2006). Furthermore Bishop (2006), affirms that the number of basis functions in SVM models is usually much smaller than the number of training points. Although they increase with the size of the training set, it still has the capacity to be computationally faster than other classifiers. The choice of kernel is also an equally crucial parameter (Burges, 1998) as it gives SVMs the capacity to insert the data into a higher-dimensional space, so that data that is not linearly separable in the original input space can be separable in a higher-dimensional one (Russell and Peter, 2010). The use of radial basis function (RBF) kernel has been the most common choice in recent studies as it generally provides a good trade-off between time efficiency and accuracy (Jodzani et al., 2019; Pedregosa et al., 2011; Friedman, 2013). In this study, three options of kernels on the grid search parameters were: polynomial, sigmoid and RBF. The range of regularization 'C' and γ parameters were set to 0.1, 110,100, and 1,0.1,0.01,0.001 respectively.

3.3.2.2.4 Logistic Regression

LR, also known as logit regression or MaxEnt, is a parametric supervised classification algorithm based on general linear models. The concept behind LR is that the classifier takes a set of input variables and creates an estimate probability for the target variable. The parameter grid established for the LR grid search was defined by a choice of penalty parameters l_1 , l_2 , *elasticnet*, or none and regularization 'C' parameter values. The optimisation algorithm was set to the options of *liblinear*, *sag*, *saga*, *lbfgs* which are termed the solvers. Empirical studies suggest that the use of the solver depends on the amount of data available (Buitinck et al., 2013). In small datasets, for example, *liblinear* can be considered a good choice whereas *saga* and *sag* can be faster for large datasets. The latter is also considered a good choice for high-dimensional data. Furthermore, in multiclass problems, the multinomial loss can only be handled by the solvers *saga*, *sag*, *lbfgs* and *newton-cg*. The scaling is also important as the solvers *saga* and *sag* can only reach faster convergence on features with proximal scales (Buitinck et al., 2013). For this study, three LR models were created with different sets of grid search parameters. Each model was trained in datasets 1 and 2, thus leading to 6 trained LRs.

3.3.2.2.5 Multilayer Perceptron

MLP is a feedforward neural network composed by an input layer, a number of hidden layers, an output layer and loss functions. Each layer is connected to the following one and that connection is controlled by a weight factor. The weights are learned using gradient descent techniques such as backpropagation during the training phase aiming to minimise the error function (Weinmann et al., 2015). MLP is considered a successful model as it uses parametric forms of the basic functions in which parameter values are adapted during training (Bishop 2006). Studies have successfully used MLPs for point cloud segmentation of urban scenes (Weinmann et al., 2015). In this study, MLPs models were trained with grid search set for the maximum number of iterations of 500, 1,000 and 2000. The optimiser options were *lbfgs*, *sgd*, *adam* and the choice of activation functions were set to *logistic*, *tanh*, *relu*. The l_2 penalty (or α) parameter

was set to the values of 0.0001, 0.001, 0.005. The number of hidden layers was defined by doing test runs from the default hidden-layer size and performing adjustments based on the results of the previous run. The remaining parameters, such as the initial learning rate and learning rate schedule for weight updates were set with Scikit-learn default values. MLP were the most intensively trained classifiers in the model selection. In total, seven MLPs were created with 7 different grid search parameter grids.

3.3.2.2.6 k-Nearest Neighbours

kNN is a memory-based method that works by assigning to each test vector the same label as the closest example from the training set (Bishop 2006). In this study, the kNN grid search parameters were set to a number of neighbours of 3, 5, 11, 19, and 25. Note that the number of neighbours has to be an odd number to avoid ties on the vote of neighbours. The weight options were set to 'uniform' or 'distance' and the choice of metrics were between Euclidean or Manhattan. Studies suggest that the choice of either Manhattan and Euclidean distances depend on whether the dimensions measured have similar or dissimilar properties. Generally, Euclidean is often recommended when measuring similar properties, whereas Manhattan is recommended for dissimilar properties (Russell and Peter 2010). Due to the use of distance metrics across feature dimensions, it is important to apply normalization to the data. This prevents generating different nearest neighbours if the scale changes across dimensions, e.g., from metres to centimetres, as the total distance will not be affected by the change of scales (Russell and Peter 2010). The remaining Scikit-learn parameters were set to default values. Here, two kNNs were trained with the same set of grid search parameters.

3.3.2.3 Model Selection

3.3.2.3.1 Grid search with cross validation

The performance of a model strongly depends on the values of hyperparameters (Schratz et al., 2019; Wu et al., 2019). Grid search is a method for performing

hyperparameter tuning to determine optimal values of each model. For each parameter configuration, a 5-fold-cross-validation was performed on the training set. When fitting the grid search method on a dataset, all possible combinations of parameter values are evaluated, and the best combination is maintained. In this study, each classifier and assigned parameter grid were trained in both dataset 1 and dataset 2. The selection of parameter grids for the grid searches of each classifier was based on both recommended literature and empirical analysis after each run. Each grid search process resulted in the best accuracy classifier for that specific parameter grid, along with the best combination of parameters that resulted in that classification. In total, 18 variations of the 6 classification algorithms mentioned above were trained.

3.3.2.3.2 *Performance assessment*

To evaluate the performance of the classification algorithms developed in this study, the classification output of each algorithm was compared against the ground-truth and the *f1* and AUC scores were calculated. k-fold cross-validation was applied and the *f1* score for each fold was obtained with the mean and standard deviation of the total of folds. k-fold cross validation is a performance evaluator widely used in supervised learning. In the validation process, the training set is split into k smaller sets, or folds. In each split, the model is trained using k-1 of the smaller sets of the training data and the remaining fold is used for the validation. This is executed until the model completes the round of k folds (Buitinck et al., 2013). The percentage difference between two classifier accuracies was calculated by the difference between the accuracies divided by their average and multiplied by 100. Run times (CPU and wall times) for classifier training and validation were also computed as this is also a critical factor influencing decision-making for ML pipelines (Rudall, 1978).

For the purpose of model comparisons, the classifiers were separated into two groups: Group 1—classifiers trained with 1,000 samples and Group 2—classifiers trained with 10,000 samples. The accuracy assessment was performed in two phases, namely: first accuracy assessment and second accuracy assessment (k-fold cross-validation). ROC curves and AUC were produced for each classifier to evaluate the interclass performance. The ROC curve is obtained by a threshold variation on the discriminant

values of the classifier. The curve is a representation of the ratio of the true positives against the ratio of false negatives (Rudall, 1978), depicting the relative trade-offs between benefits (true positives) and costs (false positives) (Fawcett, 2006). The AUC is equivalent to the probability that the classification model will classify a randomly chosen sample into the given class, thus giving a relative measure of the quality of the classifier for each class (Fawcett, 2006).

3.4 Results

3.4.1 3D Reconstructions

The dense cloud generated from the photogrammetry process was composed of 90,912,889 points. The depth difference between the on-mound and off-mound parts was approximately (± 20 m). The on-mound section represents the coral reef area, with relative higher abundance of coral colonies and coral patches. Figure 3.2 shows the planar view of the 3D reconstruction of the on-mound section and its relative ground-truth labels generated from the expert annotation. The class distribution of the ground-truth labels in the on-mound area shows that the percentage of LCF (green) and DCF (yellow) are approximately the same, 4%, SD (red) represents 32% and finally, the class CR (blue) represented the majority of samples with 61% (graph c) on Figure 3.2).

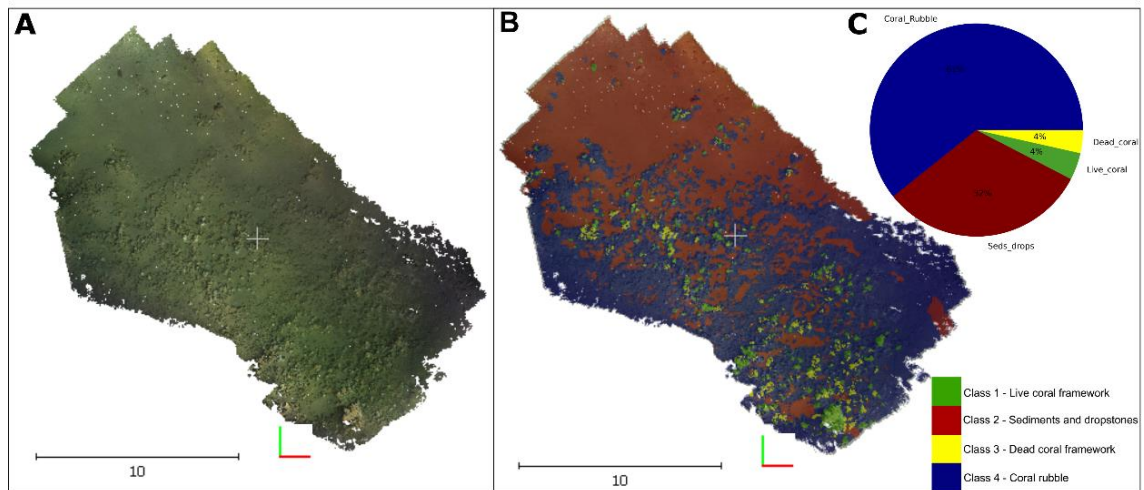


Figure 3.2: (A) Original 3D dense cloud reconstruction of the on-mound section of the Piddington Mound (B) its relative ground-truth labels (C) Percentage class distribution of the reconstructed area.

3.4.2 Multiclass Classification Results

3.4.2.1 Model Selection

Results of the grid search show that, from the 18 classifiers, only 6 classifiers or 33.3% obtained accuracies below <60% (red dotted line in Figure 3.3).

In order to make an objective comparison of the most efficient classifiers, the classifiers that yielded $f1 > 60\%$ on the first accuracy assessment and $f1 > 73\%$ (lowest accuracy value obtained) on the second accuracy assessment were selected for an in-depth analysis. Supplementary Table 3.2 in Supplementary Material summarises the results of the top performing classifiers trained in each group with their respective $f1$ accuracies of the first accuracy assessment, $f1$ accuracy of the cross-validation, best combination of parameters from the grid search and finally, the processing time to train each model. The sections below describe the results of the model selection of each of the groups of algorithms trained, including parameter selection, $f1$ accuracy of group 1 and group 2, accuracy variations and training times.

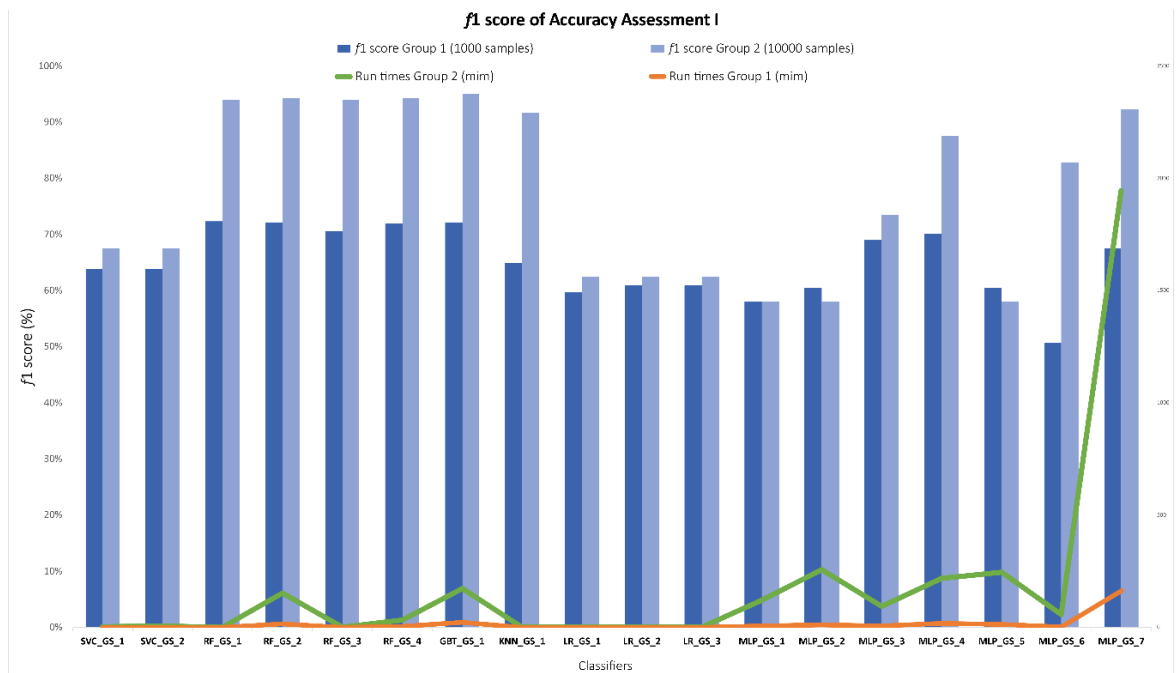


Figure 3.3: Bar plot showing the $f1$ accuracy results of all 18 classifiers grouped by algorithm type. Light blue bars represent classifiers trained in group 2 (dataset 2, 10,000 samples) and dark blue bars represent classifiers trained in group 1 (dataset 1, 1,000 samples). The red dotted line indicates $f1 < 60\%$ threshold. Run times (in minutes) for group 1 (orange) and group 2 (green) represented in the secondary axis on the right are plotted against $f1$ accuracy.

3.4.2.1.1 Support Vector Machines

Two SVM classifiers were trained with two different options of kernel parameters. The first SVM (SVC_GS_1), also referred as support vector classifier (SVC) herein, was trained with two choices of kernels: RBF, and sigmoid. The second (SVC_GS_2) with was trained with 3 kernel options: RBF, polynomial and sigmoid. The choice range of the penalty parameter C and the gamma parameter were equal for both. Each of these SVC models was trained in the dataset 1 and dataset 2, resulting on four different trained classifiers: namely SVC_GS_1_1000, SVC_GS_1_10000, SVC_GS_2_1000 and SVC_GS_2_10000. All variations of SVCs chose the combination of 'C': 100, 'gamma': 1, 'kernel': 'rbf' as their best parameters. Among them, the best accuracy SVCs were SVC_GS_1_1000 and SVC_GS_2_10000 (Supplementary Table 3.2). The accuracy variation between these classifiers across group 1 and group 2 was 3.62% which represented a percentage difference of 5.51% and a 5.67% increase in $f1$ scores from group 1 to group 2. In addition, the percentage difference on the cross-validation accuracies was of 0.14%.

3.4.2.1.2 *Random Forest*

In the four RF classifiers trained, the number of estimators varied at different ranges, going from 10 to 1,000 in steps of 10 or 10 to 100 in steps of 10. Classifiers with the highest accuracies on the first accuracy assessment also held the larger number of estimators (1,000). Among these classifiers the best accuracy RFs on group 1 was RF_GS_1_1000 ('max_features': 1, 'n_estimators': 90) and RF_GS_2_10000 ('max_features': 2, 'n_estimators': 1,000) on group 2 (Supplementary Table 3.2). The accuracy variation between these classifiers was 21.98% on the first accuracy assessment, which represents a 26.38% difference and a 30.40% increase in accuracy from the best accuracy RF on group 1 to the best accuracy classifiers in the group 2 (Figure 3.3). The overall intra-model accuracy (RF with same model parameters trained in group 1 and group 2) also showed an increase of 31.16% from RFs trained in group 1 to RF trained in group 2. The difference was less pronounced on the cross-validation accuracies, showing an accuracy difference of 0.67% and only an increase of 0.67% from the RF in group 1 to the RF in group 2. The overall intra-model accuracy difference on the cross-validation assessment was 0.032%. The processing time of the RF_GS_2_10000 was the third longest of all classifiers (2 h 31 min 52 s), staying behind of the top performing GBT (2 h 52 min 56 s), and MLP (1 day 8 h 25 min 8 s).

3.4.2.1.3 *Gradient Boosting Trees*

GBT was the classifier with the highest accuracy among all classifiers, reaching an accuracy of 95.11% on the first accuracy assessment and 80.46% on the cross-validation. The top GBT, namely GBT_GS_1_10000 was trained in group 2 with the combination of the parameters: 'max_depth': 9, 'n_estimators': 1,000, 'subsample': 0.5, 'learning_rate': 0.1. The second GBT, GBT_GS_1_1000 was trained in group 1 and reached an *f1* accuracy of 72.15%. The combination of parameters that yielded this classifier was 'max_depth': 7, 'n_estimators': 1,000, 'subsample': 0.7, 'learning_rate': 0.1. Both classifiers chose the maximum number of estimators set on the grid search (1,000) (Supplementary Table 3.2). The accuracy variation between both GBTs on the first accuracy assessment was 22.95%, which represents a 27.45% difference and a 31.81% accuracy increase from the GBT trained in group 1 and the GBT trained in group 2. The cross-validation percentage differences show a much lower gap, with a

decrease of <1% (0.16%) from GBT_GS_1_1000 to GS_GS_1_10000. The processing time of the GBT_GS_1_10000 was the second longest of all classifiers (2 h 52 min 56 s), only staying behind of the top performing MLP (1 day, 8 h 25 min 8 s).

3.4.2.1.4 *k-Nearest Neighbours*

The kNN was also among the top-performing classifiers, with a *f1* accuracy of 91.6% on the first accuracy assessment and 76.18% on the cross-validation. The first of the two kNNs trained with equal parameters, namely, KNN_GS_1_1000, trained in group 1 resulted in an *f1* accuracy of 64.9% and *f1* accuracy of 76.02% on the cross-validation. The second kNN was trained in group 2, namely KNN_GS_1_10000, which yielded the aforementioned *f1* of 91.6%. Both models chose the same set of parameters: 'metric': 'manhattan', 'n_neighbours': 3, 'weights': 'distance' (Supplementary Table 3.2). The percentage difference between the accuracies of these classifiers was 34.18%. Overall, the accuracy of the top-performing classifier KNN_GS_1_10000 (group 2) represented an increase of 41.14% on the accuracy relative to the KNN_GS_1_1000 (group 1). kNNs were among the algorithms with the fastest run times, requiring only 2.54s for training of the KNN_GS_1_10000.

3.4.2.1.5 *Logistic Regression*

Among the LRs, the best-performing classifiers provided an accuracy of 62.4% and a 74.1% accuracy on the cross-validation for the LR on group 2, namely LR_GS_2_10000. The combination of grid search parameters that resulted in the classifiers were 'C': 100, 'Penalty': 'l2', 'solver': 'sag'. The best LR on group 1 provided an *f1* score of 60.95% and 74.01% on the cross-validation. This classifier was created by the grid search with the following set of parameters: 'C': 100, 'Penalty': 'l1', 'solver': 'liblinear' (Supplementary Table 3.2). The percentage difference between the accuracies of these two classifiers was 2.35%. There was a 2.37% increase in the *f1* accuracy of LR_GS_2_10000 in relation to LR_GS_3_1000. The overall intra-model accuracy (LRs with the same model parameters but trained in group 1 and group 2) also showed an accuracy increase of 3.21% for LRs trained in group 2, i.e., larger datasets, in comparison to group 1. The overall result put the LRs among the classifiers that yielded the lowest accuracies with an average *f1* of 60.51% and 62.4% for LRs in group 1 and group 2, respectively. However, it was also one of the algorithms with the fastest training times (<5 s).

3.4.2.1.6 Multilayer Perceptrons

Each of the seven generated MLPs was trained in both group 1 and group 2, resulting in a total of 14 trained MLPs. One of these MLPs, the MLP_GS_7_10000 trained in group 2, was among the top four classifiers in this study. The MLP_GS_7_10000 produced an *f1* of 92.3% on the first accuracy run and 77.7% on the cross-validation. The combination of parameters that resulted in this classifier were: 'hidden_layer_sizes': (200, 200, 200, 200, 200, 200, 200, 200, 200), 'activation': 'tanh', 'solver': 'adam', 'learning rate': '0.0001', 'max_iter': 2000, 'early_stopping': 'false'. Among group 1, the best MLP was MLP_GS_4_1000, with an *f1* of 70.1% on the first accuracy assessment and 76.9% on the cross-validation. The choice of parameters from the grid search were: hidden_layer_sizes': (80, 80, 80, 80, 80, 80, 80), 'activation': 'tanh', 'solver': 'adam', 'learning rate': '0.0001', 'max_iter': 2000, 'early_stopping': 'false' (Supplementary Table 3.2). The percentage difference of the MLP_GS_7_10000 and the MLP_GS_4_1000 was 27.33%. The first represented a 31.66% *f1* increase relative to the latter. The overall intra-model *f1* accuracy showed a 16.98% increase in the accuracy of MLPs trained in group 2 (10,000 samples dataset), in relation to group 1 (1,000 samples dataset). The processing time of the MLP_GS_7_10000 was the longest of all classifiers (1 day, 8 h 25 min 8 s), followed by GBT (2 h 52 min 56 s) and RF (2 h 31 min 52 s). It was noted that there was a substantial increase in the run time with the increase of dataset sizes. The classifier MLP_GS_7 had a training time of 2 h 42 min 47 s on group 1. When trained in group 2, the same classifier required 1 day, 8 h 25 min 8 s to complete its training phase. Considering that the same exact parameters were used, this represents a 1,094.90% increase in the run time. The run time percentage difference of run times between the classifier of best accuracy (GBT_GS_1_10000) and the MLP_GS_7_10000 is 167.34%, which exemplifies the trade-off between run time and accuracy.

3.4.2.2 Classification Output

The classification outputs of the top four classifiers: 1) GBT_GS_1_10000, 2) RF_GS_2_10000 3) MLP_GS_7_10000 and 4) KNN_GS_1_10000 are shown in Figure

3.4. In this study, classifiers that were above our established threshold of $f1 > 90\%$ were ranked as the top-performing classifiers. The difference between the classification results and the ground-truth was calculated for each of the aforementioned classifiers (Figure 3.5).

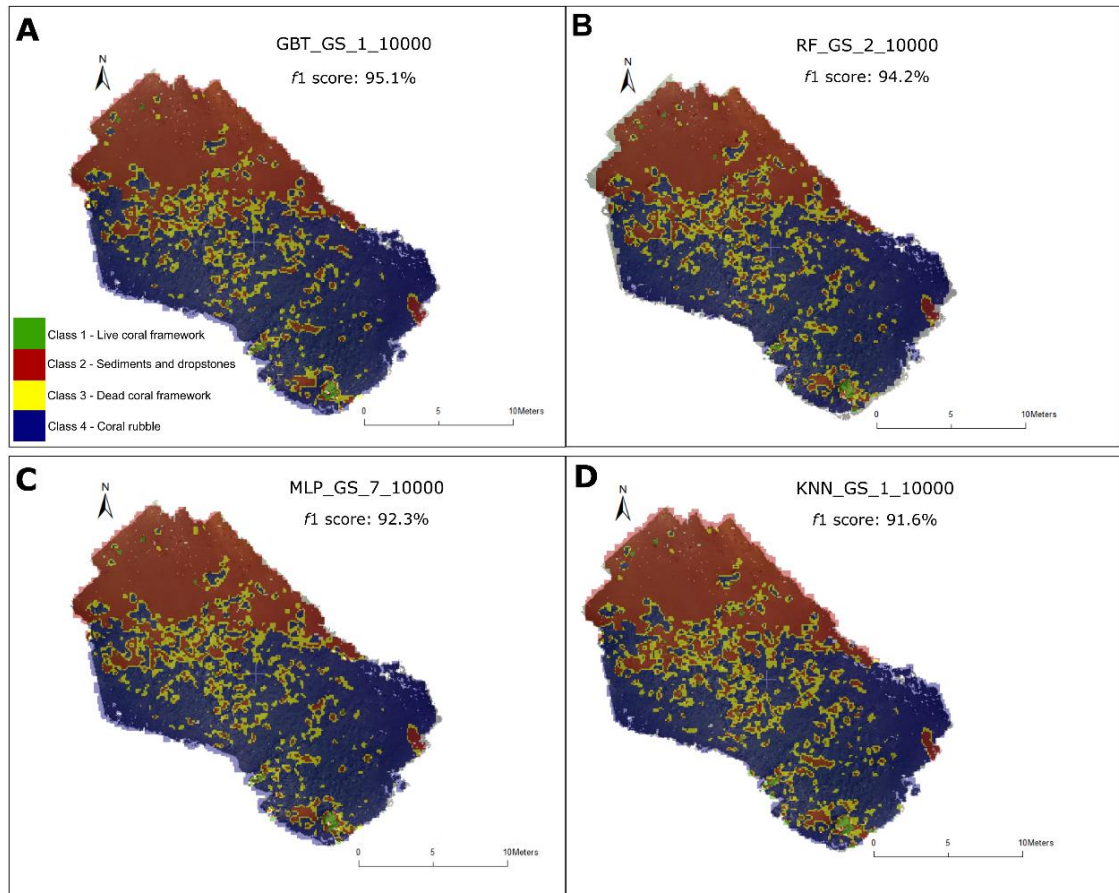


Figure 3.4: Classification outputs of the top four performing classifiers ($f1$ score $> 90\%$). (A) Classification output of the GBT classifier GBT_GS_1_10000, $f1$ score: 95.1% (B) Classification output of the RF classifier RF_GS_2_10000, $f1$ score: 94.2% (C) Classification output of the MLP classifier MLP_GS_7_10000, $f1$ score: 92.3% (D) Classification output of the KNN classifier KNN_GS_1_10000, $f1$ score: 91.6%.

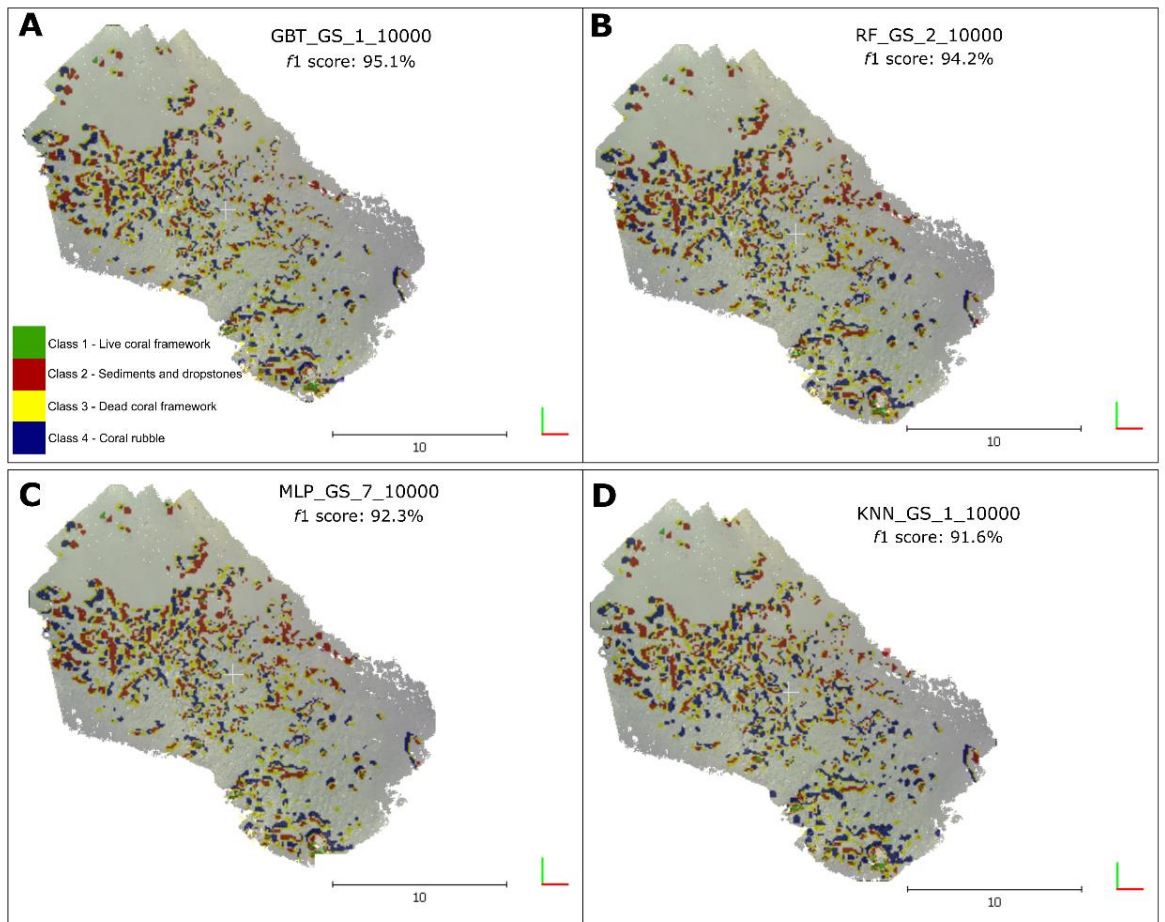


Figure 3.5: Difference of class distribution from the ground-truth labels against the classification output labels of the top four performing classifiers ($f1$ score $> 90\%$). (A) Difference of classification output vs. ground truth of the GBT classifier GBT_GS_1_10000, $f1$ score: 95.1% (B) Difference of classification output vs. ground truth of the RF classifier RF_GS_2_10000, $f1$ score: 94.2% (C) Difference of classification output vs. ground truth of the MLP classifier MLP_GS_7_10000, $f1$ score: 92.3% (D) Difference of classification output vs. ground truth of the KNN classifier KNN_GS_1_10000, $f1$ score: 91.6%.

ROC curves were calculated for these classifiers (Figure 3.6) and AUC scores were calculated for each of the four labels. Points located on the upper right near the X axis typically represent classifiers that make positive classifications based on strong evidence.

Herein, classifiers with the lowest accuracies were those below our established threshold of $f1 < 60\%$. Note that the ROC curves for each label are farther away from the upper left (0, 1) (Figure 3.7).

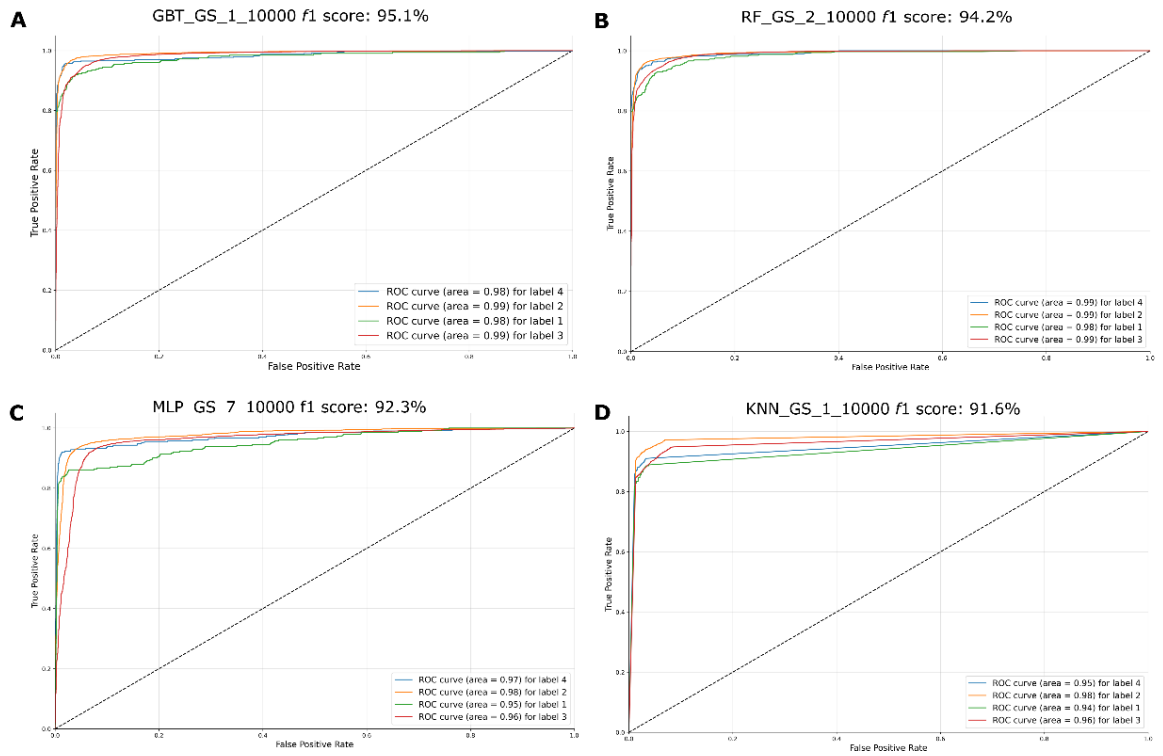


Figure 3.6: ROC curves of the four best-performing classifiers ($f1 > 90\%$). The name of the classifiers and their $f1$ score obtained on the first accuracy assessment were placed on the top of their respective graph. The AUC score for each label is placed on the lower right side of each graph. Label 1 = LCV, label 2 = SD, label 3 = DCF, label 4 = CR. (A) ROC curve of GBT classifier GBT_GS_1_10000, $f1$ score: 95.1% (B) ROC curve of the RF classifier RF_GS_2_10000, $f1$ score: 94.2% (C) ROC curve of the output of the MLP classifier MLP_GS_7_10000, $f1$ score: 92.3% (D) ROC curve of the KNN classifier KNN_GS_1_10000, $f1$ score: 91.6%.

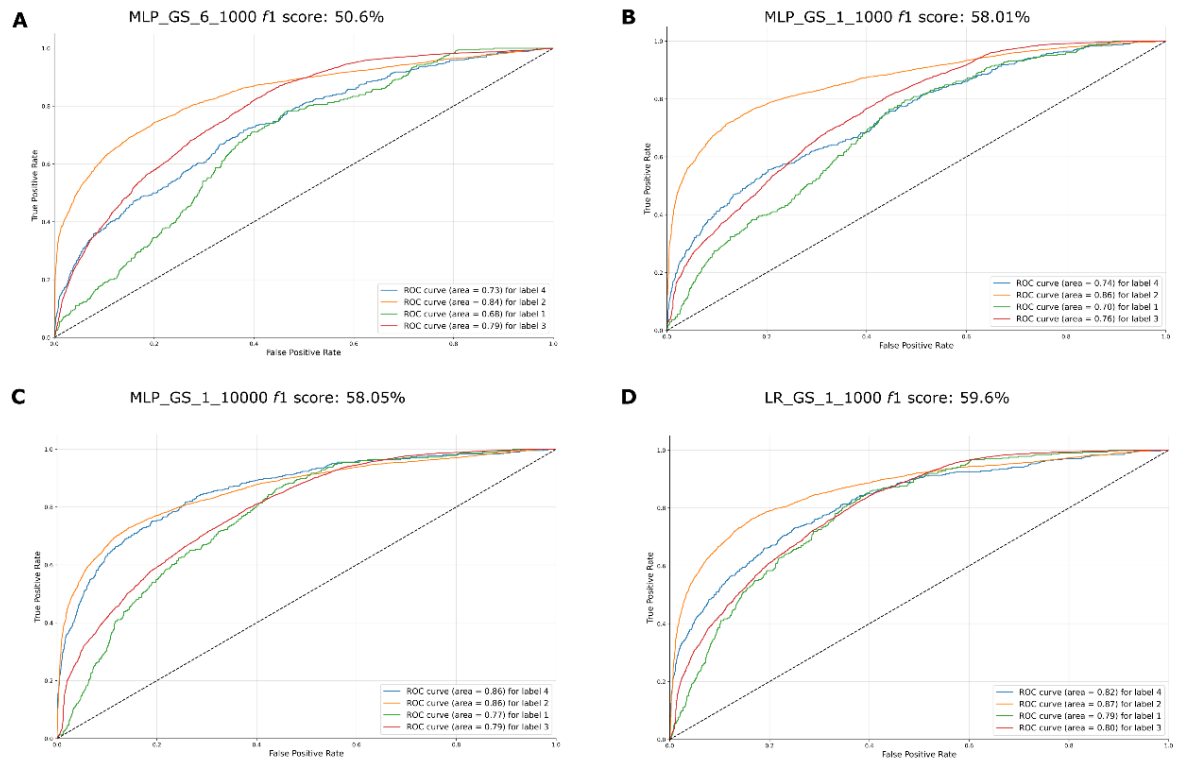


Figure 3.7: ROC curve of the worst performing classifiers ($f1 < 60\%$). The name of the classifiers and their $f1$ score obtained on the first accuracy assessment were placed on the top their respective graph. The AUC score for each label is placed on the lower right side of each graph. Label 1 = LCF, label 2 = SD, label 3 = DCF, label 4 = CR. (A) ROC curve of MLP classifier MLP_GS_6_1000, $f1$ score: 50.6% (B) ROC curve of the MLP classifier MLP_GS_1_1000, $f1$ score: 58.1% (C) ROC curve of output of the MLP classifier MLP_GS_1_10000, $f1$ score: 58.08% (D) ROC curve of the LR classifier LR_GS_1_1000, $f1$ score: 59.6%.

3.5 Discussion

The Piddington Mound is a highly dynamic area with confirmed temporal (Bohlukos et al., 2019) and facies changes (Lim et al., 2018a; Conti et al., 2019). Studies show that mound surface changed by almost 20% from 2011 to 2015. The CR, DCF, and SD classes showed variations of $<7.5\%$, whereas the LCF remained similar of the 4 years given their inherent slow growth rates (Lim et al., 2018a). Further studies developed at species level found a concerning decline in biodiversity in the same time interval, especially in the percentage coverage of *Madrepora oculata* with linear decline rates estimated at 0.17%/year (Bohlukos et al., 2019). This study shows that, in 2021, this section of the Piddington Mound used had the same proportion of LCF and DCF the

on-mound area (4%) followed by the SD class, representing 32% and finally, the class CR which represented the majority of samples (61%) (Figure 3.2, graph c).

In this study, 241.7 GB worth of data were transformed into an ecologically meaningful and compact dataset (<5.2 gigabytes) that allows for analyses of intra-habitat patterns of the study area. This represents one of the key advantages of 3D photogrammetry and SfM for seabed habitat mapping. Furthermore, 3D reconstructions, orthomosaics and DEMs of CWC derived from video data allows for contextualised analysis of coral colonies and associated fauna (Price et al., 2021). The increasing use of such datasets indicates an advancement in relation to per-image analyses, which may hinder the investigation of spatial patterns, volume density and structural complexity variations.

3.5.1 Machine Learning And 3D Reconstructions Of Coral Reef Environments

The results show that four ML algorithms yielded *f1* accuracies of >90% and were able to successfully discern between classes (Figure 3.6), especially those with usually similar characteristics, e.g., coral rubble and dead coral, which is a task that is often challenging to both the machine and the human eye (Bryson et al., 2013; Beijbom et al., 2015; Hopkinson et al., 2020). Four algorithms, i.e., LR and three variations of the MLP yielded accuracies below our minimum threshold of 60%. Given the absence of similar studies in 3D photogrammetry and ML in CWC habitats, the results herein contribute to delineating the suitability of specific algorithms for initial assessments, providing key information to future studies in CWC habitats.

3.5.2 Classifier Performance

The classifiers GBT, RF, MLP and kNN trained in group 2 (dataset of 10,000 samples) were the most accurate classifiers on the first assessment, in that order. Nonetheless, the percentage difference between the top-ranked classifier, GBT (*f1* = 95.11%) and the fourth-ranked classifier, kNN (*f1* = 91.7%) in the first accuracy assessment was low, approximately 3.65%. These results agree with other experimental comparison studies applied to high- resolution satellite imagery for land use/land cover (Jodzani

et al., 2019). Jodzani et al. (2019) showed that MLPs models were the most accurate for those cases. However, there was a small difference in the classification accuracies between these and other algorithms like SVMs and GBTs. Therefore, the use of these algorithms is still versatile to deal with mapping of complex landscapes (Jodzani et al., 2019). The study also showed that the use of CNNs for the same classification task does not necessarily lead to more accurate results when compared to common classifiers. This agrees with other studies which compared the use of SVMs and sparse auto-encoders for multispectral imagery classifications, where SVMs outperformed auto-encoders (Liu et al., 2017).

Herein, the performance of MLP classifiers trained in this study also agrees with the aforementioned studies. Whilst one of the trained MLPs yielded one of the highest accuracies (MLP_GS_7_10000, *f1* score 92.3%), three of the 14 trained MLPs yielded the lowest accuracies (MLP_GS_1_1000, MLP_GS_1_1000, MLP_GS_6_1000) (Figure 3.3), dropping the overall MLP average performance to 67.62%. Grid search results showed that MLPs were prone to choose hidden layer options with more neurons on them. In addition, all MLP classifiers selected the solver *adam* for weight optimization as the final parameter on the grid search. *Adam* represents a stochastic gradient-based optimizer (Kingma and Lei 2015). The solver is recommended for noisy or sparse gradients and is recommended for problems with large data or parameters (Kingma and Lei 2015). Empirical studies performed in *Scikit-learn* also suggest that *Adam* is highly robust for large datasets while converging fast and giving good performances (Buitinck et al., 2013).

RFs have been widely applied for a number of classification tasks in remote sensing (Pal 2005; Rodriguez-Galiano et al., 2012; Belgiu and Drăgu 2016) and specifically, in marine and coastal studies (Seiler et al., 2012; Gauci et al., 2016; Robert et al., 2016; Misiuk et al., 2019; Zelada Leon et al., 2020; Price et al., 2022). In our study, the RF was among the top four classifiers. The *f1* score average across all RFs trained was 82.9%. Our analysis showed that using a smaller dataset resulted in models with a lower number of estimators and lower accuracy. However, the suitability of the RF for our classification task can be influenced by a number of factors, one of them is the way RF deals with decision trees in the classification. Studies affirm that RF models

reduce the correlation between the decision trees in the ensemble by randomly sampling features, which can lead to an increase in accuracy when compared to other ensemble methods (Jodzani et al., 2019).

SVMs have been successfully applied for remote sensing applications (Melgani and Bruzzone 2004; Deilmai et al., 2014; Liu et al., 2017) and automated image analysis (Friedman 2013; Beijbom et al., 2012). In a few cases, SVM-based classifications have outperformed other common classification algorithms, such as kNN and decision trees (Friedman, 2013; Beijbom et al., 2012), especially when considering the amount of training data available (Liu et al., 2017). Similar to Friedman (2013) the results herein show that the best-performance SVM was created with RBF kernel. Studies have also suggested that SVM can perform well in cases where there are few training samples (Melgani and Bruzzone 2004). In this study, it was noticed that the SVM were indeed robust with respect to sample size variations, resulting in a small percentage increase of 5.67% when trained in group 1 and group 2. Nonetheless, kernel methods can be sensitive to over-fitting, and the kernel choice has been considered the biggest limitation of the SVM approach (Burges 1998; Liu et al., 2017). Although this limitation was addressed by testing a range of kernel options on the grid-search, the SVMs yielded an undistinguished performance on the first accuracy assessment compared to other classifiers. However, they matched the performance of the top four algorithms on the second accuracy assessment, i.e., k-fold cross-validation. It was noted that one of the advantages of the SVM is that, depending on the choice of kernel, the run times are considerably lower when compared to the top four classifiers. However, the kernel choice will have a considerable impact on the processing as there are data limitations when using specific kernels in accordance with the Big O notation (Chivers and Sleightholme 2015). For example, the polynomial kernel is not advised when the dataset has more than 10,000 samples as the SVM training time scales at least quadratically with the number of samples (Tsang et al., 2005).

kNNs yielded the 4th place in our classifiers rank ($f1$ score = 91.6%) whilst having the lowest training time (2.54 s). Studies performed with ROV-derived images have found that kNNs have also outperformed SVMs and NNs in smaller datasets (Shihavuddin et

al., 2013). However, when datasets get larger, their effectiveness reduces (Shihavuddin et al., 2013). As mentioned previously, the choice of weighted distance for the kNN can often be evaluated by the similarity across feature dimensions (Russell and Peter, 2010). In our grid search results, both kNNs trained in group 1 and group 2 chose Manhattan distance among the parameter grid of the best accuracy models. This suggests that the classifier may have interpreted the feature dimensions as dissimilar. kNNs can suffer with the curse of dimensionality when facing high-dimensionality data (Russell and Peter 2010) therefore, reducing the dimensions of the feature space with, e.g., PCA can increase kNN accuracy (Shihavuddin et al., 2013). A similar issue can happen with the MLPs as, although MLPs can reduce the weight of irrelevant variables close to zero, they may take a long time to converge and consequently, to find a local minimum (Settles and Burr, 2003).

GBT was the most successful classifier in our study, with an *f1* accuracy of 95.11% on the first accuracy assessment. Accordingly, studies suggest that GBTs have outstanding performance when compared to RF, SVMs and NN in different classification tasks (Caruana and Niculescu-Mizil, 2006; Becker et al., 2018). In studies using bathymetric data to predict diversity and abundance of fish, GBTs were considered the most appropriate technique to select meaningful predictors (Pittman et al., 2009). However, GBTs may be more impacted by the amount of training data in relation to other classifiers, like SVMs. Our study revealed that GBTs had a 31.81% accuracy increase from the GBT trained in group 1 and the GBT trained in group 2, which suggests that the amount of sample data may have a strong impact on the classification. It is also noteworthy this GBT had the second-longest processing time (2 h 52 min 56 s).

Our results show that the LR was among the classifiers with the worst performance on the first accuracy assessment. Studies have shown that the parametric nature of LR classifiers can lead to a more constrained model with limited complexity (Russell and Peter, 2010). Previous comparison studies also suggested that Naïve Bayes, logistic regression and variations decision trees are among the poorest-performing algorithms (Caruana and Niculescu-Mizil 2006). However, this is dependent on the type of task performed. Hence, generalisations should be made with caution.

3.5.3 Sample Size And Accuracy Variation

The quantity of training data is one of the biggest challenges in effectively applying ML for automated seabed mapping (Beijbom et al., 2012; Zurowietz et al., 2018; Williams et al., 2019; Durden et al., 2021). Results on the 1,000 sample dataset and 10,000 sample dataset show that voting ensemble classifiers like kNNs, RF, GBT have better performance and benefit more from a larger dataset than kernel methods such as SVM (Figure 3.3). The small difference in *f1* scores between variations of the same algorithms like SVM (5.51%) and LR (2.35%) suggests that these algorithms are more robust to dataset size variations. As previously mentioned, studies affirm that SVM can perform well in cases where there are few training samples (Melgani and Bruzzone 2004).

Results show that RF is highly sensitive to data size, showing a percentage increase of approximately 30.40% on the average *f1* accuracy from 1,000 samples to 10,000 samples datasets. GBT had a 31.81% increase in the average *f1* accuracy when trained in 10,000 sample datasets. kNN had a 41.23% increase in the average accuracy when trained in the 10,000 samples dataset. MLPs showed a percentage increase of 16.98% on the accuracy when trained in the 10,000 samples dataset. In contrast, LR showed only a 2.37% increase on the average *f1* accuracy. Although this low variation can indicate a positive stability across different sample sizes, it is noteworthy that the LR behaved poorly in all test runs. Similarly, SVMs showed a regular resistance to the dataset variations, with a difference of less than 6% (5.51%) on the average *f1* accuracy from group 1 to group 2, noting that the overall performance was also low. The stability of SVMs against different dataset sizes may be due to their ability to handle high- dimensionality data with a relatively low number of training samples (Melgani and Bruzzone 2004; Jodzani et al., 2019). This is explained by the general concept behind SVMs, which relies on the separation of classes with a maximum plane of separability, using boundary points to create the decision margin, thus making it independent of the dimensionality of feature space (Dixon et al., 2008).

The number of parameters implies the need for more training samples and computational requirements (Liu et al., 2017). The amount of training data required by NNs increases exponentially with the increase of feature dimensionality of the input data (Dixon et al., 2008). Similar to automated classification studies with seabed images (Durden et al., 2021), our results show that overall classification is improved by increasing the size of the training dataset.

On the other hand, cross-validation results showed that there is an increase in the *f1* scores of the classifiers in group 1. The classifiers trained with 1,000 samples showed a better performance in the *f1* accuracy for each fold *k* in the *k*-fold cross-validation. The opposite trend was found for group 2, the accuracy dropped and stabilized on the same level as the classifiers of group 1. Therefore, whilst evaluating the performance of the classifiers on parts of the dataset, i.e., cross-validation, the performance of the classifiers of group 1 was similar to the classifiers in group 2. This indicates that in particular instances and metrics, such as when using cross-validation instead of only a single validation set, the classifiers may be used interchangeably. Additionally, cross-validation may be a suitable approach to avoid overfitting when having small sample sets. Overall, in the case of deep-water environments, collecting a large number of labelled samples, dealing with naturally imbalanced datasets and the lack of benchmark data are limitations that need to be overcome in order to advance to the deep learning spectrum (Beijbom et al., 2012; Durden et al., 2021). The choice of classifiers based on their parametric or non-parametric properties is also important when considering the dataset sizes. In the case of parametric models, such as LR, the number of parameters it needs to make a decision is independent of how much data is used. This property can be useful when datasets are small, as in this case, it is convenient to have a strong constraint on the hypothesis to avoid overfitting (Russell and Peter 2010). However, when the dataset is large, it is better to have more flexible models where the data can have more influence on the learning pattern. Hence, non-parametric models, such as kNNs which cannot be characterized by a delimited set of parameters, can be a better fit. As mentioned, the disadvantage of some non-parametric methods is the amount of data samples necessary.

Another important aspect is the training run times of algorithms in each group. The run times of group 1 algorithms were significantly lower than those in the group 2. It is acknowledged that, despite the fact that MLPs are efficient, the training is time-consuming (Dixon et al., 2008). A relevant example of run time differences is the classifier MLP_7. Although this MLP had 26.8% decrease in $f1$ scores when trained in group 1, the run time was 91.63% faster. These results can be taken into consideration when evaluating not only the loss versus run time ratio, but also the processing resources required to run MLPs and the accuracy desired. This is supported by the grid search results, which show that the MLPs yielded similar accuracies in both groups, i.e., independent of the dataset size they were trained with. As NNs, the need for a number of training samples in MLPs can exponentially increase with the dimension of the input of feature space (Dixon et al., 2008). The results herein contribute to informing the user about the *ad hoc* strategy to be used when considering the accuracy variation in relation to the processing time. Thus, the user needs to evaluate a set of variables, ranging from the project timeframe, type of object of interest and the computer resources available.

3.6 Conclusions

Six state-of-art ML classifiers were applied and evaluated for the multiclass classification of high-resolution 3D reconstructions of CWCs environments. A workflow for classification using photogrammetry and ML was proposed for CWC environments of the Irish margin. The multiclass classification results show that certain algorithms proved to be more suited for the specific classification task proposed here, namely: GBTs, RF, kNN, and MLP with $f1 > 90$. In contrast, the worst-performing classifiers were LR, and two variations of MLP with $f1 < 60\%$. Furthermore, the results suggest that the overall classification is improved by increasing the size of the training dataset. However, it is possible to reach high accuracy results with datasets of 10,000 samples and medium accuracy results with datasets of 1,000 samples. The analysis of the 3D reconstructions shows that, in 2021, this section of the Piddington Mound used had the same proportion of LCF and DCF the on-mound

area (4%). The CR class dominated the majority of the samples with 61%, followed by the SD class, representing 32%. The study developed herein shows that ML and photogrammetry enable automated classification of habitats associated with CWC. The proposed workflow will allow for improvements to environmental monitoring strategies by increasing coverage area and optimising data processing.

3.7 References

- Addamo, A. Ma, Vertino, A., Stolarski, J., García-Jiménez, R., Taviani, M., and Machordom, Annie (2016). Merging scleractinian genera: The overwhelming genetic similarity between solitary *Desmophyllum* and colonial *Lophelia*. *BMC Evol. Biol.* 16 (1), 108–117. doi:10.1186/s12862-016-0654-8
- Agisoft LLC (2020). Agisoft metashape user manual. Professional Edition, St. Petersburg Publisher: Agisoft LLC, 160. https://www.agisoft.com/pdf/metashape-pro_1_7_en.pdf (accessed March 12, 2022).
- Althaus, F., Williams, A., Schlacher, T. A., Kloser, R. J., Green, M. A., Barker, B. A., et al. (2009). Impacts of bottom trawling on deep-coral ecosystems of seamounts are long-lasting. *Mar. Ecol. Prog. Ser.* 397, 279–294. doi:10.3354/meps08248
- Appah, J. K. M., Lim, A., Harris, K., O’Riordan, R., O’Reilly, L., Wheeler, A. J., et al. (2020). Are non-reef habitats as important to benthic diversity and composition as coral reef and rubble habitats in Submarine Canyons? Analysis of controls on benthic megafauna distribution in the Porcupine Bank Canyon, NE Atlantic. *Front. Mar. Sci.* 7, 831. doi:10.3389/fmars.2020.571820
- Becker, C. E., Häni, N., d’Angelo, E., and Strecha, C. (2018). Classification of aerial photogrammetric 3D point clouds. *Photogramm. Eng. remote Sens.* 84 (5), 287–295. doi:10.14358/PERS.84.5.287
- Beijbom, O., Edmunds, P. J., Roelfsema, C., Smith, J., Kline, D. I., Neal, B. P., et al. (2015). Towards automated annotation of benthic survey images: Variability of human experts and operational modes of automation. *PLoS ONE* 10 (7), e0130312–e0130322. doi:10.1371/journal.pone.0130312
- Beijbom, O., Peter, J., Kline, D. I., Mitchell, B. G., and Kriegman, D. (2012). Automated annotation of coral reef survey images. *Proc. IEEE Comput. Soc. Conf. Comput. Vis. Pattern Recognit.*, 1170. –77. doi:10.1109/CVPR.2012.6247798
- Belgiu, M., and Drăgu, L. (2016). Random forest in remote sensing: A review of applications and future directions. *ISPRS J. Photogrammetry Remote Sens.* 114, 24–31. doi:10.1016/j.isprsjprs.2016.01.011
- Bergh, J. v. d., Chirayath, V., Li, A., Torres-Pérez, J. L., and Segal-Rozenhaimer, M. (2021). NeMO-net – gamifying 3D labeling of multi-modal reference datasets to support automated marine habitat mapping. *Front. Mar. Sci.* 8. doi:10.3389/fmars.2021.645408
- Bishop, C. M. (2006). *Pattern recognition and machine learning*. Information science and statistics. New York: Springer. <https://link.springer.com/book/9780387310732>.
- Boolukos, C. M., Lim, A., O’Riordan, R. M., and Wheeler, A. J. (2019). Cold-water corals in decline – a temporal (4 Year) species abundance and biodiversity appraisal of

complete photomosaiced cold-water coral reef on the Irish margin. *Deep Sea Res. Part I Oceanogr. Res. Pap.* 146, 44–54. doi:10.1016/j.dsr.2019.03.004

Bryson, M., Johnson-Roberson, M., Pizarro, O., and Williams, S. B. (2013). Colour-consistent structure-from-motion models using underwater imagery. *Robotics Sci. Syst.* 8, 33–40. doi:10.7551/mitpress/9816.003.0010

Buda, M., Maki, A., and Maciejki, A. (2018). A systematic study of the class imbalance problem in convolutional neural networks. *Neural Netw.* 106, 249–259. doi:10.1016/j.neunet.2018.07.011

Buhl-Mortensen, L., Gooday, A. J., Levin, L. A., Priede, I. G., Buhl-Mortensen, P., et al. (2010). Biological structures as a source of habitat heterogeneity and biodiversity on the deep ocean margins. *Mar. Ecol.* 31 (1), 21–50. doi:10.1111/j. 1439-0485.2010.00359.x

Buitinck, L., Louppe, G., Blondel, M., Pedregosa, F., Mueller, A., Grisel, O., et al. (2013). API design for machine learning software: Experiences from the scikit-learn project, 1–15. <http://arxiv.org/abs/1309.0238>.

Burges, C. J. C. (1998). A tutorial on support vector machines for pattern recognition. *Data Min. Knowl. Discov.* 28, 121–167. doi:10.1023/a:1009715923555

Burns, D., Gates, R. D., and Takabayashi, M. (2015a). Integrating structure-from-motion photogrammetry with geospatial software as a novel technique for quantifying 3D ecological characteristics of coral reefs. *PeerJ* 2015 (7), e1077. doi:10.7717/peerj.1077

Burns, J. H. R., Delparte, D., Gates, R. D., and Takabayashi, M. (2015b). Utilizing underwater three-dimensional modeling to enhance ecological and biological studies of coral reefs. *Int. Arch. Photogramm. Remote Sens. Spat. Inf. Sci.*, 61–66. XL-5/W5 (5W5): 61–66. doi:10.5194/isprsarchives-XL-5-W5-61-2015

Calders, K., Stuart, P., Ferrari, R., Leon, J., Armston, J., Asner, G. P., et al. (2020). 3D imaging insights into Forests and coral reefs. *Trends Ecol. Evol.* 35 (1), 6–9. doi:10.1016/j.tree.2019.10.004

Carrivick, J. L., Smith, M. W., and Quincey, D. J. (2016). *Structure from motion in the geosciences*. Chichester, UK: John Wiley & Sons. doi:10.1002/9781118895818

Caruana, R., and Niculescu-Mizil, A. (2006). “An empirical comparison of supervised learning algorithms,” in *ICML 2006 - Proceedings of the 23rd International Conference on Machine Learning*, 161–168.

Castelvecchi, D. (2016). The black box of AI. *Nature* 538 (7623), 20–23. doi:10.1038/538020a

Chawla, N. V., Bowyer, K. W., Hall, L. O., and Philip Kegelmeyer, W. 2002. “Smote: Synthetic minority over-sampling technique.” *jair.* 16, 321. doi:10.1613/jair.953

- Chivers, I., and Sleightholme, J. (2015). "An introduction to algorithms and the Big O notation," in Introduction to programming with fortran: With coverage of fortran 90. Third Edition (Cham: Springer International Publishing), 95, 771–674. doi:10.1007/978-3-319-17701-4
- Clippele, L. H., Ramiro-Sánchez, B., Kazanidis, G. J. Vad, S. Turner, R. N. Glud, and Roberts, J. M. (2021). Mapping cold-water coral biomass: An approach to derive ecosystem functions. *Coral Reefs* 40 (1), 215–231. doi:10.1007/s00338-020-02030-5
- Cocito, S., Sgorbini, S., Peirano, A., and Valle, M. (2003). 3-D reconstruction of biological objects using underwater video technique and image processing. *J. Exp. Mar. Biol. Ecol.* 297 (1), 57–70. doi:10.1016/S0022-0981(03)00369-1
- Conti, L. A., Lim, A., and Wheeler, A. J. (2019). High resolution mapping of a cold-water coral mound. *Sci. Rep.* 9 (1), 1016. doi:10.1038/s41598-018-37725-x
- Costello, M. J., McCrea, M., Freiwald, A., Lundälv, T., Jonsson, L., Bett, B. J., et al. (2005). "Role of cold-water *Lophelia pertusa* coral reefs as fish habitat in the NE atlantic," in Cold-water corals and ecosystems (Springer Berlin Heidelberg), 771–805. doi:10.1007/3-540-27673-4_41
- Courtney, L. A., Fisher, W. S., Raimondo, S., Oliver, L. M., and Davis, W. P. (2007). Estimating 3-dimensional colony surface area of field corals. *J. Exp. Mar. Biol. Ecol.* 351 (1–2), 234–242. doi:10.1016/j.jembe.2007.06.021
- Deilmay, B. R., Ahmad, B. B., and Zabihi, H. (2014). Comparison of two classification methods (MLC and SVM) to extract land use and land cover in johor Malaysia. *IOP Conf. Ser. Earth Environ. Sci.* 20 (1), 012052. doi:10.1088/1755-1315/20/1/012052
- Dixon, B., and Candade, N. (2008). Multispectral landuse classification using neural networks and support vector machines: One or the other, or both? *Int. J. Remote Sens.* 29 (4), 1185–1206. doi:10.1080/01431160701294661
- Dorey, N., Gjelsvik, Ø., Kutti, T., and Janina, V. (2020). Broad thermal tolerance in the cold-water coral *Lophelia pertusa* from arctic and boreal reefs. *Front. Physiol.* 10, 1636–1712. doi:10.3389/fphys.2019.01636
- Dorschel, B., Hebbeln, D., Foubert, A., White, M., and Wheeler, A. J. (2007). Hydrodynamics and cold-water coral facies distribution related to recent sedimentary processes at Galway mound west of Ireland. *Mar. Geol.* 244 (1–4), 184–195. doi:10.1016/j.margeo.2007.06.010
- Dorschel, B. (2003). Late quaternary development of a deep-water carbonate mound in the northeast atlantic. PhD Thesis, 90. Geowissenschaften PhD.
- Durden, J. M., Brett Hosking, B., and Ruhl, H. A. (2021). Automated classification of fauna in seabed photographs: The impact of training and validation dataset size, with

- considerations for the class imbalance. *Prog. Oceanogr.* 196, 102612. doi:10.1016/j.pocean.2021.102612
- Fawcett, T. (2006). An introduction to ROC analysis. *Pattern Recognit. Lett.* 27 (8), 861–874. doi:10.1016/j.patrec.2005.10.010
- Ferrari, R., Figueira, W. F., Pratchett, M. S., Boube, T., Adam, A., and Byrne, M. (2017). 3D photogrammetry quantifies growth and external erosion of individual coral colonies and skeletons. *Sci. Rep.* 7 (1), 16737–16739. doi:10.1038/s41598-017-16408-z
- Figueira, W., Ferrari, R., Weatherby, E., Porter, Ae, Hawes, S., and Byrne, M. (2015). Accuracy and precision of habitat structural complexity metrics derived from underwater photogrammetry. *Remote Sens.* 7 (12), 16883–16900. doi:10.3390/rs71215859
- Fosså, J. H., Mortensen, P. B., and Furevik, D. M. (2002). The deep-water coral *Lophelia pertusa* in Norwegian waters: Distribution and fishery impacts. *Hydrobiologia* 471, 1–12. doi:10.1023/A:1016504430684
- Foubert, A., Beck, T., Wheeler, A. J., Jan, O., Grehan, A., Klages, M., et al. (2006). “New view of the Belgica mounds, porcupine Seabight, NE atlantic: Preliminary results from the polarstern ARK-XIX/3a ROV cruise,” in *Cold-water corals and ecosystems* (Berlin/Heidelberg: Springer-Verlag), 403–15. doi:10.1007/3-540-27673-4_20
- Foubert, A., Huvenne, V. A. I., Wheeler, A., Kozachenko, M., Opderbecke, J., and Henriët, J.-P. (2011). The Moira mounds, small cold-water coral mounds in the porcupine Seabight, NE atlantic: Part B—evaluating the impact of sediment dynamics through high-resolution ROV-borne bathymetric mapping. *Mar. Geol.* 282 (1–2), 65–78. doi:10.1016/j.margeo.2011.02.008
- Freiwald, A., and Roberts, J. M. (2005). *Cold-water corals and ecosystems*. Springer Berlin Heidelberg. doi:10.1007/3-540-27673-4
- Freiwald, A. (2002). “Reef-forming cold-water corals,” in *Ocean margin systems* (Springer Berlin Heidelberg), 365–85. doi:10.1007/978-3-662-05127-6_23
- Friedman, A. (2013). *Automated interpretation of benthic stereo imagery*. University of Sydney.
- Friedman, J. H. (2001). Greedy function approximation: A gradient boosting machine. *Ann. Stat.* 29 (5), 1189–1232. doi:10.1214/aos/1013203451
- Fu, T., Ma, L., Li, M., and Brian, A. (2018). Using convolutional neural network to identify irregular segmentation objects from very high-resolution remote sensing imagery. *J. Appl. Rem. Sens.* 12 (02), 1. doi:10.1117/1.jrs.12. 025010
- Fukunaga, A., and Burns, J. H. R. (2020). Metrics of coral reef structural complexity extracted from 3D mesh models and digital elevation models. *Remote Sens.* 12 (17), 2676. doi:10.3390/RS12172676

- Gauci, A., Deidun, A., and Abela, J. (2016). Machine learning for benthic sand and maerl classification and coverage estimation in coastal areas around the Maltese islands. *J. Appl. Res. Technol.* 14 (5), 338–344. doi:10.1016/j.jart.2016.08.003
- Gilardi, Nicolas (1995). Comparison of four machine learning algorithms for spatial data analysis. *Evaluation* 1–16.
- Goatley, C. H. R., and Bellwood, D. R. (2011). The roles of dimensionality, canopies and complexity in ecosystem monitoring. *PLoS ONE* 6 (11), e27307. doi:10.1371/journal.pone.0027307
- González-Rivero, M., Beijbom, O., Rodriguez-Ramirez, A., Dominic, E., Bryant, P., et al. (2020). Anjani Ganase, Yeray Gonzalez-Marrero, Ana Herrera-Reveles, et al Monitoring of Coral Reefs Using Artificial Intelligence: A Feasible and Cost- Effective Approach. *Remote Sens.* 12 (3), 489–522. doi:10.3390/rs12030489
- Gori, A., Ferrier-Pagès, C., Hennige, S. J., Murray, F., Rottier, C., Wicks, L. C., et al. (2016). Physiological response of the cold-water coral *Desmophyllum dianthus* to thermal stress and ocean acidification. *PeerJ* 2016 (2), e1606–e1616. doi:10.7717/peerj.1606
- Graham, N. A. J., and Nash, K. L. (2013). The importance of structural complexity in coral reef ecosystems. *Coral Reefs* 32 (2), 315–326. doi:10.1007/s00338-012-0984-y
- Guinan, J., Grehan, A. J., Dolan, M. F. J., and Brown, C. (2009). Quantifying relationships between video observations of cold-water coral cover and seafloor features in rockall trough, west of Ireland. *Mar. Ecol. Prog. Ser.* 375, 125–138. doi:10.3354/meps07739
- Gutierrez-Heredia, L., Benzoni, F., Murphy, E., and Reynaud, E. G. (2016). End to end digitisation and analysis of three-dimensional coral models, from communities to corallites. *PLoS ONE* 11 (2), e0149641. doi:10.1371/journal.pone.0149641
- Hengl, T., Nussbaum, M., Wright, M. N., Heuvelink, G. B. M., and Gräler, Benedikt (2018). Random forest as a generic framework for predictive modeling of spatial and spatio-temporal variables. *PeerJ* 2018 (8), e5518. doi:10.7717/peerj.5518
- Henry, L. A., and Murray Roberts, J. (2017). “Global biodiversity in cold-water coral reef ecosystems,” in *Marine animal Forests: The ecology of benthic biodiversity hotspots* (Springer International Publishing), 235–56. doi:10.1007/978-3-319-21012-4_6
- Hopkinson, B. M., KingOwenJohnson-Roberson, A. C. D. P. M., Long, M. H., Bhandarkar, Suchendra M., Long, M. H., and Bhandarkar, S. M. (2020). Automated classification of three-dimensional reconstructions of coral reefs using convolutional neural networks. *PLoS ONE* 15 (3), e0230671. doi:10.1371/journal.pone.0230671
- House, J. E., Viviana Brambilla, L. M., Pizarro, O., Madin, J. S., Dornelas, M., Madin, J. S., et al. (2018). Moving to 3D: Relationships between coral planar area, surface area and volume. *Surf. Area PeerJ* 2018 (2), e4280. doi:10.7717/peerj.4280

- Huang, Z., Brooke, B. P., and Harris, P. T. (2011). A new approach to mapping marine benthic habitats using physical environmental data. *Cont. Shelf Res.* 31 (31), 4–16. doi:10.1016/j.csr.2010.03.012
- Huvenne, V. A. I., Blondel, Ph, and Henriët, J. P. (2002). Textural analyses of sidescan sonar imagery from two mound provinces in the porcupine Seabight. *Mar. Geol.* 189 (3–4), 323–341. doi:10.1016/S0025-3227(02)00420-6
- Jodzani, S. E., Brian, J. E., and Chen, D. (2019). Comparing deep neural networks , ensemble classifiers , and support vector machine algorithms. *Remote Sens.* 11 (1), 1–24. doi:10.3390/rs11141713
- Karara, G., Hajji, R., and Poux, F. (2021). 3D point cloud semantic augmentation: Instance segmentation of 360° panoramas by deep learning techniques. *Remote Sens.* 13 (18), 3647. doi:10.3390/rs13183647
- Kingma, D. P., and Lei, J. (2015). “Adam: A method for stochastic optimization,” in 3rd International Conference on Learning Representations, ICLR 2015 (Conference Track Proceedings).1–15
- Kornder, N. A., Cappelletto, J., Mueller, B., Zalm, M. J. L., Stephanie, J., Martinez, M. J. A. V., et al. (2021). Implications of 2D versus 3D surveys to measure the abundance and composition of benthic coral reef communities. *Coral Reefs* 40, 1137–1153. doi:10.1007/s00338-021-02118-6
- Lange, I. D., and Perry, C. T. (2020). A quick, easy and non-invasive method to quantify coral growth rates using photogrammetry and 3D model comparisons. *Methods Ecol. Evol.* 11 (6), 714–726. doi:10.1111/2041-210X.13388
- Last, F., Douzas, G., and Bacao, F. (2017). Oversampling for imbalanced learning based on K-means and SMOTE. 1–19. doi:10.1016/j.ins.2018.06.056
- Leon, J. X., Roelfsema, C. M., Saunders, M. I., and Phinn, S. R. (2015). Measuring coral reef terrain roughness using ‘structure-from-motion’ close-range photogrammetry. *Geomorphology* 242, 21–28. doi:10.1016/j.geomorph.2015.01.030
- Lim, A., Adam, K., Arnaubec, A., and Andrew, J. (2018b). Seabed image acquisition and survey design for cold water coral mound characterisation. *Mar. Geol.* 395, 22–32. doi:10.1016/j.margeo.2017.09.008
- Lim, A., Huvenne, V. A. I., Vertino, A., Spezzaferri, S., and Wheeler, A. J. (2018a). New insights on coral mound development from groundtruthed high-resolution ROV-mounted multibeam imaging. *Mar. Geol.* 403, 225–237. doi:10.1016/j.margeo.2018.06.006
- Lim, A., O’Reilly, L., Macêdo Cruz de Oliveira, L., and Strachan, R. (2020a). CE20011 cruise report: Systematic monitoring survey of the Moira mound chain (SyMonS_MoM). https://www.ucc.ie/en/media/research/marinegeo/mgpdfs/SyMonS_MoM_CE20011_Cruise_Report.pdf.

- Lim, A. (2017). Spatio – temporal patterns and controls on cold-water coral reef development : The Moira mounds. Offshore Ireland: Porcupine Seabight.
- Lim, A., Wheeler, A. J., Price, D. M., O'Reilly, L., Harris, K., and Conti, L. (2020c). Influence of benthic currents on cold-water coral habitats: A combined benthic monitoring and 3D photogrammetric investigation. *Sci. Rep.* 10 (1), 19433. doi:10.1038/s41598-020-76446-y
- Lim, A., Wheeler, A. J., and Arnaubec, A. (2017). High-resolution facies zonation within a cold-water coral mound: The case of the Piddington mound, porcupine Seabight, NE atlantic. *Mar. Geol.* 390, 120–130. doi:10.1016/j. margeo.2017.06.009
- Lim, A., Wheeler, A. J., and Conti, L. (2020b). Cold-water coral habitat mapping: Trends and developments in acquisition and processing methods. *Geosciences* 11 (1), 9. doi:10.3390/geosciences11010009
- Liu, P., Kim, K., Wang, L., and Huang, F. (2017). SVM or deep learning? A comparative study on remote sensing image classification. *Soft Comput.* 21 (23), 7053–7065. doi:10.1007/s00500-016-2247-2
- Lowe, D. G. (1999). “Object recognition from local scale-invariant features,” in *Proceedings of the Seventh IEEE International Conference on Computer Vision (IEEE)*, 1150–1157. doi:10.1109/ICCV.1999.790410
- Luckhurst, B. E., and Luckhurst, K. (1978). Analysis of the influence of substrate variables on coral reef fish communities. *Mar. Biol.* 49 (4), 317–323. doi:10.1007/BF00455026
- Ma, L., Li, M., Ma, X., Cheng, L., Du, P., and Liu, Yongxue (2017). A review of supervised object-based land-cover image classification. *ISPRS J. Photogrammetry Remote Sens.* 130, 277–293. doi:10.1016/j.isprsjprs.2017.06.001
- Mahmood, A., Bennamoun, M., An, S., Sohel, F. A., Boussaid, F., Hovey, Re, et al. (2019). Deep image representations for coral image classification. *IEEE J. Ocean. Eng.* 44 (1), 121–131. doi:10.1109/JOE.2017.2786878
- Melgani, F., and Bruzzone, L. (2004). Classification of hyperspectral remote sensing–90, 1778.
- Misiuk, B., Diesing, M., Aitken, A., Brown, C. J., Edinger, Evan N., and Bell., Trevor (2019). A spatially explicit comparison of quantitative and categorical modelling approaches for mapping seabed sediments using random forest. *Geosci. Switz.* 9 (6), 254–334. doi:10.3390/geosciences9060254
- Modasshir, Md, Rahman, S., Youngquist, O., and Rekleitis, I. (2018). “Coral identification and counting with an autonomous underwater vehicle,” in *2018 IEEE international conference on robotics and biomimetics ROBIO (December, 2018)*, 524–529. doi:10.1109/ROBIO.2018.8664785

- Mohamed, H., Nadaoka, K., and Nakamura, T. (2022). Automatic semantic segmentation of benthic habitats using images from towed underwater camera in a complex shallow water environment, 1–22.
- Mohamed, H., Nadaoka, K., and Nakamura, T. (2020). Towards benthic habitat 3D mapping using machine learning algorithms and structures from motion photogrammetry. *Remote Sens.* 12 (1), 127. doi:10.3390/rs12010127
- Mol, B. De, Kozachenko, M., Wheeler, A., Alvares, H., Henriët, J., and Olu-Le Roy, K. (2007). Thérèse mound: A case study of coral bank development in the Belgica mound province, porcupine Seabight. *Int. J. Earth Sci.* 96 (1), 103–120. doi:10.1007/s00531-005-0496-x
- Mortensen, L., Martin, H., Brattegård, T., and Farestveit, R. (1995). Deep water bioherms of the scleractinian coral *Lophelia pertusa* (L.) at 64° n on the Norwegian shelf: Structure and associated megafauna. *Sarsia* 80 (2), 145–158. doi:10.1080/00364827.1995.10413586
- Mountrakis, Giorgos, Jungo, Im, and Ogole, Caesar (2011). Support vector machines in remote sensing: A review. *ISPRS J. Photogrammetry Remote Sens.* 66 (3), 247–259. doi:10.1016/j.isprsjprs.2010.11.001
- Oliveira, L., Lim, A., Conti, L. A., and Wheeler, A. J. (2021). 3D classification of cold-water coral reefs: A comparison of classification techniques for 3D reconstructions of cold-water coral reefs and seabed. *Front. Mar. Sci.* 8. doi:10.3389/fmars.2021.640713
- Pal, M. (2005). Random forest classifier for remote sensing classification. *Int. J. Remote Sens.* 26 (1), 217–222. doi:10.1080/01431160412331269698
- Pascoe, K. H., Fukunaga, A., Kosaki, R. K., and Burns, J. H. R. (2021). 3D assessment of a coral reef at lalo atoll reveals varying responses of habitat metrics following a catastrophic hurricane. *Sci. Rep.* 11 (1), 12050. doi:10.1038/s41598-021-91509-4
- Pedregosa, F., Varoquaux, G., Gramfort, A., Michel, V., Bertrand, T., Grisel, O., et al. (2011). Scikit-Learn: Machine learning in Python. *J. Mach. Learn. Res.* 12, 2825–2830.
- Pierce, J., Butler, M. J. I. V., Rzhano, Y., Kim, L., and Jennifer, A. (2021). Classifying 3-D models of coral reefs using structure-from-motion and multi-view semantic segmentation. *Front. Mar. Sci.* 0, 1623. doi:10.3389/FMARS.2021.706674
- Pittman, Sn J., Costa, B. M., and Tim, A. (2009). Using lidar bathymetry and boosted regression trees to predict the diversity and abundance of fish and corals. *J. Coast. Res.* 10053, 27–38. doi:10.2112/si53-004.1
- Pizarro, O., Friedman, A., Bryson, M., Williams, S. B., and Madin, J. (2017). A simple, fast, and repeatable survey method for underwater visual 3D benthic mapping and monitoring. *Ecol. Evol.* 7 (6), 1770–1782. doi:10.1002/ece3.2701

- Poux, F., Neuville, R., and Gilles, A. (2018). 3D point cloud semantic modelling: Integrated framework for indoor spaces and furniture. *Remote Sens.* 10 (9), 1412. doi:10.3390/rs10091412
- Price, D. M., Felgate, S. L., Huvenne, V. A. I., James, S., Carpenter, S., Barry, C., et al. (2022). Quantifying the intra-habitat variation of seagrass beds with unoccupied aerial Vehicles (UAVs).
- Price, D. M., Lim, A., Callaway, A., Eichhorn, M. P., Wheeler, A. J., Lo Iacono, C., et al. (2021). Fine-scale heterogeneity of a cold-water coral reef and its influence on the distribution of associated taxa. *Front. Mar. Sci.* 8. doi:10.3389/fmars.2021.556313
- Price, K. R., Callaway, A., Lo Iacono, C., Hall, R. A., Huvenne, A. I., and Huvenne, V. A. I. (2019). Using 3D photogrammetry from ROV video to quantify cold-water coral reef structural complexity and investigate its influence on biodiversity and community assemblage. *Coral Reefs* 38 (5), 1007–1021. doi:10.1007/s00338-019-01827-3
- Qi, C. R., Su, H., Mo, K., and Leonidas, J. (2017). “PointNet: Deep learning on point sets for 3D classification and segmentation,” in *Proceedings - 30th IEEE Conference on Computer Vision and Pattern Recognition. CVPR 2017* 2017-Janua: 77–85. doi:10.1109/CVPR.2017.16
- Robert, K., Jones, B., Roberts, J. M., and Huvenne, V. A. I. (2016). Improving predictive mapping of deep-water habitats: Considering multiple model outputs and ensemble techniques. *Deep Sea Res. Part I Oceanogr. Res. Pap.* 113, 80–89. doi:10.1016/j.dsr.2016.04.008
- Roberts, J. M., Wheeler, A., Freiwald, A., and Cairns, S. (2009). *Cold-water corals*. Cambridge University Press. doi:10.1017/CBO9780511581588
- Roberts, J. M., Harvey, S. M., Lamont, P. A., Gage, J. D., and Humphery, J. D. (2000). Seabed photography, environmental assessment and evidence for deep-water trawling on the continental margin west of the hebrides. *Hydrobiologia* 441, 173–183. doi:10.1023/A:1017550612340
- Rodriguez-Galiano, V. F., Ghimire, B., Rogan, J., Chica-Olmo, M., and Rigol-Sanchez, J. P. (2012). An assessment of the effectiveness of a random forest classifier for land-cover classification. *ISPRS J. Photogrammetry Remote Sens.* 67 (1), 93–104. doi:10.1016/j.isprsjprs.2011.11.002
- Roelfsema, C. M., Lyons, M., Murray, N., Kovacs, E. M., Kennedy, E., Markey, K., et al. (2021). Workflow for the generation of expert-derived training and validation data: A view to global scale habitat mapping. *Front. Mar. Sci.* 8, 643381. doi:10.3389/fmars.2021.643381
- Rogers, A. (1999). The biology of *Lophelia pertusa* (linnaeus 1758) and other deep-water reef-forming corals and impacts from human activities. *Int. Rev. Hydrobiology* 84 (4), 315–406. doi:10.1002/iroh.199900032

- Rudall, B. H. (1978). Lecture notes in computer science. Vol. 15—L-Systems. *Int. J. Bio-Medical Comput.* 9 (3), 242. doi:10.1016/0020-7101(78)90038-7
- Russell, S. J., and Peter, N. (2010). *Artificial intelligence: A modern approach*. 3rd ed., 4. Upper Saddle River, NJ: Prentice-Hall.
- Schratz, P., Muenchow, J., Iturritxa, E., Richter, J., and Alexander, B. (2019). Hyperparameter tuning and performance assessment of statistical and machine-learning algorithms using spatial data. *Ecol. Model.* 406, 109–120. doi:10.1016/j.ecolmodel.2019.06.002
- Seiler, J., Friedman, A., Steinberg, D., Barrett, N., Williams, A., and Neil, J. (2012). Image-based continental shelf habitat mapping using novel automated data extraction techniques. *Cont. Shelf Res.* 45, 87–97. doi:10.1016/j.csr.2012.06.003
- Settles and Burr, H. (2003). "Feature spaces," in *Computer sciences 540: Introduction to artificial intelligence* (University of Wisconsin Madison). https://pages.cs.wisc.edu/~bsettles/cs540/lectures/16_feature_spaces.pdf.
- Shang, X., Robert, K., Misiuk, B., Mackin-McLaughlin, J., and Zhao, J. (2021). Self-adaptive analysis scale determination for terrain features in seafloor substrate classification. *Estuar. Coast. Shelf Sci.* 254, 107359. doi:10.1016/j.ecss.2021.107359
- Shihavuddin, A. S. M., Gracias, N., Garcia, R., Gleason, A., and Gintert, B. (2013). Image-based coral reef classification and thematic mapping. *Remote Sens.* 5 (4), 1809–1841. doi:10.3390/rs5041809
- Storlazzi, C. D., Dartnell, P., Hatcher, G. A., and Gibbs, Ann E. (2016). End of the chain? Rugosity and fine-scale bathymetry from existing underwater digital imagery using structure-from-motion (SfM) technology. *Coral Reefs* 35 (3), 889–894. doi:10.1007/s00338-016-1462-8
- Summers, G., Lim, A., and Wheeler, A. J. (2021). A scalable, supervised classification of seabed sediment waves using an object-based image analysis approach. *Remote Sens.* 13 (12), 2317. doi:10.3390/rs13122317
- Thierens, M., Browning, E., Pirlet, H., Loutre, M.-F., Dorschel, B., Huvenne, V. A. I., et al. (2013). Cold-water coral carbonate mounds as unique palaeo-archives: The plio-pleistocene challenger mound record (NE atlantic). *Quat. Sci. Rev.* 73, 14–30. doi:10.1016/j.quascirev.2013.05.006
- Titschack, J., Baum, D., De Pol-Holz, R., López Correa, M., Forster, Nina, Flögel, Sascha, et al. (2015). Aggradation and carbonate accumulation of Holocene Norwegian cold-water coral reefs. *Sedimentology* 62 (7), 1873–1898. doi:10.1111/sed.12206
- Tsang, I. W., Kwok, J. T., and Cheung, P. M. (2005). Core vector machines: Fast SVM training on very large data sets. *J. Mach. Learn. Res.* 6, 363–392.

- Turley, C. M., Roberts, J. M., and Guinotte, J. M. (2007). Corals in deep-water: Will the unseen hand of ocean acidification destroy cold-water ecosystems? *Coral Reefs* 26 (3), 445–448. doi:10.1007/s00338-007-0247-5
- Urbina-barreto, I., Garnier, R., Simon, E., Pinel, R., Mahamadaly, Vt, Facon, M., et al. (2021). Which method for which purpose ? A comparison of line intercept transect and underwater photogrammetry methods for coral reef surveys. *Front. Mar. Sci.* 8, 636902. doi:10.3389/fmars.2021.636902
- Urbina-Barreto, I., Simon, E., Guilhaumon, F., Bruggemann, J. H., Pinel, R., Kulbicki, M., et al. (2022). Underwater photogrammetry reveals new links between coral reefscape traits and fishes that ensure key functions. *Ecosphere* 13 (2), 1–18. doi:10.1002/ecs2.3934
- Walker, J., Bennett, P., and Thornton, B. (2021). “Towards observation condition agnostic fauna detection and segmentation in seafloor imagery for biomass estimation,” in *Oceans 2021: San diego – porto* (IEEE), 1–8. doi:10.23919/OCEANS44145.2021.9705692
- Weinmann, M., Jutzi, B., Hinz, S., and Mallet, C. (2015). Semantic point cloud interpretation based on optimal neighborhoods, relevant features and efficient classifiers. *ISPRS J. Photogrammetry Remote Sens.* 105, 286–304. doi:10.1016/j.isprsjprs.2015.01.016
- Wheeler, A. J., Beck, T., Klages, M., Grehan, A., and Xavier Monteys, F. (2005a). “Deep-water coral mounds on the porcupine bank, Irish margin: Preliminary results from the polarstern ARK-XIX/3a ROV cruise,” in *Cold-water corals and ecosystems* (Berlin, Heidelberg: Springer Berlin Heidelberg), 393–402. doi:10.1007/3-540-27673-4_19
- Wheeler, A. J., Ferdelman, T., Freiwald, A., Hebbeln, D., and Henriot, J. P. (2007). Cold-water coral ecosystem functioning through time in the deep sea : The example of cold-water coral carbonate mounds in the northeast atlantic (from IODP307 to EuroMARC - CARBONATE)” 9.
- Wheeler, A. J., J Bett, B., M Billett, D. S., Masson, D. G., and Mayor, D. J. (2005b). The impact of demersal trawling on northeast atlantic deepwater coral habitats: The case of the Darwin mounds, United Kingdom. *Am. Fish. Soc. Symposium* 41, 807
- Wheeler, A. J., Kozachenko, M., Henry, L.-A., Foubert, A., de Haas, H., Huvenne, V. A. I., et al. (2011). The Moira mounds, small cold-water coral banks in the porcupine Seabight, NE atlantic: Part A—an early stage growth phase for future coral carbonate mounds? *Mar. Geol.* 282 (1–2), 53–64. doi:10.1016/j.margeo.2010.08.006
- Williams, I. D., Couch, C., Beijbom, O., Oliver, T., Vargas-Angel, B., Schumacher, B., et al. (2019). Leveraging automated image analysis tools to Transform our capacity to assess status and trends of coral reefs. *Front. Mar. Sci.* 6 (APR). doi:10.3389/fmars.2019.00222

- Wu, J., Chen, X., Zhang, H., Dong, X., Lei, H., and Deng, S. (2019). Hyperparameter optimization for machine learning models based on bayesian optimization. *J. Electron. Sci. Technol.* 17 (1), 26–40. doi:10.11989/JEST.1674-862X. 80904120
- Xu, Y., Tuttas, S., Ludwig, H., and Stilla, U. (2018). Voxel-based segmentation of 3D point clouds from construction sites using a probabilistic connectivity model. *Pattern Recognit. Lett.* 102, 67–74. doi:10.1016/j.patrec.2017.12.016
- Young, G. C. (2018). Convolutional neural networks predict fish abundance from underlying coral reef texture.
- Yu, Xi, Ma, Y., Farrington, S., Reed, J., Ouyang, B., and JosePrincipe, C. (2019). Fast segmentation for large and sparsely labeled coral images. *Proc. Int. Jt. Conf. Neural Netw.* 2019-July. doi:10.1109/IJCNN.2019.8852014
- Yuval, M., Gal EyalTchernov, D., Loya, Y., Murillo, A. C., and Treibitz, T. (2021). Repeatable semantic reef-mapping through photogrammetry, 1–19.
- Zelada Leon, A. I., HuvenneBenoist, N\ M. A., Ferguson, M., J Bett, B., Russell, B., et al. (2020). Assessing the repeatability of automated seafloor classification algorithms, with application in marine protected area monitoring. *Remote Sens.* 12 (10), 1572. doi:10.3390/rs12101572
- Zhang, X., Chen, G., Wang, W., Wang, Q., and Fan, D. (2017). Object-based land- cover supervised classification for very-high-resolution UAV images using stacked denoising autoencoders. *IEEE J. Sel. Top. Appl. Earth Obs. Remote Sens.* 10 (7), 3373–3385. doi:10.1109/JSTARS.2017.2672736
- Zurowietz, M., Langenkämper, D., Hosking, B., Ruhl, H. A., and Tim Nattkemper, W. (2018). MAIA-A machine learning assisted image annotation method for environmental monitoring and exploration. *Plos One* 13 (11), e0207498. doi:10.1371/journal.pone.0207498

3.8 Supplementary Materials

Supplementary Table 3.2: Summary of *f1* accuracies results of the top performing classifiers in group 1 and group 2. The first column “Classifiers” shows the given names of each classifier. Names ending at “1000” indicates the number of samples to which the classifiers were trained i.e., Group 1. Similarly, classifier names ending in “10000” indicates this version of the classifier was trained on Group 2, i.e., 10000 samples.

Classifiers	<i>f1</i> score (%)	<i>f1</i> cross val scores (%)	Best parameters	Run times
SVC_GS_1_1000	63.8	76.06	{'C': 100, 'gamma': 1, 'kernel': 'rbf'}	3.4s
SVC_GS_1_10000	67.4	75.95	{'C': 100, 'gamma': 1, 'kernel': 'rbf'}	5min 53secs
RF_GS_1_1000	72.3	79.5	{'Max_features': 1, 'n_estimators': 90}	9.26s
RF_GS_2_10000	94.28	80.04	{'Max_features': 2, 'n_estimators': 1000}	2h 31min 52s

GBT_GS_1_1000	72.1 5	80.5 9	{'Classifier': gradientboostingclassifier(max_depth=7, n_estimators=1000, subsample=0.7),'classifier__learning_rate': 0.1, 'classifier__max_depth': 7,'classifier__n_estimators': 1000,'classifier__subsample': 0.7}	23m in 12s
GBT_GS_1_10000	95.1 %	80.4 6	{'Classifier': gradientboostingclassifier(max_depth=9, n_estimators=1000, subsample=0.5),'classifier__learning_rate': 0.1, 'classifier__max_depth': 9,'classifier__n_estimators': 1000,'classifier__subsample': 0.5}	2h 52m in 56s
KNN_GS_1_1000	64.9	76.0 2	{'Metric': 'manhattan', 'n_neighbors': 3, 'weights': 'distance'}	485 ms
KNN_GS_1_10000	91.6	76.1 8	{'Metric': 'manhattan', 'n_neighbors': 3, 'weights': 'distance'}	2.54 s
LR_GS_3_1000	60.9 5	74.0 1	{'Classifier': logisticregression(c=100, max_iter=1000, penalty='l1', solver='liblinear'), 'classifier__c': 100,'classifier__max_iter': 1000,'classifier__penalty':'l1','classifier__solver': 'liblinear'}	
LR_GS_2_10000	62.4	74.1	{'Classifier': logisticregression(c=100, random_state=0, solver='sag'),'classifier__c': 100,'classifier__penalty': 'l2','classifier__solver': 'sag'}	37.7 s

MLP_GS_4_1 000	70.1	76.9	{'Estimator': mlpclassifier(activation='tanh', hidden_layer_sizes=(80, 80, 80, 80, 80, 80, 80),learning_rate_init=0.0001,max_iter=2000, random_state=0),'estimator__activation': 'tanh','estimator__alpha': 0.0001,'estimator__early_stopping': false,'estimator__hidden_layer_sizes': (80, 80, 80, 80, 80, 80, 80), 'estimator__learning_rate_init':0.0001,'estimat or__max_iter': 2000,'estimator__solver': 'adam'}	18m in 54s
MLP_GS_7_1 0000	92.3	77.5	{'Estimator': mlpclassifier(activation='tanh', alpha=0.005, hidden_layer_sizes=(200, 200, 200, 200, 200, 200, 200, 200, 200, 200), learning_rate_init=0.0001, max_iter=2000, random_state=0),'estimator__activation': 'tanh', 'estimator__alpha':0.005,'estimator__early_stoppi ng': false, 'estimator__hidden_layer_sizes': (200, 200, 200, 200, 200, 200, 200, 200, 200), 'estimator__learning_rate_init': 0.0001, 'estimator__max_iter': 2000, 'estimator__solver': 'adam'}	1d 8h 25m in 6s

3.8.1 Supplementary overview of the classification algorithms used in the study

Random Forest

According to the definition of (Breiman, 2001) RF classifier consists of a group of tree-structured classifiers where the vectors are independent and identically distributed random vectors, and each tree casts a vote for the most popular class input. The average of predictions of individual trees result on the final prediction (Breiman, 2001) Combining trees grown using random features can produce improved accuracy when compared to one single tree. Ensemble learning methods consist of a collection, or ensemble of hypotheses and their predictions from the hypothesis space (Russell and Norvig, 2010). As part of the ensemble method spectrum,

In this study, the grid search and cross validation using the Random Forest algorithm was performed to find the best number of estimators i.e., number of trees, and the number of maximum features to be considered for the best split. The number of estimators was set with options of ranging from 10 to 1000 and the number of features was set to a range of 1 to 7 for the first sets of RFs. The scikit-learn options 'auto' and 'log2' were also considered. When the maximum feature parameter is set to 'auto', it takes the square root of the number of features whereas when it is set to 'log2', it takes the binary logarithm of the number of features. The best performance RF model was selected based on the accuracy considering the permutation of the grid search parameters. The other parameters were set to the default of Scikitlearn class. The full list of parameters can be found in the ScikitLearn webpage.

Gradient Boosted Trees

Here, the parameter grid defined to find the optimal GBT parameters with the grid search were: learning rate, number of estimators, the maximum depth of estimators and the subsample rate. The learning rate was set to options of 0.0001, 0.001, 0.01, 0.1, 1. The number of estimators was defined to 10, 50, 100, 500 and 1000. The subsample rate was set to a range of 0.5, 0.7 and 1. Although the default subsampling value in scikit-learn is set to 1, we decided to expand the range of values to include other two values, 0.7 and 0.5, which is the suggested value of subsampling according to Buitinck et al. (2013). It is noteworthy that, if subsampling is set to a value > 1 , the classifier changes to Stochastic Gradient Boosting (Buitinck et al., 2013)

Support Vector Machines

In SVM, the regularization parameter 'C' and gamma (γ) are crucial parameters. The 'C' parameter (or penalty parameter) defines the level of complexity of the decision function in relation to misclassified samples. Therefore, small 'C' values correspond to more regularization. The gamma parameter (or margin of tolerance) is a kernel coefficient that defines the level of influence that a single sample has over other samples. The higher the gamma, the larger the influence of a single point in relation to closer samples (Pedregosa et al., 2011). The choice of kernel is also an equally crucial parameter (Burgess, 1998).

Logistic regression

In LR, probabilities describing possible outcomes of a trial are modelled into a logistic function (S-shaped) instead of a linear function, as in the case of Linear Regression. As a parametric model, LR summarizes the data with a range of parameters of fixed size, independent of the number of the training samples (Russell and Norvig, 2010). LR uses the maximum likelihood estimation (MLE) to obtain the model coefficients to connect predictors to the target variable. MLE is applied to find the best set of parameters with the greatest probability for predicting the observed data (Czepiel, 2002).

Multilayer Perceptron

MLP are generally composed by an input layer, a number of hidden layers, an output layer and loss functions. The hidden layer sizes i.e number of neurons in each layer, the activation function, the solver, the penalty and the learning rate are defined by the user according to the type of problem. The weights are learned using gradient descent techniques such as backpropagation during the training phase, aiming to minimise the error function (Weinmann et al., 2015). MLP is considered a successful model as it uses parametric forms of the basic functions in which parameter values are adapted during training (Bishop, 2006).

When training the MLPs, the choice of stop criterion is relevant because it prevents overfitting, particularly in cases where deep networks are used (Jodzani et al., 2019). One of the stopping criteria can be ending the training process after a number of iterations is reached by setting a maximum number of iterations to the classifier.

K-Nearest Neighbours (KNN)

Considering a number of training vectors, KNNs identify the k-nearest neighbours of these training vectors to assign the test vector with the class label of the majority class of the nearest neighbours (Theodoridis and Koutroumbas, 2009). The distance metrics defines how the distance is going to be measured from the training vector to its k-neighbours. The most common user-defined parameters of the KNN to evaluate are the number of neighbours, the weight function used in prediction and the distance metric.

3.8.2 Overview of the Performance assessment

***f1* Score**

f1 score is the harmonic mean between precision and recall. It varies from 0 to 1. The weighted average calculates metrics for each label and find their average weighted by the number of true instances of each label. The *f1* score using weighted average returns the weighted average of the *f1* scores of each class.

ROC Curves

The ROC curve is obtained by a threshold variation on the output values (discriminant values) of the classifier. The curve is a representation of the ratio of the true positives against the ratio of false negatives (Rudall, 1978), depicting the relative trade-offs between benefits (true positives) and costs (false positives) (Fawcett, 2006). The lower left point (0,0) in the graph represents the classifier not predicting any positive classifications (True positives), the classifier produces no false positives errors but also it does not gain any true positives false positive errors neither true positive gains. Opposite to that is the t upper right point (1,1), which represents the classifier issuing unconditionally positive classifications, independent if they are false positive or true positive). The point (0,1) represents an ideal classification, where all instances are indeed true positives. Hence, points located on the upper left near the X axis typically represent classifiers that make positive classifications based on strong evidence generally termed 'conservative' as they only predict true positives based on high confidence rates, consequently having few false positives but also having low true positive rates as trade-off (Fawcett, 2006). Following the same trend, points located on the upper right far from the X axis are considered as making positive classifications with weak evidence, classifying the majority of true positives correctly but also classifying false positives more often, hence these classifiers are generally described as 'liberal' (Fawcett, 2006). In the case of a multiclass classification, a ROC graph was produced for each class, treating the class as the positive class and the remaining classes as the negative class.

K-fold cross validation

K-fold cross validation is an estimator performance evaluator widely used in supervised learning. In k-fold cross validation, the training set is split into k smaller

sets, or folds. In each split, the model is trained using $k-1$ of the smaller sets of the training data and the remaining fold is used for the validation. This is executed until the model completes the round of k folds. The output metric is the average and standard deviations of the accuracy computed in each split. Cross validation is particularly useful in cases with low availability of samples, as it avoids portioning the data into training, validation and testing sets (Buitinck et al., 2013).

4. Cold-Water Coral Spatial Relationships Based On The Analysis Of High-Resolution Photogrammetry And Terrain Descriptors

Larissa Macedo Cruz de Oliveira, Aaron Lim, David M. Price and Andrew J. Wheeler

(Current status: ready for submission)

This chapter comprises a paper that is ready for submission to *Scientific Reports*. It is organised as follows: introduction, materials and methods, results, discussion and references.

This chapter presents the results of the second and third aims of the PhD: quantify CWC facies distribution and spatial variability and link image data to processes driving CWC reef development, respectively. Here, we explore the capabilities of SfM-derived geomorphometric variables and spatial pattern analyses to develop a fine-scale environmental analysis of a section of the Piddington Mound. A new approach to point pattern distribution using multidimensional data and distance-based methods was developed to understand facies distribution and spatial self-organisation of CWCs, whilst linking to abiotic and biotic trends previously documented for the Piddington Mound.

Candidate contributions to the study: Larissa de Oliveira conceptualised the study with contribution of Dr Aaron Lim. Larissa de Oliveira developed the methodology, carried out the data curation investigation, formal analyses, validation, data visualisation, writing of the original draft, review and editing.

Dr David Price contributed to the methodology, formal analysis, software, validation and discussions. The project was supervised by Prof Andy Wheeler, Dr Aaron Lim. The co-authors also contributed with editing, proof-reading of the manuscript and funding acquisition. Dr Aaron Lim was the chief scientist responsible for the data collected for the study during the research cruise CE20011, in which Larissa Oliveira was data manager. The project which lead to the work developed in this chapter was developed

by Larissa de Oliveira and funded through the Irish Research Council Postgraduate Scholarship awarded to Larissa Oliveira.

Abstract

Cold-water corals (CWC) play an important role in the biodiversity of deep-water habitats. Efforts to map these environments have increased as technology and access to high-resolution data advance. Structure-from-Motion (SfM) photogrammetry and density-based analyses allow the quantification of fine-scale habitat descriptors that are important to assess key CWC reef ecological traits. By combining automated 3D classification and fine-scale terrain metrics derived from SfM, we provide a qualitative and quantitative assessment of CWC habitats in the Piddington Mound, in the Belgica Mound Province, southwest of Ireland. Four facies types were adopted: 1) live coral framework 2) dead coral framework 3) coral rubble, and 4) sediments and dropstones. Geomorphometric variables were computed from digital elevation models and habitat classification was performed with supervised machine-learning algorithms. Our results show that live and dead coral facies have different terrain descriptors, occupying and creating areas of higher rugosity than compared to the coral rubble facies. Furthermore, in both live and dead coral facies, larger corals tend to appear towards the mound summit whereas small corals dominate the lower flank and flatter areas, suggesting i) the recent growth of coral colonies and ii) suboptimal conditions at the mound base. The findings herein highlight the high variability resulting from CWC mound morphological and biological traits across both regional and local scales.

4.1 Introduction

Framework forming cold-water corals (CWC) are cnidarian filter-feeding organisms typically found in regions where seawater temperatures vary between 4° to 12°C, depths of 50 to 4000 metres (Roberts et al., 2009). Apart from temperature and depth, CWCs thrive in environments with dynamic interactions among topographic heterogeneity (presence of hard substrates), current hydrodynamics (Mienis et al., 2012; Wheeler et al., 2008) and the high flux of particulate organic matter (POM) (Appah et al., 2020). Under suitable conditions, framework-building scleractinian corals such as *Lophelia pertusa* (synonymised to *Desmophyllum pertusum* in Addamo et al., 2016) and *Madrepora oculata* produce three-dimensional (3D) calcium carbonate structures that can form small patches (Wilson, 1979a), reefs (Masson et al., 2003; Roberts et al., 2006; Victorero et al., 2016), and giant carbonate mounds (Freiwald et al., 2004; Hovland and Thomsen, 1997; Huvenne et al., 2011a; Mienis et al., 2006; Wheeler et al., 2007) by incorporating current-suspended sediments (Dorschel et al., 2007; Wheeler et al., 2005; White et al., 2005).

These habitats play an important role in supporting enhanced biodiversity and providing ecosystem services for associated fauna, acting as nurseries and refugia for fish and benthic species (Costello et al., 2005; Freiwald and Roberts, 2005; Mortensen et al., 1995; Roberts et al., 2006). CWCs are also important to the global biogeochemical cycle, acting as carbon sinks of deep seas (Henry and Roberts, 2017; Oevelen et al., 2009; Titschack et al., 2009), having respiration, carbon and oxygen consumption rates over an order of magnitude higher than in noncoral areas, for example (Cathalot et al., 2015). CWCs have been documented in continental shelves, slopes and troughs (Leverette and Metaxas, 2006; Mienis et al., 2006; Mortensen et al., 1995; Savini and Corselli, 2010; Wilson, 1979b), fjords (Fosså et al., 2006, 2002; Titschack et al., 2015) and submarine canyons (De Mol et al., 2011; Huvenne et al., 2011b; Orejas et al., 2009)

Several studies have emphasised the environmental importance of CWCs as their higher structural complexity and provision of hard surfaces promote biodiversity hotspots in deep-water environments (Jonsson et al., 2004; Wheeler et al., 2007).

Habitat structural complexity is known to have a high impact on ecological interactions across scales (Crowder and Cooper, 1982). At a fine scale, distinct spatial features such as 3D structures created by scleractinian corals hold a crucial role in providing conditions to support other species (Jonsson et al., 2004; Price et al., 2019; Robert et al., 2017). Likewise, high-resolution data has proven crucial to investigate ecosystem trajectories and capture heterogeneity traits in coral reef dynamics (Burns et al., 2015; Ferrari et al., 2016). Thus, incorporating high-resolution mapping of these ecosystems is key to investigating these fine-scale interactions (D'Urban Jackson et al., 2020; Ferrari et al., 2016; Lim et al., 2020b).

The advent of ROV-based surveys has enabled the investigation of CWC habitats and their associated fauna (Dolan et al., 2008; Heindel et al., 2010; Savini et al., 2014; Wilson et al., 2007). The study of 3D structures, however, had previously been restricted to traditional 2D mapping methods (Goatley and Bellwood, 2011) such as video/image analysis or shipboard multibeam which are known to cope poorly with vertical and 3D structures (Huvenne et al., 2011b; Robert et al., 2017). The application of *Structure-from-Motion* (SfM) photogrammetry has opened a new branch of high-resolution mapping of underwater environments, providing fine-scale, 3D analyses of benthic ecosystems in a cost and time-effective manner (Figueira et al., 2015; Pizarro et al., 2017).

Studies have used SfM to reconstruct coral reef environments in shallow (Burns et al., 2019; Fukunaga et al., 2020) and deep waters (Conti et al., 2019; Lim et al., 2020c; Price et al., 2019). The reconstructions range from millimetric, polyp size scales (Cocito et al., 2003; House et al., 2018) to metre, reef-wide scales (de Oliveira et al., 2021; Fabri et al., 2022). The application of the SfM in marine studies varies from quantifying differences in coral reefs under the impact of anthropogenic and climate hazards (Burns et al., 2020; Chen and Dai, 2021; Pascoe et al., 2021) to understanding the impact of fine-scale heterogeneity in species distribution (Fabri et al., 2019; Price et al., 2021; Urbina-Barreto et al., 2022). In a social context, SfM has also been a powerful tool to aid visualisation and augment the interaction of humans with otherwise pristine environments (Cristobal et al., 2020; de Oliveira et al., 2022b; Doležal et al., 2019).

Apart from 3D models and orthorectified photomosaics, SfM can provide high-resolution digital elevation models (DEMs). Similar to multibeam-derived DEMs, SfM DEMs provide multiple terrain descriptors at a millimetric scale. This allows for flexibility in the mapping procedure as, depending on the study aim, SfM DEMs can be downscaled to reflect wider-terrain physical features (slope, aspect, curvature) or be kept at the sub-centimetric resolution to provide important ecological descriptors of structural complexity e.g. rugosity, vector ruggedness measures, shelter volume (Fukunaga and Burns, 2020; Storlazzi et al., 2016; Urbina-barreto et al., 2020).

As a suite of methods to investigate fine-scale organism distribution, point pattern analyses (PPA) have become more common in the study of marine habitats (Prado et al., 2019; Price et al., 2021). PPAs obtained from annotations of SfM-derived photomosaics have provided valuable information in ecosystem modelling studies as the photomosaics yield contextualised data about the location of the point in relation to the terrain (Prado et al., 2020; Williams et al., 2019). However, only a few studies go beyond the traditional presence/absence point distribution to integrate 3D-specific measures e.g., size of colonies into the analysis (Fabri et al., 2019; Prado et al., 2019). Integrating variables such as the size of coral colonies into the habitat distribution mapping may allow for further analyses of CWC as colony size can be an indicator of coral growth and ecosystem health (Ferrari et al., 2017; Lange and Perry, 2020).

In this paper, we aim to investigate the density and size distribution of CWC from high-resolution photogrammetric data. Distance and density-based point pattern analyses associated with CWC habitats are obtained to analyse: i) CWC facies density distribution; ii) the relationship between the density distribution and geomorphometric features and lastly; iii) to map facies hotspots in relation to the terrain. By combining automated 3D classification and fine-scale terrain metrics derived from SfM, we integrate habitat facies with geomorphological information in a 3D space, providing novel insights about the facies distribution of a CWC mound.

4.2 Materials and Methods

4.2.1 Study area

The Belgica Mound Province (BMP), located on the eastern slope of the Porcupine Basin, NE Atlantic, is characterised by outcropping or buried conical cold-water coral giant carbonate mounds either as single or elongated clusters (De Mol et al., 2002). Different aspects of the mound and its regional setting have been studied in the last two decades (De Mol et al., 2005; Foubert et al., 2006; Huvenne et al., 2005; Wheeler et al., 2005, 2011) whilst also being widely investigated for the application of novel mapping methods (Bohlukos et al., 2019; Conti et al., 2019; Lim et al., 2018b, 2017; Price et al., 2021). Given the environmental importance of the BMP in the wider North Atlantic region, the province has been designated to a Special Area of Conservation (SAC) (SAC site number: 002327) under the EU Habitats Directive (NPWS, 2022).

Within the BMP lies the Moira Mounds, a group of small-sized CWC reefs ranging from 3 to 10 metres high and dominated by scleractinian framework-building corals (Huvenne et al., 2002). It is understood that the Moira Mounds have characteristics of mounds formed under stressed high-sediment intake conditions (Foubert et al., 2011). The Moira Mounds are subdivided into four areas: the 'upslope', 'mid-slope', 'down-slope' and 'northern area' based on the distribution of surrounding smaller mounds (Wheeler et al., 2011). The Piddington Mound, located in the down-slope area, is one of the largest of the Moira Mounds and, with documented current speeds of approximately 40 cm s^{-1} , it is considered an area favourable for mound development (Lim, 2017). The surrounding area of the mound is dominated by sediments and dropstones whereas the mound is dominated by *Lophelia pertusa* and *Madrepora oculata* colonies. These characteristics allow the Piddington Mound and surrounding mounds to be divided into four distinct facies: live coral framework, dead coral framework, coral rubble and hemipelagic sediment with dropstones, as previously described in Heindel et al. (2010), Lim et al. (2017) and also adopted in later studies (Conti et al., 2019; de Oliveira et al., 2022a).

4.2.2 Structure-from-Motion Photogrammetry

The ROV HD video data used herein were collected during the survey CE20011 onboard the Celtic Explorer (Lim et al., 2020a). The ROV *Holland 1* was mounted with a downward-facing HD Insite mini-Zeus with HDSI fibre output camera for the video acquisition. ROV positioning and navigation were acquired with a Sonardyne Ranger 2 USBL with slant range accuracy of 1.3%. The ROV was mounted with a pair of lasers spaced 10cm apart for scaling. Hence, all HD video footage acquired at 1080p had projected laser scales to allow for a correctly scaled 3D reconstruction through calibration. The ROV video survey was designed to follow an N-S grid composed of 35 equidistant lines while the ROV hovered at a speed of < 2 knots at approximately 2 metres above the seafloor to ensure a constant field of view. The ROV video data and navigation were converted into 3D models in Agisoft Metashape Professional version 1.7.2 (Agisoft, 2021). Detailed survey acquisition methods and the SfM photogrammetric pipeline can be found in de Oliveira et al. (2022a); Lim et al. (2020a).

4.2.3 Data Segmentation And Classification

The point cloud resulting from the SfM process was classified using an automated supervised classification approach developed in de Oliveira et al. (2022a). Each point in the point cloud was classified using a gradient-boosted tree (GBT) algorithm as belonging to one of the four classes outlined above, reaching an $f1$ accuracy of > 95%. The process enables fast and accurate classification of 3D data of CWC, thus providing a more accessible use of high-resolution data for CWC mapping. The point cloud was divided into semantic objects using a connected component labelling algorithm (CCL) implementation in CloudCompare. CCL connects points within a minimum distance using a heuristic graph theory approach (Samet and Tamminen, 1988). The octree level used to extract point cloud components was set to 10, based on experimental tests. The octree is the recursive partition of a cubical volume in the point cloud. The octree level defines the maximum number of cubical components that are obtained from the data. High values provide more, closely spaced components. The point-to-

object process transformed 50,000 classified points into 3096 individual point clouds, where each point cloud represented one classified object i.e. live coral framework, dead coral framework, coral rubble and hemipelagic sediment with dropstones (Table 4.1):

Table 4.1: Definition of each facies used in the study

Facies	Description
1. Live Coral Framework (LCF)	Coral presenting any signs of identifiable living parts (polyps or mucus-covered frameworks evident) although major proportions of the coral framework may be dead. Coral polyps, and skeletal casing are usually bright, white or orange in colour (Appah et al., 2020)
2. Sediments And Dropstones (SD)	Sediment (sand or mud) and dropstones, include sediment waves, ripples and scour marks.
3. Dead Coral Framework (DCF)	Coral framework which has no identifiable living parts. Identified by darker grey or brown skeleton (Appah et al., 2020)
4. Coral Rubble (CR)	Coral rubble is recognisable by biogenic material where >50% of detached dead coral fragments, shell fragments and sediment are observed (Lim et al., 2017).

The Euclidean distance concept was used to aggregate each of these point cloud objects and their respective information (X,Y, Z, R, G, B) into one dataset. To this end, the centroid of each object was calculated by calculating the mean of each set of X, Y, and Z coordinates. The Euclidean distance between each point of the point cloud object and the centroid was calculated following the equation:

$$d = \sqrt{[(x_2 - x_1)^2 + (y_2 - y_1)^2 + (z_2 - z_1)^2]}$$

Where x_1 , y_1 and z_1 are the respective centroids of each point cloud object. The mean value of the obtained Euclidean distances of each object provided information about the relationship between the location of each point in a 3D space and its centroid. Thus, the value represents the radii i.e., the size of each of the 3096 objects of the point cloud. The sizes were then categorised into 'large', 'medium' and 'small' by binning the sizes into three intervals based on minimum, and maximum values.

4.2.4 Terrain Variable Extraction From Digital Elevation Model (DEM)

The DEM resulting from the *SfM* process was used to extract the geomorphometric variables used herein. A total of 7 terrain variables (Table 4.2) were extracted using the Benthic Terrain Modeler (BTM) plug-in (Walbridge, 2018) in the geospatial processing software ArcGIS (Version 10.6). The bathymetric position index (BPI) was calculated by subtracting the DEM from the focal mean (with circle, r) following Wilson et al. (2007). To capture the wider terrain context whilst tempering the influence of coral features into terrain metrics, the variables were extracted from the DEM at a resolution of 50 cm/pixel, with exception of VRM, which was also extracted from the original DEM resolution (3.39mm/pixel). The dual resolution for VRM was selected based on its importance in delineating coral reef structural complexity and its documented scale dependence (Price et al., 2019; Richardson et al., 2017). VRM and rugosity are considered important measures of coral structural complexity as they measure the variability of a surface as the ratio of the true distance along a surface to the linear distance (Friedman et al., 2012; Storlazzi et al., 2016). In coral reef environments, these measures are generally a product of high coral cover or density (Graham and Nash, 2013; Storlazzi et al., 2016). Northness and Eastness were included as they can give information about surface exposure to the current direction (Price et al., 2021). The interaction between the terrain aspect and the current direction can directly impact facies distribution, especially in the case of filter feeders that rely on current-suspended food supply (Orejas et al., 2016). The cell values of each variable raster where the point feature was projected into were extracted and added to the attribute table of the point feature.

Table 4.2: Geomorphometric variables extracted from the DEM, the neighbourhood (kernel) size and the resolution of the DEM from which the variables were extracted

Geomorphometric variable	Neighbourhood size	Resolution
Slope (°) [0,90]	3x3	50 cm/pixel
Eastness (Sin Aspect) [-1,1]	3x3	50 cm/pixel
Northness (Cos Aspect) [-1,1]	3x3	50 cm/pixel

Curvature	3x3	50 cm/pixel
BPI	3x3	50 cm/pixel
Rugosity (Arc-Chord Ratio)	3x3	50 cm/pixel
Vector Ruggedness Measure (VRM)	3x3 and 21 x 21	50 cm/pixel and 3.39 mm/pixel

4.2.5 Point Pattern Spatial Analysis

Data were analysed using three spatial statistics methods implemented in R (4.2.2) with the package ‘spatstat’ (Baddeley, 2010), ArcMap and Python. The aim of the spatial analysis was to further understand the interaction of coral facies and the terrain. Therefore, the spatial statistics analyses were carried out with a focus on the live coral (LC) and dead coral (DC) facies.

Kernel density plots were produced to examine the point intensity distribution of the coral facies. Intensity is the average density of points i.e., expected number of points per unit area (Baddeley, 2010). The plots were created using a fixed bandwidth (sigma=1) of the intensity function and visually assessed for facies distribution in relation to the terrain and object size (Euclidean radii).

Ripley’s L-function plots were used to examine the spatial distribution of facies. L-functions provide information on whether observed points are consistent or deviant from a complete spatial randomness (CRS) pattern or uniform Poisson point process (Dixon, 2014; Ripley, 1976), thus giving information about the likelihood of clustering in each facies in relation to a given distance (r), using the centroid of each point cloud. L-functions are the transformed version of Ripley’s K function and have been used in marine ecology studies (Orejas et al., 2009; Prado et al., 2020) in conjunction with its derivatives e.g., pairwise (g) functions (Price et al., 2021).

$$L(r) = \sqrt{\frac{k(r)}{\pi}}$$

Where $L(r)$ is the transformed centred form of the k-function $k(r)$. For a uniform Poisson (completely random) point pattern, the theoretical value of $L(r) = r$. The square root transformation stabilises the variance of the estimator to improve its use with simulation envelopes and hypotheses tests (Baddeley et al., 2015, 2013).

Hypothesis tests were performed with 999 Monte Carlo simulations to generate points in CRS, where the rank of the envelope was set to 25 to define a confidence interval of 95% ($\alpha < 0.05$), considering that $\alpha = 2 * nrank / (1 + nsim)$ (Baddeley et al., 2013). The Monte Carlo simulation is structured to reject the null hypothesis if the $L(r)$ values at a given distance r fall outside the confidence envelope. Thus, deviations below the confidence interval and the estimated CRS threshold would indicate that the facies tend to be organised under a random dispersion pattern. Deviations above the confidence envelope indicate the facies are not organised randomly, tending towards a clustering pattern. The region of interest was the shape of the study area. The 'best' command was used to apply the best edge correction method in 'spatstat', which was Ripley's isotropic correction implemented for rectangular or polygonal windows (Baddeley et al., 2013)

Getis Ord General G_i^* statistics (Getis and Ord, 1992), also known as High-Low Clustering, were used to identify hotspots and cold spots of facies distributions in relation to depth and depth vs size. G-statistics are used to measure the spatial association of a variable within a specified distance of a single point (Getis and Ord, 1992). Features with high z-score and p-values (< 0.001) indicate statistically significant hotspots, where the null hypothesis of a random distribution can be rejected in favour of the clustering hypothesis. The confidence intervals (G_i_Bin) identify statistically significant hot and cold spots, where high magnitude values e.g., ± 3 reflect a 99% confidence level and a bin value of 0, shows not statistically significant points. The magnitude of the z-score (G_i^*) represents the intensity of the clustering. The higher or lower the Z-score, the more intense the clustering. Facies were encoded into binary labels (0-1) and a 'one vs. all' approach was used for the analysis, where 1 means the object belongs to those facies and 0 means it does not. Scatter plots showing the distribution of clustering intensity (z-score) in relation to depth, their significance level (G_i_bin) and Euclidean size (euc_rad) in relation to depth were produced for LC and

DC classes. The analysis was performed with the Spatial Statistics suite in ArcTool box in ArcMap (ArcGIS, 2014).

Spearman's correlation coefficients (Spearman's rank test) were obtained to investigate the non-parametric correlation between the geomorphometric variables. Spearman's correlation tests have been applied in ecological studies as an aid to understanding the species interaction with the terrain and variable selection for predictive modelling (Corbera et al., 2019; Davies et al., 2008; Sundahl et al., 2020; Wilson, 2016). The test measures the strength and direction of association between two variables. Here, the analyses were performed for the whole terrain and for each facies to detect any possible correlation variations between variables of each facies. The tests were performed in Python with the Stats package. A p -value of 0.05 was selected for the significance threshold to filter out the variable pairs that did not show statistically significant evidence of correlation. The analysis of correlation will be useful for future predictive modelling and supervised classification studies using this dataset. Tests for normality of terrain variables were performed with Shapiro-Wilk's and Kolmogorov-Smirnov tests prior to Spearman's correlation tests.

To understand and evaluate if the intensity of points depends on the variation of specific terrain variables, a non-parametric density estimate in the function of covariate analysis was performed. The density in function of covariate ("rho-hat") tests were performed for the variables DEM, slope, Northness and Eastness. These can provide information regarding the statistical likelihood of finding coral facies at specific regions and terrain values by computing a non-parametric smoother estimate of function (ρ), thus identifying how the intensity of points at each a given distance u depends on the covariate:

$$\lambda(u) = \rho(Z(u))$$

Where u is the location, $\lambda(u)$ represents the intensity at that location u and $Z(u)$ is the covariate at location u . Each test was statistically supported by Berman's Z2 test and Kolmogorov Smirnov (KS) tests. The KS test is considered a powerful test preferably used when the covariate has continuously varying numerical values. It compares the observed and expected distributions of the values of the function under the CRS

hypothesis, thus giving statistical support to the 'rho-hat' function (Baddeley, 2010). Similarly, the Berman's Z1 and Z2 tests proposed in (Berman, 1986) were used as a second statistical support to the 'rho-hat'. Both tests work under the null hypothesis that the point process is a CRS independent of the covariate (Berman, 1986).

Finally, to evaluate the influence of reef substrate on facies distribution, three point pattern models (PPM) were tested with 1) no variables, 2) only depth and 3) three variables (Northness, Eastness and depth). The variables were chosen based on their importance in describing terrain morphology and their low correlation values (Spearman's test). The best of the three models determined by the lowest Akaike Information Criterion (AIC) was endorsed by a likelihood ratio test for the CSR null hypothesis, except in cases where the best model selected was CSR. The model with the lowest AIC is considered the model that explains the greatest amount of variation using the lowest number of independent variables (Baddeley et al., 2015).

4.3 Results

4.3.1 Geomorphometric Characterisation Of The Terrain

The photogrammetric process resulted in an orthomosaic of 1.69mm/pixel resolution (Figure 4.1A) and a DEM with a 3.39 mm/pixel resolution (Figure 4.1B) covering an area of 318.53 m². The average depth of the DEM is 963.9 ± 3.56 , extending from 955.6 to 970 m. The slope at the original resolution (3.39 mm/pixel) extended from 0° to 89.64° (mean 27 ± 19.83), with steeper slopes occurring towards the higher parts of the mound. Whilst the slope at 50 cm/pixel ranged from 0° to 50.9° (mean 33.28 ± 9.23) (Figure 4.1C), whereas curvature (Figure 4.1D) showed a heterogeneous pattern towards the higher parts of the mound. Eastness (sin-aspect) (Figure 4.1E) also appeared to be higher (0.8574) at the higher parts of the mound, suggesting an eastward orientation. The homogeneity of high Northness (cos-aspect) values (Figure 4.1F), close to 1 (0.87 ± 0.23), indicated an overall downslope orientation northward. Rugosity (Figure 4.1G) and VRM values also appeared to be higher in those areas.

BPI values (Figure 4.1H) were higher around the edges of the mound, showing a higher local gradient towards the southwest and negative towards the northwest where the mound is flat. BPI values had a unimodal distribution centred around the mean.

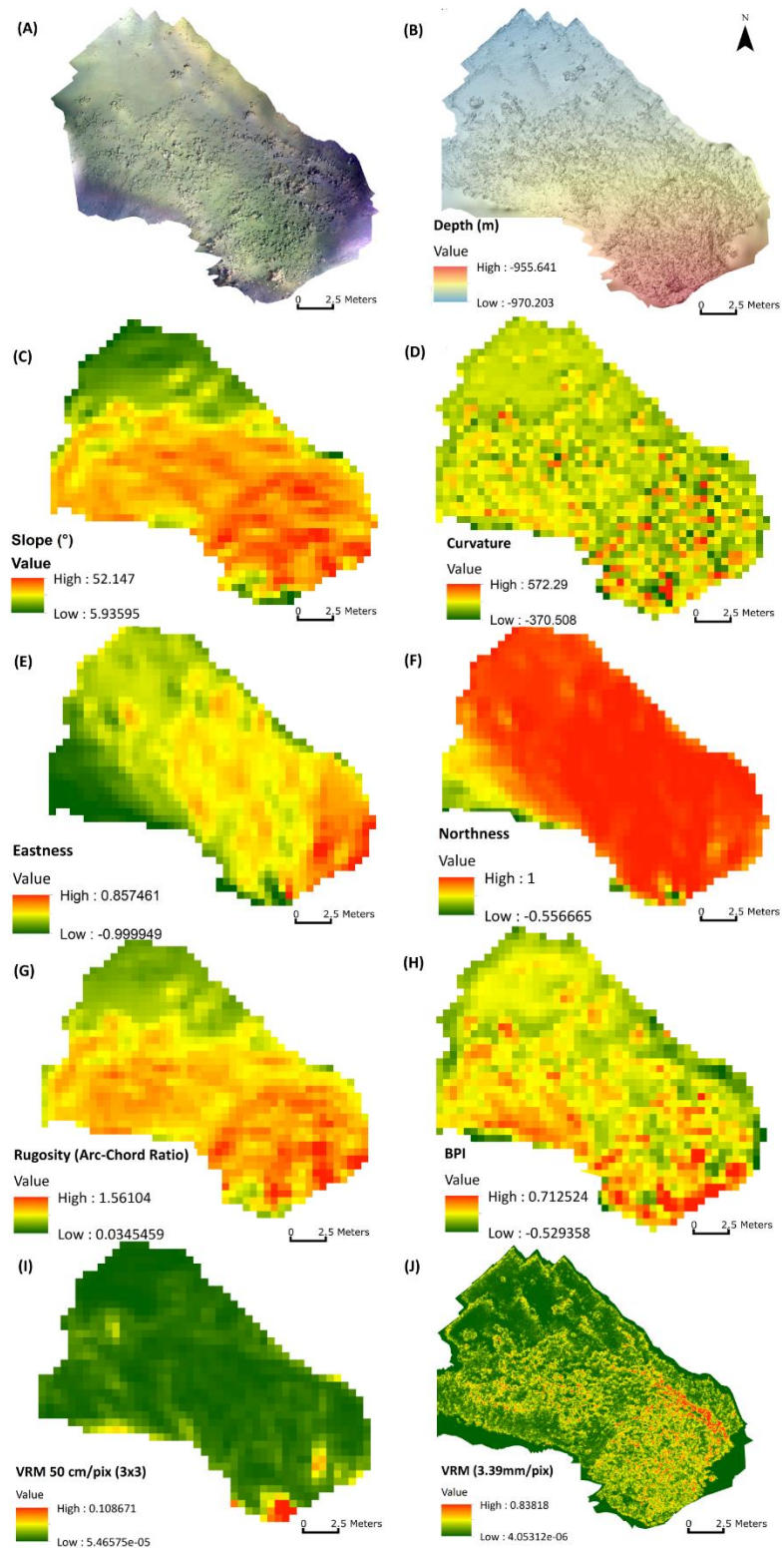


Figure 4.1: Spatial distribution of geomorphometric variables at 50cm/pixel resolution. (A) Orthomosaic (B) Hill shaded DEM (C) Slope (D) Curvature (E) Eastness (F) Northness (G) Rugosity (Arc-Chord Ratio) (H) BPI calculated with a 3x3 kernel size (I) Vector Ruggedness Measure (VRM) at 50 cm/pixel (J) VRM at 3.39mm/pixel.

4.3.2 Facies Distribution Analysis

The point cloud of the study area was segmented into 3096 semantic objects within the 4 facies outlined (LC, DC, SD, CR). The most common facies of the semantic objects is the SD facies (49%), followed by the CR facies (38.8%), LC (8.9%) and DC (3.3%) (Figure 4.2B). The LC and DC facies were represented by several ecosystem engineers such as the scleractinian CWCs *Lophelia pertusa* and *Madrepora oculata*. Both facies were observed as irregularly shaped isolated colonies and patches. The SD facies is characterised by soft sediments (sand or mud) and angular to subangular dropstones ranging from 1 to 20 cm in size. The CR facies is characterised by biogenic material e.g., coral fragments and shell fragments spread across the edges of the mound and low-relief areas.

4.3.2.1 Euclidean Radii Analysis

The LC class had a mean radius of $0.08 \pm 0.06\text{m}$ with a maximum radius of 0.49 m, whilst DC objects had a slightly larger radius with a mean of $0.12 \pm 0.07\text{m}$ and a maximum radius of 0.45 m. The larger DC and LC objects distribution were concentrated toward the top of the mound, between 955 and 960 metres depth (Figure 4.2C).

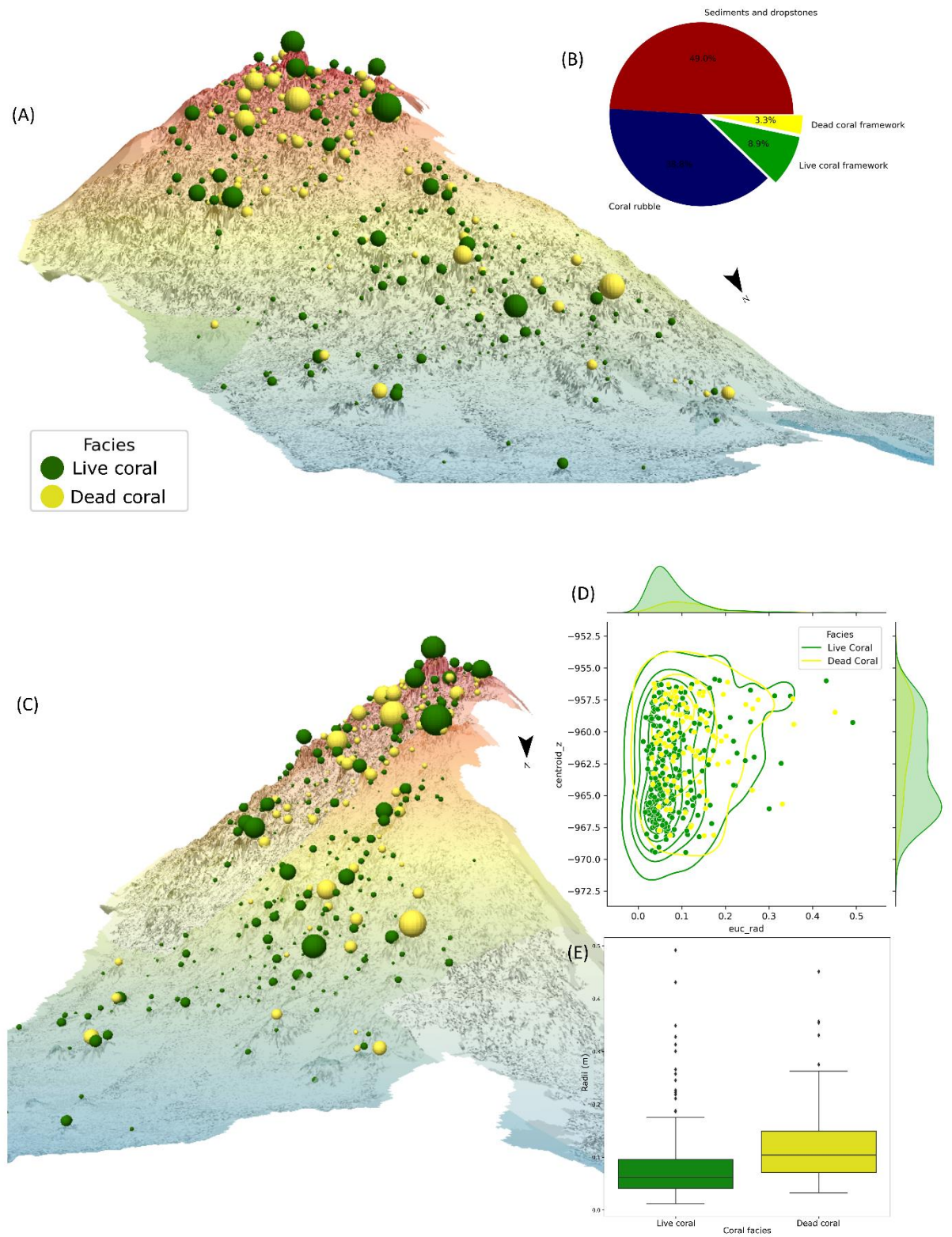


Figure 4.2: (A) Slope view of the hill shaded DEM overlaid with Euclidean radius buffers of DC (yellow) and LC facies (green) (B) Percentage of each of the four facies found in the study area. Percentages of each facies: SD = 49%, CR = 38.8%, LC = 8.9% and DC = 3.3%. (C) South facing view of the hill shaded DEM overlaid with Euclidean radius buffers (spheres) of DC and LC

facies. Spheres not to scale (D) Distribution of LC and DC facies object sizes (euc_rad) relative to depth (centroid_z). (E) Box plots of Euclidean radii distribution of LC (green), DC (yellow)

4.3.2.1 Facies distribution and geomorphometric analysis

Depth and slope

The distribution of facies in relation to the depth (Figure 4.3A) shows that the LC facies occurs within the interval of approximately 966 and 959 metres depth (962.73 ± 3.58 m), whereas DC occurs on higher sections of the mound, between 963 and 957 metres depth (960.73 ± 3.36 m). Similarly, CR occurs between 961 and 965 metres in depth (965.86 ± 3.26 m). SD is dominant in the lower parts of the mound, around 964 and 969 metres depth (963.19 ± 3.23 m). Coral classes (LC, DC, CR) were associated with steeper slopes (DC = $39.23^\circ \pm 7.026^\circ$, LC = $37.65^\circ \pm 7.034^\circ$, CR = $36.20^\circ \pm 7.062^\circ$), whilst SD facies were associated with discrete slopes (SD = $29.73^\circ \pm 9.865^\circ$) (Figure 4.3A).

Aspect

All four facies presented values of Northness above 0.90, where 1 is exactly northward and -1 is southward (Figure 4.3E). Similarly, all facies showed Eastness values below -0.1, where the value of 1 is exactly eastward and -1 is westward (Figure 4.3F). LC, DC and SD classes are oriented more northwards relative to the downslope direction (LC = 0.956 ± 0.086 , DC = 0.948 ± 0.109). The CR class appears to be slightly less oriented northwards (Northness = 0.908 ± 0.158) and more westwards (Eastness = -0.193 ± 0.336) than LC (Eastness = -0.171 ± 0.223) and DC (Eastness = -0.160146 ± 0.253). The SD facies shows lower Eastness values (Eastness = -0.246 ± 0.229), suggesting a westwards orientation.

BPI and Curvature

DC facies showed higher mean BPI (BPI= 0.066 ± 0.089) in comparison to LC facies (BPI= 0.047 ± 0.1), although the LC facies reached higher peaks of BPI (BPI=0.71) (Figure 4.3C). CR facies appeared to have the lowest mean BPI (BPI= 0.023 ± 0.1) among the coral facies. On the other hand, SD facies had negative mean BPI values (BPI= -0.027 ± 0.068).

Similarly, curvature mean values were higher for the DC facies (38.02 ± 104), followed by the LC facies (32.62 ± 94.9) and CR with significantly lower values (11.34 ± 90.56). Contrary to the DC facies, both LC and CR reached the highest peaks of curvature values (572.28 and 422.77, respectively). SD presented negative values (-17.31 ± 54.14), showing to be negatively skewed in relation to the coral facies (Figure 4.3D). The high standard deviation σ emphasises the spread-out pattern of the curvature values and the presence of outliers.

Rugosity and VRM

Rugosity mean values were also higher for the DC facies than LC facies (0.97 ± 0.17 and 0.93 ± 0.19 , respectively). CR facies presented similar values (0.91 ± 0.19). SD facies presented the lowest rugosity values with a mean of 0.74 ± 0.25 . Rugosity values showed a negatively skewed distribution across all four facies.

DC facies presented higher VRM mean values (0.006 ± 0.0004) followed by LC and CR (0.047 ± 0.007 and 0.0046 ± 0.005). Although the LC facies reached the highest peak of VRM (0.083), VRM measures across all four facies were low (0.0038 ± 0.0049) at 50cm/pixel resolution, showing low variability in the direction where surfaces are facing.

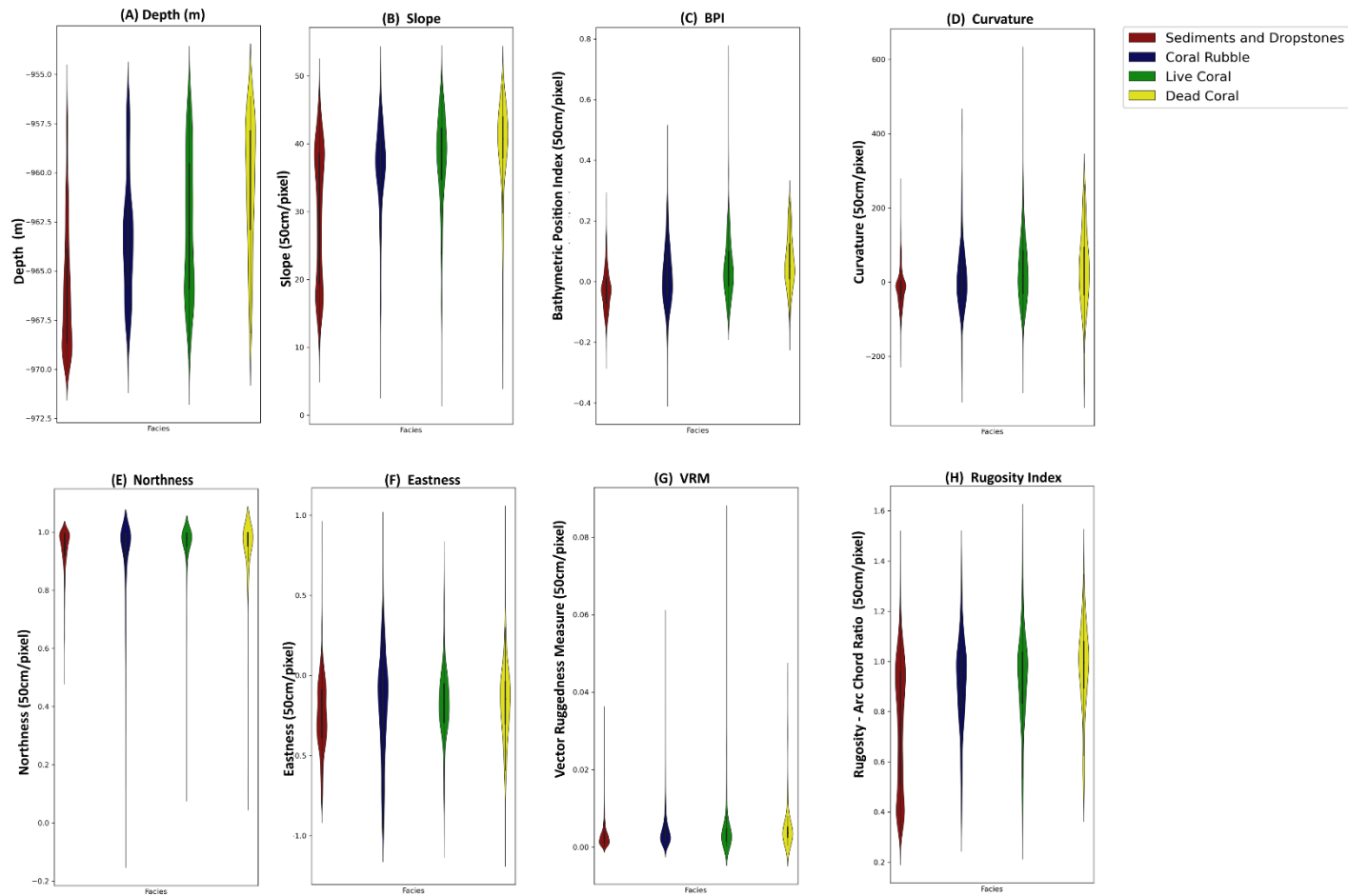


Figure 4.3: Violin box plots showing the distribution of abiotic (terrain) variables for each facies at 50cm/pixel resolution. (A) Depth (m) (B) Slope (C) Bathymetry Position Index (BPI) (D) Curvature (E) Northness (F) Eastness (G) Vector Ruggedness Measure (VRM) (H) Rugosity index (Arc-Chord Ratio).

Spearman's rank correlations among terrain variables showed that slope and depth were strongly correlated ($\rho = 0.65$ $\alpha < 0.05$) (Figure 4.4). Depth is also moderately correlated with Eastness ($\rho = 0.42$) and BPI ($\rho = 0.37$) but weakly correlated with Northness (0.26). Curvature and BPI showed a very strong correlation ($\rho = 0.73$ $\alpha < 0.05$), although the majority of terrain variables did not present statistically meaningful correlations and were therefore not considered.

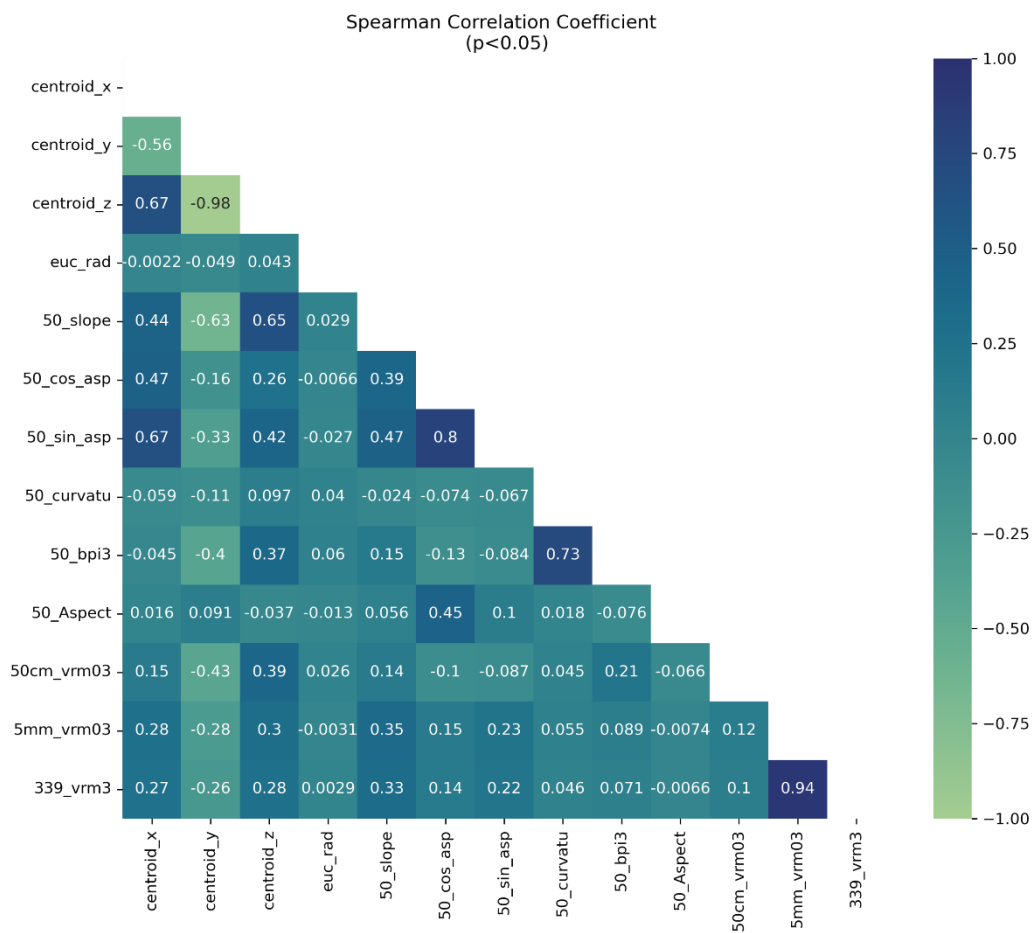


Figure 4.4: Spearman's Correlation coefficient (SCC) matrix for the entire study area (left). Only coefficients that were significant at the level of 95% were included.

Spearman's coefficients for each facies (Figure 4.5) showed that depth was moderately correlated with VRM for the LC ($\rho = 0.45$), DC ($\rho = 0.42$) and SD ($\rho = 0.43$) facies but showed a weak correlation within the CR ($\rho = 0.25$) facies. Whereas the Depth -slope relationship was strongly correlated in the SD facies ($\rho = 0.84$), moderately correlated in the LC ($\rho = 0.43$) and CR ($\rho = 0.33$) facies but substantially less

significant for DC ($\rho=0.0086$). The relationship between depth and BPI also appears to be moderately correlated across the facies, with exception of DC ($\rho=0.11$). VRM(50) and BPI also present a moderate correlation among all coral facies, but they show a negative weak relationship within the SD facies. Rugosity and slope are also strongly correlated among all facies ($\rho >0.7$).

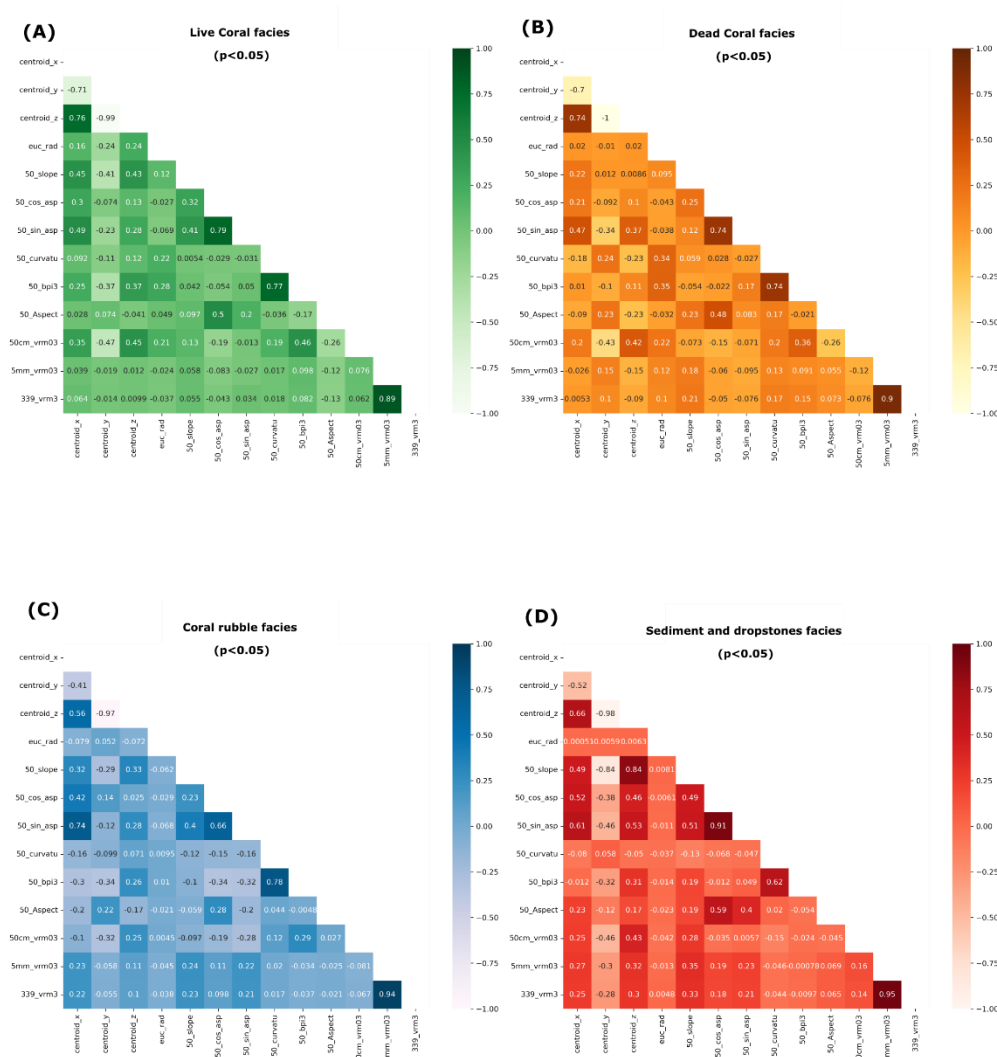


Figure 4.5: Subplots of Spearman's correlation coefficients for each facies, where green= LC, orange= DC, blue = CR, and red= SD.

4.3.2.1 Density in function of covariate

The density in function of the covariate (Smoothing Estimate of Covariate Transformation) results (Figure 4.6) shows that LC are more likely to be found at depths between -968 and -964 and -962 to -956 metres than would be expected if the

intensity was constant (*Bermans Z2 test*; $Z2 = 6.317$, $p\text{-value} < 0.001$). DC facies is likely to be found mainly at depths between -962 to -956 metres than would be expected if the intensity was constant (*Bermans Z2 test*; $Z2 = 8.689$, $p\text{-value} < 0.001$), showing that there is a relationship with depth on the distribution of both DC and LC. The distribution of LC in relation to the slope is also not random, instead, it shows a relationship to slope, especially in areas with low ($<10^\circ$) and high ($> 40^\circ$) slope values (*Bermans Z2 test*; $Z2 = 7.967$, $p\text{-value} < 0.001$; *CDF p-value* < 0.001). Slope may have an even stronger relationship to the distribution of DC facies, especially around steep areas ($> 35^\circ$) (*Bermans Z2 test*; $Z2 = 6.967$, $p\text{-value} < 0.001$; *CDF p-value* < 0.001). The intensity of LC and DC in relation to Eastness shows that LC (*Bermans Z2 test*; $Z2 = 2.719$, $p\text{-value} = 0.006$; *CDF p-value* < 0.001) and DC (*Bermans Z2 test*; $Z2 = 2.119$, $p\text{-value} = 0.034$; *CDF p-value* $= 0.034$) facies are more likely to be found at the intervals between -0.5 and 0 than if the intensity was constant, showing an influence by slope orientation in areas that the mound is oriented westwards. There was no discernible relationship between Northness and the LC and DC distribution as there was not enough variance of Northness values, which were close to 1 (LC = $0.956 \pm \alpha 0.086$, DC = $0.948 \pm \alpha 0.109$).

PPM results showed that the model with covariate depth, slope, Northness and Eastness was more suited to explain the distribution of the DC point pattern (AIC = 294.63) than the model with no covariates (AIC = 416.43). Similarly, the distribution of the LC point pattern was better explained by the model with all covariates (AIC = 422.0001) than by the hypothesis of no covariates (AIC = 579.67).

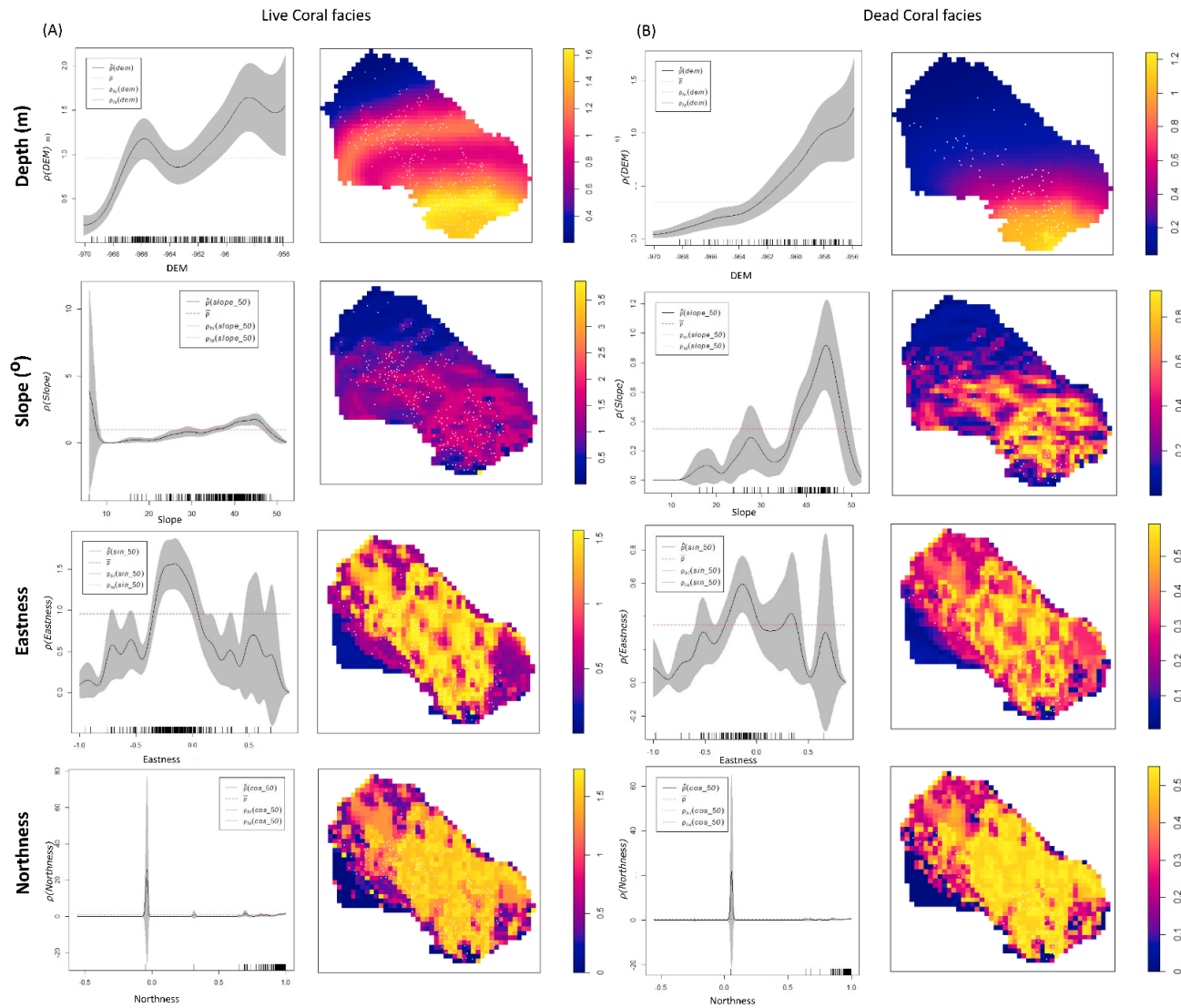


Figure 4.6: Estimated density function in relation to terrain covariates (rho-hat) for (A) live coral (LC) facies (B) and dead coral (DC) facies and respective density estimate plots. The grey area on rho-hat plots represents the 95% confidence envelope.

4.3.2.1 Density-based and hotspot analysis

Kernel estimate density plots showed that the LC and DC facies contributed to different intensity patterns. LC facies had an average intensity of 0.95 points/m², whereas DC showed an intensity of 0.34 points/m². LC facies showed two density hotspots, located towards the south of the mound and another of higher intensity hotspots towards the downslope area (Figure 4.7A). The DC facies, on the other hand, present one hotspot located towards the south, at shallower depths (approx. 955.64 m) (Figure 4.7B). Although both facies indicated an affinity towards the top of the mound, the DC hotspots were denser in shallower areas. The differences in density distribution are also emphasised across different coral sizes. The density plots by Euclidean radii size (Figure 4.7G and Figure 4.7H) showed that, in both LC and DC, larger corals tend to appear higher up towards the mound summit. Small corals distribution (Figure 4.7C and Figure 4.7D), show a similar trend to the overall intensity distribution whereas medium and larger LC and DC objects contribute to density hotspots in different mound areas (Figure 4.7E, F, G, H).

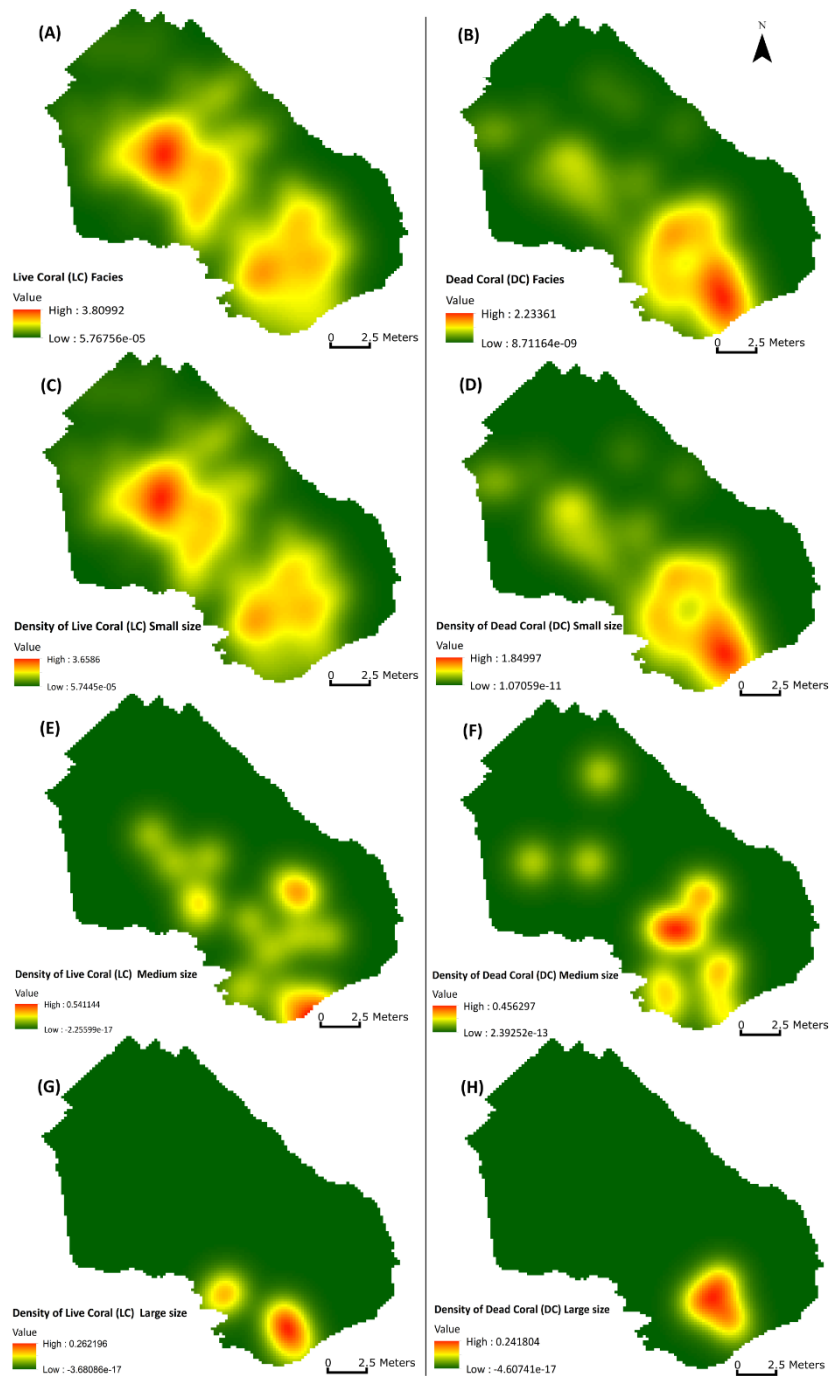


Figure 4.7: Kernel estimate intensity plots of number of points per m^2 ($\sigma=1$) of Live coral (LC) facies (left) and Dead coral (DC) facies (right) separated in (A) LC facies all sizes (B) DC facies all sizes (C) LC of small size (Euclidean radius $\leq 0.17m$) (D) DC of small size (E) LC of medium size (Euclidean radius $\leq 0.33 m$) (F) DC of medium size (G) LC of large sizes (Euclidean radius $\leq 0.49m$) (H) DC of large sizes.

Hotspot analysis (Getis- Ord G_i^*)

The distribution of LC shows high confidence hotspots throughout the entire mound but more intense clusters (Z score > 4) are located towards higher parts of the mound,

between 956 and 962 m water depth (Figure 4.8A). The Euclidean radius of the LC facies does not visually appear to be related to the intensity of the clustering. The hotspots of DC are concentrated towards the higher parts of the mound but the higher confidence hotspots show a less heterogeneous distribution, concentrated from 954 to 964 m water depth and with higher intensity clusters (Z score > 4) within these depth intervals (Figure 4.8B). Similarly, the Euclidean radii do not appear to be related to the intensity of the clustering.

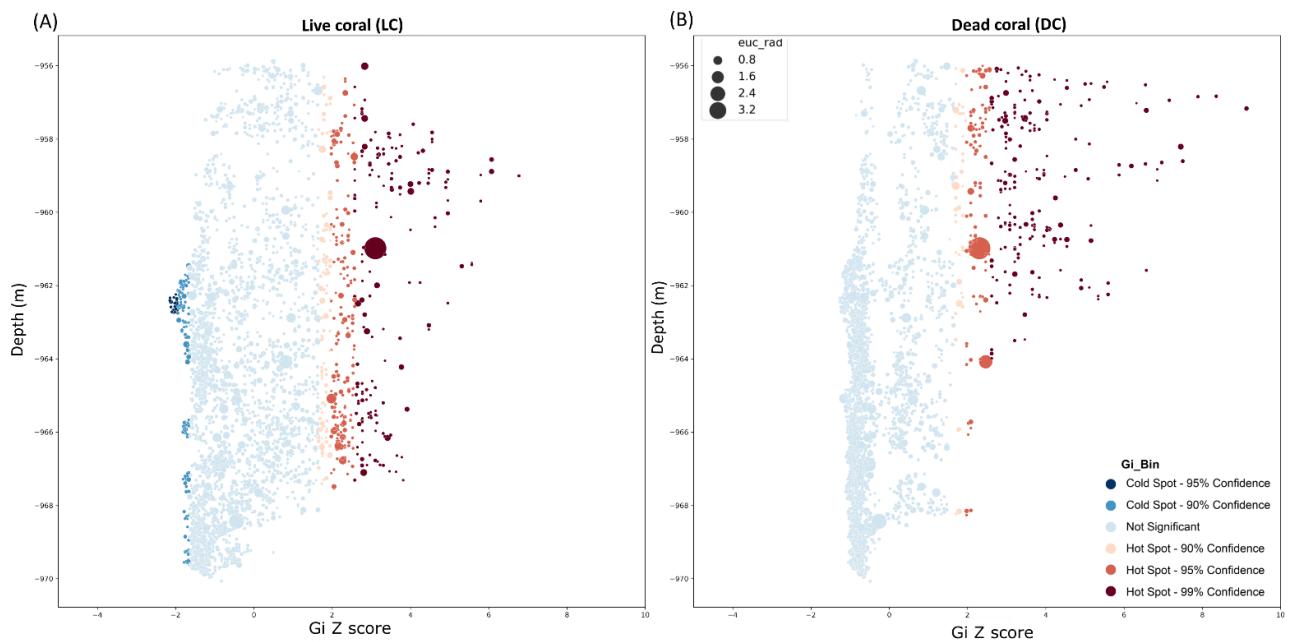


Figure 4.8: Scatter plots showing the High-Low clustering (Getis-Ord General G) results of (A) Live coral (LC) facies (B) Dead coral (DC) facies. Gi Z-score (X axis) shows the intensity of the clustering vs. depth (y-axis). The sizes of the circles represent the relative Euclidean radii of the facies sphere.

4.3.2.2 Multiscale cluster analysis

The results of both LC and DC indicate that a typical point has more neighbours than would be expected if the pattern were completely random, thus, showing a clustering pattern (Figure 4.9). LC facies shows an initial clustering of points at distances close to zero suggesting a relationship between the point and itself or other points, which is followed by a dispersion pattern ($L^{\wedge} < 0$) at $r \sim 0.2m$. Though this happens within the confidence envelope ($ci = 95\%$), there may be acceptance of the null hypothesis. As the distance band (r) increases, L^{\wedge} indicates a stronger clustering-like pattern than expected in a CRS pattern, from distances > 0.3 onwards. The DC facies show a similar pattern within the confidence envelope, but a clustering-like pattern appears to be more evident from distances $> 0.2m$.

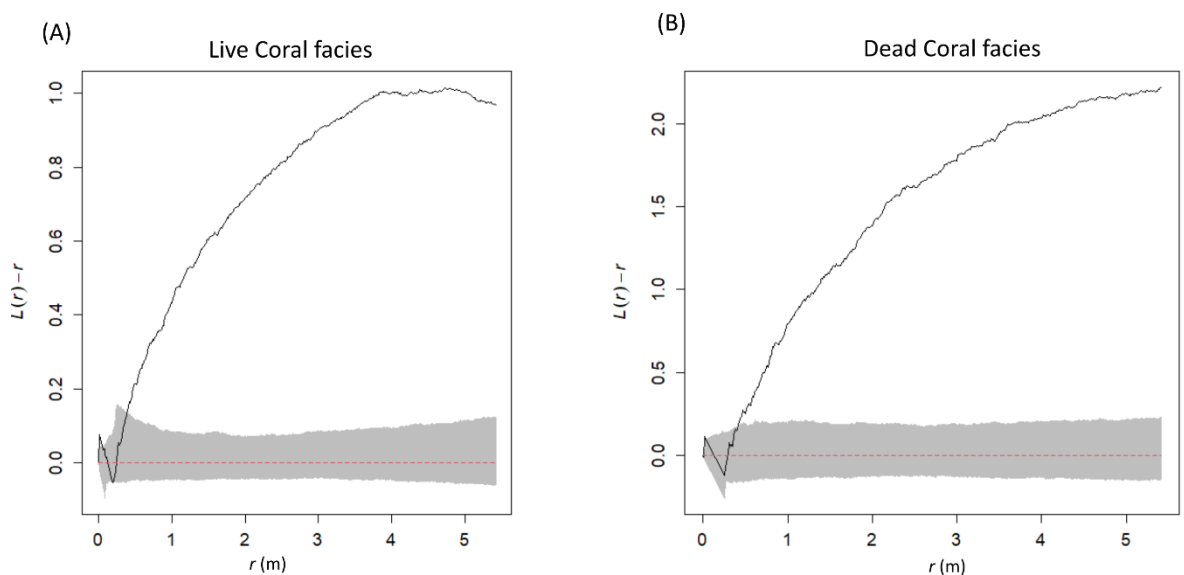


Figure 4.9: L-function plots showing the clustering likelihood in relation to the distance of each point ($r(m)$) of (A) Live coral (LC) facies and (B) dead coral (DC) facies. The grey shaded area represents the confidence interval of 95% from 999 Montecarlo simulations ($nrank=25$).

4.4 Discussion

The spatial variability of scleractinian corals that contribute to the CWC habitats in the North Atlantic has been subject of exploration for many decades (Purser et al., 2013). Several studies have incorporated 3D SfM photogrammetry and its high-resolution data products to map CWC distribution on mounds and reefs (Price et al., 2019), on vertical walls (Casoli et al., 2021; Robert et al., 2017) and in the vicinity of submarine canyons (de Oliveira et al., 2021; Lim et al., 2020c). In this study, we develop an approach to analyse CWC mound facies distribution by coupling the 3D information of each object and their fine-scale terrain variables with point pattern distance and density analysis. The transformation of thousands of labelled points into meaningful point objects that carry 3D information about each facies object demonstrates a novel use of these methodologies to further investigate facies distribution and coral mound development. The geomorphometric metrics derived from the SfM process enabled the quantification of the underlying structural complexity inherent to coral facies and sediment-dominated regions.

The study area is part of the Piddington Mound, the largest of the cold-water coral Moira Mounds, which has been previously characterised by its habitat heterogeneity across substrate facies (Lim et al., 2017) which are known to influence benthic distribution in different environmental settings (Borcard and Legendre, 2002; Savini et al., 2014). Here, the variability of facies distribution was shown by general density trends and clustering analyses of coral facies including for both living and dead coral.

Comparable to Lim et al. (2017), the sediment and dropstones (SD) facies also occur predominantly where the seabed is relatively flat around the protruding mound feature. The DC framework, LC framework and CR coexist, as shown by the proximity of distribution towards shallower areas, or peak of the mound (Figure 4.3). This proximity is reflective of normal coral growth whereby coral growth leaves behind bare dead skeletons and gradual breakdown results in coral rubble. In settings where sedimentation is more prevalent, the dead coral below the live coral is buried (Wheeler et al., 2005). This was not the case for the DC facies found here, as the dead

corals were larger in size and retained the vertical structure, not showing significant visual signs of burial. This suggests that the sediment deposition is not prevalent in this area or that the structure left behind had not existed long enough for significant burial. This is corroborated by Lim (Lim, 2017) which suggest that the area is subjected to erosion or at least non deposition based on the presence of ice-rafted debris (IRD) and Holocene muds, which have been previously documented to be linked with non-sedimentation in other areas such as the Rockwall Trough (de Haas et al., 2009). Furthermore, the region is influenced by dynamic environmental conditions, as evidenced by the change in sediment and coral facies over an interval of 4 years (Bohlukos et al., 2019). Thus, the hotspots of DC facies around the summit, along with the previously documented coral decline suggest that the contemporary environment is stressed and that summit conditions may be too hydrodynamic for optimal coral growth (Bohlukos et al., 2019)

Similar to the findings herein, other studies have reported a zonation trend with the prevalence of sediments and dropstones in the deeper water parts of the mound while the coral facies dominate marginal areas within steeper slopes and upslope areas and whilst the dead coral and coral rubble occur around the mound, the LC facies dominates the northernmost parts (Conti et al., 2019; Lim et al., 2017). CWC tend to settle or grow on elevated structures where access to food supply is facilitated by faster-flowing waters (Freiwald, 2002; Roberts et al., 2003). Considering that both segments are proximal to each other, this pattern suggests that this study region may be under similar abiotic conditions, being under the influence of northerly directed prevailing currents.

The concentration of coral facies around the mound summit can be explained by these abiotic drivers. However, it may not explain the higher density of LC facies in the downslope areas, where sediments and dropstones are dominant. This distribution may suggest that LC facies in that region may be driven by the presence of hard substrate instead. Thus, emphasising the role of sediment heterogeneity in the distribution of benthic fauna (Lacharité and Metaxas, 2017). The size of the corals in that region also corroborates with this hypothesis as the corals in the downslope area are predominantly small, between 1 and 17 cm (Figure 4.2). The relationship between

the size of the coral and the presence of dropstones may indicate early stages of mound development, where young corals rely on hard substrate to cement on (Lim et al., 2018a; Roberts et al., 2006) thus suggesting both an active coral growth (Foubert et al., 2011; Wheeler et al., 2011) and relatively recent coral colonies latching on these dropstones (Lim et al., 2018a) .

Studies have associated coral rubble with bioerosion of exposed surfaces (Titschack et al., 2015) that can be caused by currents (Wilson, 1979) and higher mean current speeds (Lim et al., 2020c). As such, the distribution of CR facies along the edges of the mound may be explained by two factors: i) higher current speeds and ii) steepened slopes that may cause eroded bioclasts from the peak of the mound to slide down onto flatter parts (Lim et al., 2017) following the slope orientation. This is also supported by the importance of aspect variables in the PPM, 'rho-hat' and Spearman correlation analyses, which may indicate the influence of localised abiotic drivers e.g., currents as also suggested in other studies (Price et al., 2021). The eroded bioclasts are likely originating from the dead coral facies that dominate the peak of the mound between 963 and 957 metres depth (960.73 ± 3.36 m). Furthermore, current speeds may also interact with coral size. Whilst larger corals can baffle the flow and create a protection against bioerosion, smaller corals may lack this baffling capacity becoming more exposed to currents speeds, and consequently erosion.

The distribution of facies in relation to water depth reflects the zonation around the area as a clear transition from sediment-dominated facies to coral facies as water depth increases, i.e., up the flanks of the mound (Figure 4.2). The presence of coral (both LC and DC) appeared linked with the slope, Eastness and BPI. These links have been noted before at larger scales (Davies et al., 2008; Guinan et al., 2009; Heindel et al., 2010; Masson et al., 2003; Mogstad et al., 2022; Sundahl et al., 2020), whereby residual currents (and their direction) and internal tides may act as a driving mechanism (Frederiksen et al., 1992). On the nearby Propeller Mounds, for example, live coral facies appear restricted to the upper slopes of the giant mound ridges (Heindel et al., 2010). The centimetric scale observation herein shows that DC and LC facies tend to occupy steep west-facing slopes, and positive bathymetric features e.g., local crests, whilst CR and SD facies tend to occur in low relief areas. This may reflect

the corals' ability to feed, protruding into the water column or oriented more vertically in order to feed on particles passing by and influence the local current regime (Buhl-Mortensen et al., 2010; Corbera et al., 2022; Mienis et al., 2019).

The BPI values provide information about topographic features in the terrain indicating positive (e.g., a crest) or negative (e.g., trough features) topographic areas (Wilson et al., 2007). In this study, the BPI values for both LC and DC have a unimodal distribution pattern, but the DC facies showed a higher mean BPI than the LC facies, although the BPI of LC showed higher peaks. Whilst CR and SD facies showed lower and negative mean values, respectively. Although our data were downsampled to 50 cm (larger than all LC colonies and DC patches), the coral facies may still play a role in the BPI and slope themselves, indicative of a positive feedback mechanism for the living patches of coral to be elevated.

In shallower waters, species distribution studies using SfM to map sponges and other echinoderms also showed that the probability of occurrence of the species increases directly as BPI and roughness increase (Prado et al., 2020). This study shows that areas with high sloping terrains overlap with areas with higher rugosity (Figure 4.1) and with areas of high coral density, which highlights the response of terrain variables to the high structural complexity created by coral facies.

LC and DC facies distribution showed a different response to terrain variables such as slope and Eastness and water depth (Figure 4.6). This difference is also highlighted in the distribution patterns of the kernel density estimate plots which show distinct intensity hotspots for each of the facies. Thus, LC and DC facies may influence or be influenced by terrain characteristics differently, highlighting habitat heterogeneity within centimetric scales. The difference between LC and DC likely reflects the suitability for living portions of the reef.

Hotspot distributions of LC and DC do not entirely overlap with the areas where VRM are high at 50 cm/pixel resolution, but it seems to follow the high VRM values at very high resolutions (3.39mm/pixel). This reaffirms what has been documented in other studies where high VRM values are considered a product of higher structural complexity promoted by coral frameworks (Graham and Nash, 2013; Prado et al.,

2020; Robert et al., 2017). Rugosity mean values were also higher for the DC facies than LC facies (0.97 ± 0.17 and 0.93 ± 0.19 , respectively). This may suggest that the dead coral framework is more prone to the collapse of opening up holes in the framework increasing VRM and rugosity, whereas live corals are actively growing, more efficiently filling the framework surface.

Price et al. (2021) divided the substrate map generated from the SfM into reef (including rubble) and non-reef areas, where reef areas represented high VRM, slope and aspect sections of the mound. Although using a different approach which was focused on the facies instead of species distribution, the results herein show that coral facies also have a connection with reef-like habitats, whereas CR occupied or formed lower VRM areas than LC and DC classes, indicating lower structural complexity. This behaviour pairs with the discussion regarding the influence of biological drivers on the terrain drivers is a circular relationship.

The density plots were an important resource towards revealing different intensity patterns for LC and DC facies. Whereas LC presents two high-density hotspots, one around the mid-slope area, which is more intense, and a second less intense hotspot upslope, the DC facies present one high-intensity hotspot upslope. This pattern distribution contrasts with other studies that suggest that live coral frameworks typically occur at or proximal to mound summits (Rüggeberg et al., 2011) rather than flat regions. This highlights the danger of generalisations and the need to measure environmental drivers for LC occurrence rather than simple depth relationships. However, the difference in patterns seen between mounds may relate to local hydrodynamic regimes and also the stage of mound formation as the Piddington Mound is significantly smaller than the mounds studied by Rüggeberg et al. (2011). In other mound settings, e.g., the Hovland Mound (Rüggeberg et al., 2011) summit environments may offer optimal conditions for food supply and coral growth. Studies have also found distinctive distribution patterns among scleractinian species *Madrepora oculata* and *Lophelia pertusa*, highlighting the contrast not just between live and dead facies, but also at species level (Price et al., 2021; Purser et al., 2013).

L-function plots showed a tendency of LC and DC facies to cluster at distances higher than 0.3 metres, which can be a reflection of not only abiotic but also biotic drivers

e.g., reproductive methods of LC (Price et al., 2021). Density plots show that these facies tend to occur towards the shallower parts of the mound, surrounded by CR facies which occur along the edges. This pattern may suggest that this study section may be part of a larger mound setting as the pattern resembles sections of a proximal area described in Lim et al. (2017), where CR dominated the mound summit and fringes whereas DC and LC dominated the topmost part of the mound. Given the fact that the study area is located within the Belgica Mound Province, which has been characterised by conical mounds (De Mol et al., 2002; Foubert et al., 2006), it is likely that the study area may follow or be part of a similar conical mound in a wider environmental setting. However, the mechanisms driving the distribution patterns are unclear given the lack of studies regarding the long-term environmental drivers of the area.

LC and DC facies distribution was characterised by individual colonies and patches that reached a maximum Euclidean radii size of approximately 50 cm but an average of 12 cm. The density distribution plots showed that in both LC and DC facies, larger corals tend to appear towards shallower parts of the mound, creating particular density hotspots in the mound summit (Figure 4.7). On the other hand, small corals dominate the downslope areas dictating the overall intensity distribution (Figure 4.7C and D). Studies have suggested that CWC have a preference to settle in elevated structures where access to food supply from the incoming current is higher (Davies et al., 2008; Freiwald, 2002; Mortensen and Buhl-Mortensen, 2004) as currents may increase the vertical nutrient flux (Roberts et al., 2003). The steepness of the mound and the dominating presence of larger corals both living, and dead may reflect a topographic high generated by the capacity of corals to trap and accumulate (baffle) sediment (Heindel et al., 2010; Wheeler et al., 2005, 2007). On the other hand, but following the similar trend, the distribution of small corals was concentrated around deeper, low-sloping parts of the mound. Studies have associated this pattern as a response to low current speeds and inconsistent food supply (Davies et al., 2008; Freiwald et al., 2004). However, the presence of smaller corals in areas dominated by sediments and dropstones may also indicate that these corals are in a juvenile stage, using the hard substrate for initial development, whereas the large colonies can be long-lived.

Nonetheless, this interpretation is only possible herein with the analysis of size distribution created from the classified habitat.

The 3D size and structure of corals are indicators of many ecosystem functions (Courtney et al., 2007). For example, measurements of size can be used to infer the age of corals from estimated growth rates (Mortensen et al., 1995). When not using SfM photogrammetry, analyses of coral sizes are typically done by physical sampling or observing video transects, images or side-scan sonar images and extracting manual estimates of the size of each colony (De Clippele et al., 2021; Mortensen et al., 1995; Wheeler et al., 2011). The inclusion of body size measures provides important information about food supply, colony development, and biomass estimates (Benoist et al., 2019; De Clippele et al., 2021; Peters, 1983). However, manual size estimation methods may limit the extent to which size measurements can be integrated into study designs. The Euclidean size estimates developed herein provide an efficient approach to integrating size into high-resolution analyses.

The findings herein contribute to highlighting the existing high degree of variability resulting from morphological and biological traits of CWC mounds across not only regional but also local scales (Purser et al., 2013; Wheeler et al., 2007). Although the further interpretation of environmental controls is central to understanding the CWC habitat development, the inclusion of three-dimensional variables such as coral size at high resolution can support fine-scale observations about the environment. Marine Strategy Framework Directive advises that SACs should be monitored every 6 years (EU) 2017/848). The datasets produced herein provide a proxy for temporal studies that can inform CWC variability within time scales. These studies, which have shown a decline in CWC over the years (Bohlukos et al., 2019) are key to understanding the impact of natural and anthropogenic activities in CWC mounds, especially in the context of Marine Protected Areas which exhibit low or no recovery on grander time scales (Huvenne et al., 2016)

4.5 Conclusions

This study integrates SfM photogrammetry, terrain features and point pattern analyses to provide an approach to fine-scale environmental analysis of CWC. The results show that the corals in the downslope area are predominantly small, between 1 and 17 cm. The relationship between the size of the coral and the presence of dropstones indicates that the study region is in the early stages of coral growth development. Larger corals dominate the regions towards the mound summit, where the DC facies is marked by larger corals than the LC facies, creating different density hotspots in those areas. Furthermore, DC and LC facies tend to occupy steep west-facing slopes, and positive bathymetric features e.g., local crests, whilst CR and SD facies tend to occur in low relief areas. The relationship between coral facies and terrain variables is indicative of a positive feedback mechanism where larger corals influence the topography of the terrain and increase the structural complexity, making it a suitable environment for the growth of small colonies.

The findings of this study help to emphasize the importance of understanding the spatial structure whilst highlighting the heterogeneity of CWC habitats. Therefore, environmental management policies of these regions should disregard any homogeneity patterns based on the assumption that all CWC ecosystem areas have the same drivers and morphologies, and therefore should be granted interchangeable interpretations. SfM and photogrammetry can improve the understanding of underwater ecosystems and their key drivers whilst contributing to monitoring, management and conservation (Ferrari et al., 2016). Here, we deliver an accessible mapping approach from the automated classification (de Oliveira et al., 2022a) to the environmental analysis incorporating crucial ecosystem traits such as coral size. The findings herein will facilitate the investigation of possible changes in this and surrounding habitats, thus having valuable temporal-spatial importance towards the monitoring of vulnerable ecosystems in MPAs and SACS.

4.6 References

- Addamo, A.M., Vertino, A., Stolarski, J., García-Jiménez, R., Taviani, M., Machordom, A., 2016. Merging scleractinian genera: The overwhelming genetic similarity between solitary *Desmophyllum* and colonial *Lophelia*. *BMC Evol. Biol.* 16, 1–17. <https://doi.org/10.1186/s12862-016-0654-8>
- Agisoft, 2021. Agisoft Metashape User Manual: Professional Edition, Version 1.7. Agisoft Metashape 160.
- Appah, J.K.M., Lim, A., Harris, K., O’Riordan, R., O’Reilly, L., Wheeler, A.J., 2020. Are Non-reef Habitats as Important to Benthic Diversity and Composition as Coral Reef and Rubble Habitats in Submarine Canyons? Analysis of Controls on Benthic Megafauna Distribution in the Porcupine Bank Canyon, NE Atlantic. *Front. Mar. Sci.* 7, 831. <https://doi.org/10.3389/fmars.2020.571820>
- ArcGIS, 2014. Hot Spot Analysis (Getis-Ord G_i^*) (Spatial Statistics) Illustration Usage 1–7.
- Baddeley, A., 2010. Analysing spatial point patterns in R. Workshop Notes - Version 4.1 178–204.
- Baddeley, A., Rubak, E., Turner, R., 2015. Spatial Point Patterns, Spatial Point Patterns. <https://doi.org/10.1201/b19708>
- Baddeley, A., Turner, R., Coeurjolly, J., Cruz, M. De, Dalgaard, P., Diggle, P.J., Hardegen, A., Hering, M., Hansen, M.B., Hazelton, M., Madin, B., Mark, R., Mateu, J., Mccullagh, P., Mehlis, U., Meyer, S., Mi, X.C., Moller, J., Mudrak, E., Nielsen, L.S., Nunes, F., Rowlingson, B., Rudge, J., Safavimanesh, F., Sarkka, A., Villers, A., Vinatier, F., Wang, H., Wendrock, H., Wild, J., Wong, S., Zamboni, M.E., 2013. Package ‘ spatstat . ’
- Benoist, N.M.A., Bett, B.J., Morris, K.J., Ruhl, H.A., 2019. A generalised volumetric method to estimate the biomass of photographically surveyed benthic megafauna. *Prog. Oceanogr.* 178, 102188. <https://doi.org/10.1016/j.pocean.2019.102188>
- Berman, M., 1986. Testing for Spatial Association Between a Point Process and Another Stochastic Process. *Appl. Stat.* 35, 54. <https://doi.org/10.2307/2347865>

Bohlukos, C.M., Lim, A., O’Riordan, R.M., Wheeler, A.J., O’Riordan, R.M., Wheeler, A.J., O’Riordan, R.M., Wheeler, A.J., 2019. Cold-water corals in decline – A temporal (4 year) species abundance and biodiversity appraisal of complete photomosaiced cold-water coral reef on the Irish Margin. *Deep Sea Res. Part I Oceanogr. Res. Pap.* 146, 44–54. <https://doi.org/10.1016/j.dsr.2019.03.004>

Borcard, D., Legendre, P., 2002. All-scale spatial analysis of ecological data by means of principal coordinates of neighbour matrices. *Ecol. Modell.* 153, 51–68. [https://doi.org/10.1016/S0304-3800\(01\)00501-4](https://doi.org/10.1016/S0304-3800(01)00501-4)

Buhl-Mortensen, L., Vanreusel, A., Gooday, A.J., Levin, L.A., Priede, I.G., Buhl-Mortensen, P., Gheerardyn, H., King, N.J., Raes, M., 2010. Biological structures as a source of habitat heterogeneity and biodiversity on the deep ocean margins. *Mar. Ecol* 31, 21–50.

Burns, Delparte, D., Gates, R., Takabayashi, M., 2015. Integrating structure-from-motion photogrammetry with geospatial software as a novel technique for quantifying 3D ecological characteristics of coral reefs. *PeerJ* 3, e1077. <https://doi.org/10.7717/peerj.1077>

Burns, Fukunaga, A., Pascoe, K.H., Runyan, A., Craig, B.K., Talbot, J., Pugh, A., Kosaki, R.K., 2019. 3D HABITAT COMPLEXITY OF CORAL REEFS IN THE NORTHWESTERN HAWAIIAN ISLANDS IS DRIVEN BY CORAL ASSEMBLAGE STRUCTURE. *Int. Arch. Photogramm. Remote Sens. Spat. Inf. Sci.* XLII-2/W10, 61–67. <https://doi.org/10.5194/isprs-archives-XLII-2-W10-61-2019>

Burns, Weyenberg, G., Mandel, T., Ferreira, S.B., Gotshalk, D., Kinoshita, C.K., Marshall, M.J., Del Moral, N.A. V., Murphy, S.J., Pascoe, K.H., Runyan, A., Spengler, A.J., Wells, B.D., Wilde, D.K., Pelayo, R., 2020. A Comparison of the Diagnostic Accuracy of in-situ and Digital Image-Based Assessments of Coral Health and Disease. *Front. Mar. Sci.* 7. <https://doi.org/10.3389/fmars.2020.00304>

Casoli, E., Ventura, D., Mancini, G., Pace, D.S., Belluscio, A., Ardizzone, G., 2021. High spatial resolution photo mosaicking for the monitoring of coralligenous reefs. *Coral Reefs* 40, 1267–1280. <https://doi.org/10.1007/s00338-021-02136-4>

Cathalot, C., Van Oevelen, D., Cox, T.J.S., Kutti, T., Lavaleye, M., Duineveld, G.,

- Meysman, F.J.R., 2015. Cold-water coral reefs and adjacent sponge grounds: hotspots of benthic respiration and organic carbon cycling in the deep sea. *Front. Mar. Sci.* 2. <https://doi.org/10.3389/fmars.2015.00037>
- Chen, G.K., Dai, C.F., 2021. Using 3D photogrammetry to quantify the subtle differences of coral reefs under the impacts of marine activities. *Mar. Pollut. Bull.* 173, 113032. <https://doi.org/10.1016/j.marpolbul.2021.113032>
- Cocito, S., Sgorbini, S., Peirano, A., Valle, M., 2003. 3-D reconstruction of biological objects using underwater video technique and image processing. *J. Exp. Mar. Bio. Ecol.* 297, 57–70. [https://doi.org/10.1016/S0022-0981\(03\)00369-1](https://doi.org/10.1016/S0022-0981(03)00369-1)
- Conti, L.A., Lim, A., Wheeler, A.J., 2019. High resolution mapping of a cold water coral mound. *Sci. Rep.* 9, 1016. <https://doi.org/10.1038/s41598-018-37725-x>
- Corbera, G., Lo Iacono, C., Gràcia, E., Grinyó, J., Pierdomenico, M., Huvenne, V.A.I., Aguilar, R., Gili, J.M., 2019. Ecological characterisation of a Mediterranean cold-water coral reef: Cabliers Coral Mound Province (Alboran Sea, western Mediterranean). *Prog. Oceanogr.* 175, 245–262. <https://doi.org/10.1016/j.pocean.2019.04.010>
- Corbera, G., Lo Iacono, C., Simarro, G., Grinyó, J., Ambroso, S., Huvenne, V.A.I., Mienis, F., Carreiro-Silva, M., Martins, I., Mano, B., Orejas, C., Larsson, A., Hennige, S., Gori, A., 2022. Local-scale feedbacks influencing cold-water coral growth and subsequent reef formation. *Sci. Rep.* 12, 1–14. <https://doi.org/10.1038/s41598-022-24711-7>
- Costello, M.J., McCrea, M., Freiwald, A., Lundälv, T., Jonsson, L., Bett, B.J., van Weering, T.C.E., de Haas, H., Roberts, J.M., Allen, D., 2005. Role of cold-water *Lophelia pertusa* coral reefs as fish habitat in the NE Atlantic, in: *Cold-Water Corals and Ecosystems*. Springer Berlin Heidelberg, pp. 771–805. https://doi.org/10.1007/3-540-27673-4_41
- Courtney, L.A., Fisher, W.S., Raimondo, S., Oliver, L.M., Davis, W.P., 2007. Estimating 3-dimensional colony surface area of field corals. *J. Exp* 351, 234–242.
- Cristobal, F.R., Dodge, M., Noll, B., Rosenberg, N., Burns, J., Sanchez, J., Gotshalk, D., Pascoe, K., Runyan, A., 2020. Exploration of Coral Reefs in Hawai'i through Virtual Reality: Hawaiian Coral Reef Museum VR, in: *Practice and Experience in Advanced*

Research Computing. ACM, New York, NY, USA, NY, USA, pp. 545–546.
<https://doi.org/10.1145/3311790.3404542>

Crowder, L.B., Cooper, W.E., 1982. Habitat Structural Complexity and the Interaction Between Bluegills and Their Prey. *Ecology* 63, 1802. <https://doi.org/10.2307/1940122>

D’Urban Jackson, T., Williams, G.J., Walker-Springett, G., Davies, A.J., 2020. Three-dimensional digital mapping of ecosystems: a new era in spatial ecology. *Proc. R. Soc. B Biol. Sci.* 287, 20192383. <https://doi.org/10.1098/rspb.2019.2383>

Davies, A.J., Wisshak, M., Orr, J.C., Murray Roberts, J., 2008. Predicting suitable habitat for the cold-water coral *Lophelia pertusa* (Scleractinia). *Deep. Res. Part I Oceanogr. Res. Pap.* 55, 1048–1062. <https://doi.org/10.1016/j.dsr.2008.04.010>

De Clippele, L.H., Rovelli, L., Ramiro-Sánchez, B., Kazanidis, G., Vad, J., Turner, S., Glud, R.N., Roberts, J.M., 2021. Mapping cold-water coral biomass: an approach to derive ecosystem functions. *Coral Reefs* 40, 215–231. <https://doi.org/10.1007/s00338-020-02030-5>

de Haas, H., Mienis, F., Frank, N., Richter, T.O., Steinacher, R., de Stigter, H., van der Land, C., van Weering, T.C.E., 2009. Morphology and sedimentology of (clustered) cold-water coral mounds at the south Rockall Trough margins, NE Atlantic Ocean. *Facies* 55, 1–26. <https://doi.org/10.1007/s10347-008-0157-1>

De Mol, B., Henriët, J.-P., Canals, M., 2005. Development of coral banks in Porcupine Seabight: do they have Mediterranean ancestors? *Cold-Water Corals Ecosyst.* 515–533. https://doi.org/10.1007/3-540-27673-4_26

De Mol, B., Van Rensbergen, P., Pillen, S., Van Herreweghe, K., Van Rooij, D., McDonnell, A., Huvenne, V., Ivanov, M., Swennen, R., Henriët, J., 2002. Large deep-water coral banks in the Porcupine Basin, southwest of Ireland. *Mar. Geol.* 188, 193–231. [https://doi.org/10.1016/S0025-3227\(02\)00281-5](https://doi.org/10.1016/S0025-3227(02)00281-5)

De Mol, L., Van Rooij, D., Pirlet, H., Greinert, J., Frank, N., Quemmerais, F., Henriët, J.P., 2011. Cold-water coral habitats in the Penmarc’h and Guilvinec Canyons (Bay of Biscay): Deep-water versus shallow-water settings. *Mar. Geol.* 282, 40–52. <https://doi.org/10.1016/j.margeo.2010.04.011>

de Oliveira, L.M.C., Lim, A., Conti, L.A., Wheeler, A.J., 2022a. High-resolution 3D mapping of cold-water coral reefs using machine learning. *Front. Environ. Sci.* 10, 1–20. <https://doi.org/10.3389/fenvs.2022.1044706>

de Oliveira, L.M.C., Lim, A., Conti, L.A., Wheeler, A.J., 2021. 3D Classification of Cold-Water Coral Reefs: A Comparison of Classification Techniques for 3D Reconstructions of Cold-Water Coral Reefs and Seabed. *Front. Mar. Sci.* 8. <https://doi.org/10.3389/fmars.2021.640713>

de Oliveira, L.M.C., Oliveira, P.A. De, Lim, A., Wheeler, A.J., Conti, L.A., 2022b. Developing Mobile Applications with Augmented Reality and 3D Photogrammetry for Visualisation of Cold-Water Coral Reefs and Deep-Water Habitats. *Geosciences* 12, 356. <https://doi.org/10.3390/geosciences12100356>

Dixon, P.M., 2014. Ripley's K Function. *Wiley StatsRef Stat. Ref. Online* 3, 1796–1803. <https://doi.org/10.1002/9781118445112.stat07751>

Dolan, M.F.J., Grehan, A.J., Guinan, J.C., Brown, C., 2008. Modelling the local distribution of cold-water corals in relation to bathymetric variables: Adding spatial context to deep-sea video data. *Deep. Res. Part I Oceanogr. Res. Pap.* 55, 1564–1579. <https://doi.org/10.1016/j.dsr.2008.06.010>

Doležal, M., Vlachos, M., Secci, M., Demesticha, S., Skarlatos, D., Liarakapis, F., 2019. UNDERSTANDING UNDERWATER PHOTOGRAMMETRY for MARITIME ARCHAEOLOGY THROUGH IMMERSIVE VIRTUAL REALITY. *ISPRS Ann. Photogramm. Remote Sens. Spat. Inf. Sci.* 42, 85–91. <https://doi.org/10.5194/isprs-archives-XLII-2-W10-85-2019>

Dorschel, B., Hebbeln, D., Foubert, A., White, M., Wheeler, A.J., 2007. Hydrodynamics and cold-water coral facies distribution related to recent sedimentary processes at Galway Mound west of Ireland. *Mar. Geol.* 244, 184–195. <https://doi.org/10.1016/j.margeo.2007.06.010>

Fabri, M.C., Dugornay, O., de la Bernardie, X., Guerin, C., Sanchez, P., Arnaubec, A., Autin, T., Piasco, R., Puig, P., 2022. 3D-Representations for studying deep-sea coral habitats in the Lacaze-Duthiers Canyon, from geological settings to individual specimens. *Deep. Res. Part I Oceanogr. Res. Pap.* 187, 103831. <https://doi.org/10.1016/j.dsr.2022.103831>

- Fabri, M.C., Vinha, B., Allais, A.G., Bouhier, M.E., Dugornay, O., Gaillot, A., Arnaubec, A., 2019. Evaluating the ecological status of cold-water coral habitats using non-invasive methods: An example from Cassidaigne canyon, northwestern Mediterranean Sea. *Prog. Oceanogr.* 178, 102172. <https://doi.org/10.1016/j.pocean.2019.102172>
- Ferrari, R., Figueira, W.F., Pratchett, M.S., Boube, T., Adam, A., Kobelkowsky-Vidrio, T., Doo, S.S., Atwood, T.B., Byrne, M., 2017. 3D photogrammetry quantifies growth and external erosion of individual coral colonies and skeletons. *Sci. Rep.* 7, 1–9. <https://doi.org/10.1038/s41598-017-16408-z>
- Ferrari, R., McKinnon, D., He, H., Smith, R.N., Corke, P., González-Rivero, M., Mumby, P.J., Upcroft, B., 2016. Quantifying multiscale habitat structural complexity: A cost-effective framework for underwater 3D modelling. *Remote Sens.* 8. <https://doi.org/10.3390/rs8020113>
- Figueira, W., Ferrari, R., Weatherby, E., Porter, A., Hawes, S., Byrne, M., 2015. Accuracy and Precision of Habitat Structural Complexity Metrics Derived from Underwater Photogrammetry. *Remote Sens* 7, 16883–16900.
- Fosså, J.H., Lindberg, B., Christensen, O., Lundälv, T., Svellingen, I., Mortensen, P.B., Alvsvåg, J., 2006. Mapping of *Lophelia* reefs in Norway: experiences and survey methods. *Cold-Water Corals Ecosyst.* 359–391. https://doi.org/10.1007/3-540-27673-4_18
- Fosså, J.H., Mortensen, P.B., Furevik, D.M., 2002. The deep-water coral *Lophelia pertusa* in Norwegian waters: Distribution and fishery impacts. *Hydrobiologia* 471, 1–12. <https://doi.org/https://doi.org/10.1023/A:1016504430684>
- Foubert, A., Beck, T., Wheeler, A.J., Opderbecke, J., Grehan, A., Klages, M., Thiede, J., Henriët, J.-P., 2006. New view of the Belgica Mounds, Porcupine Seabight, NE Atlantic: preliminary results from the Polarstern ARK-XIX/3a ROV cruise, in: *Cold-Water Corals and Ecosystems*. Springer-Verlag, Berlin/Heidelberg, pp. 403–415. https://doi.org/10.1007/3-540-27673-4_20
- Foubert, A., Huvenne, V.A.I., Wheeler, A., Kozachenko, M., Opderbecke, J., Henriët, J.-P., 2011. The Moira Mounds, small cold-water coral mounds in the Porcupine

- Seabight, NE Atlantic: Part B—Evaluating the impact of sediment dynamics through high-resolution ROV-borne bathymetric mapping. *Mar. Geol.* 282, 65–78. <https://doi.org/10.1016/j.margeo.2011.02.008>
- Frederiksen, R., Jensen, A., Westerberg, H., 1992. The distribution of the scleractinian coral *Lophelia pertusa* around the Faroe islands and the relation to internal tidal mixing. *Sarsia* 77, 157–171. <https://doi.org/10.1080/00364827.1992.10413502>
- Freiwald, A., 2002. Reef-Forming Cold-Water Corals, in: *Ocean Margin Systems*. Springer Berlin Heidelberg, pp. 365--385.
- Freiwald, A., Fosså, J.H., Grehan, A., Koslow, T., Roberts, J.M., 2004. Cold-water Coral Reefs: out of sight - no longer out of mind. *UNEP-WCMC Biodiversity Series 22*, UNEP-WCMC Biodiversity Series. [s.n.]. <https://doi.org/10.5962/bhl.title.45025>
- Freiwald, A., Roberts, J.M., 2005. *Cold-Water Corals and Ecosystems*, *Cold-Water Corals and Ecosystems*. Springer Berlin Heidelberg, Berlin, Heidelberg. <https://doi.org/10.1007/3-540-27673-4>
- Friedman, A., Pizarro, O., Williams, S.B., Johnson-Roberson, M., 2012. Multi-Scale Measures of Rugosity, Slope and Aspect from Benthic Stereo Image Reconstructions. *PLoS One* 7. <https://doi.org/10.1371/journal.pone.0050440>
- Fukunaga, A., Burns, J.H.R., 2020. Metrics of coral reef structural complexity extracted from 3D mesh models and digital elevation models. *Remote Sens.* 12, 2676. <https://doi.org/10.3390/RS12172676>
- Fukunaga, A., Burns, J.H.R., Pascoe, K.H., Kosaki, R.K., 2020. Associations between benthic cover and habitat complexity metrics obtained from 3D reconstruction of coral reefs at different resolutions. *Remote Sens.* 12. <https://doi.org/10.3390/rs12061011>
- Getis, A., Ord, J.K., 1992. The Analysis of Spatial Association by Use of Distance Statistics. *Geogr. Anal.* 24, 189–206. <https://doi.org/10.1111/j.1538-4632.1992.tb00261.x>
- Goatley, C.H.R., Bellwood, D.R., 2011. The roles of dimensionality, canopies and complexity in ecosystem monitoring. *PLoS One* 6.

- Graham, N.A.J., Nash, K.L., 2013. The importance of structural complexity in coral reef ecosystems. *Coral Reefs* 32, 315–326. <https://doi.org/10.1007/s00338-012-0984-y>
- Guinan, J., Grehan, A., Dolan, M., Brown, C., 2009. Quantifying relationships between video observations of cold-water coral cover and seafloor features in Rockall Trough, west of Ireland. *Mar. Ecol. Prog. Ser.* 375, 125–138. <https://doi.org/10.3354/meps07739>
- Heindel, K., Titschack, J., Dorschel, B., Huvenne, V.A.I., Freiwald, A., 2010. The sediment composition and predictive mapping of facies on the Propeller Mound-A cold-water coral mound (Porcupine Seabight, NE Atlantic). *Cont. Shelf Res.* 30, 1814–1829. <https://doi.org/10.1016/j.csr.2010.08.007>
- Henry, L.-A., Roberts, J.M., 2017. Global Biodiversity in Cold-Water Coral Reef Ecosystems, in: Rossi, S., Bramanti, L., Gori, A., Orejas, C. (Eds.), *Marine Animal Forests*. Springer International Publishing, Cham, pp. 235–256. https://doi.org/10.1007/978-3-319-21012-4_6
- House, J.E., Brambilla, V., Bidaut, L.M., Christie, A.P., Pizarro, O., Madin, J.S., Dornelas, M., 2018. Moving to 3D: relationships between coral planar area, surface area and volume. *PeerJ* 6, e4280. <https://doi.org/10.7717/peerj.4280>
- Hovland, M., Thomsen, E., 1997. Cold-water corals - Are they hydrocarbon seep related?, in: *Marine Geology*. Elsevier, pp. 159–164. [https://doi.org/10.1016/S0025-3227\(96\)00086-2](https://doi.org/10.1016/S0025-3227(96)00086-2)
- Huvenne, V.A.I., Beyer, A., de Haas, H., Dekindt, K., Henriët, J.-P., Kozachenko, M., Olu-Le Roy, K., Wheeler, A.J., 2005. The seabed appearance of different coral bank provinces in the Porcupine Seabight, NE Atlantic: results from sidescan sonar and ROV seabed mapping. *Cold-Water Corals Ecosyst.* 535–569. https://doi.org/10.1007/3-540-27673-4_27
- Huvenne, V.A.I., Blondel, P., Henriët, J.P., 2002. Textural analyses of sidescan sonar imagery from two mound provinces in the Porcupine Seabight. *Mar. Geol.* 189, 323–341. [https://doi.org/10.1016/S0025-3227\(02\)00420-6](https://doi.org/10.1016/S0025-3227(02)00420-6)
- Huvenne, V.A.I., Tyler, P.A., Masson, D.G., Fisher, E.H., Hauton, C., Hühnerbach, V.,

Bas, T.P., Wolff, G.A., 2011a. A picture on the wall: Innovative mapping reveals cold-water coral refuge in submarine canyon. *PLoS One* 6. <https://doi.org/10.1371/journal.pone.0028755>

Huvenne, V.A.I., Tyler, P.A., Masson, D.G., Fisher, E.H., Hauton, C., Hühnerbach, V., Bas, T.P., Wolff, G.A., 2011b. A picture on the wall: Innovative mapping reveals cold-water coral refuge in submarine canyon. *PLoS One* 6, 1–9. <https://doi.org/10.1371/journal.pone.0028755>

Jonsson, L.G., Nilsson, P.G., Floruta, F., Lundälv, T., 2004. Distributional patterns of macro- and megafauna associated with a reef of the cold-water coral *Lophelia pertusa* on the Swedish west coast. *Mar. Ecol. Prog. Ser.* 284, 163–171. <https://doi.org/10.3354/meps284163>

Lacharité, M., Metaxas, A., 2017. Hard substrate in the deep ocean: How sediment features influence epibenthic megafauna on the eastern Canadian margin. *Deep. Res. Part I Oceanogr. Res. Pap.* 126, 50–61. <https://doi.org/10.1016/j.dsr.2017.05.013>

Lange, I.D., Perry, C.T., 2020. A quick, easy and non-invasive method to quantify coral growth rates using photogrammetry and 3D model comparisons. *Methods Ecol. Evol.* 11, 714–726. <https://doi.org/10.1111/2041-210X.13388>

Leverette, T.L., Metaxas, A., 2006. Predicting habitat for two species of deep-water coral on the Canadian Atlantic continental shelf and slope, in: *Cold-Water Corals and Ecosystems*. Springer-Verlag, pp. 467–479. https://doi.org/10.1007/3-540-27673-4_23

Lim, A., 2017. Spatio – temporal Patterns and Controls on Cold-water Coral Reef Development : The Moira Mounds , Porcupine Seabight , Offshore Ireland. Porcupine Seabight, Offshore Ireland.

Lim, A., Huvenne, V.A.I., Vertino, A., Spezzaferri, S., Wheeler, A.J., 2018a. New insights on coral mound development from groundtruthed high-resolution ROV-mounted multibeam imaging. *Mar. Geol.* 403, 225–237. <https://doi.org/10.1016/j.margeo.2018.06.006>

Lim, A., Kane, A., Arnaubec, A., Wheeler, A.J., 2018b. Seabed image acquisition and

survey design for cold water coral mound characterisation. *Mar. Geol.* 395, 22–32. <https://doi.org/https://doi.org/10.1016/j.margeo.2017.09.008>

Lim, A., Wheeler, A.J., Arnaubec, A., 2017. High-resolution facies zonation within a cold-water coral mound: The case of the Piddington Mound, Porcupine Seabight, NE Atlantic. *Mar. Geol.* 390, 120–130. <https://doi.org/10.1016/j.margeo.2017.06.009>

Lim, O'Reilly, L., Summer, G., de Oliveira, L.M.C., Strachan, R., Lim, O'Reilly, L., Summer, G., de Oliveira, L.M.C., Strachan, R., 2020a. CE20011 Cruise Report: Systematic Monitoring Survey of the Moira Mound Chain (SyMonS_MoM).

Lim, Wheeler, A.J., Conti, L., 2020b. Cold-Water Coral Habitat Mapping: Trends and Developments in Acquisition and Processing Methods. *Geosciences* 11, 9. <https://doi.org/10.3390/geosciences11010009>

Lim, Wheeler, A.J., Price, D.M., O'Reilly, L., Harris, K., Conti, L., 2020c. Influence of benthic currents on cold-water coral habitats: a combined benthic monitoring and 3D photogrammetric investigation. *Sci. Rep.* 10, 19433. <https://doi.org/10.1038/s41598-020-76446-y>

Masson, D., Bett, B., Billett, D.S., Jacobs, C., Wheeler, A., Wynn, R., 2003. The origin of deep-water, coral-topped mounds in the northern Rockall Trough, Northeast Atlantic. *Mar. Geol.* 194, 159–180. [https://doi.org/10.1016/S0025-3227\(02\)00704-1](https://doi.org/10.1016/S0025-3227(02)00704-1)

Mienis, F., Bouma, T., Witbaard, R., van Oevelen, D., Duineveld, G., 2019. Experimental assessment of the effects of coldwater coral patches on water flow. *Mar. Ecol. Prog. Ser.* 609, 101–117. <https://doi.org/10.3354/meps12815>

Mienis, F., Duineveld, G.C.A., Davies, A.J., Ross, S.W., Seim, H., Bane, J., van Weering, T.C.E., 2012. The influence of near-bed hydrodynamic conditions on cold-water corals in the Viosca Knoll area, Gulf of Mexico. *Deep Sea Res. Part I Oceanogr. Res. Pap.* 60, 32–45. <https://doi.org/10.1016/j.dsr.2011.10.007>

Mienis, F., van Weering, T., de Haas, H., de Stigter, H., Huvenne, V., Wheeler, A., 2006. Carbonate mound development at the SW Rockall Trough margin based on high resolution TOBI and seismic recording. *Mar. Geol.* 233, 1–19. <https://doi.org/10.1016/j.margeo.2006.08.003>

Mogstad, A.A., Løvås, H.S., Sture, O., Johnsen, G., Ludvigsen, M., 2022. Remote Sensing of the Tautra Ridge: An Overview of the World's Shallowest Cold-Water Coral Reefs. *Front. Mar. Sci.* 9, 1–18. <https://doi.org/10.3389/fmars.2022.848888>

Mortensen, P.B., Buhl-Mortensen, L., 2004. Distribution of deep-water gorgonian corals in relation to benthic habitat features in the Northeast Channel (Atlantic Canada). *Mar. Biol.* 144, 1223–1238. <https://doi.org/10.1007/s00227-003-1280-8>

Mortensen, P.B., Hovland, M., Brattegard, T., Farestveit, R., 1995. Deep water bioherms of the scleractinian coral *Lophelia pertusa* (L.) at 64° n on the Norwegian shelf: Structure and associated megafauna. *Sarsia* 80, 145–158. <https://doi.org/10.1080/00364827.1995.10413586>

NPWS, 2022. NPWS Belgica Mound Province SAC (site code: 002327) Conservation objectives supporting document-Marine Habitats.

Oevelen, D. van, Duineveld, G., Lavaleye, M., Mienis, F., Soetaert, K., Heip, C.H.R., 2009. The cold-water coral community as hotspot of carbon cycling on continental margins: A food-web analysis from Rockall Bank (northeast Atlantic). *Limnol. Oceanogr.* 54, 1829–1844. <https://doi.org/10.4319/lo.2009.54.6.1829>

Orejas, C., Gori, A., Lo Iacono, C., Puig, P., Gili, J.M., Dale, M.R.T.T., 2009. Cold-water corals in the Cap de Creus canyon, northwestern Mediterranean: Spatial distribution, density and anthropogenic impact. *Mar. Ecol. Prog. Ser.* 397, 37–51. <https://doi.org/10.3354/meps08314>

Orejas, C., Gori, A., Rad-Menéndez, C., Last, K.S., Davies, A.J., Beveridge, C.M., Sadd, D., Kiriakoulakis, K., Witte, U., Roberts, J.M., 2016. The effect of flow speed and food size on the capture efficiency and feeding behaviour of the cold-water coral *Lophelia pertusa*. *J. Exp. Mar. Bio. Ecol.* 481, 34–40. <https://doi.org/10.1016/j.jembe.2016.04.002>

Pascoe, K.H., Fukunaga, A., Kosaki, R.K., Burns, J.H.R., 2021. 3D assessment of a coral reef at Lalo Atoll reveals varying responses of habitat metrics following a catastrophic hurricane. *Sci. Rep* 11, 12050.

Peters, R.H., 1983. *The Ecological Implications of Body Size*. Cambridge University

Press. <https://doi.org/10.1017/CBO9780511608551>

Pizarro, O., Friedman, A., Bryson, M., Williams, S.B., Madin, J., 2017. A simple, fast, and repeatable survey method for underwater visual 3D benthic mapping and monitoring. *Ecol. Evol.* 7, 1770–1782. <https://doi.org/10.1002/ece3.2701>

Prado, E., Rodríguez-Basalo, A., Cobo, A., Ríos, P., Sánchez, F., 2020. 3D fine-scale terrain variables from underwater photogrammetry: A new approach to benthic microhabitat modeling in a circalittoral Rocky shelf. *Remote Sens.* 12, 2466. <https://doi.org/10.3390/RS12152466>

Prado, E., Sánchez, F., Rodríguez-Basalo, A., Altuna, Á., Cobo, A., 2019. Analysis of the population structure of a gorgonian forest (*Placogorgia* sp.) using a photogrammetric 3D modeling approach at Le Danois Bank, Cantabrian Sea. *Deep. Res. Part I Oceanogr. Res. Pap.* 153. <https://doi.org/10.1016/j.dsr.2019.103124>

Price, D.M., Lim, A., Callaway, A., Eichhorn, M.P., Wheeler, A.J., Lo Iacono, C., Huvenne, V.A.I., 2021. Fine-Scale Heterogeneity of a Cold-Water Coral Reef and Its Influence on the Distribution of Associated Taxa. *Front. Mar. Sci.* 8. <https://doi.org/10.3389/fmars.2021.556313>

Price, D.M., Robert, K., Callaway, A., Lo Iacono, C., Hall, R.A., Huvenne, V.A.I., 2019. Using 3D photogrammetry from ROV video to quantify cold-water coral reef structural complexity and investigate its influence on biodiversity and community assemblage. *Coral Reefs* 38, 1007–1021. <https://doi.org/10.1007/s00338-019-01827-3>

Purser, A., Orejas, C., Gori, A., Tong, R., Unnithan, V., Thomsen, L., 2013. Local variation in the distribution of benthic megafauna species associated with cold-water coral reefs on the Norwegian margin. *Cont. Shelf Res.* 54, 37–51. <https://doi.org/10.1016/j.csr.2012.12.013>

Richardson, L.E., Graham, N.A.J., Hoey, A.S., 2017. Cross-scale habitat structure driven by coral species composition on tropical reefs. *Sci. Rep.* 7, 1–11. <https://doi.org/10.1038/s41598-017-08109-4>

Ripley, B.D., 1976. The second-order analysis of stationary point processes. *J. Appl. Probab.* 13, 255–266. <https://doi.org/10.2307/3212829>

- Robert, K., Huvenne, V.A.I.I., Georgiopoulou, A., Jones, D.O.B.B., Marsh, L., Carter, D.O.G., Chaumillon, L., 2017. New approaches to high-resolution mapping of marine vertical structures. *Sci. Rep.* 7, 1–14. <https://doi.org/10.1038/s41598-017-09382-z>
- Roberts, J.M., Long, D., Wilson, J.B., Mortensen, P.B., Gage, J.D., 2003. The cold-water coral *Lophelia pertusa* (Scleractinia) and enigmatic seabed mounds along the north-east Atlantic margin: Are they related? *Mar. Pollut. Bull.* 46, 7–20. [https://doi.org/10.1016/S0025-326X\(02\)00259-X](https://doi.org/10.1016/S0025-326X(02)00259-X)
- Roberts, J.M., Wheeler, A., Freiwald, A., Cairns, S., 2009. Cold-Water Corals, Cold-Water Corals: The Biology and Geology of Deep-Sea Coral Habitats. Cambridge University Press. <https://doi.org/10.1017/CBO9780511581588>
- Roberts, Wheeler, A.J., Freiwald, A., 2006. Reefs of the Deep: The Biology and Geology of Cold-Water Coral Ecosystems. *Science* (80-.). 312, 543–547. <https://doi.org/10.1126/science.1119861>
- Rüggeberg, A., Flögel, S., Dullo, W.C., Hissmann, K., Freiwald, A., 2011. Water mass characteristics and sill dynamics in a subpolar cold-water coral reef setting at Stjernsund, northern Norway. *Mar. Geol.* 282, 5–12. <https://doi.org/10.1016/j.margeo.2010.05.009>
- Samet, H., Tamminen, M.K., 1988. Efficient Component Labeling of Images of Arbitrary Dimension Represented by Linear Bintree. *IEEE Trans. Pattern Anal. Mach. Intell.* 10, 579–586. <https://doi.org/10.1109/34.3918>
- Savini, A., Corselli, C., 2010. High-resolution bathymetry and acoustic geophysical data from Santa Maria di Leuca Cold Water Coral province (Northern Ionian Sea-Apulian continental slope). *Deep. Res. Part II Top. Stud. Oceanogr.* 57, 326–344. <https://doi.org/10.1016/j.dsr2.2009.08.014>
- Savini, A., Vertino, A., Marchese, F., Beuck, L., Freiwald, A., 2014. Mapping cold-water coral habitats at different scales within the Northern Ionian Sea (central Mediterranean): An assessment of coral coverage and associated vulnerability. *PLoS One* 9, 2002–2005. <https://doi.org/10.1371/journal.pone.0087108>
- Storlazzi, C.D., Dartnell, P., Hatcher, G.A., Gibbs, A.E., 2016. End of the chain? Rugosity

and fine-scale bathymetry from existing underwater digital imagery using structure-from-motion (SfM) technology. *Coral Reefs* 35, 889–894. <https://doi.org/10.1007/s00338-016-1462-8>

Sundahl, H., Buhl-Mortensen, P., Buhl-Mortensen, L., 2020. Distribution and Suitable Habitat of the Cold-Water Corals *Lophelia pertusa*, *Paragorgia arborea*, and *Primnoa resedaeformis* on the Norwegian Continental Shelf. *Front. Mar. Sci.* 7, 1–22. <https://doi.org/10.3389/fmars.2020.00213>

Titschack, J., Baum, D., De Pol-Holz, R., López Correa, M., Forster, N., Flögel, S., Hebbeln, D., Freiwald, A., 2015. Aggradation and carbonate accumulation of Holocene Norwegian cold-water coral reefs. *Sedimentology* 62, 1873–1898. <https://doi.org/10.1111/sed.12206>

Titschack, J., Thierens, M., Dorschel, B., Schulbert, C., Freiwald, A., Kano, A., Takashima, C., Kawagoe, N., Li, X., 2009. Carbonate budget of a cold-water coral mound (Challenger Mound, IODP Exp. 307). *Mar. Geol.* 259, 36–46. <https://doi.org/10.1016/j.margeo.2008.12.007>

Urbina-barreto, I., Pinel, R., Fr, L., Mahamadaly, V., Elise, S., Kulbicki, M., Quod, J., Dutrieux, E., 2020. Quantifying the shelter capacity of coral reefs using photogrammetric 3D modeling : From colonies to reefscales. *Ecol. Indic.* 107151. <https://doi.org/10.1016/j.ecolind.2020.107151>

Urbina-Barreto, I., Elise, S., Guilhaumon, F., Bruggemann, J.H., Pinel, R., Kulbicki, M., Vigliola, L., Mou-Tham, G., Mahamadaly, V., Facon, M., Bureau, S., Peignon, C., Dutrieux, E., Garnier, R., Penin, L., Adjeroud, M., 2022. Underwater photogrammetry reveals new links between coral reefscape traits and fishes that ensure key functions. *Ecosphere* 13, 1–18. <https://doi.org/10.1002/ecs2.3934>

Victorero, L., Blamart, D., Pons-Branchu, E., Mavrogordato, M.N., Huvenne, V.A.I.I., 2016. Reconstruction of the formation history of the Darwin Mounds, N Rockall Trough: How the dynamics of a sandy contourite affected cold-water coral growth. *Mar. Geol.* 378, 186–195. <https://doi.org/10.1016/j.margeo.2015.12.001>

Walbridge, S., 2018. Unified Geomorphological Analysis Workflows with Benthic Terrain Modeler. *Geosciences* 8, 94. <https://doi.org/10.3390/geosciences8030094>

Wheeler, A.J., Beyer, A., Freiwald, A., de Haas, H., Huvenne, V.A.I.I., Kozachenko, M., Olu-Le Roy, K., Opderbecke, J., 2007. Morphology and environment of cold-water coral carbonate mounds on the NW European margin. *Int. J. Earth Sci.* 96, 37–56. <https://doi.org/10.1007/s00531-006-0130-6>

Wheeler, A.J., Kozachenko, M., Henry, L.-A., Foubert, A., de Haas, H., Huvenne, V.A.I.A.I., Masson, D.G.G., Olu, K., 2011. The Moira Mounds, small cold-water coral banks in the Porcupine Seabight, NE Atlantic: Part A—an early stage growth phase for future coral carbonate mounds? *Mar. Geol.* 282, 53–64. <https://doi.org/10.1016/j.margeo.2010.08.006>

Wheeler, A.J., Kozachenko, M., Masson, D.G., Huvenne, V.A.I., 2008. Influence of benthic sediment transport on cold-water coral bank morphology and growth: the example of the Darwin Mounds, north-east Atlantic. *Sedimentology* 55, 1875–1887. <https://doi.org/10.1111/j.1365-3091.2008.00970.x>

Wheeler, Kozachenko, M., Beyer, A., Foubert, A., Huvenne, V.A.I., Klages, M., Masson, D.G., Olu-Le Roy, K., Thiede, J., 2005. Sedimentary processes and carbonate mounds in the Belgica Mound province, Porcupine Seabight, NE Atlantic, in: *Cold-Water Corals and Ecosystems*. Springer Berlin Heidelberg, Berlin, Heidelberg, pp. 571–603. https://doi.org/10.1007/3-540-27673-4_28

White, M., Mohn, C., de Stigter, H., Mottram, G., 2005. Deep-water coral development as a function of hydrodynamics and surface productivity around the submarine banks of the Rockall Trough, NE Atlantic. *Cold-Water Corals Ecosyst.* 503–514. https://doi.org/10.1007/3-540-27673-4_25

Williams, I.D., Couch, C., Beijbom, O., Oliver, T., Vargas-Angel, B., Schumacher, B., Brainard, R., 2019. Leveraging automated image analysis tools to transform our capacity to assess status and trends on coral reefs. *Front. Mar. Sci.* 6. <https://doi.org/10.3389/fmars.2019.00222>

Wilson, 1979a. 'Patch' development of the deep-water coral *Lophelia pertusa* (L.) on Rockall Bank. *J. Mar. Biol. Assoc. United Kingdom* 59, 165–177. <https://doi.org/10.1017/S0025315400046257>

Wilson, 1979b. The distribution of the coral *Lophelia pertusa* (L.) [*L. prolifera* (Pallas)]

in the north-east Atlantic. *J. Mar. Biol. Assoc. United Kingdom* 59, 149–164.
<https://doi.org/10.1017/S0025315400046245>

Wilson, A.M., 2016. Lateral transport of suspended particulate matter in nepheloid layers along the Irish continental margin - a case study of the Whittard Canyon, North-East Atlantic Ocean. *Earth Ocean Sci. Sch. Nat. Sci. Natl. Univ. Ireland, Galw.*

Wilson, M.F.J., O'Connell, B., Brown, C., Guinan, J.C., Grehan, A.J., 2007. Multiscale Terrain Analysis of Multibeam Bathymetry Data for Habitat Mapping on the Continental Slope. *Mar. Geod.* 30, 3–35.
<https://doi.org/10.1080/01490410701295962>

5. Developing Mobile Applications with Augmented Reality and 3D Photogrammetry for Visualisation of Cold-Water Coral Reefs and Deep-Water Habitats

Larissa Macedo Cruz de Oliveira*, Priscila Almeida de Oliveira, Aaron Lim, Andrew J. Wheeler and Luis Americo Conti

(Current status: Published, Geosciences MDPI)

DOI: <https://doi.org/10.3390/geosciences12100356>

This chapter comprises a paper that is published in the journal Geosciences MDPI.

de Oliviera, L.M.C., de Oliveira, P.A., Lim, A., Wheeler, A.J., Conti, L. (2022). Developing mobile applications with augmented reality and 3D photogrammetry for visualisation of cold-water coral reefs. *Geosciences* 12, 356.

This chapter is organised as follows: introduction, materials and methods, results, discussion and references.

The study in this chapter aimed to fulfil the fourth aim of the PhD: to develop new forms of visualisation of 3D data of underwater environments. The chapter was motivated by the fact CWC habitats are generally located in pristine environments and unlike most of their tropical counterparts, their accessibility is hindered by depth or terrain topography, which contributes to the need to raise awareness to their existence and importance. Here, SfM, AR and game development engines were integrated to create the Coral APP, a visualisation platform for CWC habitats, that allow users with a smartphone and internet connection to interact with 3D reconstructions of these habitats. Furthermore, the suitability of different 3D reconstructions for the mobile app was assessed based on three criteria to investigate the requirements for 3D resolution within the mobile app. Thus, this chapter contributes to informing future research about the available technology and data

requirements for AR applications. To the first author's knowledge, this is the first study to develop a visualisation application for 3D reconstructions of CWC reef habitats.

Candidate contributions to the study: Larissa de Oliveira conceptualised developed the methodology of the study with Priscila Almeida and Prof Luis A. Conti. Larissa de Oliveira, carried out data curation, project administration, investigation, formal analyses, software programming, data visualisation, supervision, writing and editing of the original draft with Priscila Almeida. Larissa Oliveira carried out the editing and submission of the manuscript.

For this study, Larissa de Oliveira was funded through the Irish Research Council Postgraduate Scholarship awarded to Larissa Oliveira: Advancing Seabed Mapping Techniques for Deep-water Habitat Classification in Submarine Canyons (ASMaT) - GOIPG/2020/1659. Prof Luis Conti conceptualised the study and contributed to the methodology. Larissa de Oliveira and Priscila Almeida developed the methodology, investigation, data visualisation, writing of the original abstract. Larissa de Oliveira developed the 3D models developed in the study and Priscila Almeida developed the Unity workflow to produce the APP. The project which lead to the work developed in this chapter was developed by Larissa de Oliveira and funded through the Irish Research Council Postgraduate Scholarship awarded to Larissa Oliveira. Dr Aaron Lim was the chief scientist responsible for the data collected for the study during the research cruise CE20011, in which Larissa Oliveira was data manager. The project was supervised by Prof Andy Wheeler, Dr Aaron Lim and Prof Luis Conti. These co-authors also contributed with editing and proof-reading of the manuscript and funding acquisition.

Abstract

Cold-water coral (CWC) reefs are considered “hotspots” of biodiversity in deep-sea environments. Like tropical coral reefs, these habitats are subject to climate and anthropogenic threats. The use of remotely operated vehicles (ROVs) in combination with three-dimensional (3D) modelling and augmented reality (AR) has enabled detailed visualisation of terrestrial and marine environments while promoting data accessibility and scientific outreach. However, remote environments such as CWC reefs still present challenges with data acquisition, which impacts the further understanding of these environments. This study aims to develop a mobile application using structure-from-motion (SfM) 3D photogrammetric data and AR for the visualisation of CWC reefs. The mobile application was developed to display 3D models of CWC reefs from the Piddington Mound area, southwest of Ireland. The 3D models were tested at different resolutions to analyse the visualisation experience and trade-off between resolution and application size. The results from the 3D reconstructions with higher resolution indicate that the combination of SfM, AR, and mobile phones is a promising tool for raising awareness and literacy regarding CWC and deep-water habitats. This study is the first of its kind to showcase CWC habitats accessible to anyone, anywhere with a mobile phone and internet connectivity.

5.1 Introduction

Cold-water coral (CWC) ecosystems are structural three-dimensional (3D) deep-water habitats that mostly rely on robust mapping technologies to enable detailed analyses and monitoring of these reefs (Conti et al., 2019; Price et al., 2019; Robert et al., 2017). CWC ecosystems form complex reef structures on the seabed and are considered “hotspots” for biodiversity in deep-sea environments as they are able to baffle sediments and act as nurseries and shelter to thousands of deep-sea species (Hebbeln et al., 2020, 2019; Henry and Roberts, 2016; Miller et al., 2012). Moreover, coral reefs can form large 3D carbonate structures (Roberts et al., 2006; Wheeler et al., 2007) and provide important ecosystem services (Aanesen et al., 2015; Armstrong et al., 2014), thus promoting an increase in biomass relative to their surrounding areas (Lim et al., 2020b; Miller and Spoolman, 2015). However, research and analyses related to the geographic distribution and conditions of CWC, and other deep-water habitats are scarce mainly because of data acquisition limitations related to the accessibility and extent of these environments (Armstrong et al., 2014; Oevelen et al., 2009). These factors lead to challenges in understanding their key processes and controls, hence promoting awareness of these environments to the wider community is difficult (Danovaro et al., 2004). Furthermore, CWC reefs are considered vulnerable marine ecosystems (Auster et al., 2011; Fabri et al., 2014; Hebbeln et al., 2019) given their exposure to a range of direct and indirect disturbances such as climate change (Cathalot et al., 2015), ocean acidification (Frank et al., 2011; Miller and Spoolman, 2015; Roberts and Cairns, 2014; Turley et al., 2007), and fishing activities like bottom trawling (Althaus et al., 2009; Coughlan et al., 2015; Huvenne et al., 2016). Given these factors, regional efforts have been made to place CWC reefs and mounds as marine protected areas (MPAs) and special areas of conservation (SACs) (Clark, 2006; Davies et al., 2017; Lim et al., 2020b). However, protective measures against global change threats, encouragement of sustainable practices, and raising awareness actions are still limited (Hebbeln et al., 2020).

Marine habitats and archaeologically important underwater sites usually require remote mapping and diving technologies. This dependency leads to limitations in the

accessibility to these environments (Liestøl, 2019). In coastal areas, activities such as touristic diving is one of the most popular recreational activities. However, these activities can directly impact the marine environment (Chen et al., 2012) and pose a significant risk for divers (Barker and Roberts, 2004). In the case of coral reefs, which are sensitive to several environmental factors, the physical contact entailed when exploring these areas can cause direct and indirect impacts on the corals, such as structural damages and habitat disturbance due to sediment resuspension (Jameson et al., 1999; Sorice et al., 2007). In order to mitigate these risks in shallow and coastal water habitats, researchers have introduced the concept of 'dry diving' (Liestøl, 2019). In the context of underwater data visualisation, dry diving represents a new alternative way to access study sites without the need for physical diving by utilising augmented reality (AR) (Liestøl et al., 2021).

The conditions are different for deep-water environments, as the accessibility is limited by water depth and pressure. In this case, the use of remotely operated vehicles (ROVs) or autonomous-underwater vehicles (AUVs) has emerged as relatively new survey technologies that can aid the mapping of ocean features through the acquisition of high-resolution (HD) bathymetric and video data, physico-chemical measurements, and ecological sampling (De Clippele et al., 2017; Kwasnitschka et al., 2013; Lim et al., 2020c). These technologies, when coupled with novel mapping methods such as 3D photogrammetry and structure-from-motion (SfM), can be used for in-depth environmental observations using 2D and 3D perceptions (de Oliveira et al., 2021; House et al., 2018; Laranjeira et al., 2020).

SfM is a relatively new photogrammetry technique that has been increasingly applied to geospatially reconstruct different environments such as seabed habitats (Conti et al., 2019; Price et al., 2019), forests and grasslands (Cunliffe et al., 2016; Panagiotidis et al., 2016), mangroves (Navarro et al., 2020; Otero et al., 2018; Warfield and Leon, 2019), and rock outcrops (Weidner et al., 2021). SfM can provide fine-scale 3D reconstructions with millimetric to centimetric spatial resolutions, which allows for detailed mapping of different environmental and terrain descriptors (Smith et al., 2016).

Underwater photogrammetry has become progressively more common since the introduction of ROVs (Kwasnitschka et al., 2013). It is considered a non-destructive seabed mapping technique that enables representations and measurements of marine environments (Li et al., 1997), combining both metric and interpretative tasks. The use of SfM photogrammetry has been widely employed as a time and cost-effective method for high-resolution seabed mapping from AUVs/ROVs derived video data (Anelli et al., 2019; Burns et al., 2019, 2015; House et al., 2018; Robert et al., 2017; Storlazzi et al., 2016). The SfM technique is used to generate 3D models from a sequence of 2D images by detecting multiple matching features on these images and reconstructing a 3D point cloud (Carrivick et al., 2016; Smith et al., 2016). Photogrammetry-derived 3D models have an increasing importance towards the mapping of such environments as these models allow the visualization and high-resolution analyses of otherwise pristine and secluded areas (Foucault and Miskowiec, 1986).

In contrast with conventional photogrammetry, SfM utilises a set of algorithms such as the scale invariant feature transform (SIFT) algorithm (Lowe, 2004) to identify matching features in the image sequence and calculates the orientation and location from the difference of positions of the matched features. From these calculations, a sparse 3D point cloud is derived. The sparse cloud is usually refined to a finer resolution with multi-view stereo (MVS) methods (Carrivick et al., 2016). Unlike laser scanning techniques, SfM is not limited to temporal frequency as it does not rely on laser pulse frequency or beam spacing and can offer point cloud data with comparable accuracy to point clouds generated from those sources, at lower costs. Therefore, it offers a wide range of opportunities to characterise surface topography in high and multi-temporal resolution to map elevation, volumetric, and position variations, which are key to understanding earth surface processes (Carrivick et al., 2016).

Likewise, AR represents a promising technique that has been increasingly discussed in different fields, such as archaeology and management of underwater cultural heritages (Bruno et al., 2019; Čejka et al., 2020). AR has gained popularity with educational and touristic applications for providing the possibility to disseminate knowledge in sustainable and accessible ways without requiring the physical presence

of users at the study site, thus helping with damage prevention of historical sites (Loureiro et al., 2020) and supporting environmental preservation (Cristobal et al., 2020).

Virtual reality (VR) and AR are similar, but distinct and complementary technologies within a concept of “mixed reality” or more freely translated “immersive reality” (IR) (Barrile et al., 2019; Chen et al., 2012; Cristobal et al., 2020; Han et al., 2021; Markowitz et al., 2018; Monteiro and Montanha, 2019). AR and VR can be considered symmetrical (and continuous) reflections of each other in relation to what each technology seeks to accomplish and deliver to the user. While a VR environment enables the user’s interaction experience with immersive environments through multisensory interfaces, AR is characterized by projecting computational images on physical surfaces, increasing the informational and, consequently, perceptual and cognitive level we have of the environments, objects, and people around us (Arena et al., 2022; Billinghamurst and Duenser, 2012; Bimber and Raskar, 2005; Borba, 2014; Carmigniani and Furht, 2011; Cipresso et al., 2018; Dunleavy et al., 2009; Feiner et al., 1993; Fernández-Batanero et al., 2022; Kaufmann, 2003; Lee, 2012; Loureiro et al., 2020; Scholz and Smith, 2016). In this sense, VR and AR are two forms of innovative platforms essentially focused on the production and consumption of content.

In the scientific field, the use of AR and VR has gained motion in the past few years, especially during the global COVID-19 pandemic, when remote teaching was widely adopted. AR platforms such as Labster (Labster, 2011) and ClassVR (ClassVR, 2022) have been created to simulate scientific laboratory spaces for teaching experiments. Web platforms such as Sketchfab (Denoyel et al., 2012) have increased data sharing and visualization for the general public. Advances have also been made in the field of geosciences with the development of VR platforms for field mapping, such as and VRGeosciences (VRgeoscience, 2022). However, these technologies are usually not open-source and rely on the use of specific hardware, i.e., desktops and VR sets, which can often be inaccessible. The use of mobile devices, on the other hand, provides a more accessible alternative towards promoting knowledge with AR.

Studies suggest that integrating the visualisation of seafloor elements with AR techniques can be beneficial for increasing situational awareness, especially in the

case of deep-water habitats (Laranjeira et al., 2020), where depth and pressure conditions make diving, or any sort of human access, nearly impractical. VR experiments have been developed to provide remote diving experiences with an alternative to reduce damage to marine environments and risk to divers (Chen et al., 2012; Cristobal et al., 2020) and for representing coral habitats reconstructed with photogrammetry techniques (Cristobal et al., 2020). Similarly, other studies have used AR to represent underwater sites (Barrile et al., 2019; Doležal et al., 2019; Rizvic et al., 2019) such as the iMareCulture project (“i-MareCulture – H2020 funded EU research and innovation project,” 2020). Recent studies have used AR with the aid of waterproof devices to visualise objects during dives (Bruno et al., 2019; Čejka et al., 2020) and to explore shipwrecks (Liestøl et al., 2021). However, marine habitats remain underexplored in terms of AR applications, and questions related to its use in education and training remain unanswered. For example, information regarding incurring costs, efficiency between AR systems, and the methods used (Cipresso et al., 2018; Shelton and Hedley, 2004), as well as how to identify factors and conditions that affect the effectiveness of an AR system (Sotiriou and Bogner, 2008), are yet to be explored. Therefore, it is important to investigate the potential of AR applications to allow novel, more inclusive surveying and optimise educational experiences (Loureiro et al., 2020).

The aim of the study is to integrate SfM, AR, and game designing techniques to develop a visualisation platform for CWC and deep-water habitats video data and to analyse its applicability for educational and data accessibility purposes. By developing the proposed application (APP), this study aims to contribute towards (i) promoting the accessibility to 3D reconstructed datasets via mobile phones; (ii) facilitating the visualisation of deep-water environments such as CWC reefs; (iii) applying AR visualisation frameworks to CWC reefs and adjacent deep-sea habitats; and (iv) evaluating the outcomes of the APP in relation to 3D model resolutions. To this end, game engines and 3D photogrammetry were combined to develop a mobile APP of 3D models at different resolutions and user acceptance was assessed. The APP will provide further understanding on the resolution changes and optimal parameters for an application built for a particular environment such as CWC of the Piddington

Mound, southwest of Ireland. To the best of our knowledge, the study herein is the first study to combine these three applications to enable the visualisation of deep-water habitats as 3D reconstructions.

5.2 Materials and Methods

The proposed framework was applied to CWC reefs of the Piddington Mound area, located in the Purcupine Seabight, the NE Atlantic (Figure 5.1). This study was executed in three stages: (1) data acquisition; (2) 3D modelling with SfM photogrammetry; and (3) Android APP development.

5.2.1 Data Acquisition

5.2.1.1 Study Area

The Piddington Mound is a highly dynamic CWC mound (Boolukos et al., 2019) located approximately 300 km southwest of Ireland, in the Belgica Mound Province (BMP) (Figure 5.1) at a depth of approximately 960 metres. Given the presence of CWC mound features, including giant carbonate mounds and important deep-sea ecosystems, part of the BMP province is a designated SAC under the EU Habitats Directive (European Union Habitats Directive, 2016). The BMP comprises a range of mound structures, also including small CWC reefs (approximately 30 m across and 10 m tall) known as Moira Mounds (Lim et al., 2017; Wheeler et al., 2005). The Piddington Mound is located in the downslope area of these mounds and the main scleractinian framework-forming species are *Lophelia pertusa* (synonymised to *Desmophyllum pertusum* (Addamo et al., 2016)) and *Madrepora oculata* (De Mol et al., 2002; Wheeler et al., 2007). Sponge hotspots of *Aphrocallistes sp.* have also been documented (Conti et al., 2019). Local currents have been estimated to reach between 34 and 40 cm s⁻¹ (Dorschel et al., 2007; Lim et al., 2018). Owing to the high sediment influx in the area, the mounds have been considered to represent mound formation under stressed conditions (Foubert et al., 2011; Lim et al., 2017). The Piddington Mound was selected for this study given the extensive mapping efforts in the area (Boolukos et al., 2019; Conti et al., 2019; Lim et al., 2018, 2017) and evidence of temporal changes in benthic and sedimentological facies (Boolukos et al., 2019; Conti et al., 2019; Lim et al., 2018).

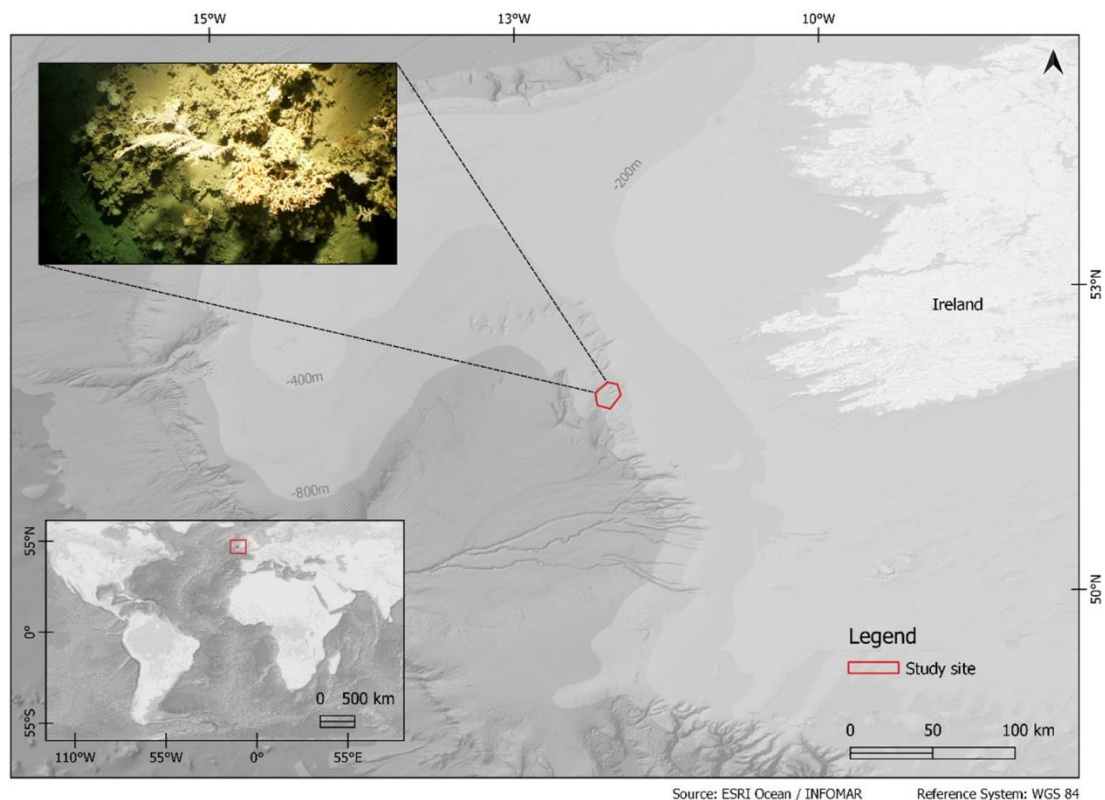


Figure 5.1: Location of the study site in the Piddington Mound, Belgica Mound Province area relative to the Irish margin. Upper left: extracted HD video frame of the study site.

5.2.1.2 Video Survey

The HD video data used to generate the 3D model were collected using the *Holland 1* ROV during the research cruise CE20011 in 2020 (Lim et al., 2020a). The video surveys were performed with the ROV at approximately 2 m above the sea floor with a survey speed of approximately <math><0.2</math> knots. For the CE20011 survey, the ROV was equipped with an HDTV video camera (HD Insite mini-Zeus with HD SDI fibre output), and Kongsberg OE 14–208 digital stills camera systems were used. The *Holland 1* is mounted with two deep-sea lasers spaced at 10 cm for scaling. Positioning data were acquired with a Sonardyne Ranger 2 ultra-short baseline (USBL) beacon with an accuracy of 1.3% of slant range. Video data were acquired at 50 frames/second at 1080-pixel resolution and stored as .mov files (de Oliveira et al., 2021). In total, 8 h of HD video data were surveyed.

5.2.2 3D Models with Structure-from-Motion Photogrammetry

ROVs HD video data, extracted video frames, and camera positioning information were used for the 3D photogrammetric reconstructions used herein. The photogrammetry pipeline was implemented in Agisoft Metashape Professional v1.6 (Agisoft, 2021) following the work of de Oliveira et al. (2021). From the SfM workflow, a 3D model and its respective texture file representing the CWC reef images were created. The SfM workflow is represented in Figure 5.2.

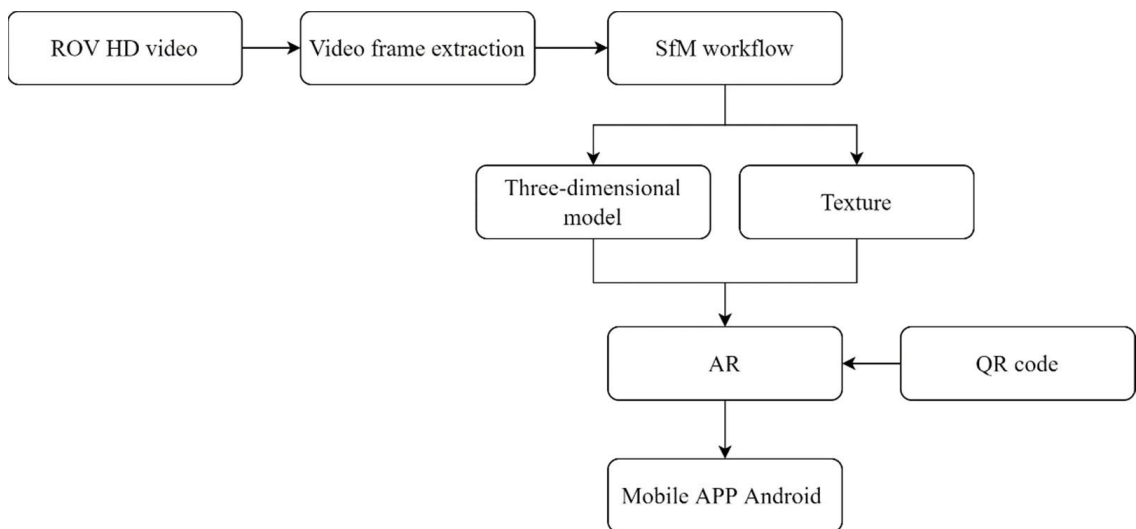


Figure 5.2: Generalised workflow of the methodology from the video acquisition to the APP development.

The video frames used for the photogrammetry were extracted in Blender (version 2.78) at a rate of one frame per second and resolution of 1920×1080 pixels (de Oliveira et al., 2021). Extracted frames were imported into Agisoft Metashape Professional v1.6 together with their respective USBL positioning information. Key and tie point limits were selected empirically according to the results of each photo alignment run. Camera alignment was followed by camera optimisation to refine camera orientation parameters and triangulated tie point coordinates. The 3D model reconstruction parameters were set to arbitrary, with source data from depth maps and the interpolation enabled. The resulting dense cloud georeferenced the frame-relative positioning data (X and Y coordinates, depth, yaw, pitch, roll, and accuracy (°)).

Dense clouds were scaled using HD camera lasers spaced at 10 cm as a reference. After the dense clouds were optimised, the meshes and texture from the images were derived. The texture was created using the generic mapping mode with the mosaic blending mode. The hole filling and the ghosting filter were applied in all model reconstructions. Finally, the textured 3D models, orthomosaics, and DTMs were produced. The texture was exported as .jpg format and the 3D models were exported in .obj format for the subsequent AR part of the study. Habitat characterisation of each site was performed through a visual assessment of dense cloud and orthomosaics considering main seabed morphologies, scaled measurements of sedimentological features (dropstones, pebbles, and so on), identification of the main framework forming CWC, and associated species.

5.2.3 Three-Dimensional Android APP Development

The AR APP was generated with the Vuforia Engine and Android Studio platforms that provide support for Android smartphone APP development in Unity (version 2018.4.30f1) (Unity Technologies, 2021). A simplified workflow of the use of each platform is represented in Figure 5.3.

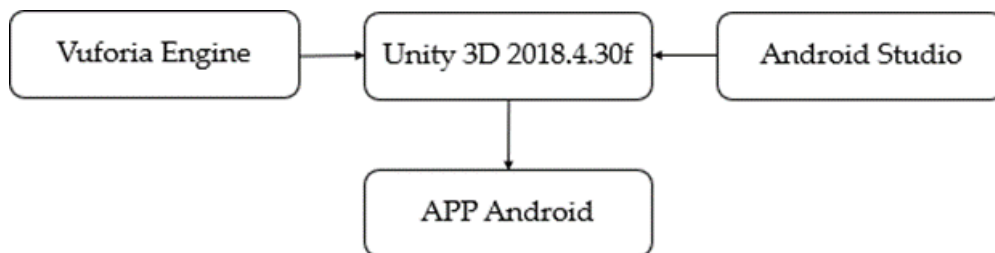


Figure 5.3: Workflow of the platforms used in the development of the Android APP.

Unity is a game engine for creating interactive content and has graphic capabilities for lighting, rendering, and importing 3D models in several formats (Unity Technologies, 2021). When installing Unity, it is important to enable Microsoft Visual Studio, if it is not yet installed on the desktop, and the supports for the Vuforia Engine (Vuforia, 2015) and Android Studio (Microsoft, n.d.).

The first part of generating the AR project consisted of searching for an image to encapsulate the 3D object. The image serves as an object that the code can read to

retrieve the 3D object. The image used in this study was a web-generated HD image of a QR Code to which the URL link with the project license generated by Vuforia was embedded. Although the QR Code was used for didactic purposes, any image can be used. Next, the QR Code was registered on the Vuforia Engine website, where a project license was obtained for the application of the AR project on Unity 3D. Subsequently, a database of the device type was created on the same Vuforia Engine website, where the QR Code was added and downloaded in the Unity Editor format.

The second part of the process consisted of setting up the project in Unity 3D, enabling Vuforia augmented reality supported and importing the database downloaded from the Vuforia Engine website. Then, the QR Code and the AR camera, responsible for reproducing the object in AR, were added. In the Vuforia Engine settings, inside Unity 3D, the license generated together with the database was applied. The 3D object and texture referring to the CWC reef were added, with positions and resolutions in the project in relation to the QR Code.

The AR visualisation was tested in Unity 3D by pointing the QR Code image at the desktop webcam. For the mobile version of the APP, the project was exported into Unity 3D with an Android Studio integration. Android Studio enables the creation of an Android Application Pack (APK) file for smartphones with an Android system. Finally, the APP file with the APK extension is generated and is ready to be downloaded and installed onto smartphones. Further examples of the use of these platforms for AR can be found in Cieza and Lujan (2018) and Liu et al. (2018). User perception was evaluated based on the interaction of the APP when used by an average smartphone user, with either a scientific or non-scientific background.

5.3 Results

5.3.1 Photogrammetry

In total, four models (named A, B, C, and D) were used for the development of the study. For the reconstruction of the models from the HD video data, the tie point limit and key point limits for Model D and B were set to 2000 and 20,0000, respectively.

For Models A and C, the tie and key point limits were set to 20,000 and 200,000 points, respectively. The resulting texture resolution was 4096 × 4096 pixels across all models. The 3D models measure from 3.76 m² to 21.47 m² in area. In total, 2894 images were used to reconstruct the sites from which the models A, B, C, and D were derived. Table 5.1 contains further details for each model used.

Table 5.1: Metadata of each 3D model used in the study.

3D model name	Number of Faces	Number of Vertices	Area (m ²)	Resolution (Number of faces/Area (m ²))	Texture size (pixels)	Total Number of Frames	Scale error (m)	Android application Size (MB)
A	1,124,301	4,177,311	3.776	297,749.21	4,096 x 4,096	613	0.07513	106
B	462,589	232,453	14.535	31,825.87	4,096 x 4,096	1122	0.05767	56.5
C	6,285,480	3,154,610	21.477	292,660.99	4,096 x 4,096	613	0.038187	163
D	44,000	22,122	10.71	4,108.31	4,096 x 4,097	1159	0.07513	49.3

5.3.1.1 Habitat Characterisation

Model A

Model A is a reconstruction of an area of approximately 3.7 m² at a depth of 967 metres. The site is characterised by coral patches and thickets varying from 0.2 metres to approximately 1.2 metres high spread across the extent of the model. The patches are formed by scleractinian coral species *Lophelia pertusa* and *Madrepora oculata* in live and dead forms and, more predominantly, coral rubble. There are occurrences of sponges *Aphrocallistes Beatrix*; soft corals and black corals, e.g., *Leiopathes sp.* and *Stichopathes cf. abyssicola*; and sea urchins (*Echinus sp.*). The seabed is composed of soft sediments overlaid by dropstones with pebbles, cobbles varying from 1 cm to 8 cm, and biogenic fragments (shells and coral fragments).

Model B

Model B is a section of a reconstructed area of 14.56 m² at a depth of approximately 970 metres. The study site is characterised by the presence of coral frameworks of *Lophelia pertusa* and *Madrepora oculata* in the form of patches and individual colonies of live and dead coral frameworks. The presence of coral rubble and coral fragments is higher relative to the other models. The section used to construct Model B is particularly dominated by coral rubble and coral fragments, with occurrences of sponges *Aphrocallistes Beatrix* and black corals *Stichopathes cf. abyssicola*. Visual assessment indicates that the seabed is composed of soft sediments (mud and sand) with occurrences of sedimentary bedforms (ripples and sediment waves) and rounded to subrounded dropstones varying from 1 cm to 10 cm, which occur in abundance to the south of the transect.

Model C

Model C represents an area of 21.47 m² at a depth of approximately 968.7 metres. Similar to Model A, the area is characterised by coral patches and thickets varying from 0.2 metres to approximately 1.2 metres high spread across the extent of the model. The coral species *Lophelia pertusa* and *Madrepora oculata* are the most abundant framework forming species, occurring as patches, thickets, and individual colonies in both living and dead forms. The presence of sponges *Aphrocallistes Beatrix*; soft corals, e.g. *Leiopathes sp.*; black corals, e.g., *Stichopathes cf. abyssicola*; and sea urchins (*Echinus sp.*) was also found. The sediment is composed of soft sediments (sand and mud) and dropstones varying from 1 cm to 8 cm in size with sub centimetric shell and coral fragments.

Model D

Model D is a 3D reconstruction of an area of 10.71 m² at a depth of approximately 969 metres. The section is composed of small colonies <30 cm high and individual coral colonies of *Lophelia pertusa* and *Madrepora oculata* with the presence of sponges *Aphrocallistes Beatrix*. The occurrence of coral rubble is scarce and limited to the surroundings of the small mounds, occasionally forming thickets. The seabed is

composed of soft sediments (mainly sand and mud) with the presence of bidirectional sediment waves and subangular to subrounded dropstones. The presence of shell and coral fragments is also scarce in the area.

5.3.2 The Coral APP

The installation of the APP from files in APK format was easily completed on an Android smartphone with a display of 1280 × 720 pixels and 1 GB of RAM. The installation of each APK takes approximately 3 min, depending on the internet connection speed. The resulting APP was tested using smartphones with Android version 8.1 or superior. The visualisation of the 3D CWC reef models produced by the Coral APP can be seen in Figure 5.4. By starting the APP and pointing the smartphone camera at the QR Code on the map seen in the background of Figure 5.4, the 3D model of the CWC can be interactively visualised.

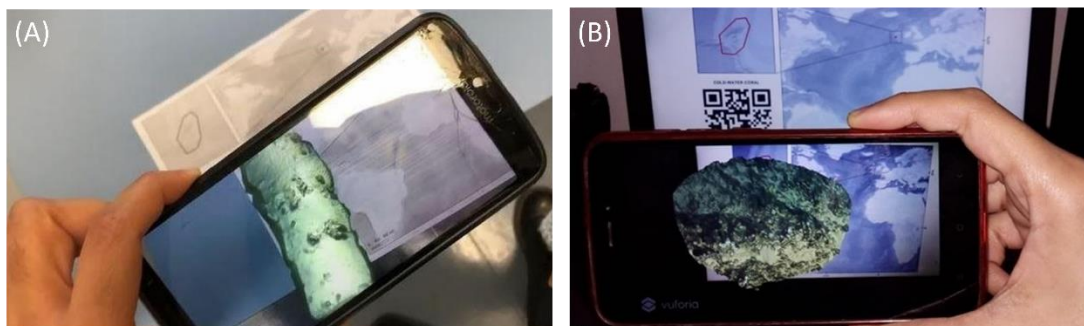


Figure 5.4: Demonstration of AR APP integration with the mobile phone and QR Code of two models. The background image shows the map of the study area in relation to Ireland and the QR Code for interaction: (a) demonstration of APP visualisation of Model D and (b) demonstration of APP visualisation of Model B.

The methodology presented was tested on the four 3D models of CWC runs using the SfM technique. The 3D models A, B, C, and D were used for the development of different APPs to understand the performance of visualisation by reading a QR Code on the smartphone. Figure 5.5 shows the AR projects of the four 3D models generated

in Unity 3D. Experiments in the Unity 3D desktop showed that the visualisation of the models in which the resolution, i.e., relation between the number of faces and the extent of the 3D models, was higher than 200,000 faces/area (m²) allowed the better understanding the environment. In these higher resolution models (e.g., model A), the manipulation of the objects in terms of zoom, rotation, and interaction when viewed via a desktop was superior in relation to the other models (Figure 5.5). However, they required a higher computational cost for the generation of the APP for mobile visualisation, which lead to a drop in the resulting model resolution.

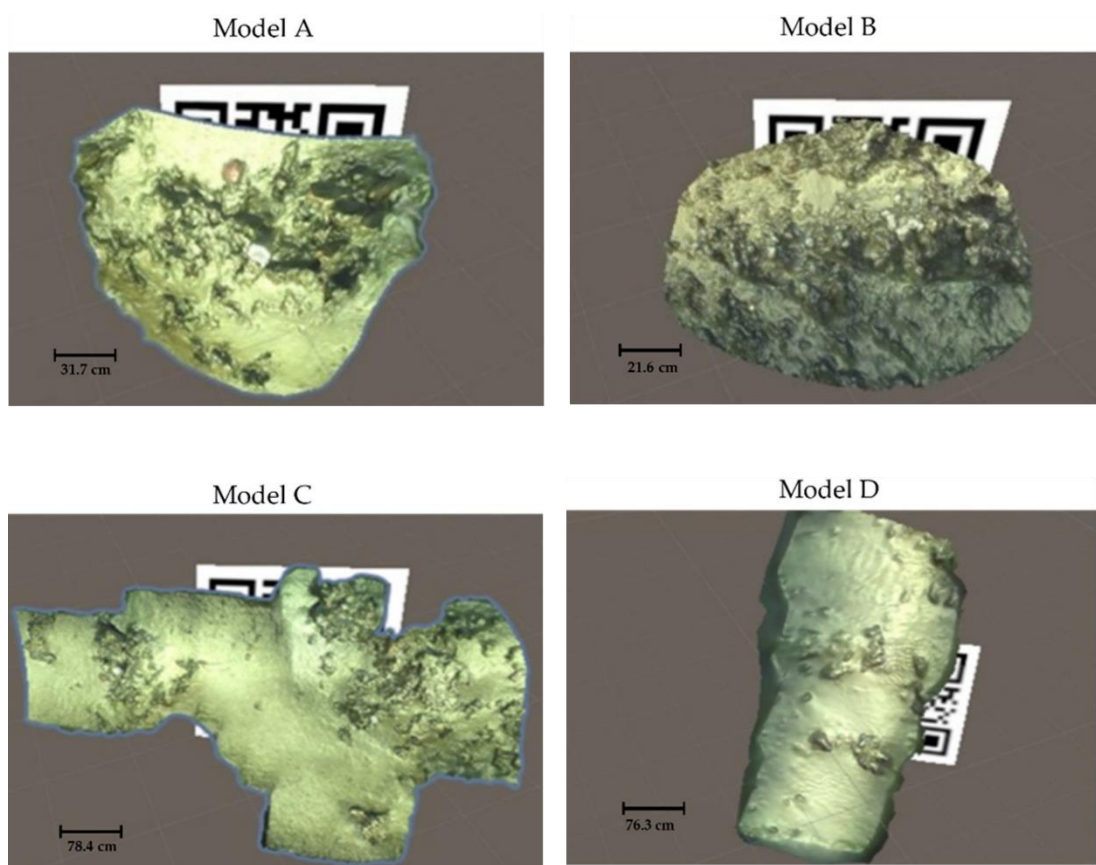


Figure 5.5: Three-dimensional models of CWC: Model A with 1,124,301 faces and 4,177,311 vertices at a resolution of 297,749.21 faces/area (m²); Model B with 462,589 faces and 232,453 vertices at a resolution of 31,825.87 faces/area (m²); Model C with 6,285,480 faces and 3,154,610 vertices at 292,660.99 faces/area (m²); Model D with 44,000 faces and 22,122 vertices at 4108.31 faces/area (m²), with A extracted from C.

The results showed that the size of the APP installation file (APK) in MB increased with the number of facies of each model (Figure 5.6). During the APP mobile assessment, it was possible to identify a few difficulties interacting with larger resolution models,

such as Model C, which had 6,285,480 faces, 3,154,610 vertices, and was 163 MB in size. User interaction movements such as intra axis rotation and changing zooms were limited owing to the model resolution (number of faces and vertices) and size. This can be because of the large size of the APP installation file (163 MB), which is the largest of the models tested. On the other hand, Model D, which is two orders of magnitude smaller than Model C, presented a smooth interaction. This is possibly because of the smaller number of faces and vertices of Model D, as well as the size of the APP installation file (49.3 MB), which is approximately 69% smaller than that of Model C. Similarly, Model B, with a similar APP size (56.5 MB), contributed to making the interaction in AR easier, at the expense of providing fewer CWC details (Figure 5.5). Model A (Figure 5.5), with 1,124,301 faces, 4,177,311 vertices, and 106 MB in size, which has a higher resolution than Models B and D, presented an easier interaction with the APP and a higher level of detail of objects. This evidences the trade-off between the resolution and the APP file size.

For example, Model A is approximately 82.1% smaller considering the number of faces in relation to Model C, and while the latter has a higher number of faces and vertices, the former presents a richer interaction at the expense of representing a smaller area. In Figure 5.6, it is noted that the number of faces influences the size of the APP. Contrarily, the number of vertices, which reflects the resolution i.e., level of detail of the model, does not vary with the size of the APP.

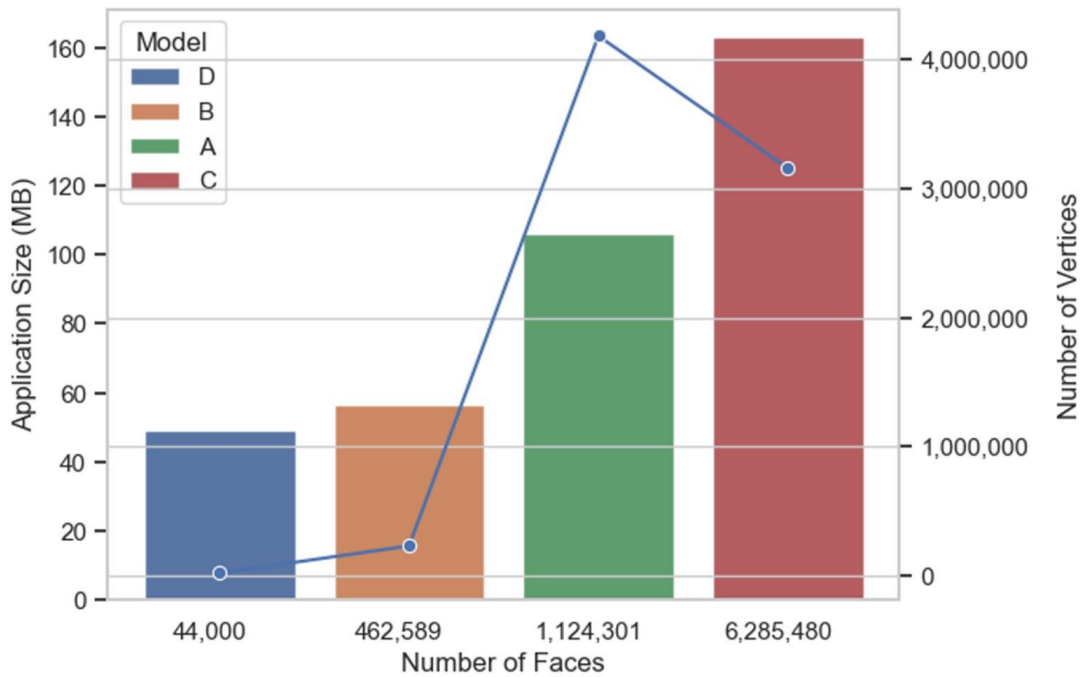


Figure 5.6: Relationship of the number of faces (x-axis) and number of vertices (blue trend line) in relation to the size of the APP in MB (y-axis).

5.4 Discussion

Overall, APP demonstrations showing Models D and B presented in Figure 5.4 (subfigures (a) and (b), respectively) represented smooth-to-run models owing to three criteria: (i) the generated APP occupied less space in the smartphone memory, (ii) the QR Code was read quickly, and (iii) it was possible to manipulate and interact easily with the 3D object, satisfying the proposal of this study. However, the higher resolution Model A (Figure 5.5 and Figure 5.7) presented a better trade-off among the three factors. Although Model A represented a small extent, it provided a higher level of detail at a reasonable APP file size that can allow smoother interactions in standard smartphones (Figure 5.6).

Three-dimensional reconstructions, when represented in a high resolution and at multiple scales, allow observations beyond the visual human aspect, such as the geographical distribution, seabed terrain variability (rugosity and slope measures) (Leon et al., 2015; Storlazzi et al., 2016), and morphological variations of CWC (Price et al., 2019). These variations can express environmental indicators that strongly dictate mound structure such as current dynamics, supply of organic particles, and

vertical and bottom sediments that influence the growth of coral mounds (Wheeler et al., 2007). In Figure 5.5 and Figure 5.7 it was possible to observe the contrast of the texture and roughness of the models and associate it with the seabed elements, such as shells, sediment morphology, and corals. Although this contrast was less pronounced in the models in Figure 5.4, where the 3D view as well as textures and roughness were compromised, the results herein help outline a minimum threshold for the number of faces and vertices and, consequently, the resolution of the models to be used.

The developed APP can facilitate the dissemination of knowledge by raising awareness regarding the importance of understanding and monitoring these environments towards coral health and conservation, especially considering that CWC has been affected by climate and anthropogenic threats such as rising temperatures, increased ocean acidity (Roberts and Cairns, 2014), and bottom trawling (Althaus et al., 2009).



Figure 5.7: View of Model A (297,749.21 faces/m² resolution) and Model D (4,108.31 faces/m² resolution) from Unity 3D desktop. Here, it is possible to see the resolution differences between models.

Scleractinian corals are naturally 3D reef-forming frameworks (Lim et al., 2020b; Mienis et al., 2019). With the combination of AR and 3D photogrammetry, it is possible to visualise the 3D model of coral reef formations, which is a fundamental aspect in understanding these habitats (Burns et al., 2015; House et al., 2018; McKinnon et al., 2011). In the marine sciences field, the 3D perception derived from 3D photogrammetry and SfM techniques can leverage remote mapping and explorations

for scientists and decision makers looking to understand and manage these deep-sea environments. Moreover, the 3D visualisation using AR can be a didactic and low-cost alternative to show how coral structures can appear in various types of environments. The use of this technology may help students and researchers in studies related to not only CWC, but also other deep-water environments such as submarine canyons and hydrothermal vents. The interaction with the models makes it easy to observe the environment in which the corals are inserted, showing these marine ecosystems in a more visual way. Users can interactively rotate the 3D object and zoom while moving the camera closer or further away from the QR Code, making the learning process more interesting when compared with visualisation provided by videos or images, for example.

Mobile AR can increase data accessibility, as users only need their smartphone and can learn about CWC from anywhere. In a wider scenario, mobile AR creates the potential for scientific dissemination of these environments and encourages the protection of underwater ecosystems by arousing curiosity among agencies that can begin to protect reefs. This is especially true in the case of 3D models built from SfM, which are usually heavy to visualise and, therefore, end up depending on desktop environments and specialized software.

The map for the visualisation of the 3D model built from SfM in the context of the Atlantic Ocean can be seen in Figure 5.8, and the APP is available online for other users on (<https://drive.google.com/drive/folders/1Nf36dtLtCCQKts40Kqha8D9hSCWluFzU>).

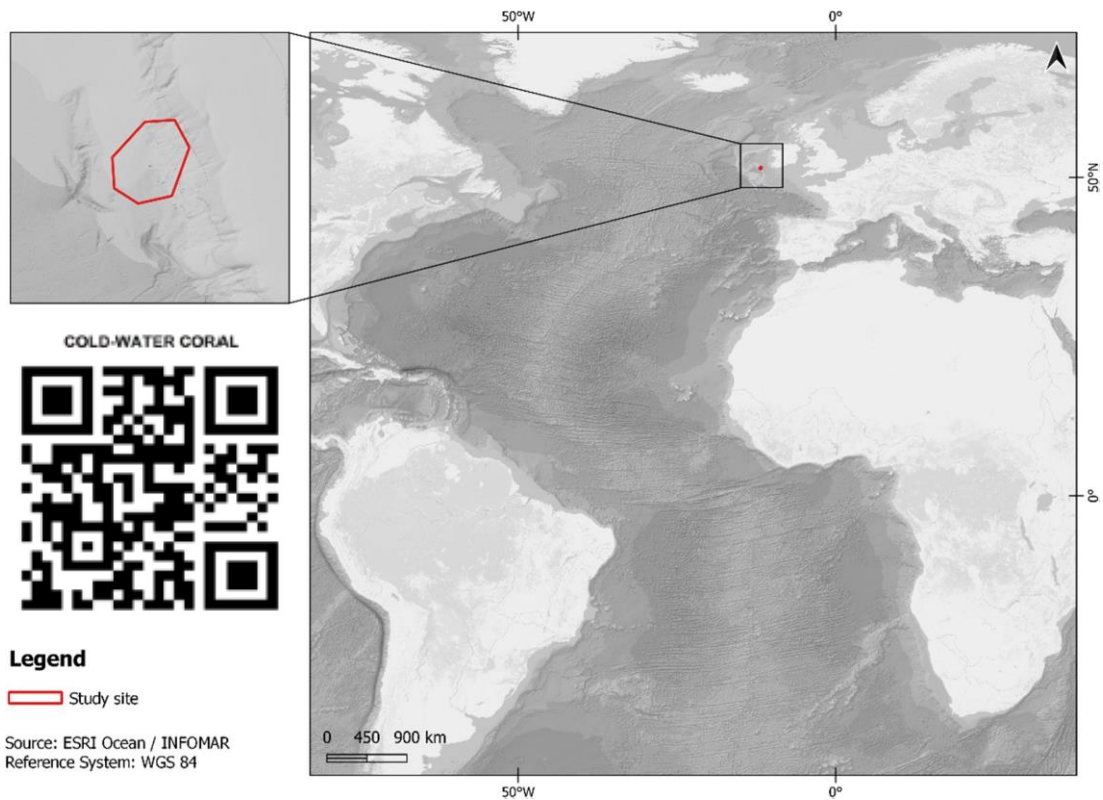


Figure 5.8: Interactive map for the AR app visualisation. After downloading the APP (APK) on their phone, the user can open app and scan the QR Code (left) on the map.

5.5 Conclusions

The production of a digital representation of CWC topography and constituent elements allowed the reconstruction of the CWC seascape in a virtual 3D environment. The use of AR integrated with GIS (georeferenced data) facilitates exploring large regions at a high resolution, leading to field scale experiences with varying levels of immersion, and it has been used in a wide range of fields including geoscience research and education. CWC reefs were selected for mobile AR visualisation for two main reasons: (i) they are important deep-sea ecosystems that are often located in secluded and complex terrains and (ii) these habitats have a fundamental role in sustaining local biodiversity by acting as hotspots for different species (Roberts and Hirshfield, 2004); therefore, there is an increasing need to map and monitor them. The results of the AR visualisation by Android smartphones from the APP exported in the Unity 3D software showed that visualisation was satisfactory

for resolutions higher than 200,000 faces/ m². However, there was a trade-off between resolution and APP size as 3D models with many faces and vertices presented a better result in terms of the level of detail of object, but had limitations in the size of the APP.

SfM photogrammetry produces 3D point clouds, orthorectified images, and accurate digital elevation models (Pizarro et al., 2017), and has been used to quantify the structural complexity of coral reef habitats (Anelli et al., 2019; Pizarro et al., 2017; Price et al., 2019). The integration of SfM and AR potentializes the visualisation of these reefs in new perspectives. Additionally, AR can provide additional support to ROVs mapping surveys. The interactive AR visualisation of CWC via a smartphone can increase the accessibility of data visualisation and awareness of CWC's environmental importance.

Overall, the results show that it was possible to combine digital technologies such as ROVs, 3D modelling, and mobile AR as a subsidy for the interactive visualisation of CWC. Studies suggest that users who explore virtual spaces can form more cognitive associations (Buchner et al., 2022) with scientific content, and can better learn and retain information related to the causes and effects of different phenomena, such as ocean acidification, for example. Thus, AR visualisation can endorse the environmental importance of underwater ecosystems through educational outreach and ocean literacy actions that encourage the understanding of complex structures such CWC, which can ultimately increase the community's interest in protecting coral reefs (Kasinathan et al., 2021). Furthermore, the dissemination of information about the services associated with CWC can stimulate decision-makers to take initiatives to protect CWC (Armstrong et al., 2014). Future studies should involve a wider user acceptance testing (UAT) survey (Cimperman, 2006), including AR-related problems faced by teachers and students (Fernández-Batanero et al., 2022; Lee, 2012), to test the efficiency and usability of the APP in different geographical settings (Jung et al., 2018).

5.6 References

- Aanesen, M., Armstrong, C., Czajkowski, M., Falk-Petersen, J., Hanley, N., Navrud, S., 2015. Willingness to pay for unfamiliar public goods: Preserving cold-water coral in Norway. *Ecol. Econ.* 112, 53–67. <https://doi.org/10.1016/j.ecolecon.2015.02.007>
- Addamo, A.M., Vertino, A., Stolarski, J., García-Jiménez, R., Taviani, M., Machordom, A., García-Jiménez, R., Taviani, M., Machordom, A., García-Jiménez, R., Taviani, M., Machordom, A., 2016. Merging scleractinian genera: The overwhelming genetic similarity between solitary *Desmophyllum* and colonial *Lophelia*. *BMC Evol. Biol.* 16, 1–17. <https://doi.org/10.1186/s12862-016-0654-8>
- Agisoft, 2021. Agisoft Metashape User Manual: Professional Edition, Version 1.7. Agisoft Metashape 160.
- Althaus, F., Williams, A., Schlacher, T.A., Kloser, R.J., Green, M.A., Barker, B.A., Bax, N.J., Brodie, P., Schlacher-Hoenlinger, M.A., 2009. Impacts of bottom trawling on deep-coral ecosystems of seamounts are long-lasting. *Mar. Ecol. Prog. Ser.* 397, 279–294. <https://doi.org/10.3354/meps08248>
- Anelli, M., Julitta, T., Fallati, L., Galli, P., Rossini, M., Colombo, R., 2019. Towards new applications of underwater photogrammetry for investigating coral reef morphology and habitat complexity in the Myeik Archipelago, Myanmar. *Geocarto Int.* 34, 459–472. <https://doi.org/10.1080/10106049.2017.1408703>
- Arena, F., Collotta, M., Pau, G., Termine, F., 2022. An Overview of Augmented Reality. *Computers.* <https://doi.org/10.3390/computers11020028>
- Armstrong, C.W., Foley, N.S., Kahui, V., Grehan, A., 2014. Cold water coral reef management from an ecosystem service perspective. *Mar. Policy* 50, 126–134. <https://doi.org/10.1016/j.marpol.2014.05.016>
- Auster, P.J., Gjerde, K., Heupel, E., Watling, L., Grehan, A., Rogers, A.D., 2011. Definition and detection of vulnerable marine ecosystems on the high seas: problems with the “move-on” rule. *ICES J. Mar. Sci.* 68, 254–264. <https://doi.org/10.1093/icesjms/fsq074>

- Barker, N.H.L., Roberts, C.M., 2004. Scuba diver behaviour and the management of diving impacts on coral reefs. *Biol. Conserv.* 120, 481–489. <https://doi.org/10.1016/j.biocon.2004.03.021>
- Barrile, V., Fotia, A., Bernardo, E., 2019. The submerged heritage: a virtual journey in our. *Int. Arch. Photogramm. Remote Sens. Spat. Inf. Sci.* XLII-2/W10, 17–24. <https://doi.org/10.5194/isprs-archives-XLII-2-W10-17-2019>
- Billinghurst, M., Duenser, A., 2012. Augmented reality in the classroom. *Computer (Long. Beach. Calif.)*. 45, 56–63.
- Bimber, O., Raskar, R., 2005. Spatial augmented reality: merging real and virtual worlds. CRC press.
- Boolukos, C.M., Lim, A., O’Riordan, R.M., Wheeler, A.J., O’Riordan, R.M., Wheeler, A.J., O’Riordan, R.M., Wheeler, A.J., 2019. Cold-water corals in decline – A temporal (4 year) species abundance and biodiversity appraisal of complete photomosaiced cold-water coral reef on the Irish Margin. *Deep Sea Res. Part I Oceanogr. Res. Pap.* 146, 44–54. <https://doi.org/10.1016/j.dsr.2019.03.004>
- Borba, E.Z., 2014. Imersão visual e corporal: paradigmas da percepção em simuladores. *Narrat. Comun. Complexificadas II—A Forma. SantaCruz do Sul Edunisc* 239–256.
- Bruno, F., Barbieri, L., Mangeruga, M., Cozza, M., Lagudi, A., Čejka, J., Liarokapis, F., Skarlatos, D., 2019. Underwater augmented reality for improving the diving experience in submerged archaeological sites. *Ocean Eng.* 190, 106487. <https://doi.org/10.1016/j.oceaneng.2019.106487>
- Buchner, J., Buntins, K., Kerres, M., 2022. The impact of augmented reality on cognitive load and performance: A systematic review. *J. Comput. Assist. Learn.* 38, 285–303. <https://doi.org/10.1111/jcal.12617>
- Burns, Fukunaga, A., Pascoe, K.H., Runyan, A., Craig, B.K., Talbot, J., Pugh, A., Kosaki, R.K., 2019. 3D HABITAT COMPLEXITY OF CORAL REEFS IN THE NORTHWESTERN HAWAIIAN ISLANDS IS DRIVEN BY CORAL ASSEMBLAGE STRUCTURE. *Int. Arch. Photogramm. Remote Sens. Spat. Inf. Sci.* XLII-2/W10, 61–67.

<https://doi.org/10.5194/isprs-archives-XLII-2-W10-61-2019>

- Burns, J.H.R., Delparte, D., Gates, R., Takabayashi, M., 2015. Integrating structure-from-motion photogrammetry with geospatial software as a novel technique for quantifying 3D ecological characteristics of coral reefs. *PeerJ* 3, e1077. <https://doi.org/10.7717/peerj.1077>
- Carmigniani, J., Furht, B., 2011. Augmented Reality: An Overview, in: *Handbook of Augmented Reality*. Springer New York, New York, NY, pp. 3–46. https://doi.org/10.1007/978-1-4614-0064-6_1
- Carrivick, J.L., Smith, M.W., Quincey, D.J., 2016. *Structure from Motion in the Geosciences*. John Wiley & Sons, Ltd, Chichester, UK. <https://doi.org/10.1002/9781118895818>
- Cathalot, C., Van Oevelen, D., Cox, T.J.S., Kutti, T., Lavaleye, M., Duineveld, G., Meysman, F.J.R., 2015. Cold-water coral reefs and adjacent sponge grounds: hotspots of benthic respiration and organic carbon cycling in the deep sea. *Front. Mar. Sci.* 2. <https://doi.org/10.3389/fmars.2015.00037>
- Čejka, J., Zsíros, A., Liarokapis, F., 2020. A hybrid augmented reality guide for underwater cultural heritage sites. *Pers. Ubiquitous Comput.* 24, 815–828. <https://doi.org/10.1007/s00779-019-01354-6>
- Chen, T.C., Ku, K.C., Ying, T.C., 2012. A process-based collaborative model of marine tourism service system - The case of Green Island area, Taiwan. *Ocean Coast. Manag.* 64, 37–46. <https://doi.org/10.1016/J.OCECOAMAN.2012.04.009>
- Cieza, E., Lujan, D., 2018. Educational Mobile Application of Augmented Reality Based on Markers to Improve the Learning of Vowel Usage and Numbers for Children of a Kindergarten in Trujillo. *Procedia Comput. Sci.* 130, 352–358. <https://doi.org/10.1016/j.procs.2018.04.051>
- Cimperman, R., 2006. *UAT Defined: A Guide to Practical User Acceptance Testing (Digital Short Cut)*. Pearson Education.
- Cipresso, P., Giglioli, I.A.C., Raya, M.A., Riva, G., 2018. The Past, Present, and Future of Virtual and Augmented Reality Research: A Network and Cluster Analysis of the

- Literature. *Front. Psychol.* 9. <https://doi.org/10.3389/fpsyg.2018.02086>
- Clark, M.R., 2006. Seamounts, deep-sea corals and fisheries: vulnerability of deep-sea corals to fishing on seamounts beyond areas of national jurisdiction. UNEP/Earthprint.
- ClassVR, 2022. Student Wearing ClassVR Headset Virtual Reality for Schools [WWW Document].
- Conti, L.A., Lim, A., Wheeler, A.J., 2019. High resolution mapping of a cold water coral mound. *Sci. Rep.* 9, 1016. <https://doi.org/10.1038/s41598-018-37725-x>
- Coughlan, M., Wheeler, A.J., Dorschel, B., Lordan, C., Boer, W., Van Gaever, P., De Haas, H., Mörz, T., 2015. Record of anthropogenic impact on the Western Irish Sea mud belt. *Anthropocene* 9, 56–69. <https://doi.org/10.1016/j.ancene.2015.06.001>
- Cristobal, F.R., Dodge, M., Noll, B., Rosenberg, N., Burns, J., Sanchez, J., Gotshalk, D., Pascoe, K., Runyan, A., 2020. Exploration of Coral Reefs in Hawai'i through Virtual Reality: Hawaiian Coral Reef Museum VR, in: *Practice and Experience in Advanced Research Computing*. ACM, New York, NY, USA, NY, USA, pp. 545–546. <https://doi.org/10.1145/3311790.3404542>
- Cunliffe, A.M., Brazier, R.E., Anderson, K., 2016. Ultra-fine grain landscape-scale quantification of dryland vegetation structure with drone-acquired structure-from-motion photogrammetry. *Remote Sens. Environ.* 183, 129–143. <https://doi.org/10.1016/j.rse.2016.05.019>
- Danovaro, R., Dell'Anno, A., Pusceddu, A., 2004. Biodiversity response to climate change in a warm deep sea. *Ecol. Lett.* 7, 821–828. <https://doi.org/10.1111/j.1461-0248.2004.00634.x>
- Davies, J.S., Guillaumont, B., Tempera, F., Vertino, A., Beuck, L., Ólafsdóttir, S.H., Smith, C.J., Fosså, J.H., van den Beld, I.M.J., Savini, A., Rengstorf, A., Bayle, C., Bourillet, J.F., Arnaud-Haond, S., Grehan, A., 2017. A new classification scheme of European cold-water coral habitats: Implications for ecosystem-based management of the deep sea. *Deep. Res. Part II Top. Stud. Oceanogr.* 145, 102–

109. <https://doi.org/10.1016/j.dsr2.2017.04.014>

- De Clippele, L.H., Gafeira, J., Robert, K., Hennige, S., Lavaleye, M.S., Duineveld, G.C.A., Huvenne, V.A.I., Roberts, J.M., 2017. Using novel acoustic and visual mapping tools to predict the small-scale spatial distribution of live biogenic reef framework in cold-water coral habitats. *Coral Reefs* 36, 255–268. <https://doi.org/10.1007/s00338-016-1519-8>
- De Mol, B., Van Rensbergen, P., Pillen, S., Van Herreweghe, K., Van Rooij, D., McDonnell, A., Huvenne, V., Ivanov, M., Swennen, R., Henriët, J., 2002. Large deep-water coral banks in the Porcupine Basin, southwest of Ireland. *Mar. Geol.* 188, 193–231. [https://doi.org/10.1016/S0025-3227\(02\)00281-5](https://doi.org/10.1016/S0025-3227(02)00281-5)
- de Oliveira, L.M.C., Lim, A., Conti, L.A., Wheeler, A.J., 2021. 3D Classification of Cold-Water Coral Reefs: A Comparison of Classification Techniques for 3D Reconstructions of Cold-Water Coral Reefs and Seabed. *Front. Mar. Sci.* 8. <https://doi.org/10.3389/fmars.2021.640713>
- Denoyel, A., Pinson, C., Passet, P.A., 2012. Sketchfab - The best 3D viewer on the web [WWW Document]. URL <https://sketchfab.com/> (accessed 9.15.22).
- Doležal, M., Vlachos, M., Secci, M., Demesticha, S., Skarlatos, D., Liarokapis, F., 2019. UNDERSTANDING UNDERWATER PHOTOGRAMMETRY for MARITIME ARCHAEOLOGY THROUGH IMMERSIVE VIRTUAL REALITY. *ISPRS Ann. Photogramm. Remote Sens. Spat. Inf. Sci.* 42, 85–91. <https://doi.org/10.5194/isprs-archives-XLII-2-W10-85-2019>
- Dorschel, B., Hebbeln, D., Foubert, A., White, M., Wheeler, A.J., 2007. Hydrodynamics and cold-water coral facies distribution related to recent sedimentary processes at Galway Mound west of Ireland. *Mar. Geol.* 244, 184–195.
- Dunleavy, M., Dede, C., Mitchell, R., 2009. Affordances and limitations of immersive participatory augmented reality simulations for teaching and learning. *J. Sci. Educ. Technol.* 18, 7–22.
- European Union Habitats Directive, 2016. European Union Habitats(Porcupine Bank Canyon Special Area of Conservation 003001) Regulations2016. Ireland.

- Fabri, M.-C., Pedel, L., Beuck, L., Galgani, F., Hebbeln, D., Freiwald, A., 2014. Megafauna of vulnerable marine ecosystems in French mediterranean submarine canyons: Spatial distribution and anthropogenic impacts. *Deep Sea Res. Part II Top. Stud. Oceanogr.* 104, 184–207. <https://doi.org/10.1016/j.dsr2.2013.06.016>
- Feiner, S., MacIntyre, B., Seligmann, D., 1993. Knowledge-based augmented reality. *Commun. ACM* 36, 53–62.
- Fernández-Batanero, J.M., Montenegro-Rueda, M., Fernández-Cerero, J., 2022. Use of Augmented Reality for Students with Educational Needs: A Systematic Review (2016–2021). *Societies* 12, 36. <https://doi.org/10.3390/soc12020036>
- Foubert, A., Huvenne, V.A.I., Wheeler, A., Kozachenko, M., Opderbecke, J., Henriët, J.-P., 2011. The Moira Mounds, small cold-water coral mounds in the Porcupine Seabight, NE Atlantic: Part B---Evaluating the impact of sediment dynamics through high-resolution ROV-borne bathymetric mapping. *Mar. Geol.* 282, 65–78.
- Foucault, M., Miskowiec, J., 1986. Of other spaces. *diacritics* 16, 22–27.
- Frank, N., Freiwald, A., López Correa, M., Wienberg, C., Eisele, M., Hebbeln, D., Van Rooij, D., Henriët, J.P., Colin, C., van Weering, T., de Haas, H., Buhl-Mortensen, P., Roberts, J.M., De Mol, B., Douville, E., Blamart, D., Hatté, C., 2011. Northeastern Atlantic cold-water coral reefs and climate. *Geology* 39, 743–746. <https://doi.org/10.1130/G31825.1>
- Han, X., Liu, J., Tan, B., Duan, L., 2021. Design and Implementation of Smart Ocean Visualization System Based on Extended Reality Technology. *J. Web Eng.* <https://doi.org/10.13052/jwe1540-9589.20215>
- Hebbeln, D., Portilho-Ramos, R. da C., Wienberg, C., Titschack, J., 2019. The Fate of Cold-Water Corals in a Changing World: A Geological Perspective. *Front. Mar. Sci.* 6. <https://doi.org/10.3389/fmars.2019.00119>
- Hebbeln, D., Wienberg, C., Dullo, W.C., Freiwald, A., Mienis, F., Orejas, C., Titschack, J., 2020. Cold-water coral reefs thriving under hypoxia. *Coral Reefs* 39, 853–859.

<https://doi.org/10.1007/s00338-020-01934-6>

Henry, L.-A., Roberts, J.M., 2016. Global Biodiversity in Cold-Water Coral Reef Ecosystems, in: *Marine Animal Forests*. Springer International Publishing, Cham, pp. 1–21. https://doi.org/10.1007/978-3-319-17001-5_6-1

House, J.E., Brambilla, V., Bidaut, L.M., Christie, A.P., Pizarro, O., Madin, J.S., Dornelas, M., 2018. Moving to 3D: relationships between coral planar area, surface area and volume. *PeerJ* 6, e4280. <https://doi.org/10.7717/peerj.4280>

Huvenne, V.A.I., Bett, B.J., Masson, D.G., Le Bas, T.P., Wheeler, A.J., 2016. Effectiveness of a deep-sea cold-water coral Marine Protected Area, following eight years of fisheries closure. *Biol. Conserv.* 200, 60–69. <https://doi.org/10.1016/j.biocon.2016.05.030>

i-MareCulture – H2020 funded EU research and innovation project [WWW Document], n.d. URL <https://imareculture.eu/> (accessed 9.15.22).

Jameson, S.C., Ammar, M.S.A., Saadalla, E., Mostafa, H.M., Riegl, B., 1999. A coral damage index and its application to diving sites in the Egyptian Red Sea. *Coral reefs* 18, 333–339.

Jung, T.H., Lee, H., Chung, N., tom Dieck, M.C., 2018. Cross-cultural differences in adopting mobile augmented reality at cultural heritage tourism sites. *Int. J. Contemp. Hosp. Manag.* 30, 1621–1645. <https://doi.org/10.1108/IJCHM-02-2017-0084>

Kasinathan, V., Al-Sharafi, A.T.A., Zamnah, A., Appadurai, N.K., Thiruchelvam, V., Mustapha, A., 2021. Augmented reality in ocean’s secrets: educational application with attached book for students. *Linguist. Cult. Rev.* 5, 1123–1137. <https://doi.org/10.21744/lingcure.v5ns1.1498>

Kaufmann, H., 2003. Collaborative augmented reality in education. *Inst. Softw. Technol. Interact. Syst. Vienna Univ. Technol.* 2–4.

Kwasnitschka, T., Hansteen, T.H., Devey, C.W., Kutterolf, S., 2013. Doing fieldwork on the seafloor: Photogrammetric techniques to yield 3D visual models from ROV video. *Comput. Geosci.* 52, 218–226.

<https://doi.org/10.1016/j.cageo.2012.10.008>

Labster, n.d. Reimagining the future of education [WWW Document]. 2022. URL <https://www.labster.com/about/>

Laranjeira, M., Arnaubec, A., Brignone, L., Dune, C., Opderbecke, J., 2020. 3D Perception and Augmented Reality Developments in Underwater Robotics for Ocean Sciences. *Curr. Robot. Reports* 1, 123–130. <https://doi.org/10.1007/s43154-020-00014-5>

Lee, K., 2012. Augmented reality in education and training. *TechTrends* 56, 13–21.

Leon, J.X., Roelfsema, C.M., Saunders, M.I., Phinn, S.R., 2015. Measuring coral reef terrain roughness using ‘Structure-from-Motion’ close-range photogrammetry. *Geomorphology* 242, 21–28. <https://doi.org/10.1016/j.geomorph.2015.01.030>

Li, R., Li, H., Zou, W., Smith, R.G., Curran, T.A., 1997. Quantitative photogrammetric analysis of digital underwater video imagery. *IEEE J. Ocean. Eng.* 22, 364–375. <https://doi.org/10.1109/48.585955>

Liestøl, G., 2019. Augmented Reality Storytelling – Narrative Design and Reconstruction of a Historical Event in situ. *Int. J. Interact. Mob. Technol.* 13, 196. <https://doi.org/10.3991/ijim.v13i12.11560>

Liestøl, G., Bendon, M., Hadjidaki-Marder, E., 2021. Augmented Reality Storytelling Submerged. Dry Diving to a World War II Wreck at Ancient Phalasarna, Crete. *Heritage* 4, 4647–4664. <https://doi.org/10.3390/heritage4040256>

Lim, A., Huvenne, V.A.I., Vertino, A., Spezzaferri, S., Wheeler, A.J., 2018. New insights on coral mound development from groundtruthed high-resolution ROV-mounted multibeam imaging. *Mar. Geol.* 403, 225–237. <https://doi.org/10.1016/j.margeo.2018.06.006>

Lim, A., Wheeler, A.J., Arnaubec, A., 2017. High-resolution facies zonation within a cold-water coral mound: The case of the Piddington Mound, Porcupine Seabight, NE Atlantic. *Mar. Geol.* 390, 120–130. <https://doi.org/10.1016/j.margeo.2017.06.009>

Lim, A., O’Reilly, L., Summer, G., de Oliveira, L.M.C., Strachan, R., Lim, O’Reilly, L.,

- Summer, G., de Oliveira, L.M.C., Strachan, R., 2020a. CE20011 Cruise Report: Systematic Monitoring Survey of the Moira Mound Chain (SyMonS_MoM).
- Lim, A., Wheeler, A.J., Conti, L., 2020b. Cold-Water Coral Habitat Mapping: Trends and Developments in Acquisition and Processing Methods. *Geosciences* 11, 9. <https://doi.org/10.3390/geosciences11010009>
- Lim, A., Wheeler, A.J., Price, D.M., O'Reilly, L., Harris, K., Conti, L., 2020c. Influence of benthic currents on cold-water coral habitats: a combined benthic monitoring and 3D photogrammetric investigation. *Sci. Rep.* 10, 19433. <https://doi.org/10.1038/s41598-020-76446-y>
- Liu, X., Sohn, Y.-H., Park, D.-W., 2018. Application Development with Augmented Reality Technique using Unity 3D and Vuforia. *Int. J. Appl. Eng. Res.* 13, 15068–15071.
- Loureiro, S.M.C., Guerreiro, J., Ali, F., 2020. 20 years of research on virtual reality and augmented reality in tourism context: A text-mining approach. *Tour. Manag.* <https://doi.org/10.1016/j.tourman.2019.104028>
- Lowe, G., 2004. Sift-the scale invariant feature transform. *Int. J* 2, 2.
- Markowitz, D.M., Laha, R., Perone, B.P., Pea, R.D., Bailenson, J.N., 2018. Immersive Virtual Reality Field Trips Facilitate Learning About Climate Change. *Front. Psychol.* 9. <https://doi.org/10.3389/fpsyg.2018.02364>
- McKinnon, D., He, H., Upcroft, B., Smith, R.N., 2011. Towards automated and in-situ, near-real time 3-D reconstruction of coral reef environments. *Ocean. - MTS/IEEE Kona, Progr. B.* <https://doi.org/10.23919/oceans.2011.6106982>
- Microsoft, n.d. Android Studio | Android Developers.
- Mienis, F., Bouma, T., Witbaard, R., van Oevelen, D., Duineveld, G., 2019. Experimental assessment of the effects of coldwater coral patches on water flow. *Mar. Ecol. Prog. Ser.* 609, 101–117. <https://doi.org/10.3354/meps12815>
- Miller, G.T., Spoolman, S., 2015. *Environmental science*. Cengage Learning.
- Miller, R.J., Hocevar, J., Stone, R.P., Fedorov, D. V, 2012. Structure-Forming Corals and Sponges and Their Use as Fish Habitat in Bering Sea Submarine Canyons. *PLoS*

One 7, 1–9. <https://doi.org/10.1371/journal.pone.0033885>

Monteiro, J.H.F., Montanha, G.K., 2019. Desenvolvimento de aplicação em Realidade Virtual. *Tekhne e Logos* 10, 99–111.

Navarro, A., Young, M., Allan, B., Carnell, P., Macreadie, P., Ierodiaconou, D., 2020. The application of Unmanned Aerial Vehicles (UAVs) to estimate above-ground biomass of mangrove ecosystems. *Remote Sens. Environ.* 242, 111747. <https://doi.org/10.1016/j.rse.2020.111747>

Oevelen, D. van, Duineveld, G., Lavaleye, M., Mienis, F., Soetaert, K., Heip, C.H.R., 2009. The cold-water coral community as hotspot of carbon cycling on continental margins: A food-web analysis from Rockall Bank (northeast Atlantic). *Limnol. Oceanogr.* 54, 1829–1844. <https://doi.org/10.4319/lo.2009.54.6.1829>

Otero, V., Van De Kerchove, R., Satyanarayana, B., Martínez-Espinosa, C., Fisol, M.A. Bin, Ibrahim, M.R. Bin, Sulong, I., Mohd-Lokman, H., Lucas, R., Dahdouh-Guebas, F., 2018. Managing mangrove forests from the sky: Forest inventory using field data and Unmanned Aerial Vehicle (UAV) imagery in the Matang Mangrove Forest Reserve, peninsular Malaysia. *For. Ecol. Manage.* 411, 35–45. <https://doi.org/10.1016/j.foreco.2017.12.049>

Panagiotidis, D., Surovy, P., Kuželka, K., 2016. Accuracy of Structure from Motion models in comparison with terrestrial laser scanner for the analysis of DBH and height influence on error behaviour. *J. For. Sci.* 62, 357–365. <https://doi.org/10.17221/92/2015-JFS>

Pizarro, O., Friedman, A., Bryson, M., Williams, S.B., Madin, J., 2017. A simple, fast, and repeatable survey method for underwater visual 3D benthic mapping and monitoring. *Ecol. Evol.* 7, 1770–1782. <https://doi.org/10.1002/ece3.2701>

Price, D.M., Robert, K., Callaway, A., Lo Iacono, C., Hall, R.A., Huvenne, V.A.I., 2019. Using 3D photogrammetry from ROV video to quantify cold-water coral reef structural complexity and investigate its influence on biodiversity and community assemblage. *Coral Reefs* 38, 1007–1021. <https://doi.org/10.1007/s00338-019-01827-3>

- Rizvic, S., Boskovic, D., Okanovic, V., Sljivo, S., Zukic, M., 2019. Interactive digital storytelling: bringing cultural heritage in a classroom. *J. Comput. Educ.* 6, 143–166. <https://doi.org/10.1007/s40692-018-0128-7>
- Robert, K., Huvenne, V.A.I.I., Georgiopoulou, A., Jones, D.O.B.B., Marsh, L., Carter, D.O.G., Chaumillon, L., 2017. New approaches to high-resolution mapping of marine vertical structures. *Sci. Rep.* 7, 1–14. <https://doi.org/10.1038/s41598-017-09382-z>
- Roberts, J.M., Cairns, S.D., 2014. Cold-water corals in a changing ocean. *Curr. Opin. Environ. Sustain.* 7, 118–126. <https://doi.org/10.1016/j.cosust.2014.01.004>
- Roberts, S., Hirshfield, M., 2004. Deep-sea corals: Out of sight, but no longer out of mind. *Front. Ecol. Environ.* 2, 123–130. [https://doi.org/10.1890/1540-9295\(2004\)002\[0123:DCOOSB\]2.0.CO;2](https://doi.org/10.1890/1540-9295(2004)002[0123:DCOOSB]2.0.CO;2)
- Roberts, Wheeler, A.J., Freiwald, A., 2006. Reefs of the Deep: The Biology and Geology of Cold-Water Coral Ecosystems. *Science* (80-.). 312, 543–547. <https://doi.org/10.1126/science.1119861>
- Scholz, J., Smith, A.N., 2016. Augmented reality: Designing immersive experiences that maximize consumer engagement. *Bus. Horiz.* 59, 149–161. <https://doi.org/10.1016/j.bushor.2015.10.003>
- Shelton, B.E., Hedley, N.R., 2004. Exploring a cognitive basis for learning spatial relationships with augmented reality. *Technol. Instr. Cogn. Learn.* 1, 323.
- Smith, M.W., Carrivick, J.L., Quincey, D.J., 2016. Structure from motion photogrammetry in physical geography. *Prog. Phys. Geogr.* 40, 247–275. <https://doi.org/10.1177/0309133315615805>
- Sorice, M.G., Oh, C.-O., Ditton, R.B., 2007. Managing scuba divers to meet ecological goals for coral reef conservation. *AMBIO A J. Hum. Environ.* 36, 316–322.
- Sotiriou, S., Bogner, F.X., 2008. Visualizing the invisible: augmented reality as an innovative science education scheme. *Adv. Sci. Lett.* 1, 114–122.
- Storlazzi, C.D., Dartnell, P., Hatcher, G.A., Gibbs, A.E., 2016. End of the chain? Rugosity and fine-scale bathymetry from existing underwater digital imagery using

- structure-from-motion (SfM) technology. *Coral Reefs* 35, 889–894. <https://doi.org/10.1007/s00338-016-1462-8>
- Turley, C.M., Roberts, J.M., Guinotte, J.M., 2007. Corals in deep-water: will the unseen hand of ocean acidification destroy cold-water ecosystems? *Coral Reefs* 26, 445–448. <https://doi.org/10.1007/s00338-007-0247-5>
- Unity Technologies, 2021. Real-time solutions. Endless opportunities. [WWW Document]. Unity Webseite. URL <https://unity.com/>
- VRgeoscience, 2022. Digital Outcrop Modelling [WWW Document].
- Vuforia, 2015. Vuforia Engine [WWW Document]. Vuforia. URL <https://developer.vuforia.com/>
- Warfield, A.D., Leon, J.X., 2019. Estimating Mangrove Forest Volume Using Terrestrial Laser Scanning and UAV-Derived Structure-from-Motion. *Drones* 3, 32. <https://doi.org/10.3390/drones3020032>
- Weidner, L., Walton, G., Krajnovich, A., 2021. Classifying rock slope materials in photogrammetric point clouds using robust color and geometric features. <https://doi.org/10.13140/RG.2.2.35632.89604>
- Wheeler, A.J., Beyer, A., Freiwald, A., de Haas, H., Huvenne, V.A.I.I., Kozachenko, M., Olu-Le Roy, K., Opderbecke, J., 2007. Morphology and environment of cold-water coral carbonate mounds on the NW European margin. *Int. J. Earth Sci.* 96, 37–56. <https://doi.org/10.1007/s00531-006-0130-6>
- Wheeler, Kozachenko, M., Beyer, A., Foubert, A., Huvenne, V.A.I., Klages, M., Masson, D.G., Olu-Le Roy, K., Thiede, J., 2005. Sedimentary processes and carbonate mounds in the Belgica Mound province, Porcupine Seabight, NE Atlantic, in: *Cold-Water Corals and Ecosystems*. Springer Berlin Heidelberg, Berlin, Heidelberg, pp. 571–603. https://doi.org/10.1007/3-540-27673-4_28

6. Conclusions

6.1 Concluding remarks

This thesis presents four pathways to the investigation of the role of 3D habitat mapping in understanding CWC habitats.

To understand the de facto application of SfM to deep-water habitats, the existing methods available to analyse the data and the implications of multidimensionality, a study in the Porcupine Bank Canyon was developed. The findings corroborated answering the following research questions:

What software-based methods for 3D point cloud classification are available?

In [Chapter 2](#), we leveraged image processing tools embedded in commercial and open-source software to develop two methods to classify CWC in 3D (Multiscale Geometrical Classification (MGC), Colour and Geometrical Classification (CGC) and compare them to benchmark object-based image Classification (OBIA) method. Upon investigating the suitability of several GIS and 3D analysis software such as MeshLab, eCognition, CloudCompare, Blender, Agisoft Metashape ArcGis, Qgis, three methods to classify 3D models of CWC habitats were built, tested and their performance was assessed with a classification of CWC habitats between two classes, “coral”, which referred to the coral colonies and coral fragments and “seabed”, which referred to sediments, dropstones without signs of coral coverage. The balanced accuracy and accuracy scores averaged 67.2%, ranging to up to 74% for the 3D methods, showing that the MGC method is more appropriate for complex scenes with high environmental variability (Brodu and Lague, 2012). Nonetheless, these findings highlighted the paucity of accessible methods to classify fine-scale data and motivated the study design that resulted in [Chapter 3](#).

What is the cost, in terms of data loss, of using 2D data for 3D objects?

[Chapter 2](#) also showed that with the exception of the CGC method, all methods required similar amounts of data processing, which was mainly allocated to segmentation, labelling, and parameter-tuning, e.g., manual segmentation and labelling in MGC and manual classification in the OBIA method. To test the possible data loss in handling 2D and 3D data, two manual annotation schemes were used to

provide a baseline and ground truth for the methods, and percentage class distributions were compared. We show that there is a higher distribution of coral class within the 3D dense-cloud annotation in comparison to the OBIA method in 50% of the models with a difference of up to 4.45% in the percentage of coral (mean of 3.02%). The average distribution ratio of coral and seabed calculated from 3D methods and the OBIA method was 0.2%, showing that there is potentially an impact of at least a magnitude order of a tenth of the value in using 2D methods to represent objects that are naturally 3D structures. Although this difference may not appear significant, it has the potential to impact studies that rely on biomass measures from coral structural complexity, and landscape ecology being propagated across fine and mesoscales (millimetres to hundreds of metres).

What are the main advantages and disadvantages of the 3 different 3D workflows identified within this study?

The applications of SfM as a non-destructive, cost-effective method to reconstruct deep-water environments have been discussed throughout the thesis. The 3D models allowed for the quantification of habitat facies in the Porcupine Bank Canyon which otherwise would only be possible with the manual delineation of classes. The reconstructions serve as a temporal archive to complement previous studies and understand any spatiotemporal changes in the PBC. The techniques used to reconstruct and georeference the 3D models from video and ROV positioning have been transferred to reconstruct other areas such as the Moira Mounds.

However, as the *modus operandum* of machine learning applications, the amount of data to train classifiers should be carefully evaluated, as well as the particularities of regions of interest. In this case, the abundance of coral rubble and octocorals needs to be accounted for as they present similar values within the intensity range and present irregular boundaries. Furthermore, 3D photogrammetric surveys yield centimetric to millimetric resolutions that are computationally heavy and require significant data resources. The need to explore subsampling techniques to handle the data efficiently but without losing information is highly crucial. The results also demonstrated that most off-the-shelf algorithms at the time the study had been

released needed to be adapted for seabed classification. These findings motivated the study design of Chapter 3.

In [Chapter 3](#), the aim was to advance from the software-based methods by integrating the use of supervised machine learning algorithms into a multiclass 3D classification framework of the Piddington Mound area building upon the identified challenges outlined in [Chapter 2](#). To this end, six machine learning algorithms were tested, namely: Support Vector Machines, Random Forests, Gradient Boosting Trees, k-Nearest Neighbours, Logistic Regression and Multilayer Perceptron trained in two datasets of different sizes (1,000 samples and 10,000 samples) to understand the performance behaviour upon changing the quantity of training data. A section of the Piddington Mound was classified into four classes based on previous facies distribution studies, in this case, live coral framework (LCF), dead coral framework (DCF) and coral rubble (CR), apart from sediments and drop stones (SD). The results of this work answered the following questions:

Can Machine Learning be used for the classification of 3D point clouds of coral reef environments?

In [Chapter 3](#), a workflow was developed using machine learning and SfM that transformed 241.7 GB worth of data into an ecologically meaningful and compact dataset (<5.2 gigabytes) of the Piddington Mound area. Results show that it is possible to use ML algorithms in 3D point cloud data of CWC reefs and four ML algorithms yielded *f1* accuracies of >90%, being able to successfully discern between classes, especially those with similar features such as coral rubble and dead coral. Reservations regarding the training data size and execution time were made. The results showed that although MLP had 26.8% decrease in *f1* scores when trained on the smaller dataset (group 1), the run time was 91.63% faster, thus highlighting and quantifying the trade-offs of ML algorithms for CWC habitat classification.

The classification developed in [Chapter 3](#) was used for fine-scale analyses of intra-habitat patterns of the study area, which allowed the environmental study design of [Chapter 4](#).

Which Machine Learning classifiers produce the highest classification accuracy?

Given the absence of similar studies in 3D photogrammetry and ML in CWC habitats, the results herein delineated the suitability of specific algorithms for initial assessments, providing key information to future studies in CWC habitats. The classifiers GBT, RF, MLP and kNN trained in group 2 (dataset of 10,000 samples) were the most accurate classifiers on the first assessment, in that order. The *f1* accuracy of these four classifiers ranged from 95.11% (GBT) to 91.7% (kNN). The percentage difference among *f1* accuracies was low, approximately 3.65% which corroborates the interchangeability of algorithms, as documented in other studies (Jodzani et al., 2019; Liu et al., 2017).

Which parameters and variables can provide a better classification outcome?

To account for the wide range of possible parameters and variables that can be used in machine learning, model selection was performed with grid-search with a five-fold cross validation in both datasets. This was used to ensure that all possible combinations of parameter values were evaluated. The grid search results showed that MLPs were prone to choose hidden layer options with more neurons on them. In addition, all MLP classifiers selected the solver *adam* for weight optimisation as the final parameter on the grid search. In RF, for example, the analyses showed that using a smaller dataset resulted in models with a lower number of estimators and lower accuracy which is possibly due to how RF deals with decision trees in the classification. Another example given was the SVMs. [Chapter 3](#) shows that SVM responded unanimously to the choice of RBF kernel in all the best-performance SVMs. Furthermore, the chapter also gathered new information about suitability of polynomial kernels to dataset sizes, showing constraints when datasets have more than 10,000 samples.

What is the minimum density of points required to accurately classify a point cloud model with ML?

To answer this RQ, the original point cloud which was composed of approximately 90,000,000 points, was down sampled using as criteria the feasibility of carrying out complete workflow in the hardware used (Figure 3.2). This guaranteed that the workflow could be performed in end-user hardware, with > 64 GB of RAM. To this end, the point cloud was down sampled from the original value, to 5,000,000, 1,000,000,

500,000, 50,000, 10,000 and finally 1000. The values of 10,000 to 1000 were chosen based on the ML performance on the used hardware to yield a performance comparison.

Results these datasets show that voting ensemble classifiers like kNNs, RF, GBT have a greater response in *f1* accuracy when trained in larger datasets than kernel methods such as SVM. For example, GBTs and RFs had an increase of approximately 30% in accuracy when trained on the larger dataset, On the other hand, results suggest that SVM and LR are more robust to dataset size variations, given the small difference in *f1* scores between variations of the same algorithms like SVM (5.51%) and LR (2.35%). However, the training times act in favour of smaller datasets for certain algorithms such as MLPs. Overall, the results in [Chapter 3](#) support the quantification of the impact of training size on machine learning datasets which have not been previously quantified.

In [Chapter 4](#), SfM, ML, geomorphometric variables and Euclidean distance size distribution from the segmented facies were combined into a fine-scale environmental analysis of a section of the Piddington Mound. This body of work answered the following questions:

What is the distribution of each facies?

The most common facies of the semantic objects was the sediment and dropstones facies (SD) (49%), mainly concentrated downslope towards the deeper parts of the mound, followed by the coral rubble (CR) facies (38.8%), located around the edges of the mound. Live coral (LC) (8.9%) and dead coral (DC) (3.3%) both occurred at steeper slopes, around the shallower parts of the mound. However, LC facies also appeared in downslope, deeper areas.

Is there a pattern in coral distribution and size of corals ?

Density plots showed that the live coral facies presented two high density hotspots, one around the mid-slope area which is more intense (approx., 3.79 points/ m²) followed by a second less intense (2.46 expected points/m²) hotspot upslope. Whilst the dead coral facies presented one dense intensity hotspot (2.17 points/m²) upslope, at higher depths. Furthermore, larger DC and LC objects distribution were

concentrated toward the top of the mound, between 955 and 960 metres depth whilst smaller LC objects were concentrated downslope. The hotspots of LC and DC towards the higher parts of the mound corroborate to the hypothesis that CWC tend to settle on elevated structures where access to food supply is facilitated by faster flowing waters. On the other hand, the distribution of smaller corals in the downslope areas may have two explanations: i) it reflects mound growth or expansion were corals latch on to the existing hard substrate or ii) slower growth rates due to suboptimal conditions at the mound base.

Do corals have a preference in habitat?

The relationships between geomorphometric variables and facies spatial distribution were quantified to understand more about possible habitat preferences. Smoothing Estimate of Covariate Transformation (RhoHat) results showed that LC are more likely to be found at depths between -968 and -964 and -962 to -956 metres than would be expected if the intensity was constant. DC facies estimates were more conservative, showing that dead corals are more likely to be found mainly at depths between -962 to -956 metres than would be expected if the depth intensity was constant. There was also a strong relationship between both facies and steep slopes and westwards oriented slopes. The results also highlight the circular relationship among coral facies and the terrain, as at fine scales, the terrain ruggedness and VRM may be a response to the influence of the coral facies themselves.

Are coral facies clustered or dispersed?

[Chapter 4](#) results show that dead coral facies have a clustering pattern that becomes more evident from point distances greater than 0.2 metres, whereas live coral facies tend to appear more clustered in distances greater than 0.3 metres. Getis-Ord Gi Hotspot analyses also show that the intensity of clustering is stronger towards the higher parts of the mound. The findings of this study contribute to highlighting the high degree of variability resulting from morphological and biological traits of CWC mounds across not only regional but also local scales as coral facies have different terrain descriptors. Furthermore, it shows how environmental interpretations can be drawn from 3D fine-scale data.

Finally, [Chapter 5](#) provided a further insight to the contribution of 3D data to accessible visualisation and outreach whilst answering the following questions:

Can SfM and augmented reality (AR) be applied in outreach activities to promote access to deep-water environments?

CWC habitats are generally located in pristine environments and unlike their tropical counterparts, it was noted that there is a necessity to raise awareness to their existence and importance. By coupling SfM, AR and game development engines, we created a visualisation platform for CWC habitats, the Coral APP, which allows anyone with a smartphone and internet connection to interact with 3D reconstructions of these habitats. With the Coral APP, the user can point the phone to a provided QR code and see 3D models of CWC habitats.

What technologies are currently available to aid visualisation of these habitats?

Apart from the Coral APP, [Chapter 5](#) also delivered an overview of the current technologies and initiatives available for geoscience applications such as VRGeosciences and general AR applications such as Labster, ClassVR and SketchFab. In marine sciences, the overview highlighted EU funded projects for underwater cultural heritage such as the IMareCulture project, funded by Horizon2020. However, the literature review also highlighted the need for information about the requirements to develop visualisation applications of 3D underwater reconstructions.

What are the specificities of 3D data necessary to develop successful mobile applications?

For the development of the APP, we used georeferenced 3D meshes of one location around the Piddington Mound. We evaluated the performance of the applications based on three criteria: (i) how much memory the APP occupies in the smartphone (ii) how fast the QR Code was read (iii) possibility to manipulate and interact easily with the 3D object. The results showed that the size of the APP installation file (APK) in MB increased with the number of facies of each model. Furthermore, the APP visualisation in Android smartphones from exported in the Unity 3D software showed that visualisation was satisfactory for resolutions higher than 200,000 faces/m². However, there was a trade-off between resolution and APP size as 3D models with many faces

and vertices presented a better result in terms of the level of detail of object, but had limitations in the size of the APP.

Contributions

Considering the findings outline above, the main contributions of this thesis are:

- I. It shows how machine learning algorithms can learn patterns that connect 3D high-resolution models to geological and ecological data (fulfilling Aims I, II and III)
- II. How researchers can leverage 3D photogrammetry and augmented reality to increase the accessibility to deep-water environments (fulfilling Aims IV and V)
- III. How current technologies can be explored and adapted to map CWC habitats (fulfilling Aims I,III, IV and V)
- IV. It investigates the advantages and limitations of pursuing 3D mapping (fulfilling Aim I and V)
- V. The photogrammetric methods presented herein for creating and analysing 3D datasets of CWC habitat scenes have wide implications for habitat monitoring and ecological research. The 3D models produced are a non-destructive unique aid for recording reef structure that allows for analyses and comparisons over time and the integration with multi-scale metrics. (fulfilling Aim IV)

Limitations

The research findings and conclusions herein are outlined in the context of contemporary and inherent limitations. These have been discussed throughout the chapters and key aspects are reiterated here.

Even though technology is advancing, there are still processing obstacles intrinsic to handling multi-dimensional, high-resolution data. The limitations of end-user hardware and software have shaped the development of methods to process 3D datasets, which require the integration of appropriate techniques to reduce the computational cost of these applications.

It is acknowledged that density estimates of megafauna derived from visual observations depend on underlying factors related to survey design such as the focal

length, bottom distance and observer bias (Christiansen, 1993). The video acquisition method plays a crucial role in the quality of the reconstruction. Thus, there is a limitation of SfM to model structural elements with occluded features as often cameras cannot deal with object occlusion and canopy structures (Friedman, 2013; Young, 2017). As such, the quality of terrain reconstructions varies heavily depending on the angle of the camera mounted to the ROV. As of yet, there is no current agreement on best practices, especially regarding the use of downward-facing or oblique-facing cameras as this depends on the topography of the terrain and the object of interest that is being investigated. As SfM is a relatively new technique, most of the video archives are not particularly suitable for reconstruction.

It is also important to highlight the relatively small extent of the research areas, which corroborates with the importance of integrating multiscale datasets into a holistic approach to mapping CWC. Although orthomosaics pose an advance to batch-image and video analyses, there is a limitation of the SfM method to reconstruct larger areas (hundreds of m² to km²) both because of the computing power required and survey design limitations. SfM presents challenges for acquiring data over greater distances given underwater light attenuation and ROV motion constraints (Menna et al., 2018). Furthermore, the lack of granularity of 3D models poses limitations in identifying organisms at the species level (Pierce et al., 2021)

Generating data for machine-learning models is also a crucial task which heavily depends on human-resources and domain expertise. One of the main limitations of deploying machine learning models is the lack of training data, especially for deep-water habitats, which also comes with the sampling bias due to the open interpretation of the environment. With the computational costs and the relative novelty of 3D methods, researchers face understory complexity of exploring an unknown field which requires domain knowledge and capacity building.

However, researchers are now aware of these limitations and there is ongoing work to overcome these challenges. **In fact, one of the most exciting aspects about this research is the perception of being on the edge of the challenge, as part of the building blocks of new concepts and subsequently paving way to new methods that will benefit future research.**

6.2 Future Directions

This thesis highlights the synergy between seabed habitat mapping, computer vision and machine learning. As such, it proposes five new directions for future research of CWC habitats from 3D photogrammetry, and venues of study that are particularly relevant to advancing from the findings of this thesis. First, there is a need for establishing survey design protocols for 3D data acquisition of deep-water environments. Secondly, integrating new benchmark datasets of CWC reefs around the world is crucial for the improvement of automated supervised classification and the advance to robust deep learning models . Similarly, given the well-known constraints of generating training data, the development of unsupervised machine learning approaches to lighten the need for manual annotation input of classifiers is an important step toward advances. For example, methods such region-growing and super pixel algorithms such as Simple Linear Iterative Clustering (SLIC) have been explored within the scopes of this thesis (see [Appendix III](#)) and would hugely benefit future research if further developed. Thirdly, it is also crucial to raise awareness to the importance of fine-scale analyses in habitat investigations and marine spatial planning. The findings gathered herein emphasise the role of fine-scale heterogeneity in CWC ecosystem services. Lastly, generating, curating and analysing high-resolution data is a task that requires interdisciplinarity, thus, promoting capacity building to integrate different knowledge domains, such as computer vision and data sciences will increase the potential of research in marine sciences.

Appendix I

Additional Data Acquired And Processed

Table 0.1 Total of video frames per ROV transect used in the 3D reconstructions of the study area analysed in Chapter 3,4 and 5

Transect	First_Image	Last_Image	Total	Section	Steps_FPS
SM_D12_L37_1	SM_D12_L37_142442	SM_D12_L37_148130	238	on-mound	24_1
SM_D12_L38_1	SM_D12_L38_131525	SM_D12_L38_137117	234	on-mound	24_1
SM_D12_L39_1	SM_D12_L39_0183	SM_D12_L39_6951	285	on-mound	24_1
SM_D12_L40_1	SM_D12_L40_12154	SM_D12_L40_17218	212	on-mound	24_1
SM_D12_L41_1	SM_D12_41_22106	SM_D12_41_27338	219	on-mound	24_1
SM_D12_L42_1	SM_D12_42_31440	SM_D12_42_37416	250	on-mound	24_1
SM_D12_L43_1	SM_D12_L43_39816	SM_D12_L43_44760	207	on-mound	24_1
SM_D12_L44_1	SM_D12_44_47342	SM_D12_44_52718	225	on-mound	24_1
SM_D12_L45_1	SM_D12_L45_55840	SM_D12_L45_61240	226	on-mound	24_1
SM_D12_L46_1	SM_D12_46_63618	SM_D12_46_67722	172	on-mound	24_1
SM_D12_L47_1	SM_D12_47_70845	SM_D12_47_73893	128	on-mound	24_1
SM_D12_L48_1	SM_D12_L48_76586	SM_D12_L48_82010	227	on-mound	24_1
SM_D12_L48.1_1	SM_D12_L48.1_85241	SM_D12_L48.1_90713	230	on-mound	24_1
SM_D12_L48.1_TO_49	SM_D12_L48.1_TO_49_90740	SM_D12_L48.1_TO_49_93284	107	on-mound	
SM_D12_L49_1	SM_D12_49_93284	SM_D12_49_99596	264	on-mound	24_1
SM_D12_L49_TO_L49.1	SM_D12_L49_TO_49.1_99606	SM_D12_L49_TO_49.1_104502	223	off-mound	
SM_D12_L49.1_1	SM_D12_49.1_104513	SM_D12_49.1_108065	149	off-mound	24_1
SM_D12_L49.1_L50_1	SM_D12_49.1_50_108084	SM_D12_49.1_50_112740	194	off-mound	
SM_D12_L50_1	SM_D12_L50_112760	SM_D12_L50_117008	178	off-mound	24_1
SM_D12_L51_1	SM_D12_51_121686	SM_D12_51_127134	228	off-mound	24_1
SM_D12_L52_1	SM_D12_L52_132131	SM_D12_L52_136979	203	off-mound	24_1
SM_D12_L53_1	SM_D12_L53_142576	SM_D12_L53_148024	237	off-mound	24_1
SM_D12_L54_1	SM_D12_54_154736	SM_D12_54_160112	225	off-mound	24_1
SM_D12_L55.1_1	SM_D12_55.1_167900	SM_D12_55.1_172172	179	off-mound	24_1
SM_D12_L56_1	SM_D12_L56_0301	SM_D12_L56_5197	205	off-mound	24_1

SM_D12_L57_1	SM_D12_57_7746	SM_D12_57_12450	197	off-mound	24_1
SM_D12_L58_1	SM_D12_L58_15330	SM_D12_L58_19074	157	off-mound	24_1
SM_D12_L59_1	SM_D12_59_21778	SM_D12_59_27274	230	off-mound	24_1
SM_D12_L60_1	SM_D12_L60_29371	SM_D12_L60_33787	185	off-mound	24_1
SM_D12_L61_1	SM_D12_61_37189	SM_D12_61_40213	127	off-mound	24_1
SM_D12_L62_1	SM_D12_62_46978	SM_D12_62_51826	203	off-mound	24_1
SM_D12_L63_1	SM_D12_63_56476	SM_D12_63_61012	190	off-mound	24_1
SM_D12_L64_1	SM_D12_64_66993	SM_D12_64_72849	245	off-mound	24_1
SM_D12_L65_1	SM_D12_L65_76351	SM_D12_L65_81607	220	off-mound	24_1
SM_D12_L66_1	SM_D12_66_83369	SM_D12_66_86513	132	off-mound	24_1
SM_D12_L67_1	SM_D12_L67_89304	SM_D12_L67_95400	255	off-mound	24_1
Total:			7386		
Average:			205.1666		
			667		
Total on-mound:			3224		
Average of images per transect on-mound			214.9333		
			333		
Total off-mound			4162		

Table 0.2: Comparison among frame extraction tools to analyse the impact of frame extraction on the photogrammetry reconstruction workflow.

	FFMPEG		Blender		Open CV
File size of each frame	11.1 MB		15.8MB		3.08 MB
Bit Depth	48	64		24	
General					
Cameras	100	100		100	
Aligned cameras	100	100		100	
Coordinate system	Local Coordinates (m)		Local Coordinates (m)		Local Coordinates (m)
Rotation angles	Yaw, Pitch, Roll		Yaw, Pitch, Roll		Yaw, Pitch, Roll
Point Cloud					
Points	3,723 of 6,503		3,739 of 6,834		3,851 of 6,497
RMS reprojection error	0.147982 (0.417229 pix)		0.142521 (0.40022 pix)		0.14904 (0.433484 pix)
Max reprojection error	0.505093 (4.53993 pix)		0.473255 (5.24274 pix)		0.756495 (6.53604 pix)
Mean key point size	2.67028 pix		2.61581 pix		2.7046 pix
Point colors	3 bands, uint16		3 bands, uint16		3 bands, uint8
Key points	No		No		No
Average tie point multiplicity	39.0737	39.0755		38.9406	
Alignment parameters					
Accuracy	High		High		High
Generic preselection	Yes		Yes		Yes
Reference preselection	No		No		No
Key point limit	20,000	20,000		20,000	
Tie point limit	2,000	2,000		2,000	
Guided image matching	No		No		No
Adaptive camera model fitting	Yes		Yes		Yes
Matching time	21 seconds		23 seconds		17 seconds
Matching memory usage	148.56 MB		159.31 MB		97.72 MB
Alignment time	2 minutes 14 seconds		2 minutes 19 seconds		2 minutes 24 seconds

Alignment memory usage	38.26 MB	20.02 MB	16.35 MB
Optimization parameters			
Parameters	f, cx, cy, k1-k3, p1, p2	f, cx, cy, k1-k3, p1, p2	f, cx, cy, k1-k3, p1, p2
Adaptive camera model fitting	Yes	Yes	Yes
Optimization time	3 seconds	3 seconds	4 seconds
Software version	1.6.5.11249	1.6.5.11249	1.6.5.11249
File size	5.94 MB	6.24 MB	5.90 MB
Depth Maps			
Count	100	100	100
Depth maps generation parameters			
Quality	High	High	High
Filtering mode	Aggressive	Aggressive	Aggressive
Processing time	13 minutes 55 seconds	13 minutes 13 seconds	12 minutes 16 seconds
Memory usage	1.20 GB	1.23 GB	982.64 MB
Software version	1.6.5.11249	1.6.5.11249	1.6.5.11249
File size	72.66 MB	72.52 MB	75.97 MB
Dense Point Cloud			
Points	1,100,622	1,156,442	1,069,737
Point colors	3 bands, uint16	3 bands, uint16	3 bands, uint8
Depth maps generation parameters			
Quality	High	High	High
Filtering mode	Aggressive	Aggressive	Aggressive
Processing time	13 minutes 55 seconds	13 minutes 13 seconds	12 minutes 16 seconds
Memory usage	1.20 GB	1.23 GB	982.64 MB
Dense cloud generation parameters			
Max neighbors	50	50	50
Processing time	3 minutes 42 seconds	3 minutes 42 seconds	3 minutes 48 seconds
Memory usage	1.80 GB	1.80 GB	1.63 GB
Software version	1.6.5.11249	1.6.5.11249	1.6.5.11249
File size	19.12 MB	20.13 MB	14.32 MB

Model				
Faces	96,150	115,116	95,287	
Vertices	48,144	57,628	47,704	
Vertex colors	3 bands, uint8		3 bands, uint8	3 bands, uint8
Depth maps generation parameters				
Quality	High		High	High
Filtering mode	Aggressive		Aggressive	Aggressive
Processing time	13 minutes 55 seconds		13 minutes 13 seconds	12 minutes 16 seconds
Memory usage	1.20 GB		1.23 GB	982.64 MB
Reconstruction parameters				
Surface type	Arbitrary		Arbitrary	Arbitrary
Source data	Depth maps		Depth maps	Depth maps
Interpolation	Enabled		Enabled	Enabled
Strict volumetric masks	No		No	No
Processing time	31 seconds		33 seconds	31 seconds
Memory usage	904.82 MB		646.64 MB	965.64 MB
Software version	1.6.5.11249		1.6.5.11249	1.6.5.11249
File size	2.20 MB		2.64 MB	2.18 MB

Chapter 2

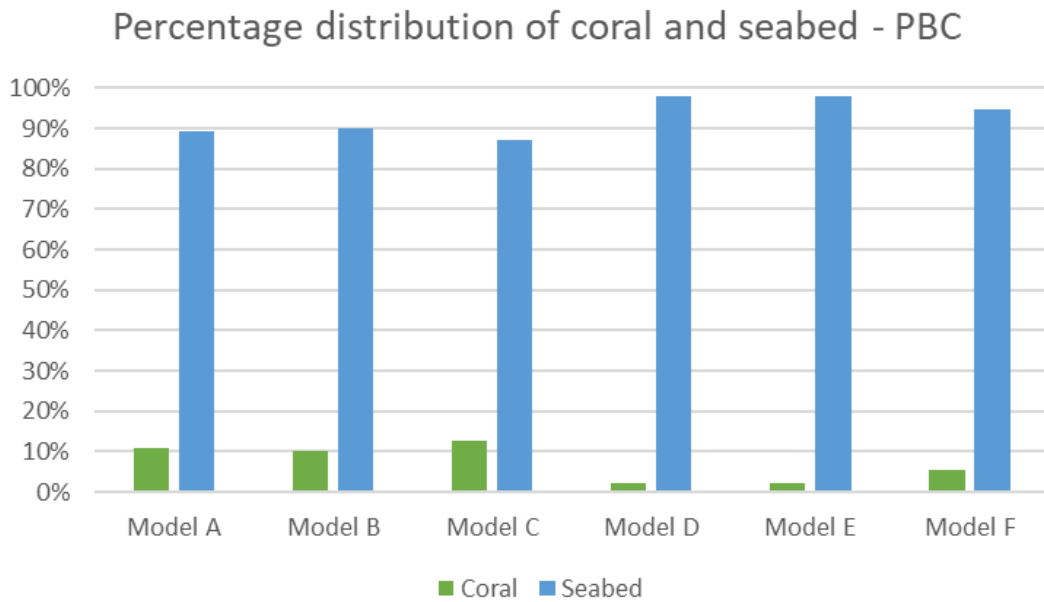


Figure 0.1 Class distribution of each 3D model reconstructed from the Porcupine Bank Canyon (PBC)

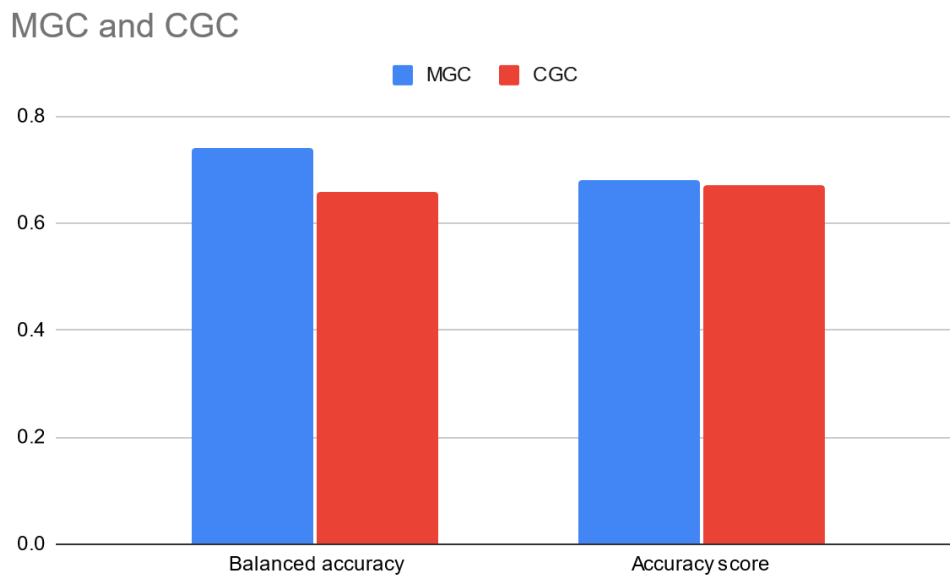


Figure 0.2 Accuracy comparison between the Multiscale Geometric Classification method (MGC) and the Colour Geometrical Classification (CGC) method

Table 0.3 Summary of comparisons among the MGC, CGC and OBIA methods

	MGC	CGC	OBIA
Advantages	Addressed coral colonies and coral patches more precisely	Minimal user input required	Automatic segmentation process
	Able to identify seabed coverage in all 3D reconstructions	Pre-training is not necessary	Successfully distinguished coral rubble from sediment
	It can be reapplied to classify similar coral reef environments	Suitable for fast identification of seabed distribution	Our observations agree with previous studies: orthomosaics can be useful for high-resolution habitat mapping of large areas (Lim et al., 2017; Conti et al., 2019).
Disadvantages	Susceptible to object occlusion and canopy effects created by objects	Susceptible to object occlusion and canopy effects created by objects.	Although orthomosaics and DEMs provide height information that is useful for larger scale models, they can be limiting for high-resolution analyses.
	Occasionally tended to under classify coral	Tended to overclassify corals	
	Amount of training data required to train the classifier	Sensitive to terrain surface variations	
		Low RGB variability, resulted in slightly different classification outputs with the CGC method not being able to recognise seabed as compared to the method MGC	
Remarks	As for most of the classification methods, training data size and availability should be evaluated prior to choosing the methodology as it directly impacts the performance of the classifier	In previous studies, the algorithm performed well for the detection of buildings and roads , but it misclassified vegetation and ground, especially in datasets containing hills and non-flat surfaces (Becker et al., 2018)	3D metrics derived from vector dispersion and triangulation in dense clouds can provide more detailed information for characterising individual coral colonies and benthic species (Fukunaga and Burns, 2020)

Chapter 3

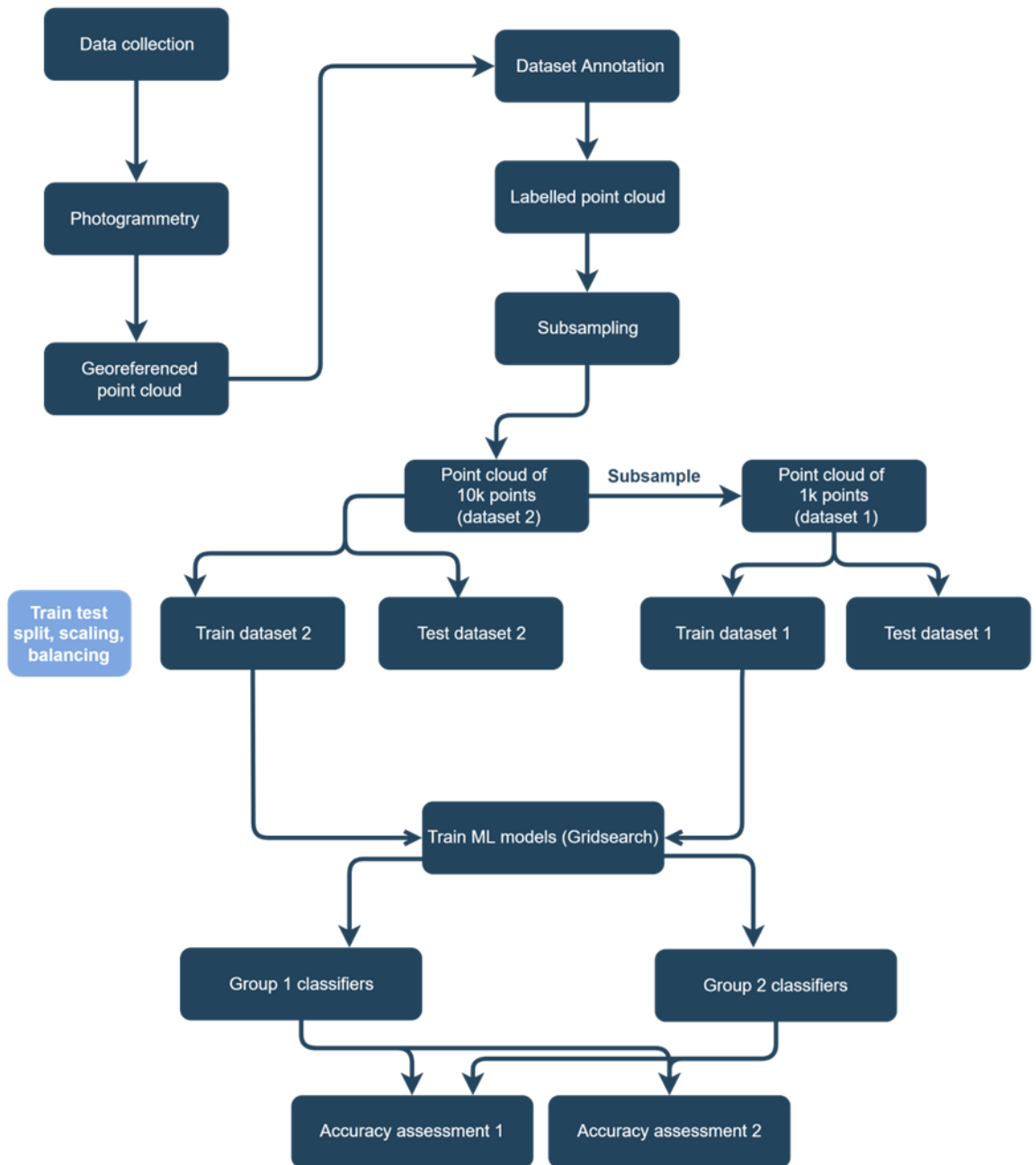


Figure 0.3 Workflow of the study design developed for Chapter 3

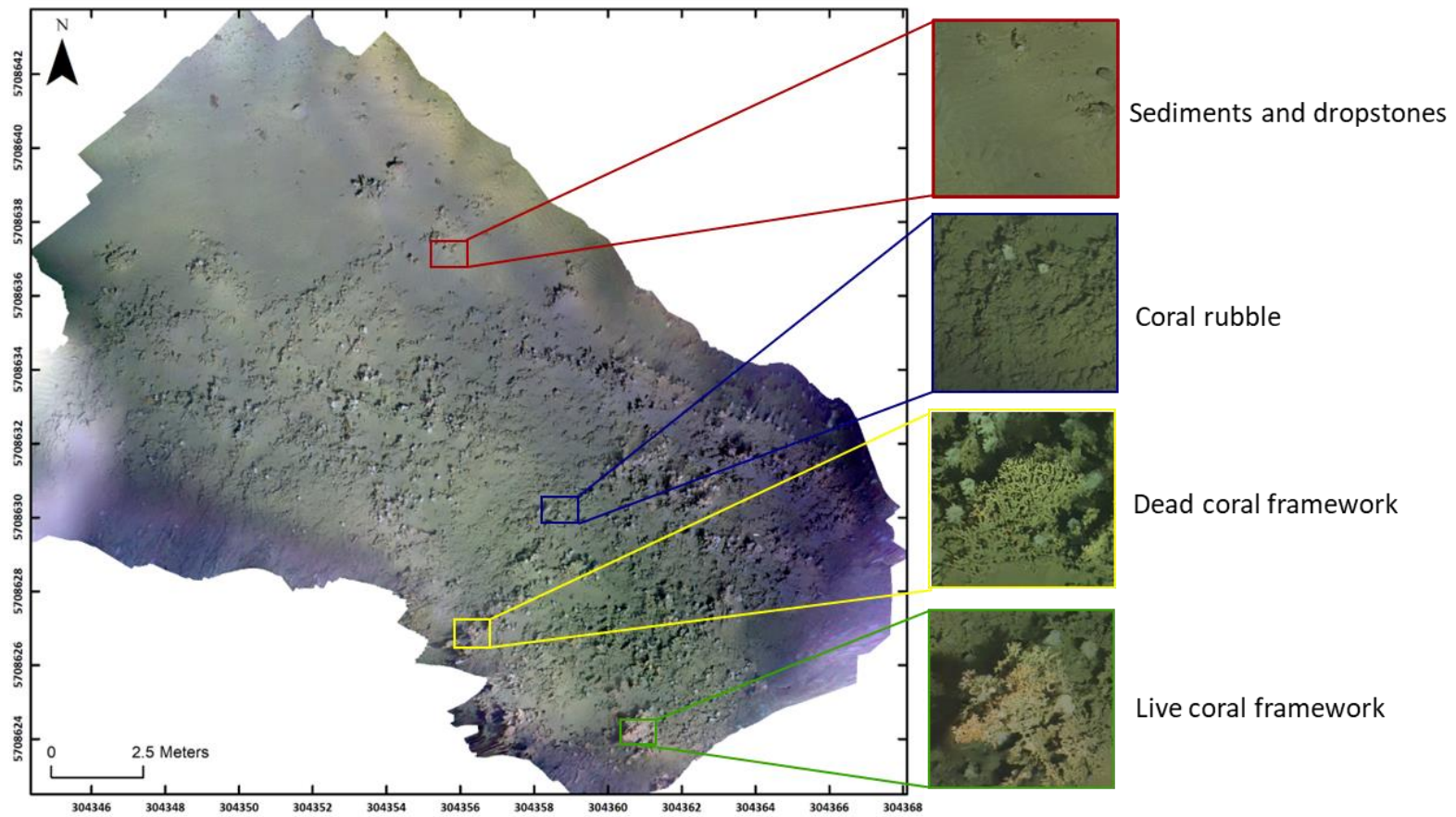


Figure 0.4 Examples of the four facies categorised in the study

Chapter 4

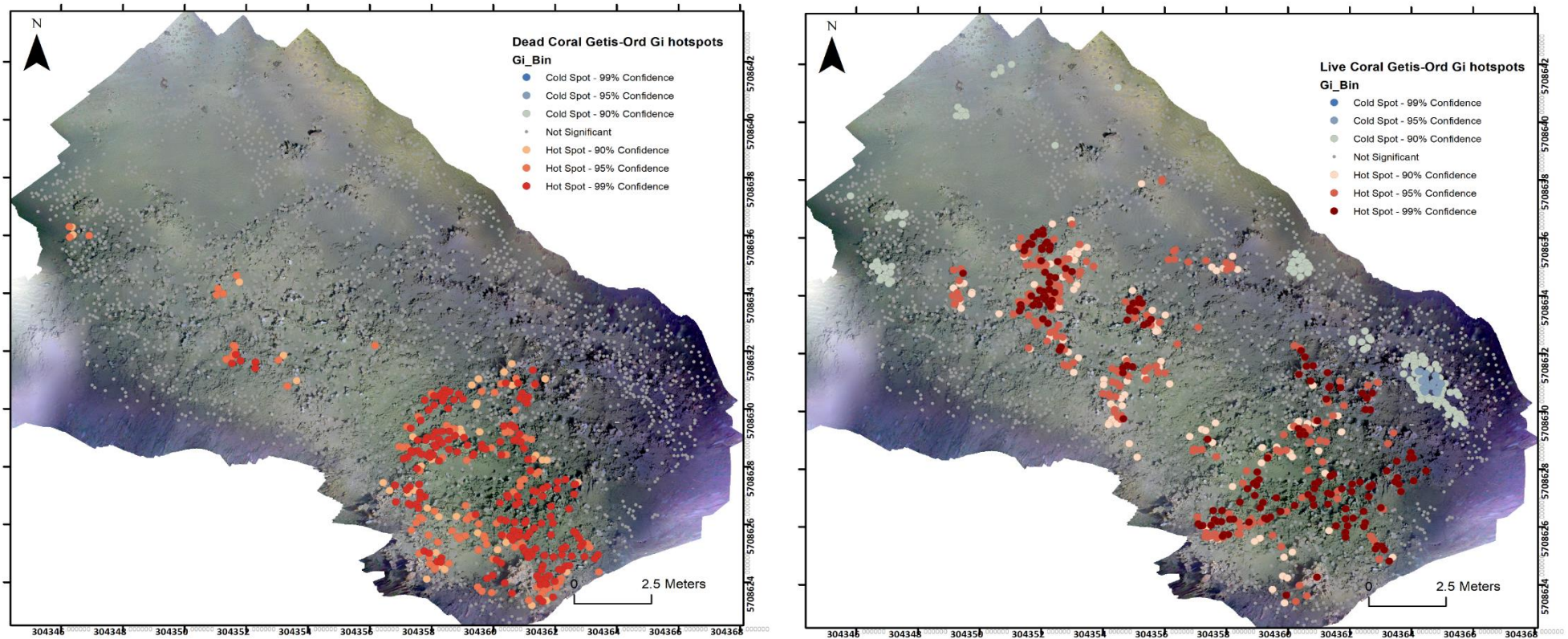
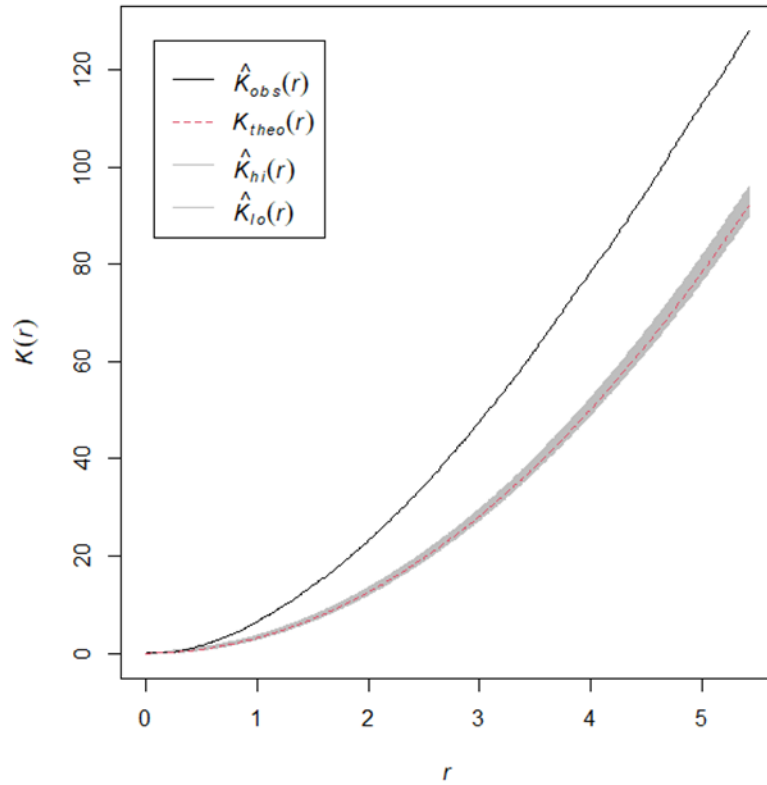


Figure 0.5: Getis Ord Gi hotspot results for the Dead coral facies (left) and Live coral facies (right)

Live coral Facies

RK_ENV



Dead coral Facies

RK_ENV

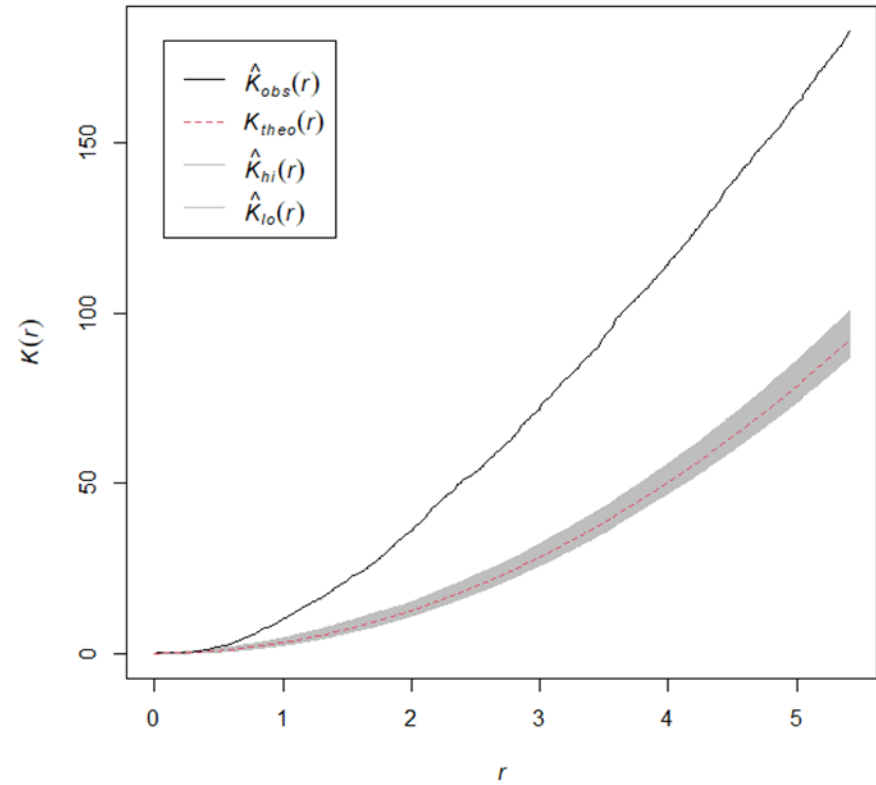


Figure 0.6 Ripley's K function plots for Live coral facies (left) and Dead coral facies (right). The shaded grey area represents the 95% confidence bands.

Live coral (LC) facies

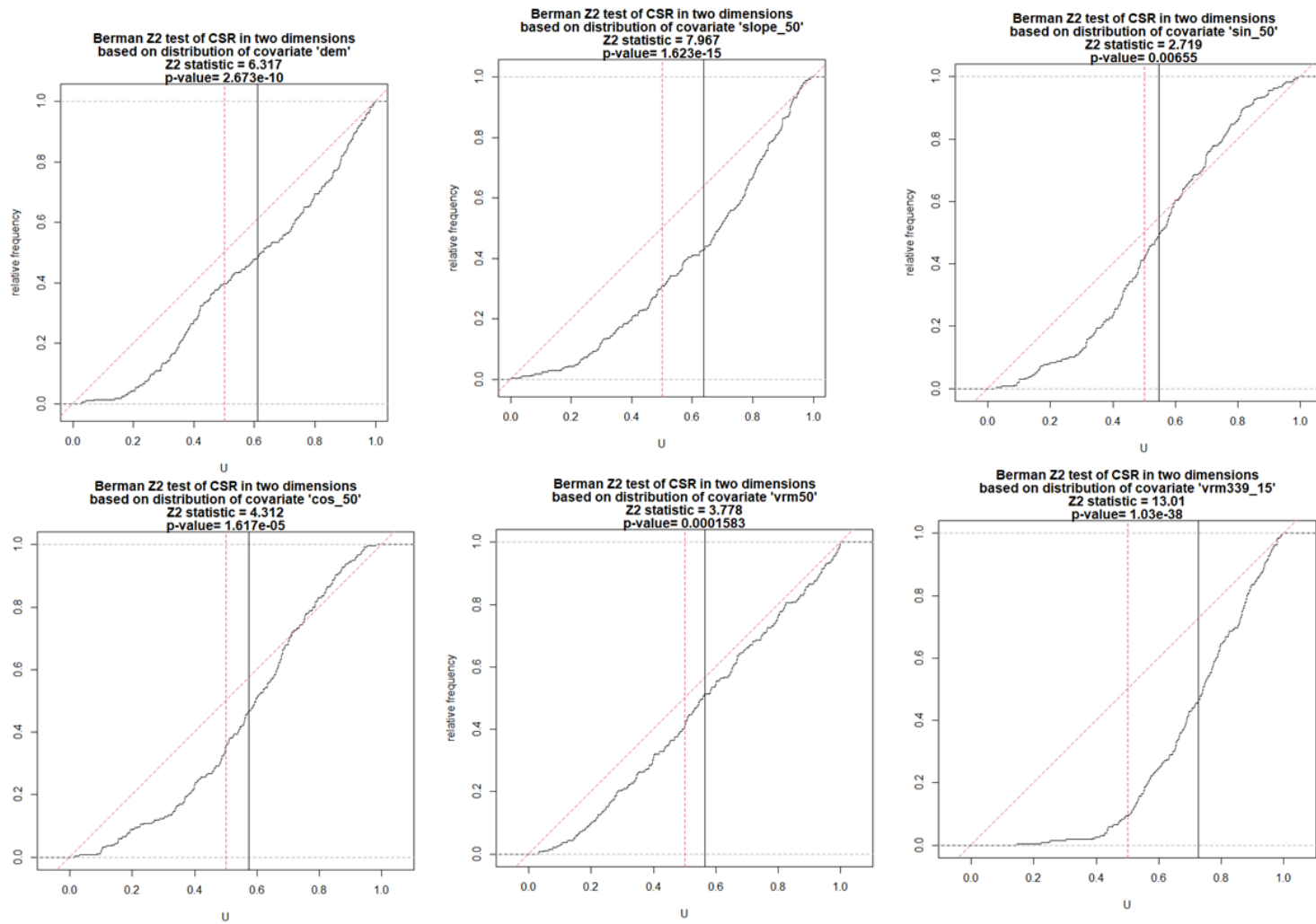


Figure 0.8 Berman's Z2 tests for the density in function of covariate tests of Live Coral facies (Rho-hat function)

Dead coral (DC) facies

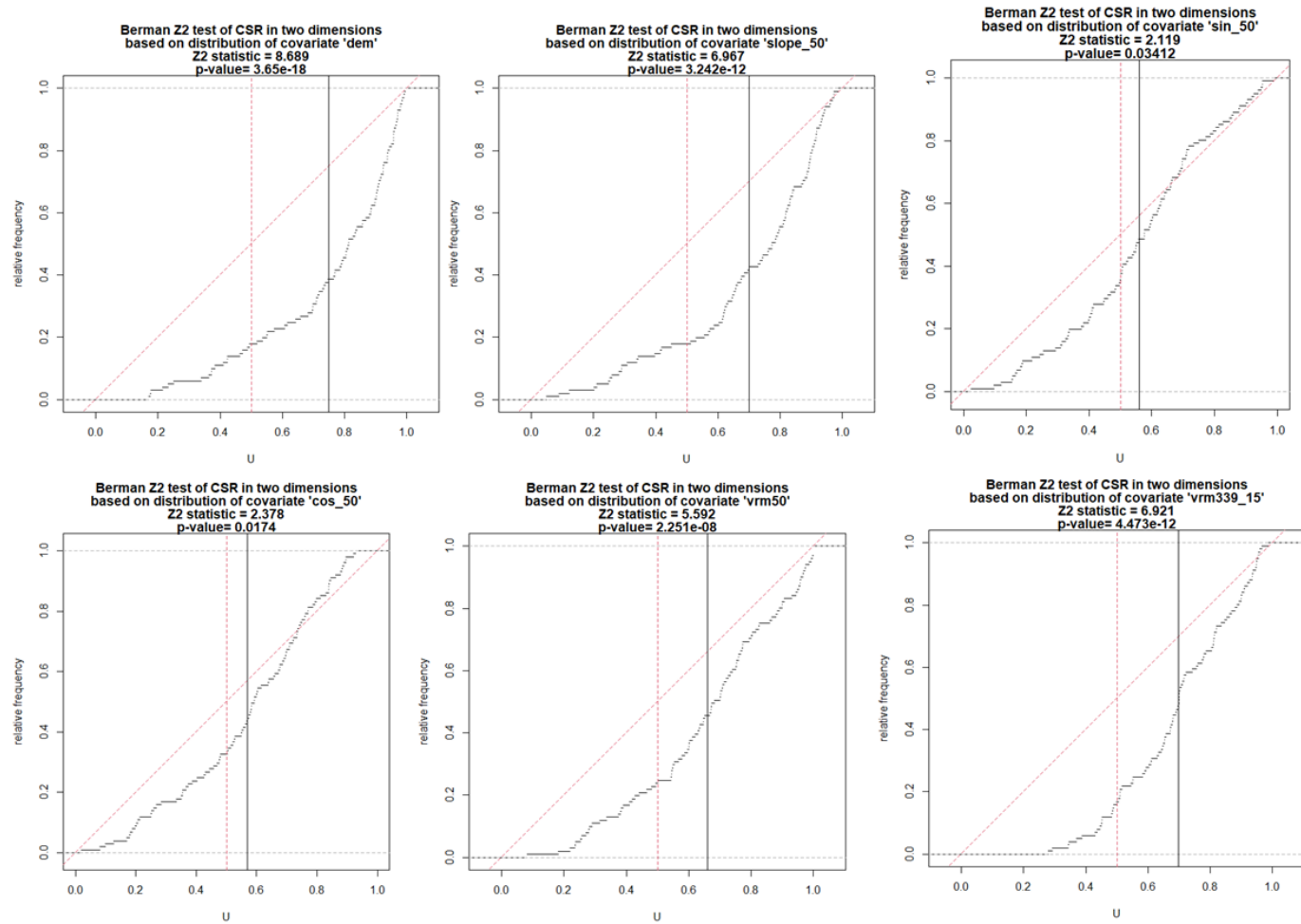
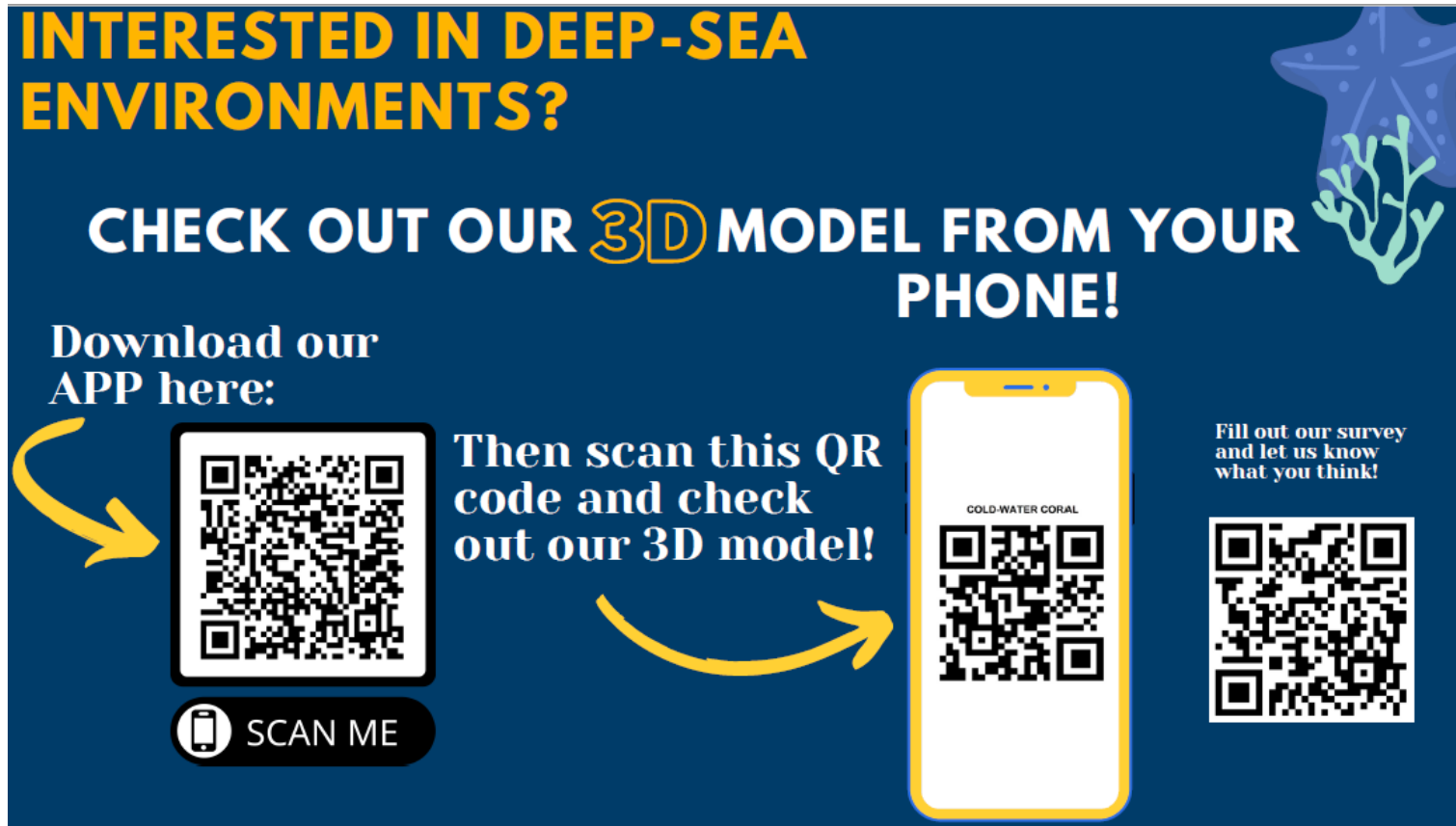


Figure 0.9 Figure 0.7 Berman's Z2 tests for the density in function of covariate tests of Dead Coral facies (Rhoat function)



INTERESTED IN DEEP-SEA ENVIRONMENTS?

CHECK OUT OUR 3D MODEL FROM YOUR PHONE!

Download our APP here:

Then scan this QR code and check out our 3D model!

Fill out our survey and let us know what you think!

SCAN ME

GOLD-WATER CORAL

The flyer features a dark blue background with yellow and white text. It includes two QR codes: one for downloading the app and another for a survey. A smartphone graphic displays the app interface with the text 'GOLD-WATER CORAL' and a QR code. A starfish and coral illustration is in the top right corner. A yellow arrow points from the first QR code to the smartphone, and another points from the smartphone to the second QR code.

Figure 0.10: Coral APP flyer used in outreach events in 2022

Appendix II

List of published peer-reviewed papers during the PhD

- **de Oliveira, L. M. C.**, Lim, A., Conti, L. A., & Wheeler, A. J. (2022). High-resolution 3D mapping of cold-water coral reefs using machine learning. *Frontiers in Environmental Science*, 10. <https://doi.org/10.3389/fenvs.2022.1044706>
- **de Oliveira, L.M.C.**; Oliveira, P.A.de. Oliveira; Lim, A.; Wheeler, A.J.; Conti, L.A. Developing Mobile Applications with Augmented Reality and 3D Photogrammetry for Visualisation of Cold-Water Coral Reefs and Deep-Water Habitats. *Geosciences* 2022, 12, 356. <https://doi.org/10.3390/geosciences12100356>
- **de Oliveira, L.M.C.**, Lim, A., Conti, L.A. & Wheeler, A.J. (2021). 3D classification of cold-water coral reefs: A comparison of classification techniques for 3D reconstructions of cold-water coral reefs and seabed. *Frontiers in Marine Science*. doi: 10.3389/fmars.2021.640713 (**awarded with Delap Student Prize – Bronze Award for best peer-reviewed academic paper**)
- **de Oliveira, L.M.C.**, Stefano, P.H.P., Vedana, L.A. et al. (2020) A hydrogeological impact survey on the largest onshore oil field in Brazil: physicochemical and total petroleum hydrocarbon (TPH) analyses in the south of Japaratuba River Basin, Sergipe. *Environ Earth Sci* 79, 383 (2020). doi: <https://doi.org/10.1007/s12665-020-09121-0> (from Bachelor Thesis)
- Appah, J. K. M., Lynch, S. A., Lim, A., O’ Riordan, R., O’Reilly, L., **de Oliveira, L.**, & Wheeler, A. J. (2022). A health survey of the reef forming scleractinian cold-water corals *Lophelia pertusa* and *Madrepora oculata* in a remote submarine canyon on the European continental margin, NE Atlantic. *Journal of Invertebrate Pathology*, 192(June), 107782. <https://doi.org/10.1016/j.jip.2022.107782>
- Article contribution “Automatic Seabed Image Classification: Where Are We Going With It?” *Deep-Sea Life Issue 15*, pg 23: [Online Deep-Sea Life Issue 15](#)

Projects supervised during the PhD

Master's thesis in Bioinformatics "Semantic coral reef mapping through image annotation and analysis: An example from cold-water corals in the Northeast Atlantic" – Supervisee: David Mark Dalton

ABSTRACT

Cold-water coral reefs hold an important ecological role in benthic ecosystems by harbouring aquatic species and are an important part of nutrient cycling in marine environments. Cold-water coral reefs themselves have become under threat from anthropogenic actions such as Climate Change. An effective way of monitoring coral reef health is the assessment of the biological composition of these environments over time. This way researchers can spot changes in the abundance of coral species which can indicate a healthy ecosystem or a reef that is in danger of dying. Over recent years there has been advancements in underwater image acquisition and in high resolution mapping of benthic environments. The use of machine learning has emerged as an exciting tool that can be used to extract information from images and marine biologists are now using deep-learning models such as Convolutional Neural Networks (CNN) to create datasets of marine images.

To use these machine learning methods, ground truth annotations of the underwater images must be created to train the models into 'learning' the features of the dataset, which can then be used to assess the biological composition. The creation of ground truth annotations is a task that takes a lot of time and expert knowledge and this is where the scientific bottleneck is, the speed at which underwater images are being collected cannot be matched by the manual annotation of these images to train machine learning models.

With the use of patch-based image classification and CNN's this task can be automated and provide as many sparse labels per image as required. Once these sparse labels are created, researchers will be able to use these models and labels to study the area or

similar locations without having to create their own manual annotations, reducing the research time significantly. This study has researched the best manual annotation tools for benthic analysis and used this to start an annotated dataset of coral reefs in Ireland of the Piddington Mound, NE Porcupine Seabight. With these annotations and the use of a CNN, enough sparse annotations have been created for the dataset. An algorithm Fast-MSS has been employed on these images to create dense labels from the sparse annotations of these images. These dense labels will be used to create a 3-D reconstructed surface model of the Piddington Mound in the future.

The contributions of this thesis will help move coral reef analysis forward by providing the first set of sparse and dense labels for a reef offshore Ireland. This will make research more time efficient and easier to observe changes in the community composition of benthic environments in the future.

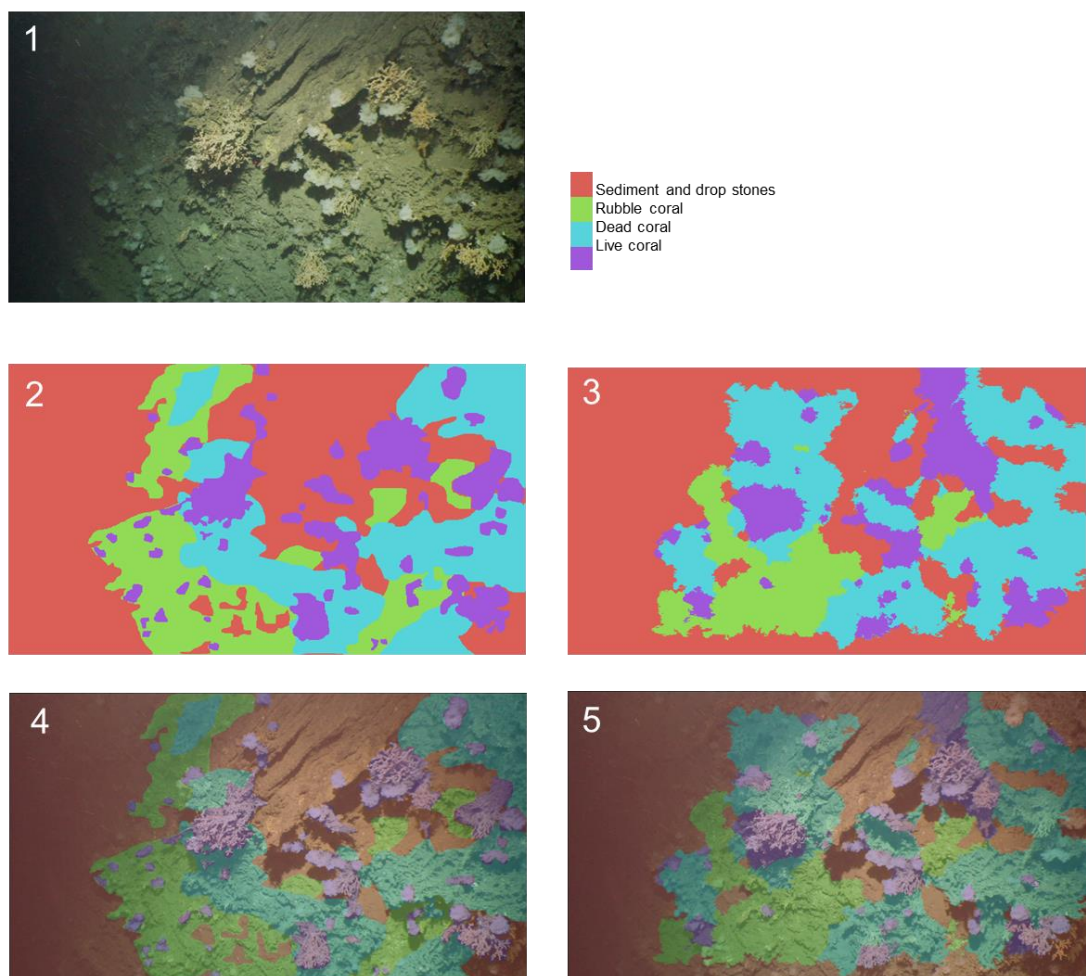


Figure 0.1: Results of the MSc project (1) an image from the Piddington Mound dataset, (2) the ground-truth dense labels manually created of this image (3) the dense labels created for this image using the Fast-MSS algorithm (4) An image overlay of the ground truth image and

the actual image, and () An image overlay of the Fast-MSS image and the actual image (Credits: David Dalton, MSc student)

PhD candidate contributions: Larissa Oliveira was responsible for developing the project, supervising the project, advising the student, managing the project, securing infrastructure, data curation, thesis proof-reading.

Grants and awards obtained during the PhD

- **ESAI Postgraduate Researcher of the Year 2022** – winner of the Environmental Sciences Association of Ireland national award for postgraduate researchers
- **Delap Student Prize – Bronze Award** for best peer-reviewed academic paper for the first PhD paper
- **Helmholtz Visiting Researcher Grant** – funded by Helmholtz Information & Data Science Academy for a 3-month Research Internship at GEOMAR, Kiel (in Summer, 2023)
- **4th Marine Imaging Workshop Travel Grant (€500)**– funded by ISblue and Schmidt Ocean Institute
- **GeoHab Ron Mcdowell Student Support Award 2022 (€700)**
- **College of Science, Engineering & Food Science (SEFS) Travel Bursary Award 2022 (€500)**
- **Marine Institute Networking & Marine Research Communication Awards 2022 (€700)**
- **Commended for best poster presentation** at 64th Irish Geological Research Meeting (IGRM) 2021, *Online*, March, 2021;
- **Government of Ireland Postgraduate Scholarship 2020 (€54,124.86)** - for PhD in University College Cork - ASMaT Project - from October 2020 to October 2022;

- **Commended for best poster presentation** at 63rd Irish Geological Research Meeting (IGRM) 2020, Athlone, March, 2020;
- **Science Foundation of Ireland Scholarship** - for Master's by Research in University College Cork - MMonKey_Pro Project - from March 2019 to March 2021;
- **Travel Grant Eurofleets+ Blue Skills Lab** (€300) - AUV Workshop & Training 2019

Appendix V

Academic roles and extracurricular activities

Role title: Marine Geosciences Demonstrator

Location: Atlantic Technological University - Strategic Marine Alliance for Research and Training (SMART)

Job description: Responsible for teaching different offshore data collection and sampling methods (multibeam and sub bottom profiler data acquisition and sediment grab acquisition) on board of research vessels, introduce concepts of marine survey planning at local and large scales, demonstrate use of marine software for data acquisition and processing

Role Title: Postgraduate representative of the School of BEES Equality, Diversity, Inclusion and Wellbeing (EDIW) committee

Location: School of Biological, Earth and Environmental Sciences, UCC, Ireland

Date: January 2019 to present

Job description: As a representative and member of the working group for the Athena Swan Silver Award 2021, I idealised and co-organised the first BEES EDIW event “Diversity in BEES career paths and UCC initiatives on EDIW” focused on undergraduate and postgraduate students. The event was designed to highlight UCC EDIW initiatives and the diversity of careers and possible academic paths within BEES staff, students and alumni.

Role Title: IGEO2022 Organising committee member - Social Media and Registration Officer

Irish Geosciences Early Career Symposium (iGEO2022)

Date: June 2021 to June 2022

Job description: I was part of the organising committee of the Irish Geosciences Early Career Symposium (iGEO2022) acting as Social Media and Registration Officer. I was responsible for content creation, Social Media management and registration administrative duties. I collaborated with funding acquisition through grant writing and prospecting sponsorships. The job provided me with teamwork and communication skills, as well as experience with financial and administrative activities such as research account management and dealing with HEI suppliers.

Role Title: UCC Campus Connect Student Ambassador

Location: University College Cork

Date: January 2019 to 2021

Job description: The UCC Campus Connect project was developed to create a mobile platform to welcome and support new students coming to UCC during the COVID-19 pandemic. As a UCC Campus Connect Ambassador, I was responsible for providing virtual support to incoming national and international undergraduates, addressing questions regarding academic modules, and administrative matters through the UCC Campus Connect app.

Role Title: Module tutor for courses in Geology and Environmental Sciences

- GL1001 – Introduction to Geology
- GL1004 – Geological Evolution of Ireland
- AD1084 – Introduction to Earth Sciences

Location: University College Cork

Job description: I was responsible for creating activities and curate content for students, demonstrate practical activities, correct and assist with module assignments, address module questions during and after lectures, field work assistance

Conference presentations

1. **de Oliveira, L.M.C., Lim, A., Conti, L.A. & Wheeler, A.J. (2022).** “Classification of cold-water coral (CWC) reefs in high resolution on: using 3D photogrammetry and machine learning for CWC habitat classification of the Piddington Mound, southwest of Ireland” – **Oral presentation at 4th Marine Imaging Workshop**, Brest, France, 2022
2. **de Oliveira, L.M.C., Lim, A., Conti, L.A. & Wheeler, A.J. (2022).** “3D Photogrammetric Classification Of Cold-water Coral Reefs with Machine Learning – Preliminary Results from Piddington Mound, Ne Atlantic” - **Oral presentation at International Conference on Seafloor Forms, Processes and Evolution 2022**, Valletta, Malta
3. **de Oliveira, L.M.C.** “3D Classification of Cold-Water Coral Reefs: using photogrammetry and machine learning for the classification of CWC habitats in the North Atlantic – The journey” - **Oral presentation BEES Research Day for Delap Prize**
4. **de Oliveira, L.M.C., Lim, A., Conti, L.A. & Wheeler, A.J. (2022).** “3D Photogrammetric Classification Of Cold-Water Coral Reefs With Machine Learning – Preliminary Results From Piddington Mound, Ne Atlantic” - **Oral presentation at GEOHAB 2022**, Venice, Italy
5. **de Oliveira, L.M.C., Lim, A., Conti, L.A. & Wheeler, A.J. (2021).** “3D Classification of Cold-Water Coral Reefs: A Comparison of Classification Techniques for 3D Reconstructions of Cold-Water Coral Reefs and Seabed” - **Oral Presentation at iAtlantic General Assembly, 2021**, online
6. **de Oliveira, L.M.C., Lim, A., Conti, L.A. & Wheeler, A.J. (2021).** “3D Classification of Cold-Water Coral Reefs: A Comparison of Classification Techniques for 3D Reconstructions of Cold-Water Coral Reefs and Seabed”- **Oral Presentation at INCISE, 2021**, online

7. **de Oliveira, L.M.C.** “UCC Brazilian PhD & Postdoc Showcase” - showcasing the ASMaT PhD project results – **Oral presentation at FAUBAI2021**, online
8. **de Oliveira, L.M.C.**, Lim, A., Conti, L.A. & Wheeler, A.J. (2021). “3D classification of cold-water coral reefs: A comparison of classification techniques for 3D reconstructions of cold-water coral reefs and seabed” – **Oral Presentation at GEOHAB 2021**, online
9. **de Oliveira, L.M.C.**, Lim, A., Conti, L.A. & Wheeler, A.J. (2021). “Use of 3D photogrammetry for advancing seabed mapping techniques for deep-water habitat classification in Submarine Canyons” – Poster presentation 64th Irish Geological Research Meeting (IGRM 2021) – **Honorable mention for Best Postgraduate poster**, online
10. **de Oliveira, L.M.C.**, Lim, A., Conti, L.A. & Wheeler, A.J. (2021). “Use of 3D data in Advancing seabed mapping techniques for cold-water coral habitat classification in submarine canyons” – Poster presentation at 63rd Irish Geological Research Meeting (IGRM 2020)- **Honorable mention for Best Postgraduate poster**, Athlone, Ireland
11. **de Oliveira, L.M.C.**, “Life as a Marine Geoscientist” - **Oral presentation at “Pathfinders” event by Irish Association for Women in Geosciences**, Cork Ireland

Appendix VII

Research cruises undertaken as part of, and during the PhD

Total of research expeditions during PhD: 8

2021 (Total of cruises: 4)

CV21026 - SMART NUIG Multidisciplinary Offshore Operations in Marine Science 2021 (Marine Geosciences Instructor)

CV21030 - SMART BSc UCC Multidisciplinary Offshore Operations in Marine Science 2021 (Marine Geosciences Instructor)

CV21031 - SMART UCC Postgraduate Offshore Environmental Geology 2021 (Marine Geosciences Instructor)

CE21016 – Benthic Lander Recovery/Redeployment (Night shift leader)

2020 (Total of cruises: 1)

CE20011 – Systematic Monitoring Survey of the Moira Mound Chain (SyMonS_MoM) (Day shift scientist)

2019 (Total of cruises: 3)

DY108-109 – CLASS – Climate-linked Atlantic System Science - RRS Discovery cruise to the Darwin Mounds, Rockall Bank and Rockall Trough (Scientist representative for Ireland)

CE19014 – Monitoring Changes in Submarine Canyon Coral Habitats II (Night shift scientist)

CE19008 – Monitoring Changes in Submarine Canyon Coral Habitats I (Night shift scientist)

Appendix VIII

Courses completed during the PhD

Total of courses during PhD: 17

2022 (Total of courses: 3)

Date: 30th October to 5th of November 2022

Title of training course: **EUROFLEETS+ Blue Skills: Autonomous Underwater Vehicle (AUV) training/ Workshop**

UCC module code (if relevant): N/A

Location: Gothenburg University, Sweden

Date: October 2022

Title of training course: **Proficiency in Security Awareness (PSA)**

UCC module code (if relevant): N/A

Location: Remote, Securewest Training

Date: 29th of June, 2022

Title of training course: **Deep Learning Pytorch: Image segmentation project**

UCC module code (if relevant): N/A

Location: Remote, Coursera

2021 (Total of courses: 3)

Date: 2nd to the 9th of July, 2021

Title of training course: **Vision Understanding and Machine intelligence (VISUM) Summer School**

UCC module code (if relevant): N/A

Location: Remote, Institute for Systems and Computer Engineering, Technology and Science (INESC TEC), Portugal

Date: Academic year 2020/21 – Semester 1 and 2

Title of training course: **Statistics and Data Analysis for Postgraduate research students (10 credits)**

UCC module code (if relevant): ST6013

Location: University College Cork, Cork, Ireland

Date: Academic year 2020/21 – Semester 1 and 2

Title of training course: **Skills in Public engagement of Science (5 credits)**

UCC module code (if relevant): PG6029

Location: University College Cork, Cork, Ireland

2020 (Total of courses: 6)

Date: 17th to 25th of August 2020

Title of training course: **Oxford Machine Learning Summer School 2020**

Location: Remote - University of Oxford (transferred to online due COVID-19)

Date: 24th of June 2020

Title of training course: **“How to approach a review” – Professor Peir Pufhal**

Location: Remote, Seds Online

Date: 19th to 25th of February 2020

Title of training course: **Eurofleets + Floating University RV Celtic Voyager** – “Mapping the Ocean Floor: An Introduction to Practical Aspects of Hydrographic Surveying”

Location: Cork, Ireland

Date: 7th to 8th of February 2020

Title of training course: **R and Statistics training course**

Location: University College Cork, Ireland

Date: Academic Year 2019/20 - Semester 2

Title of training course: **Programming in Python for Data Science Applications (5 credits)**

UCC module code (if relevant): CS6507

Location: UCC, Western Gateway Building

Date: Academic Year 2019/20 - Semester 1 and 2

Title of training course: **Teaching and Learning Module for Graduate Studies (5 credits)**

UCC module code (if relevant): PG6003

Location: UCC, Main Campus

2019 (Total of courses: 5)

Date: 26th of November 2019

Title of training course: **Machine Learning Onramp – MathWorks training course**

Location: Online

Date: 29th of November 2019

Title of training course: **Writing and Preparing a Journal Article for Publication by Elsevier**

Location: UCC, Cavanagh Pharmacy Building

Date: 9th of November 2019

Title of training course: **Epigeum Research Integrity Course by Oxford University Press**

Location: Remote, Epigeum Online Course System

Date: 30th May, 2019

Title of training course: **Artificial Intelligence (AI) Workshop with Microsoft Azure**

Location: University College Cork, Ireland

Date: 10th of May 2019

Title of training course: **Personal Survival Techniques (PST) STCW 95**

Location: National Maritime College of Ireland – NMCI, Ringaskiddy, Co. Cork

Compiled list of references

- Aanesen, M., Armstrong, C., Czajkowski, M., Falk-Petersen, J., Hanley, N., Navrud, S., 2015. Willingness to pay for unfamiliar public goods: Preserving cold-water coral in Norway. *Ecol. Econ.* 112, 53–67. <https://doi.org/10.1016/j.ecolecon.2015.02.007>
- Addamo, A.M., Vertino, A., Stolarski, J., García-Jiménez, R., Taviani, M., Machordom, A., García-Jiménez, R., Taviani, M., Machordom, A., García-Jiménez, R., Taviani, M., Machordom, A., 2016. Merging scleractinian genera: The overwhelming genetic similarity between solitary *Desmophyllum* and colonial *Lophelia*. *BMC Evol. Biol.* 16, 1–17. <https://doi.org/10.1186/s12862-016-0654-8>
- Agisoft-LLC, 2020. Agisoft Metashape User Manual: Professional Edition, Version 1.6. Agisoft LLC 160.
- Akbani, R., Kwek, S., Japkowicz, N., 2004. Applying Support Vector Machines to Imbalanced Datasets, in: *European Conference on Machine Learning*. pp. 39–50.
- Alonso, I., Yuval, M., Eyal, G., Treibitz, T., Murillo, A.C., 2019. CoralSeg: Learning coral segmentation from sparse annotations. *J. F. Robot.* 36, 1456–1477. <https://doi.org/10.1002/rob.21915>
- Althaus, F., Williams, A., Schlacher, T.A., Kloser, R.J., Green, M.A., Barker, B.A., Bax, N.J., Brodie, P., Schlacher-Hoenlinger, M.A., 2009. Impacts of bottom trawling on deep-coral ecosystems of seamounts are long-lasting. *Mar. Ecol. Prog. Ser.* 397, 279–294. <https://doi.org/10.3354/meps08248>
- Anelli, M., Julitta, T., Fallati, L., Galli, P., Rossini, M., Colombo, R., 2019. Towards new applications of underwater photogrammetry for investigating coral reef morphology and habitat complexity in the Myeik Archipelago, Myanmar. *Geocarto Int.* 34, 459–472. <https://doi.org/10.1080/10106049.2017.1408703>
- Appah, J.K.M., Lim, A., Harris, K., O’Riordan, R., O’Reilly, L., Wheeler, A.J., 2020b. Are Non-reef Habitats as Important to Benthic Diversity and Composition as Coral Reef and Rubble Habitats in Submarine Canyons? Analysis of Controls on Benthic

Megafauna Distribution in the Porcupine Bank Canyon, NE Atlantic. *Front. Mar. Sci.* 7, 831. <https://doi.org/10.3389/fmars.2020.571820>

ArcGIS, 2014. Hot Spot Analysis (Getis-Ord G_i^*) (Spatial Statistics) Illustration Usage 1–7.

Arena, F., Collotta, M., Pau, G., Termine, F., 2022. An Overview of Augmented Reality. *Computers*. <https://doi.org/10.3390/computers11020028>

Argentino, C., Savini, A., Panieri, G., 2022. Integrating Fine-Scale Habitat Mapping and Pore Water Analysis in Cold Seep Research: A Case Study from the SW Barents Sea, in: *World Atlas of Submarine Gas Hydrates in Continental Margins*. Springer International Publishing, Cham, pp. 505–514. https://doi.org/10.1007/978-3-030-81186-0_43

Armstrong, C.W., Foley, N.S., Kahui, V., Grehan, A., 2014. Cold water coral reef management from an ecosystem service perspective. *Mar. Policy* 50, 126–134. <https://doi.org/10.1016/j.marpol.2014.05.016>

Auster, P.J., Gjerde, K., Heupel, E., Watling, L., Grehan, A., Rogers, A.D., 2011. Definition and detection of vulnerable marine ecosystems on the high seas: problems with the “move-on” rule. *ICES J. Mar. Sci.* 68, 254–264. <https://doi.org/10.1093/icesjms/fsq074>

Baddeley, A., 2010. Analysing spatial point patterns in R. *Workshop Notes - Version 4.1* 178–204.

Baddeley, A., Rubak, E., Turner, R., 2015. *Spatial Point Patterns*, *Spatial Point Patterns*. <https://doi.org/10.1201/b19708>

Baddeley, A., Turner, R., Coeurjolly, J., Cruz, M. De, Dalgaard, P., Diggle, P.J., Hardegen, A., Hering, M., Hansen, M.B., Hazelton, M., Madin, B., Mark, R., Mateu, J., Mccullagh, P., Mehlig, U., Meyer, S., Mi, X.C., Moller, J., Mudrak, E., Nielsen, L.S., Nunes, F., Rowlingson, B., Rudge, J., Safavimanesh, F., Sarkka, A., Villers, A., Vinatier, F., Wang, H., Wendrock, H., Wild, J., Wong, S., Zamboni, M.E., 2013. Package ‘ spatstat .’

Baker, E.K., Harris, P.T., 2012. Habitat Mapping and Marine Management. *Seafloor Geomorphol. as Benthic Habitat* 23–38. <https://doi.org/10.1016/B978-0-12-385140-6.00002-5>

- Barbosa, R. V, Davies, A.J., Sumida, P.Y.G., 2019. Habitat suitability and environmental niche comparison of cold-water coral species along the Brazilian continental margin. *Deep. Res. Part I* 103147. <https://doi.org/10.1016/j.dsr.2019.103147>
- Barker, N.H.L., Roberts, C.M., 2004. Scuba diver behaviour and the management of diving impacts on coral reefs. *Biol. Conserv.* 120, 481–489. <https://doi.org/10.1016/j.biocon.2004.03.021>
- Barrile, V., Fotia, A., Bernardo, E., 2019. The submerged heritage: a virtual journey in our. *Int. Arch. Photogramm. Remote Sens. Spat. Inf. Sci.* XLII-2/W10, 17–24. <https://doi.org/10.5194/isprs-archives-XLII-2-W10-17-2019>
- Becker, C., Rosinskaya, E., Häni, N., d'Angelo, E., Strecha, C., 2018. Classification of aerial photogrammetric 3D point clouds. *Photogramm. Eng. Remote Sensing* 84, 287–295. <https://doi.org/10.14358/PERS.84.5.287>
- Beijbom, O., Edmunds, P.J., Kline, D.I., Mitchell, B.G., Kriegman, D., 2012. Automated annotation of coral reef survey images, in: *Proc. IEEE Comput. Soc. Conf. Comput. Vis. Pattern Recognit*, pp. 1170–1177. <https://doi.org/10.1109/CVPR.2012.6247798>
- Beijbom, O., Edmunds, P.J., Roelfsema, C., Smith, J., Kline, D.I., Neal, B.P., Dunlap, M.J., Moriarty, V., Fan, T.-Y.Y., Tan, C.-J.J., Chan, S., Treibitz, T., Gamst, A., Mitchell, B.G., Kriegman, D., 2015. Towards automated annotation of benthic survey images: Variability of human experts and operational modes of automation. *PLoS One* 10, 1–22. <https://doi.org/10.1371/journal.pone.0130312>
- Belgiu, M., Drăgu, L., 2016. Random forest in remote sensing: A review of applications and future directions. *ISPRS J. Photogramm. Remote Sens.* 114, 24–31. <https://doi.org/10.1016/j.isprsjprs.2016.01.011>
- Ben-Shabat, Y., Lindenbaum, M., Fischer, A., 2017. 3D Point Cloud Classification and Segmentation using 3D Modified Fisher Vector Representation for Convolutional Neural Networks.
- Benoist, N.M.A., Bett, B.J., Morris, K.J., Ruhl, H.A., 2019. A generalised volumetric method to estimate the biomass of photographically surveyed benthic megafauna. *Prog. Oceanogr.* 178, 102188. <https://doi.org/10.1016/j.pocean.2019.102188>

- Benz, U.C., Hofmann, P., Willhauck, G., Lingenfelder, I., Heynen, M., 2004. Multi-resolution, object-oriented fuzzy analysis of remote sensing data for GIS-ready information. *ISPRS J. Photogramm. Remote Sens.* 58, 239–258. <https://doi.org/10.1016/j.isprsjprs.2003.10.002>
- Berman, M., 1986. Testing for Spatial Association Between a Point Process and Another Stochastic Process. *Appl. Stat.* 35, 54. <https://doi.org/10.2307/2347865>
- Billinghurst, M., Duenser, A., 2012. Augmented reality in the classroom. *Computer (Long. Beach. Calif.)* 45, 56–63.
- Bimber, O., Raskar, R., 2005. Spatial augmented reality: merging real and virtual worlds. CRC press.
- Bishop, C.M., 2006. Pattern Recognition and Machine Learning, Information Science and Statistics. Springer New York.
- Blaschke, T., 2010. Object based image analysis for remote sensing. *ISPRS J. Photogramm. Remote Sens.* 65, 2–16. <https://doi.org/10.1016/j.isprsjprs.2009.06.004>
- Bodenmann, A., Thornton, B., Nakajima, R., Ura, T., 2017. Methods for quantitative studies of seafloor hydrothermal systems using 3D visual reconstructions. <https://doi.org/10.1186/s40648-017-0091-5>
- Boolukos, C.M., Lim, A., O’Riordan, R.M., Wheeler, A.J., O’Riordan, R.M., Wheeler, A.J., O’Riordan, R.M., Wheeler, A.J., 2019b. Cold-water corals in decline – A temporal (4 year) species abundance and biodiversity appraisal of complete photomosaiced cold-water coral reef on the Irish Margin. *Deep Sea Res. Part I Oceanogr. Res. Pap.* 146, 44–54. <https://doi.org/10.1016/j.dsr.2019.03.004>
- Borba, E.Z., 2014. Imersão visual e corporal: paradigmas da percepção em simuladores. *Narrat. Comun. Complexificadas II—A Forma. SantaCruz do Sul Edunisc* 239–256.
- Borcard, D., Legendre, P., 2002. All-scale spatial analysis of ecological data by means of principal coordinates of neighbour matrices. *Ecol. Modell.* 153, 51–68. [https://doi.org/10.1016/S0304-3800\(01\)00501-4](https://doi.org/10.1016/S0304-3800(01)00501-4)

- Brandt, A., James Griffiths, H., Schiaparelli, S., Ballerini, T., Griffiths, H., Gutt, J., Linse, K., Danis, B., Pfannkuche, O., 2014. Challenges of deep-sea biodiversity assessments in the Southern Ocean. *Adv Polar Sci* 25, 204–212. <https://doi.org/10.13679/j.advps.2014.3.00204>
- Brodersen, K.H., Ong, C.S., Stephan, K.E., Buhmann, J.M., 2010. The balanced accuracy and its posterior distribution. *Proc. - Int. Conf. Pattern Recognit.* 3121–3124. <https://doi.org/10.1109/ICPR.2010.764>
- Brodu, N., Lague, D., 2012. 3D terrestrial lidar data classification of complex natural scenes using a multi-scale dimensionality criterion: Applications in geomorphology. *ISPRS J. Photogramm. Remote Sens.* 68, 121–134. <https://doi.org/10.1016/j.isprsjprs.2012.01.006>
- Brown, C.J., Smith, S.J., Lawton, P., Anderson, J.T., 2011. Benthic habitat mapping: A review of progress towards improved understanding of the spatial ecology of the seafloor using acoustic techniques. *Estuar. Coast. Shelf Sci.* 92, 502–520. <https://doi.org/10.1016/j.ecss.2011.02.007>
- Bruno, F., Barbieri, L., Mangeruga, M., Cozza, M., Lagudi, A., Čejka, J., Liarokapis, F., Skarlatos, D., 2019. Underwater augmented reality for improving the diving experience in submerged archaeological sites. *Ocean Eng.* 190, 106487. <https://doi.org/10.1016/j.oceaneng.2019.106487>
- Bryson, M., Johnson-Roberson, M., Pizarro, O., Williams, S.B., 2013. Colour-consistent structure-from-motion models using underwater imagery. *Robot. Sci. Syst.* 8, 33–40. <https://doi.org/10.7551/mitpress/9816.003.0010>
- Buchner, J., Buntins, K., Kerres, M., 2022. The impact of augmented reality on cognitive load and performance: A systematic review. *J. Comput. Assist. Learn.* 38, 285–303. <https://doi.org/10.1111/jcal.12617>
- Buda, M., Maki, A., Mazurowski, M.A., 2018. A systematic study of the class imbalance problem in convolutional neural networks. *Neural Networks* 106, 249–259. <https://doi.org/10.1016/j.neunet.2018.07.011>

Buhl-Mortensen, L., Buhl-Mortensen, P., Dolan, M.F.J., Holte, B., 2015. The MAREANO programme – A full coverage mapping of the Norwegian off-shore benthic environment and fauna. *Mar. Biol. Res.* 11, 4–17. <https://doi.org/10.1080/17451000.2014.952312>

Buhl-Mortensen, Lene, Vanreusel, A., Gooday, A.J., Levin, L.A., Priede, I.G., Buhl-Mortensen, P., Gheerardyn, H., King, N.J., Raes, M., 2010. Biological structures as a source of habitat heterogeneity and biodiversity on the deep ocean margins. *Mar. Ecol.* 31, 21–50. <https://doi.org/10.1111/j.1439-0485.2010.00359.x>

Buhl-mortensen, P., Buhl-mortensen, L., Purser, A., 2015. Trophic Ecology and Habitat Provision in Cold-Water Coral Ecosystems, in: Rossi, S., Bramanti, L., Gori, A., Orejas Saco del Valle, C. (Eds.), *Marine Animal Forests*. Springer International Publishing, Cham, pp. 1–26. <https://doi.org/10.1007/978-3-319-17001-5>

Buitinck, L., Louppe, G., Blondel, M., Pedregosa, F., Mueller, A., Grisel, O., Niculae, V., Prettenhofer, P., Gramfort, A., Grobler, J., Layton, R., Vanderplas, J., Joly, A., Holt, B., Varoquaux, G., 2013. API design for machine learning software: experiences from the scikit-learn project 1–15.

Burges, C.J.C., 1998. A Tutorial on Support Vector Machines for Pattern Recognition. *Data Min. Knowl. Discov.* 28, 121–167.

Burke, L., Reytar, K., Spalding, M., Perry, A., 2011. *Reefs at Risk Revisited*, Defenders.

Burns, J.H.R., Delparte, D., Gates, R., Takabayashi, M., 2015a. Integrating structure-from-motion photogrammetry with geospatial software as a novel technique for quantifying 3D ecological characteristics of coral reefs. *PeerJ* 3, e1077. <https://doi.org/10.7717/peerj.1077>

Burns, J.H.R., Delparte, D., Gates, R.D., Takabayashi, M., 2015b. UTILIZING UNDERWATER THREE-DIMENSIONAL MODELING TO ENHANCE ECOLOGICAL AND BIOLOGICAL STUDIES OF CORAL REEFS. *Int. Arch. Photogramm. Remote Sens. Spat. Inf. Sci.* XL-5/W5, 61–66. <https://doi.org/10.5194/isprsarchives-XL-5-W5-61-2015>

Burns, J.H.R., Fukunaga, A., Pascoe, K.H., Runyan, A., Craig, B.K., Talbot, J., Pugh, A., Kosaki, R.K., 2019. 3D Habitat Complexity Of Coral Reefs In The Northwestern

Hawaiian Islands Is Driven By Coral Assemblage Structure. *Int. Arch. Photogramm. Remote Sens. Spat. Inf. Sci.* XLII-2/W10, 61–67. <https://doi.org/10.5194/isprs-archives-XLII-2-W10-61-2019>

Burns, J.H.R., Delparte, D., Gates, R., Takabayashi, M., 2015. Integrating structure-from-motion photogrammetry with geospatial software as a novel technique for quantifying 3D ecological characteristics of coral reefs. *PeerJ* 3, e1077. <https://doi.org/10.7717/peerj.1077>

Burns, J.H.R., Weyenberg, G., Mandel, T., Ferreira, S.B., Gotshalk, D., Kinoshita, C.K., Marshall, M.J., Del Moral, N.A. V., Murphy, S.J., Pascoe, K.H., Runyan, A., Spengler, A.J., Wells, B.D., Wilde, D.K., Pelayo, R., 2020. A Comparison of the Diagnostic Accuracy of in-situ and Digital Image-Based Assessments of Coral Health and Disease. *Front. Mar. Sci.* 7. <https://doi.org/10.3389/fmars.2020.00304>

Büscher, J. V., Form, A.U., Riebesell, U., 2017. Interactive effects of ocean acidification and warming on growth, fitness and survival of the cold-water coral *Lophelia pertusa* under different food availabilities. *Front. Mar. Sci.* 4, 1–14. <https://doi.org/10.3389/fmars.2017.00101>

Bythell, J., Pan, P., Lee, J., 2001. Three-dimensional morphometric measurements of reef corals using underwater photogrammetry techniques. *Coral Reefs* 20, 193–199. <https://doi.org/10.1007/s003380100157>

Cairns, S.D., 2007. Deep-water corals: An overview with special reference to diversity and distribution of deep-water scleractinian corals. *Bull. Mar. Sci.* 81, 311–322.

Cairns, S.D., 1995. The marine fauna of New Zealand: Scleractinia (Cnidaria: Anthozoa). *New Zeal. Oceanogr. Inst. Mem.*

Calders, K., Phinn, S., Ferrari, R., Leon, J., Armston, J., Asner, G.P., Disney, M., 2020. 3D Imaging Insights into Forests and Coral Reefs. *Trends Ecol. Evol.* 35, 6–9. <https://doi.org/10.1016/j.tree.2019.10.004>

Capra, A., Castagnetti, C., Mancini, F., Rossi, P., Capra, A., Castagnetti, C., Mancini, F., Rossi, P., 2020. Underwater Photogrammetry for Change Detection 10–14.

- Carmigniani, J., Furht, B., 2011. Augmented Reality: An Overview, in: Handbook of Augmented Reality. Springer New York, New York, NY, pp. 3–46. https://doi.org/10.1007/978-1-4614-0064-6_1
- Carrivick, J.L., Smith, M.W., Quincey, D.J., 2016. Structure from Motion in the Geosciences. John Wiley & Sons, Ltd, Chichester, UK. <https://doi.org/10.1002/9781118895818>
- Caruana, R., Niculescu-Mizil, A., 2006. An empirical comparison of supervised learning algorithms. ICML 2006 - Proc. 23rd Int. Conf. Mach. Learn. 2006, 161–168.
- Casoli, E., Ventura, D., Mancini, G., Pace, D.S., Belluscio, A., Ardizzone, G., 2021. High spatial resolution photo mosaicking for the monitoring of coralligenous reefs. Coral Reefs 40, 1267–1280. <https://doi.org/10.1007/s00338-021-02136-4>
- Castelvecchi, D., 2016. The black box of AI. Nature 538, 20–23.
- Cathalot, C., Van Oevelen, D., Cox, T.J.S., Kutti, T., Lavaleye, M., Duineveld, G., Meysman, F.J.R., 2015. Cold-water coral reefs and adjacent sponge grounds: hotspots of benthic respiration and organic carbon cycling in the deep sea. Front. Mar. Sci. 2. <https://doi.org/10.3389/fmars.2015.00037>
- Čejka, J., Zsíros, A., Liarokapis, F., 2020. A hybrid augmented reality guide for underwater cultural heritage sites. Pers. Ubiquitous Comput. 24, 815–828. <https://doi.org/10.1007/s00779-019-01354-6>
- Chance, T.S., Kleiner, A.A., Northcutt, J.G., 2000. The Autonomous Underwater Vehicle (AUV): A Cost-Effective Alternative to Deep-Towed Technology. Integr. Coast. Zo. Manag. Mag. 65–69.
- Chawla, N. V., Bowyer, K.W., Hall, L.O., Kegelmeyer, W.P., 2002. SMOTE: Synthetic Minority Over-sampling Technique. J. Artif. Intell. Res. 16, 321–357. <https://doi.org/https://doi.org/10.48550/arXiv.1106.1813>
- Chen, G., Weng, Q., Hay, G.J., He, Y., 2018. Geographic object-based image analysis (GEOBIA): emerging trends and future opportunities. GIScience Remote Sens. 55, 159–182. <https://doi.org/10.1080/15481603.2018.1426092>

- Chen, G.K., Dai, C.F., 2021. Using 3D photogrammetry to quantify the subtle differences of coral reefs under the impacts of marine activities. *Mar. Pollut. Bull.* 173, 113032. <https://doi.org/10.1016/j.marpolbul.2021.113032>
- Chen, T.C., Ku, K.C., Ying, T.C., 2012. A process-based collaborative model of marine tourism service system - The case of Green Island area, Taiwan. *Ocean Coast. Manag.* 64, 37–46. <https://doi.org/10.1016/J.OCECOAMAN.2012.04.009>
- Chivers, I., Sleightholme, J., 2015. An Introduction to Algorithms and the Big O Notation, in: *Introduction to Programming with Fortran: With Coverage of Fortran 90, 95, 2003, 2008 and 77: Third Edition*. Springer International Publishing, Cham, pp. 1–674. <https://doi.org/10.1007/978-3-319-17701-4>
- Christiansen, B., 1993. A television and photographic survey of megafaunal abundance in Central Sognefjorden, Western Norway. *Sarsia* 78, 1–8. <https://doi.org/10.1080/00364827.1993.10413515>
- Cieza, E., Lujan, D., 2018. Educational Mobile Application of Augmented Reality Based on Markers to Improve the Learning of Vowel Usage and Numbers for Children of a Kindergarten in Trujillo. *Procedia Comput. Sci.* 130, 352–358. <https://doi.org/10.1016/j.procs.2018.04.051>
- Cimperman, R., 2006. *UAT Defined: A Guide to Practical User Acceptance Testing (Digital Short Cut)*. Pearson Education.
- Cipresso, P., Giglioli, I.A.C., Raya, M.A., Riva, G., 2018. The Past, Present, and Future of Virtual and Augmented Reality Research: A Network and Cluster Analysis of the Literature. *Front. Psychol.* 9. <https://doi.org/10.3389/fpsyg.2018.02086>
- Clark, M.R., 2006. Seamounts, deep-sea corals and fisheries: vulnerability of deep-sea corals to fishing on seamounts beyond areas of national jurisdiction. UNEP/Earthprint.
- ClassVR, 2022. Student Wearing ClassVR Headset Virtual Reality for Schools [WWW Document].
- Cocito, S., Sgorbini, S., Peirano, A., Valle, M., 2003. 3-D reconstruction of biological objects using underwater video technique and image processing. *J. Exp. Mar. Bio. Ecol.* 297, 57–70. [https://doi.org/10.1016/S0022-0981\(03\)00369-1](https://doi.org/10.1016/S0022-0981(03)00369-1)

- Conti, L.A., Lim, A., Wheeler, A.J., 2019. High resolution mapping of a cold water coral mound. *Sci. Rep.* 9, 1016. <https://doi.org/10.1038/s41598-018-37725-x>
- Corbera, G., Lo Iacono, C., Gràcia, E., Grinyó, J., Pierdomenico, M., Huvenne, V.A.I., Aguilar, R., Gili, J.M., 2019. Ecological characterisation of a Mediterranean cold-water coral reef: Cabliers Coral Mound Province (Alboran Sea, western Mediterranean). *Prog. Oceanogr.* 175, 245–262. <https://doi.org/10.1016/j.pocean.2019.04.010>
- Corbera, G., Lo Iacono, C., Simarro, G., Grinyó, J., Ambroso, S., Huvenne, V.A.I., Mienis, F., Carreiro-Silva, M., Martins, I., Mano, B., Orejas, C., Larsson, A., Hennige, S., Gori, A., 2022. Local-scale feedbacks influencing cold-water coral growth and subsequent reef formation. *Sci. Rep.* 12, 1–14. <https://doi.org/10.1038/s41598-022-24711-7>
- Costanza, R., Costanza, R., Arge, R., Groot, R. De, Farber, S., Grasso, M., Hannon, B., 1996. The value of the world ' s ecosystem services and natural capital.
- Costello, M.J., McCrea, M., Freiwald, A., Lundälv, T., Jonsson, L., Bett, B.J., van Weering, T.C.E., de Haas, H., Roberts, J.M., Allen, D., 2005. Role of cold-water *Lophelia pertusa* coral reefs as fish habitat in the NE Atlantic, in: *Cold-Water Corals and Ecosystems*. Springer Berlin Heidelberg, pp. 771–805. https://doi.org/10.1007/3-540-27673-4_41
- Coughlan, M., Wheeler, A.J., Dorschel, B., Lordan, C., Boer, W., Van Gaever, P., De Haas, H., Mörz, T., 2015. Record of anthropogenic impact on the Western Irish Sea mud belt. *Anthropocene* 9, 56–69. <https://doi.org/10.1016/j.ancene.2015.06.001>
- Courtney, Lee A, Fisher, W.S., Raimondo, S., Oliver, L.M., Davis, W.P., 2007. Estimating 3-dimensional colony surface area of field corals. *J. Exp. Mar. Bio. Ecol.* 351, 234–242. <https://doi.org/10.1016/j.jembe.2007.06.021>
- Cristobal, F.R., Dodge, M., Noll, B., Rosenberg, N., Burns, J., Sanchez, J., Gotshalk, D., Pascoe, K., Runyan, A., 2020. Exploration of Coral Reefs in Hawai'i through Virtual Reality: Hawaiian Coral Reef Museum VR, in: *Practice and Experience in Advanced Research Computing*. ACM, New York, NY, USA, NY, USA, pp. 545–546. <https://doi.org/10.1145/3311790.3404542>

- Crowder, L.B., Cooper, W.E., 1982. Habitat Structural Complexity and the Interaction Between Bluegills and Their Prey. *Ecology* 63, 1802. <https://doi.org/10.2307/1940122>
- Cunliffe, A.M., Brazier, R.E., Anderson, K., 2016. Ultra-fine grain landscape-scale quantification of dryland vegetation structure with drone-acquired structure-from-motion photogrammetry. *Remote Sens. Environ.* 183, 129–143. <https://doi.org/10.1016/j.rse.2016.05.019>
- D'Urban Jackson, T., Williams, G.J., Walker-Springett, G., Davies, A.J., 2020. Three-dimensional digital mapping of ecosystems: a new era in spatial ecology. *Proc. R. Soc. B Biol. Sci.* 287, 20192383. <https://doi.org/10.1098/rspb.2019.2383>
- Danovaro, R., Dell'Anno, A., Pusceddu, A., 2004. Biodiversity response to climate change in a warm deep sea. *Ecol. Lett.* 7, 821–828. <https://doi.org/10.1111/j.1461-0248.2004.00634.x>
- Danson, E., 2002. The Economics of Scale : Using Autonomous Underwater Vehicles (AUVs) for Wide-Area Hydrographic Survey and Ocean Data Acquisition The Economics of Scale : Using Autonomous Underwater Vehicles (AUVs) for Wide-Area Hydrographic Survey and Ocean Data Acq. *Proc. XXII FIG(Fédération Int. des Géomètres) Int. Congr.* 1–15.
- Davies, A.J., Duineveld, G.C.A., van Weering, T.C.E., Mienis, F., Quattrini, A.M., Seim, H.E., Bane, J.M., Ross, S.W., 2010. Short-term environmental variability in cold-water coral habitat at Viosca Knoll, Gulf of Mexico. *Deep. Res. Part I Oceanogr. Res. Pap.* 57, 199–212. <https://doi.org/10.1016/j.dsr.2009.10.012>
- Davies, A.J., Wisshak, M., Orr, J.C., Murray Roberts, J., 2008. Predicting suitable habitat for the cold-water coral *Lophelia pertusa* (Scleractinia). *Deep. Res. Part I Oceanogr. Res. Pap.* 55, 1048–1062. <https://doi.org/10.1016/j.dsr.2008.04.010>
- Davies, J.S., Guillaumont, B., Tempera, F., Vertino, A., Beuck, L., Ólafsdóttir, S.H., Smith, C.J., Fosså, J.H., van den Beld, I.M.J., Savini, A., Rengstorf, A., Bayle, C., Bourillet, J.F., Arnaud-Haond, S., Grehan, A., 2017. A new classification scheme of European cold-water coral habitats: Implications for ecosystem-based management of the deep sea. *Deep. Res. Part II Top. Stud. Oceanogr.* 145, 102–109. <https://doi.org/10.1016/j.dsr2.2017.04.014>

De Clippele, L.H., Gafeira, J., Robert, K., Hennige, S., Lavaleye, M.S., Duineveld, G.C.A., Huvenne, V.A.I., Roberts, J.M., 2017. Using novel acoustic and visual mapping tools to predict the small-scale spatial distribution of live biogenic reef framework in cold-water coral habitats. *Coral Reefs* 36, 255–268. <https://doi.org/10.1007/s00338-016-1519-8>

De Clippele, L.H., Rovelli, L., Ramiro-Sánchez, B., Kazanidis, G., Vad, J., Turner, S., Glud, R.N., Roberts, J.M., 2021. Mapping cold-water coral biomass: an approach to derive ecosystem functions. *Coral Reefs* 40, 215–231. <https://doi.org/10.1007/s00338-020-02030-5>

de Haas, H., Mienis, F., Frank, N., Richter, T.O., Steinacher, R., de Stigter, H., van der Land, C., van Weering, T.C.E., 2009. Morphology and sedimentology of (clustered) cold-water coral mounds at the south Rockall Trough margins, NE Atlantic Ocean. *Facies* 55, 1–26. <https://doi.org/10.1007/s10347-008-0157-1>

De Leo, F.C., Vetter, E.W., Smith, C.R., Rowden, A.A., McGranaghan, M., 2014. Spatial scale-dependent habitat heterogeneity influences submarine canyon macrofaunal abundance and diversity off the Main and Northwest Hawaiian Islands. *Deep. Res. Part II Top. Stud. Oceanogr.* 104, 267–290. <https://doi.org/10.1016/j.dsr2.2013.06.015>

De Mol, B., Henriët, J.-P., Canals, M., 2005. Development of coral banks in Porcupine Seabight: do they have Mediterranean ancestors? *Cold-Water Corals Ecosyst.* 515–533. https://doi.org/10.1007/3-540-27673-4_26

De Mol, B., Kozachenko, M., Wheeler, A., Alvares, H., Henriët, J.P., Olu-Le Roy, K., 2007. Thérèse Mound: A case study of coral bank development in the Belgica Mound Province, Porcupine Seabight. *Int. J. Earth Sci* 96, 103–120. <https://doi.org/10.1007/s00531-005-0496-x>

De Mol, B., Van Rensbergen, P., Pillen, S., Van Herreweghe, K., Van Rooij, D., McDonnell, A., Huvenne, V., Ivanov, M., Swennen, R., Henriët, J., 2002. Large deep-water coral banks in the Porcupine Basin, southwest of Ireland. *Mar. Geol.* 188, 193–231. [https://doi.org/10.1016/S0025-3227\(02\)00281-5](https://doi.org/10.1016/S0025-3227(02)00281-5)

De Mol, L., Van Rooij, D., Pirlet, H., Greinert, J., Frank, N., Quemmerais, F., Henriët, J.P., 2011. Cold-water coral habitats in the Penmarc’h and Guilvinec Canyons (Bay of

- Biscay): Deep-water versus shallow-water settings. *Mar. Geol.* 282, 40–52. <https://doi.org/10.1016/j.margeo.2010.04.011>
- de Oliveira, L.M.C., Lim, A., Conti, L.A., Wheeler, A.J., 2022a. High-resolution 3D mapping of cold-water coral reefs using machine learning. *Front. Environ. Sci.* 10, 1–20. <https://doi.org/10.3389/fenvs.2022.1044706>
- de Oliveira, L.M.C., Lim, A., Conti, L.A., Wheeler, A.J., 2021. 3D Classification of Cold-Water Coral Reefs: A Comparison of Classification Techniques for 3D Reconstructions of Cold-Water Coral Reefs and Seabed. *Front. Mar. Sci.* 8. <https://doi.org/10.3389/fmars.2021.640713>
- de Oliveira, L.M.C., Oliveira, P.A. De, Lim, A., Wheeler, A.J., Conti, L.A., 2022b. Developing Mobile Applications with Augmented Reality and 3D Photogrammetry for Visualisation of Cold-Water Coral Reefs and Deep-Water Habitats. *Geosciences* 12, 356. <https://doi.org/10.3390/geosciences12100356>
- Deilmay, B.R., Ahmad, B. Bin, Zabihi, H., 2014. Comparison of two Classification methods (MLC and SVM) to extract land use and land cover in Johor Malaysia. *IOP Conf. Ser. Earth Environ. Sci.* 20. <https://doi.org/10.1088/1755-1315/20/1/012052>
- Denoyel, A., Pinson, C., Passet, P.A., 2012. Sketchfab - The best 3D viewer on the web [WWW Document]. URL <https://sketchfab.com/> (accessed 9.15.22).
- Diesing, M., Green, S.L., Stephens, D., Lark, R.M., Stewart, H.A., Dove, D., 2014. Mapping seabed sediments: Comparison of manual, geostatistical, object-based image analysis and machine learning approaches. *Cont. Shelf Res.* 84, 107–119. <https://doi.org/10.1016/j.csr.2014.05.004>
- Diesing, M., Mitchell, P., Stephens, D., 2016. Image-based seabed classification: what can we learn from terrestrial remote sensing? *ICES J. Mar. Sci. J. du Cons.* 73, 2425–2441. <https://doi.org/10.1093/icesjms/fsw118>
- Dixon, B., Candade, N., 2008. Multispectral land use classification using neural networks and support vector machines: One or the other, or both? *Int. J. Remote Sens.* 29, 1185–1206. <https://doi.org/10.1080/01431160701294661>

- Dixon, P.M., 2014. Ripley's K Function . Wiley StatsRef Stat. Ref. Online 3, 1796–1803. <https://doi.org/10.1002/9781118445112.stat07751>
- Dolan, M.F.J., Grehan, A.J., Guinan, J.C., Brown, C., 2008. Modelling the local distribution of cold-water corals in relation to bathymetric variables: Adding spatial context to deep-sea video data. Deep. Res. Part I Oceanogr. Res. Pap. 55, 1564–1579. <https://doi.org/10.1016/j.dsr.2008.06.010>
- Doležal, M., Vlachos, M., Secci, M., Demesticha, S., Skarlatos, D., Liarokapis, F., 2019. UNDERSTANDING UNDERWATER PHOTOGRAMMETRY for MARITIME ARCHAEOLOGY THROUGH IMMERSIVE VIRTUAL REALITY. ISPRS Ann. Photogramm. Remote Sens. Spat. Inf. Sci. 42, 85–91. <https://doi.org/10.5194/isprs-archives-XLII-2-W10-85-2019>
- Donovan, M.K., Alves, C., Burns, J., Drury, C., Meier, O.W., Ritson, R., Ross, W., Robert, C., Gretchen, P.D., Gringley, G., Henderson, L.M., Knapp, I.S.S., Levy, J., Logan, C.A., Mudge, L., Sullivan, C., Gates, R.D., Asner, G.P., 2022. From polyps to pixels : understanding coral reef resilience to local and global change across scales. Landsc. Ecol. <https://doi.org/10.1007/s10980-022-01463-3>
- Dorey, N., Gjelsvik, Ø., Kutti, T., Büscher, J. V, 2020. Broad Thermal Tolerance in the Cold-Water Coral *Lophelia pertusa* From Arctic and Boreal Reefs. Front. Physiol. 10, 1–12. <https://doi.org/10.3389/fphys.2019.01636>
- Dorschel, B., 2003. Late Quaternary Development of a deep-water Carbonate Mound in the northeast Atlantic. PhD thesis. Geowissenschaften PhD, 90.
- Dorschel, B., Hebbeln, D., Foubert, A., White, M., Wheeler, A.J., 2007. Hydrodynamics and cold-water coral facies distribution related to recent sedimentary processes at Galway Mound west of Ireland. Mar. Geol. 244, 184–195.
- Dorschel, B., Hebbeln, D., Foubert, A., White, M., Wheeler, A.J., 2007. Hydrodynamics and cold-water coral facies distribution related to recent sedimentary processes at Galway Mound west of Ireland. Mar. Geol. 244, 184–195. <https://doi.org/10.1016/j.margeo.2007.06.010>
- Dorschel, B., Hebbeln, D., Rüggeberg, A., Dullo, W.C., Freiwald, A., 2005. Growth and erosion of a cold-water coral covered carbonate mound in the Northeast Atlantic

during the Late Pleistocene and Holocene. *Earth Planet. Sci. Lett.* 233, 33–44. <https://doi.org/10.1016/j.epsl.2005.01.035>

Dorschel, B., Wheeler, A.J., Monteys, X., Verbruggen, K., 2010. Atlas of the Deep-Water Seabed, Atlas of the Deep-Water Seabed: Ireland. Springer Netherlands, Dordrecht. <https://doi.org/10.1007/978-90-481-9376-9>

Douarin, M., Sinclair, D.J., Elliot, M., Henry, L.A., Long, D., Mitchison, F., Roberts, J.M., 2014. Changes in fossil assemblage in sediment cores from Mingulay Reef Complex (NE Atlantic): Implications for coral reef build-up. *Deep. Res. Part II Top. Stud. Oceanogr.* 99, 286–296. <https://doi.org/10.1016/j.dsr2.2013.07.022>

Dunleavy, M., Dede, C., Mitchell, R., 2009. Affordances and limitations of immersive participatory augmented reality simulations for teaching and learning. *J. Sci. Educ. Technol.* 18, 7–22.

Durden, J.M., Bett, B.J., Schoening, T., Morris, K.J., Nattkemper, T.W., Ruhl, H.A., 2016. Comparison of image annotation data generated by multiple investigators for benthic ecology. *Mar. Ecol. Prog. Ser.* 552, 61–70. <https://doi.org/10.3354/meps11775>

Durden, J.M., Hosking, B., Bett, B.J., Cline, D., Ruhl, H.A., 2021. Automated classification of fauna in seabed photographs: the impact of training and validation dataset size, with considerations for the class imbalance. *Prog. Oceanogr.* 196, 102612. <https://doi.org/10.1016/j.pocean.2021.102612>

Elawady, M., 2015. Sparse Coral Classification Using Deep Convolutional Neural Networks.

Elliott, G.M., Shannon, P.M., Haughton, P.D.W., Praeg, D., O'Reilly, B., 2006. Mid- to Late Cenozoic canyon development on the eastern margin of the Rockall Trough, offshore Ireland. *Mar. Geol.* 229, 113–132. <https://doi.org/10.1016/j.margeo.2006.03.008>

European Union Habitats Directive, 2016. European Union Habitats(Porcupine Bank Canyon Special Area of Conservation 003001) Regulations2016. Ireland.

- Eustice, R., Pizarro, O., Singh, H., 2004. Visually augmented navigation in an unstructured environment using a delayed state history. Proc. - IEEE Int. Conf. Robot. Autom. 2004, 25–32. <https://doi.org/10.1109/robot.2004.1307124>
- Fabri, M.-C., Pedel, L., Beuck, L., Galgani, F., Hebbeln, D., Freiwald, A., 2014. Megafauna of vulnerable marine ecosystems in French mediterranean submarine canyons: Spatial distribution and anthropogenic impacts. Deep Sea Res. Part II Top. Stud. Oceanogr. 104, 184–207. <https://doi.org/10.1016/j.dsr2.2013.06.016>
- Fabri, M.C., Dugornay, O., de la Bernardie, X., Guerin, C., Sanchez, P., Arnaubec, A., Autin, T., Piasco, R., Puig, P., 2022. 3D-Representations for studying deep-sea coral habitats in the Lacaze-Duthiers Canyon, from geological settings to individual specimens. Deep. Res. Part I Oceanogr. Res. Pap. 187, 103831. <https://doi.org/10.1016/j.dsr.2022.103831>
- Fabri, M.C., Vinha, B., Allais, A.G., Bouhier, M.E., Dugornay, O., Gaillot, A., Arnaubec, A., 2019. Evaluating the ecological status of cold-water coral habitats using non-invasive methods: An example from Cassidaigne canyon, northwestern Mediterranean Sea. Prog. Oceanogr. 178, 102172. <https://doi.org/10.1016/j.pocean.2019.102172>
- Fallati, L., Saponari, L., Savini, A., Marchese, F., Corselli, C., Galli, P., 2020. Multi-temporal UAV data and object-based image analysis (OBIA) for estimation of substrate changes in a post-bleaching scenario on a Maldivian reef. Remote Sens. 12. <https://doi.org/10.3390/rs12132093>
- FAO, 2010. The state of world fisheries and aquaculture 218.
- FAO, 2009. International Guidelines for the Management of Deep-sea Fisheries in the High Seas. Rome, Italy.
- Fawcett, T., 2006. An introduction to ROC analysis. Pattern Recognit. Lett. 27, 861–874. <https://doi.org/10.1016/j.patrec.2005.10.010>
- Feiner, S., MacIntyre, B., Seligmann, D., 1993. Knowledge-based augmented reality. Commun. ACM 36, 53–62.

- Fernández-Batanero, J.M., Montenegro-Rueda, M., Fernández-Cerero, J., 2022. Use of Augmented Reality for Students with Educational Needs: A Systematic Review (2016–2021). *Societies* 12, 36. <https://doi.org/10.3390/soc12020036>
- Ferrari, R., Figueira, W.F., Pratchett, M.S., Boube, T., Adam, A., Kobelkowsky-Vidrio, T., Doo, S.S., Atwood, T.B., Byrne, M., 2017. 3D photogrammetry quantifies growth and external erosion of individual coral colonies and skeletons. *Sci. Rep.* 7, 1–9. <https://doi.org/10.1038/s41598-017-16408-z>
- Ferrari, R., Lachs, L., Pygas, D.R., Humanes, A., Sommer, B., Figueira, W.F., Edwards, A.J., Bythell, J.C., Guest, J.R., 2021. Photogrammetry as a tool to improve ecosystem restoration. *Trends Ecol. Evol.* 1–9. <https://doi.org/10.1016/j.tree.2021.07.004>
- Ferrari, R., McKinnon, D., He, H., Smith, R.N., Corke, P., González-Rivero, M., Mumby, P.J., Upcroft, B., 2016. Quantifying multiscale habitat structural complexity: A cost-effective framework for underwater 3D modelling. *Remote Sens.* 8. <https://doi.org/10.3390/rs8020113>
- Figueira, Will, Ferrari, R., Weatherby, E., Porter, A., Hawes, S., Byrne, M., 2015. Accuracy and Precision of Habitat Structural Complexity Metrics Derived from Underwater Photogrammetry. *Remote Sens.* 7, 16883–16900. <https://doi.org/10.3390/rs71215859>
- Fischler, M.A., Bolles, R.C., 1981. Random sample consensus: A Paradigm for Model Fitting with Applications to Image Analysis and Automated Cartography. *Commun. ACM* 24, 381–395. <https://doi.org/10.1145/358669.358692>
- Fisher, W.S., Davis, W.P., Quarles, R.L., Patrick, J., Campbell, J.G., Harris, P.S., Hemmer, B.L., Parsons, M., 2007. Characterizing coral condition using estimates of three-dimensional colony surface area. *Environ. Monit. Assess.* 125, 347–360. <https://doi.org/10.1007/s10661-006-9527-8>
- Flögel, S., Dullo, W.C., Pfannkuche, O., Kiriakoulakis, K., Rüggeberg, A., 2014. Geochemical and physical constraints for the occurrence of living cold-water corals. *Deep. Res. Part II Top. Stud. Oceanogr.* 99, 19–26. <https://doi.org/10.1016/j.dsr2.2013.06.006>

Foley, N.S., Rensburg, T.M. Van, Armstrong, C.W., 2010. Ocean & Coastal Management The ecological and economic value of cold-water coral ecosystems. *Ocean Coast. Manag.* 53, 313–326. <https://doi.org/10.1016/j.ocecoaman.2010.04.009>

Fosså, J.H., Lindberg, B., Christensen, O., Lundälv, T., Svellingen, I., Mortensen, P.B., Alvsvåg, J., 2006. Mapping of *Lophelia* reefs in Norway: experiences and survey methods. *Cold-Water Corals Ecosyst.* 359–391. https://doi.org/10.1007/3-540-27673-4_18

Fosså, J.H., Mortensen, P.B., Furevik, D.M., 2002. The deep-water coral *Lophelia pertusa* in Norwegian waters: Distribution and fishery impacts. *Hydrobiologia* 471, 1–12. <https://doi.org/https://doi.org/10.1023/A:1016504430684>

Foubert, A., Beck, T., Wheeler, A.J., Opderbecke, J., Grehan, A., Klages, M., Thiede, J., Henriët, J.-P., 2006. New view of the Belgica Mounds, Porcupine Seabight, NE Atlantic: preliminary results from the Polarstern ARK-XIX/3a ROV cruise, in: *Cold-Water Corals and Ecosystems*. Springer-Verlag, Berlin/Heidelberg, pp. 403–415. https://doi.org/10.1007/3-540-27673-4_20

Foubert, A., Huvenne, V.A.I., Wheeler, A., Kozachenko, M., Opderbecke, J., Henriët, J.-P., 2011. The Moira Mounds, small cold-water coral mounds in the Porcupine Seabight, NE Atlantic: Part B—Evaluating the impact of sediment dynamics through high-resolution ROV-borne bathymetric mapping. *Mar. Geol.* 282, 65–78. <https://doi.org/10.1016/j.margeo.2011.02.008>

Foucault, M., Miskowiec, J., 1986. Of other spaces. *diacritics* 16, 22–27.

Frank, N., Freiwald, A., López Correa, M., Wienberg, C., Eisele, M., Hebbeln, D., Van Rooij, D., Henriët, J.P., Colin, C., van Weering, T., de Haas, H., Buhl-Mortensen, P., Roberts, J.M., De Mol, B., Douville, E., Blamart, D., Hatté, C., 2011. Northeastern Atlantic cold-water coral reefs and climate. *Geology* 39, 743–746. <https://doi.org/10.1130/G31825.1>

Frederiksen, R., Jensen, A., Westerberg, H., 1992. The distribution of the scleractinian coral *Lophelia pertusa* around the Faroe islands and the relation to internal tidal mixing. *Sarsia* 77, 157–171. <https://doi.org/10.1080/00364827.1992.10413502>

- Freiwald, A., 2002. Reef-Forming Cold-Water Corals, in: Ocean Margin Systems. Springer Berlin Heidelberg, pp. 365–385. https://doi.org/10.1007/978-3-662-05127-6_23
- Freiwald, A., Fosså, J.H., Grehan, A., Koslow, T., Roberts, J.M., 2004a. Cold-water Coral Reefs: out of sight - no longer out of mind. UNEP-WCMC Biodiversity Series 22, UNEP-WCMC Biodiversity Series. [s.n.]. <https://doi.org/10.5962/bhl.title.45025>
- Freiwald, A., Hühnerbach, V., Lindberg, B., Wilson, J.B., Campbell, J., 2002. The Sula Reef Complex, Norwegian shelf. *Facies* 47, 179–200. <https://doi.org/10.1007/BF02667712>
- Freiwald, A., Roberts, J.M., 2005. Cold-Water Corals and Ecosystems, Cold-Water Corals and Ecosystems. Springer Berlin Heidelberg, Berlin, Heidelberg. <https://doi.org/10.1007/3-540-27673-4>
- Freiwald, A., Wilson, J.B., 1998. Taphonomy of modern deep, cold-temperate water coral reefs. *Hist. Biol.* 13, 37–52. <https://doi.org/10.1080/08912969809386571>
- Freiwald, A., Wilson, J.B., Henrich, R., 1999. Grounding pleistocene icebergs shape recent deep-water coral reefs. *Sediment. Geol.* 125, 1–8. [https://doi.org/10.1016/S0037-0738\(98\)00142-0](https://doi.org/10.1016/S0037-0738(98)00142-0)
- Friedman, A., 2013. Automated interpretation of benthic stereo imagery. University of Sydney.
- Friedman, A., Pizarro, O., Williams, S.B., Johnson-Roberson, M., 2012. Multi-Scale Measures of Rugosity, Slope and Aspect from Benthic Stereo Image Reconstructions. *PLoS One* 7. <https://doi.org/10.1371/journal.pone.0050440>
- Friedman, J.H., 2001. Greedy function approximation: A gradient boosting machine. *Ann. Stat.* 29, 1189–1232. <https://doi.org/10.1214/aos/1013203451>
- Fu, T., Ma, L., Li, M., Johnson, B.A., 2018. Using convolutional neural network to identify irregular segmentation objects from very high-resolution remote sensing imagery. *J. Appl. Remote Sens.* 12, 1. <https://doi.org/10.1117/1.jrs.12.025010>

Fukunaga, A., Burns, J.H.R., 2020. Metrics of coral reef structural complexity extracted from 3D mesh models and digital elevation models. *Remote Sens.* 12, 2676. <https://doi.org/10.3390/RS12172676>

Fukunaga, A., Burns, J.H.R., Pascoe, K.H., Kosaki, R.K., 2020. Associations between benthic cover and habitat complexity metrics obtained from 3D reconstruction of coral reefs at different resolutions. *Remote Sens.* 12. <https://doi.org/10.3390/rs12061011>

Gass, S.E., Roberts, J.M., 2006. The occurrence of the cold-water coral *Lophelia pertusa* (Scleractinia) on oil and gas platforms in the North Sea: Colony growth, recruitment and environmental controls on distribution. *Mar. Pollut. Bull.* 52, 549–559. <https://doi.org/10.1016/j.marpolbul.2005.10.002>

Gauci, A., Deidun, A., Abela, J., Zarb Adami, K., 2016. Machine Learning for benthic sand and maerl classification and coverage estimation in coastal areas around the Maltese Islands. *J. Appl. Res. Technol.* 14, 338–344. <https://doi.org/10.1016/j.jart.2016.08.003>

GEBCO, 2017. The Nippon Foundation GEBCO Seabed 2030 Mission statement [WWW Document]. URL https://www.gebco.net/documents/seabed2030_brochure.pdf (accessed 1.26.23).

Gerdes, K., Arbizu, P.M., Schwarz-Schampera, U., Schwentner, M., Kihara, T.C., 2019. Detailed mapping of hydrothermal vent fauna: A 3d reconstruction approach based on video imagery. *Front. Mar. Sci.* 6. <https://doi.org/10.3389/fmars.2019.00096>

Getis, A., Ord, J.K., 1992. The Analysis of Spatial Association by Use of Distance Statistics. *Geogr. Anal.* 24, 189–206. <https://doi.org/10.1111/j.1538-4632.1992.tb00261.x>

Gilardi, N., 1995. Comparison of four machine learning algorithms for spatial data analysis. *Evaluation* 1–16.

Goatley, C H R, Bellwood, D.R., 2011. The roles of dimensionality, canopies and complexity in ecosystem monitoring. *PLoS One* 6.

- Goatley, Christopher H R, Bellwood, D.R., 2011. The roles of dimensionality, canopies and complexity in ecosystem monitoring. *PLoS One* 6. <https://doi.org/10.1371/journal.pone.0027307>
- González-Rivero, M., Beijbom, O., Rodriguez-Ramirez, A., Bryant, D.E.P., Ganase, A., Gonzalez-Marrero, Y., Herrera-Reveles, A., Kennedy, E. V., Kim, C.J.S., Lopez-Marcano, S., Markey, K., Neal, B.P., Osborne, K., Reyes-Nivia, C., Sampayo, E.M., Stolberg, K., Taylor, A., Vercelloni, J., Wyatt, M., Hoegh-Guldberg, O., 2020. Monitoring of coral reefs using artificial intelligence: A feasible and cost-effective approach. *Remote Sens.* 12, 1–22. <https://doi.org/10.3390/rs12030489>
- Gori, A., Ferrier-Pagès, C., Hennige, S.J., Murray, F., Rottier, C., Wicks, L.C., Roberts, J.M., 2016. Physiological response of the cold-water coral *Desmophyllum dianthus* to thermal stress and ocean acidification. *PeerJ* 2016, 1–16. <https://doi.org/10.7717/peerj.1606>
- Graham, N.A.J., Nash, K.L., 2013. The importance of structural complexity in coral reef ecosystems. *Coral Reefs* 32, 315–326. <https://doi.org/10.1007/s00338-012-0984-y>
- Graham, N.A.J., Wilson, S.K., Jennings, S., Polunin, N.V.C., Bijoux, J.P., Robinson, J., 2006. Dynamic fragility of oceanic coral reef ecosystems. *Proc. Natl. Acad. Sci. U. S. A.* 103, 8425–8429. <https://doi.org/10.1073/pnas.0600693103>
- Granshaw, S.I., 1980. Bundle Adjustment Methods in Engineering Photogrammetry. *Photogramm. Rec.* 10, 181–207. <https://doi.org/10.1111/j.1477-9730.1980.tb00020.x>
- Guinan, J., Grehan, A., Dolan, M., Brown, C., 2009. Quantifying relationships between video observations of cold-water coral cover and seafloor features in Rockall Trough, west of Ireland. *Mar. Ecol. Prog. Ser.* 375, 125–138. <https://doi.org/10.3354/meps07739>
- Gutierrez-Heredia, L., Benzoni, F., Murphy, E., Reynaud, E.G., 2016. End to End Digitisation and Analysis of Three-Dimensional Coral Models, from Communities to Corallites. *PLoS One* 11. <https://doi.org/10.1371/journal.pone.0149641>

Hall-Spencer, J., Allain, V., Fosså, J.H., 2002. Trawling damage to Northeast Atlantic ancient coral reefs. *Proc. R. Soc. B Biol. Sci.* 269, 507–511. <https://doi.org/10.1098/rspb.2001.1910>

Hall-Spencer, J.M., Stehfest, K.M., Wheeler, A.J., 2009. Assessment of Coral Carbonate Mounds in the OSPAR area and the development of a monitoring program Background Information.

Han, X., Liu, J., Tan, B., Duan, L., 2021. Design and Implementation of Smart Ocean Visualization System Based on Extended Reality Technology. *J. Web Eng.* <https://doi.org/10.13052/jwe1540-9589.20215>

Harris, P.T., Whiteway, T., 2011. Global distribution of large submarine canyons: Geomorphic differences between active and passive continental margins. *Mar. Geol.* 285, 69–86. <https://doi.org/10.1016/j.margeo.2011.05.008>

Hebbeln, D., Portilho-Ramos, R. da C., Wienberg, C., Titschack, J., 2019. The Fate of Cold-Water Corals in a Changing World: A Geological Perspective. *Front. Mar. Sci.* 6. <https://doi.org/10.3389/fmars.2019.00119>

Hebbeln, D., Wienberg, C., Dullo, W.C., Freiwald, A., Mienis, F., Orejas, C., Titschack, J., 2020. Cold-water coral reefs thriving under hypoxia. *Coral Reefs* 39, 853–859. <https://doi.org/10.1007/s00338-020-01934-6>

Heindel, K., Titschack, J., Dorschel, B., Huvenne, V.A.I., Freiwald, A., 2010. The sediment composition and predictive mapping of facies on the Propeller Mound-A cold-water coral mound (Porcupine Seabight, NE Atlantic). *Cont. Shelf Res.* 30, 1814–1829. <https://doi.org/10.1016/j.csr.2010.08.007>

Hengl, T., Nussbaum, M., Wright, M.N., Heuvelink, G.B.M., Gräler, B., 2018. Random forest as a generic framework for predictive modeling of spatial and spatio-temporal variables. *PeerJ* 2018. <https://doi.org/10.7717/peerj.5518>

Hennige, S.J., Wolfram, U., Wickes, L., Murray, F., Roberts, J.M., Kamenos, N.A., Schofield, S., Groetsch, A., Spiesz, E.M., Aubin-Tam, M.E., Etnoyer, P.J., 2020. Crumbling Reefs and Cold-Water Coral Habitat Loss in a Future Ocean: Evidence of

“Coralporosis” as an Indicator of Habitat Integrity. *Front. Mar. Sci.* 7, 1–16. <https://doi.org/10.3389/fmars.2020.00668>

Henry, L.-A., Roberts, J.M., 2017. Global Biodiversity in Cold-Water Coral Reef Ecosystems, in: Rossi, S., Bramanti, L., Gori, A., Orejas, C. (Eds.), *Marine Animal Forests*. Springer International Publishing, Cham, pp. 235–256. https://doi.org/10.1007/978-3-319-21012-4_6

Hopkinson, Brian M., King, A.C., Owen, D.P., Johnson-Roberson, M., Long, M.H., Bhandarkar, S.M., 2020. Automated classification of three-dimensional reconstructions of coral reefs using convolutional neural networks. *PLoS One* 15. <https://doi.org/10.1371/journal.pone.0230671>

House, J.E., Brambilla, V., Bidaut, L.M., Christie, A.P., Pizarro, O., Madin, J.S., Dornelas, M., 2018. Moving to 3D: relationships between coral planar area, surface area and volume. *PeerJ* 6, e4280. <https://doi.org/10.7717/peerj.4280>

Hovland, M., Croker, P.F., Martin, M., 1994. Fault-associated seabed mounds (carbonate knolls?) off western Ireland and north-west Australia. *Mar. Pet. Geol.* 11, 232–246. [https://doi.org/10.1016/0264-8172\(94\)90099-X](https://doi.org/10.1016/0264-8172(94)90099-X)

Hovland, M., Thomsen, E., 1997. Cold-water corals - Are they hydrocarbon seep related?, in: *Marine Geology*. Elsevier, pp. 159–164. [https://doi.org/10.1016/S0025-3227\(96\)00086-2](https://doi.org/10.1016/S0025-3227(96)00086-2)

Huang, Z., Brooke, B.P., Harris, P.T., 2011. A new approach to mapping marine benthic habitats using physical environmental data. *Cont. Shelf Res.* 31, 4–16. <https://doi.org/10.1016/j.csr.2010.03.012>

Huvenne, V.A.I., Bett, B.J., Masson, D.G., Le Bas, T.P., Wheeler, A.J., 2016. Effectiveness of a deep-sea cold-water coral Marine Protected Area, following eight years of fisheries closure. *Biol. Conserv.* 200, 60–69. <https://doi.org/10.1016/j.biocon.2016.05.030>

Huvenne, V.A.I., Beyer, A., de Haas, H., Dekindt, K., Henriët, J.-P., Kozachenko, M., Olu-Le Roy, K., Wheeler, A.J., 2005. The seabed appearance of different coral bank provinces in the Porcupine Seabight, NE Atlantic: results from sidescan sonar and ROV

seabed mapping. *Cold-Water Corals Ecosyst.* 535–569. https://doi.org/10.1007/3-540-27673-4_27

Huvenne, V.A.I., Blondel, P., Henriot, J.P., 2002. Textural analyses of sidescan sonar imagery from two mound provinces in the Porcupine Seabight. *Mar. Geol.* 189, 323–341. [https://doi.org/10.1016/S0025-3227\(02\)00420-6](https://doi.org/10.1016/S0025-3227(02)00420-6)

Huvenne, V.A.I., Tyler, P.A., Masson, D.G., Fisher, E.H., Hauton, C., Hühnerbach, V., Bas, T.P., Wolff, G.A., 2011a. A picture on the wall: Innovative mapping reveals cold-water coral refuge in submarine canyon. *PLoS One* 6, 1–9. <https://doi.org/10.1371/journal.pone.0028755>

i-MareCulture – H2020 funded EU research and innovation project [WWW Document], n.d. URL <https://imareculture.eu/> (accessed 9.15.22).

Inter-Departmental Marine Coordination Group, 2018. *Harnessing Our Ocean Wealth An Integrated Marine Plan for Ireland.*

Ismail, K., Huvenne, V., Robert, K., 2018. Quantifying spatial heterogeneity in submarine canyons. *Prog. Oceanogr.* 169, 181–198. <https://doi.org/10.1016/j.pocean.2018.03.006>

Jameson, S.C., Ammar, M.S.A., Saadalla, E., Mostafa, H.M., Riegl, B., 1999. A coral damage index and its application to diving sites in the Egyptian Red Sea. *Coral reefs* 18, 333–339.

Jodzani, S.E., Johnson, B.A., Chen, D., 2019. Comparing Deep Neural Networks , Ensemble Classifiers , and Support Vector Machine Algorithms. *Remote Sens.* 11, 1–24.

Jones, C.G., Lawton, J.H., Shachak, M., 1994. Organisms as Ecosystem Engineers. *Ecosyst. Manag.* 130–147. https://doi.org/10.1007/978-1-4612-4018-1_14

Jonsson, L.G., Nilsson, P.G., Floruta, F., Lundälv, T., 2004. Distributional patterns of macro- and megafauna associated with a reef of the cold-water coral *Lophelia pertusa* on the Swedish west coast. *Mar. Ecol. Prog. Ser.* 284, 163–171. <https://doi.org/10.3354/meps284163>

- Jung, T.H., Lee, H., Chung, N., tom Dieck, M.C., 2018. Cross-cultural differences in adopting mobile augmented reality at cultural heritage tourism sites. *Int. J. Contemp. Hosp. Manag.* 30, 1621–1645. <https://doi.org/10.1108/IJCHM-02-2017-0084>
- Karara, G., Hajji, R., Poux, F., 2021. 3D Point Cloud Semantic Augmentation: Instance Segmentation of 360° Panoramas by Deep Learning Techniques. *Remote Sens.* 13, 3647. <https://doi.org/10.3390/rs13183647>
- Kasinathan, V., Al-Sharafi, A.T.A., Zamnah, A., Appadurai, N.K., Thiruchelvam, V., Mustapha, A., 2021. Augmented reality in ocean's secrets: educational application with attached book for students. *Linguist. Cult. Rev.* 5, 1123–1137. <https://doi.org/10.21744/lingcure.v5ns1.1498>
- Kaufmann, H., 2003. Collaborative augmented reality in education. *Inst. Softw. Technol. Interact. Syst. Vienna Univ. Technol.* 2–4.
- Kazanidis, G., Henry, L.A., Roberts, J.M., 2021. Hidden structural heterogeneity enhances marine hotspots' biodiversity. *Coral Reefs* 40, 1615–1630. <https://doi.org/10.1007/s00338-021-02114-w>
- Kenyon, N.H., Akhmetzhanov, A.M., Wheeler, A.J., van Weering, T.C.E., de Haas, H., Ivanov, M.K., 2003. Giant carbonate mud mounds in the southern Rockall Trough. *Mar. Geol.* 195, 5–30. [https://doi.org/10.1016/S0025-3227\(02\)00680-1](https://doi.org/10.1016/S0025-3227(02)00680-1)
- Kenyon, N.H., Ivanov, M.K., Akhmetzhanov, a M., 1998. Cold water carbonate mounds and sediment transport on the Northeast Atlantic margin. *IOC Tech. Ser.* 52.
- King, A., Bhandarkar, S.M., Hopkinson, B.M., 2018. A Comparison of Deep Learning Methods for Semantic Segmentation of Coral Reef Survey Images, in: 2018 IEEE/CVF Conference on Computer Vision and Pattern Recognition Workshops (CVPRW). IEEE, pp. 1475–14758. <https://doi.org/10.1109/CVPRW.2018.00188>
- Kingma, D.P., Ba, J.L., 2015. Adam: A method for stochastic optimization. 3rd Int. Conf. Learn. Represent. ICLR 2015 - Conf. Track Proc. 1–15.
- Kitahara, M.V., 2007. Species richness and distribution of azooxanthellate Scleractinia in Brazil Species richness and distribution of azooxanthellate Scleractinia in Brazil. *Bull. Mar. Sci.* 81, 497–518.

- Koch, A., Heipke, C., 2006. Semantically correct 2.5D GIS data - The integration of a DTM and topographic vector data. *ISPRS J. Photogramm. Remote Sens.* 61, 23–32. <https://doi.org/10.1016/j.isprsjprs.2006.07.005>
- Kongsberg Gruppen, 2010. The HUGIN Family : Maximizing performance.
- Koop, L., Snellen, M., Simons, D.G., 2021. An Object-Based Image Analysis Approach Using Bathymetry and Bathymetric Derivatives to Classify the Seafloor. *Geosciences* 11, 45. <https://doi.org/10.3390/geosciences11020045>
- Kornder, N.A., Cappelletto, J., Mueller, B., Zalm, M.J.L., Martinez, S.J., Vermeij, M.J.A., Huisman, J., de Goeij, J.M., 2021. Implications of 2D versus 3D surveys to measure the abundance and composition of benthic coral reef communities. *Coral Reefs*. <https://doi.org/10.1007/s00338-021-02118-6>
- Kovalenko, K.E., Thomaz, S.M., Warfe, D.M., 2012. Habitat complexity: Approaches and future directions. *Hydrobiologia* 685, 1–17. <https://doi.org/10.1007/s10750-011-0974-z>
- Kwasnitschka, T., Hansteen, T.H., Devey, C.W., Kutterolf, S., 2013. Doing fieldwork on the seafloor: Photogrammetric techniques to yield 3D visual models from ROV video. *Comput. Geosci.* 52, 218–226. <https://doi.org/10.1016/j.cageo.2012.10.008>
- Labster, n.d. Reimagining the future of education [WWW Document]. 2022. URL <https://www.labster.com/about/>
- Lacharité, M., Metaxas, A., 2017. Hard substrate in the deep ocean: How sediment features influence epibenthic megafauna on the eastern Canadian margin. *Deep. Res. Part I Oceanogr. Res. Pap.* 126, 50–61. <https://doi.org/10.1016/j.dsr.2017.05.013>
- Lange, I.D., Perry, C.T., 2020a. A quick, easy and non-invasive method to quantify coral growth rates using photogrammetry and 3D model comparisons. *Methods Ecol. Evol.* 11, 714–726. <https://doi.org/10.1111/2041-210X.13388>
- Laranjeira, M., Arnaubec, A., Brignone, L., Dune, C., Opderbecke, J., 2020. 3D Perception and Augmented Reality Developments in Underwater Robotics for Ocean Sciences. *Curr. Robot. Reports* 1, 123–130. <https://doi.org/10.1007/s43154-020-00014-5>

- Last, F., Douzas, G., Bacao, F., 2017. Oversampling for Imbalanced Learning Based on K-Means and SMOTE 1–19. <https://doi.org/10.1016/j.ins.2018.06.056>
- Lavy, A., Eyal, G., Neal, B., Keren, R., Loya, Y., Ilan, M., 2015. A quick, easy and non-intrusive method for underwater volume and surface area evaluation of benthic organisms by 3D computer modelling. *Methods Ecol. Evol.* 6, 521–531. <https://doi.org/10.1111/2041-210X.12331>
- Le Danois, E. 1887-, 1948. Les profondeurs de la mer; trente ans de recherches sur la faune sous-marine au large des côtes de France. LK -, Bibliothèque scientifique TA - TT -. Payot, Paris SE - 303 pages illustrations, maps 23 cm.
- Lecours, V., Devillers, R., Schneider, D., Lucieer, V., Brown, C., Edinger, E., 2015. Spatial scale and geographic context in benthic habitat mapping: review and future directions. *Mar. Ecol. Prog. Ser.* 535, 259–284. <https://doi.org/10.3354/meps11378>
- Lee, K., 2012. Augmented reality in education and training. *TechTrends* 56, 13–21.
- Leon, J.X., Roelfsema, C.M., Saunders, M.I., Phinn, S.R., 2015. Measuring coral reef terrain roughness using ‘Structure-from-Motion’ close-range photogrammetry. *Geomorphology* 242, 21–28. <https://doi.org/10.1016/j.geomorph.2015.01.030>
- Leverette, T.L., Metaxas, A., 2006. Predicting habitat for two species of deep-water coral on the Canadian Atlantic continental shelf and slope, in: *Cold-Water Corals and Ecosystems*. Springer-Verlag, pp. 467–479. https://doi.org/10.1007/3-540-27673-4_23
- Li, R., Li, H., Zou, W., Smith, R.G., Curran, T.A., 1997. Quantitative photogrammetric analysis of digital underwater video imagery. *IEEE J. Ocean. Eng.* 22, 364–375. <https://doi.org/10.1109/48.585955>
- Liestøl, G., 2019. Augmented Reality Storytelling – Narrative Design and Reconstruction of a Historical Event in situ. *Int. J. Interact. Mob. Technol.* 13, 196. <https://doi.org/10.3991/ijim.v13i12.11560>
- Liestøl, G., Bendon, M., Hadjidaki-Marder, E., 2021. Augmented Reality Storytelling Submerged. Dry Diving to a World War II Wreck at Ancient Phalasarna, Crete. *Heritage* 4, 4647–4664. <https://doi.org/10.3390/heritage4040256>

Lim, A., 2017. Spatio – temporal Patterns and Controls on Cold-water Coral Reef Development : The Moira Mounds , Porcupine Seabight , Offshore Ireland. Porcupine Seabight, Offshore Ireland.

Lim, A., Huvenne, V.A.I., Vertino, A., Spezzaferri, S., Wheeler, A.J., 2018a. New insights on coral mound development from groundtruthed high-resolution ROV-mounted multibeam imaging. *Mar. Geol.* 403, 225–237. <https://doi.org/10.1016/j.margeo.2018.06.006>

Lim, A., Kane, A., Arnaubec, A., Wheeler, A.J., 2018b. Seabed image acquisition and survey design for cold water coral mound characterisation. *Mar. Geol.* 395, 22–32. <https://doi.org/https://doi.org/10.1016/j.margeo.2017.09.008>

Lim, A., Wheeler, A.J., Arnaubec, A., 2017. High-resolution facies zonation within a cold-water coral mound: The case of the Piddington Mound, Porcupine Seabight, NE Atlantic. *Mar. Geol.* 390, 120–130. <https://doi.org/10.1016/j.margeo.2017.06.009>

Lim, A., O'Reilly, L., Summer, G., de Oliveira, L.M.C., Strachan, R., Lim, O'Reilly, L., Summer, G., de Oliveira, L.M.C., Strachan, R., 2020a. CE20011 Cruise Report: Systematic Monitoring Survey of the Moira Mound Chain (SyMonS_MoM).

Lim, A., Wheeler, A.J., Conti, L., 2020b. Cold-Water Coral Habitat Mapping: Trends and Developments in Acquisition and Processing Methods. *Geosciences* 11, 9. <https://doi.org/10.3390/geosciences11010009>

Lim, A., Wheeler, A.J., Price, D.M., O'Reilly, L., Harris, K., Conti, L., 2020c. Influence of benthic currents on cold-water coral habitats: a combined benthic monitoring and 3D photogrammetric investigation. *Sci. Rep.* 10, 19433. <https://doi.org/10.1038/s41598-020-76446-y>

Liu, P., Choo, K.K.R., Wang, L., Huang, F., 2017. SVM or deep learning? A comparative study on remote sensing image classification. *Soft Comput.* 21, 7053–7065. <https://doi.org/10.1007/s00500-016-2247-2>

Liu, X., Sohn, Y.-H., Park, D.-W., 2018. Application Development with Augmented Reality Technique using Unity 3D and Vuforia. *Int. J. Appl. Eng. Res.* 13, 15068–15071.

- Long, D., Roberts, J.M., Gillespie, E.J., 1999. Occurrences of *Lophelia pertusa* on the Atlantic margin. Tech. Rep. WB/99/24 44.
- Loureiro, S.M.C., Guerreiro, J., Ali, F., 2020. 20 years of research on virtual reality and augmented reality in tourism context: A text-mining approach. *Tour. Manag.* <https://doi.org/10.1016/j.tourman.2019.104028>
- Lowe, D.G., 1999. Object recognition from local scale-invariant features, in: *Proceedings of the Seventh IEEE International Conference on Computer Vision*. IEEE, pp. 1150–1157 vol.2. <https://doi.org/10.1109/ICCV.1999.790410>
- Lowe, G., 2004. Sift-the scale invariant feature transform. *Int. J* 2, 2.
- Lucieer, V., Hill, N.A., Barrett, N.S., Nichol, S., 2013. Do marine substrates ‘look’ and ‘sound’ the same? Supervised classification of multibeam acoustic data using autonomous underwater vehicle images. *Estuar. Coast. Shelf Sci.* 117, 94–106. <https://doi.org/10.1016/J.ECSS.2012.11.001>
- Luckhurst, B.E., Luckhurst, K., 1978. Analysis of the influence of substrate variables on coral reef fish communities. *Mar. Biol.* 49, 317–323. <https://doi.org/10.1007/BF00455026>
- Ma, L., Li, M., Ma, X., Cheng, L., Du, P., Liu, Y., 2017. A review of supervised object-based land-cover image classification. *ISPRS J. Photogramm. Remote Sens.* 130, 277–293. <https://doi.org/10.1016/j.isprsjprs.2017.06.001>
- Mahmood, A., Bennamoun, M., An, S., Sohel, F.A., Boussaid, F., Hovey, R., Kendrick, G.A., Fisher, R.B., 2019. Deep Image Representations for Coral Image Classification. *IEEE J. Ocean. Eng.* 44, 121–131. <https://doi.org/10.1109/JOE.2017.2786878>
- Mangini, A., Lomitschka, M., Eichstädter, R., Frank, N., Vogler, S., Bonani, G., Hajdas, I., Patzold, J., 1998. Coral provides way to age deep water. *Nature* 392, 347–348. <https://doi.org/10.1038/32804>
- Markowitz, D.M., Laha, R., Perone, B.P., Pea, R.D., Bailenson, J.N., 2018. Immersive Virtual Reality Field Trips Facilitate Learning About Climate Change. *Front. Psychol.* 9. <https://doi.org/10.3389/fpsyg.2018.02364>

Masson, D., Bett, B., Billett, D.S., Jacobs, C., Wheeler, A., Wynn, R., 2003. The origin of deep-water, coral-topped mounds in the northern Rockall Trough, Northeast Atlantic. *Mar. Geol.* 194, 159–180. [https://doi.org/10.1016/S0025-3227\(02\)00704-1](https://doi.org/10.1016/S0025-3227(02)00704-1)

Mazzini, A., Akhmetzhanov, A., Monteys, X., Ivanov, M., 2012. The Porcupine Bank Canyon coral mounds: oceanographic and topographic steering of deep-water carbonate mound development and associated phosphatic deposition. *Geo-Marine Lett.* 32, 205–225. <https://doi.org/10.1007/s00367-011-0257-8>

McCormick, M.I., 1994. Comparison of field methods for measuring surface tomography and their associations with a tropical reef fish assemblage. *Mar. Ecol. Prog. Ser.* 112, 87–96. <https://doi.org/10.3354/meps112087>

McKinnon, D., He, H., Upcroft, B., Smith, R.N., 2011. Towards automated and in-situ, near-real time 3-D reconstruction of coral reef environments. *Ocean. - MTS/IEEE Kona, Progr. B.* <https://doi.org/10.23919/oceans.2011.6106982>

Melgani, F., Bruzzone, L., 2004. Classification of Hyperspectral Remote Sensing 42, 1778–1790.

Menna, F., Nocerino, E., Remondino, F., 2018. Photogrammetric Modelling of Submerged Structures: Influence of Underwater Environment and Lens Ports on Three-Dimensional (3D) Measurements, in: *Latest Developments in Reality-Based 3D Surveying and Modelling*. MDPI, pp. 279–303. <https://doi.org/10.3390/books978-3-03842-685-1-13>

Microsoft, n.d. Android Studio | Android Developers.

Mienis, F., Bouma, T., Witbaard, R., van Oevelen, D., Duineveld, G., 2019. Experimental assessment of the effects of coldwater coral patches on water flow. *Mar. Ecol. Prog. Ser.* 609, 101–117. <https://doi.org/10.3354/meps12815>

Mienis, F., Duineveld, G.C.A., Davies, A.J., Ross, S.W., Seim, H., Bane, J., van Weering, T.C.E., 2012. The influence of near-bed hydrodynamic conditions on cold-water corals in the Viosca Knoll area, Gulf of Mexico. *Deep Sea Res. Part I Oceanogr. Res. Pap.* 60, 32–45. <https://doi.org/10.1016/j.dsr.2011.10.007>

- Mienis, F., van Weering, T., de Haas, H., de Stigter, H., Huvenne, V., Wheeler, A., 2006. Carbonate mound development at the SW Rockall Trough margin based on high resolution TOBI and seismic recording. *Mar. Geol.* 233, 1–19. <https://doi.org/10.1016/j.margeo.2006.08.003>
- Miller, G.T., Spoolman, S., 2015. *Environmental science*. Cengage Learning.
- Miller, R.J., Hocevar, J., Stone, R.P., Fedorov, D. V, 2012. Structure-Forming Corals and Sponges and Their Use as Fish Habitat in Bering Sea Submarine Canyons. *PLoS One* 7, 1–9. <https://doi.org/10.1371/journal.pone.0033885>
- Misiuk, B., Diesing, M., Aitken, A., Brown, C.J., Edinger, E.N., Bell, T., 2019. A spatially explicit comparison of quantitative and categorical modelling approaches for mapping seabed sediments using random forest. *Geosci.* 9, 1–34. <https://doi.org/10.3390/geosciences9060254>
- Moberg, F., Folke, C., 1999. Ecological goods and services of coral reef ecosystems. *Ecol. Econ.* 29, 215–233. [https://doi.org/10.1016/S0921-8009\(99\)00009-9](https://doi.org/10.1016/S0921-8009(99)00009-9)
- Modasshir, M., Rahman, S., Youngquist, O., Rekleitis, I., 2018. Coral Identification and Counting with an Autonomous Underwater Vehicle. 2018 IEEE Int. Conf. Robot. Biomimetics, ROBIO 2018 524–529. <https://doi.org/10.1109/ROBIO.2018.8664785>
- Mogstad, A.A., Løvås, H.S., Sture, O., Johnsen, G., Ludvigsen, M., 2022. Remote Sensing of the Tautra Ridge: An Overview of the World’s Shallowest Cold-Water Coral Reefs. *Front. Mar. Sci.* 9, 1–18. <https://doi.org/10.3389/fmars.2022.848888>
- Mohamed, H., Nadaoka, K., Nakamura, T., 2022. Automatic Semantic Segmentation of Benthic Habitats Using Images from Towed Underwater Camera in a Complex Shallow Water Environment 1–22.
- Mohamed, H, Nadaoka, K., Nakamura, T., 2020. Towards Benthic Habitat 3D Mapping Using Machine Learning Algorithms and Structures from Motion Photogrammetry. *Remote Sens* 12, 127.
- Mohamed, Hassan, Nadaoka, K., Nakamura, T., 2020. Towards Benthic Habitat 3D Mapping Using Machine Learning Algorithms and Structures from Motion Photogrammetry. *Remote Sens.* 12, 127. <https://doi.org/10.3390/rs12010127>

Monteiro, J.H.F., Montanha, G.K., 2019. Desenvolvimento de aplicação em Realidade Virtual. *Tekhne e Logos* 10, 99–111.

Mortensen, P.B., Buhl-Mortensen, L., 2004. Distribution of deep-water gorgonian corals in relation to benthic habitat features in the Northeast Channel (Atlantic Canada). *Mar. Biol.* 144, 1223–1238. <https://doi.org/10.1007/s00227-003-1280-8>

Mortensen, P.B., Hovland, M., Brattegard, T., Farestveit, R., 1995. Deep water bioherms of the scleractinian coral *Lophelia pertusa* (L.) at 64° n on the Norwegian shelf: Structure and associated megafauna. *Sarsia* 80, 145–158. <https://doi.org/10.1080/00364827.1995.10413586>

Mortensen, P.B., Hovland, T., Fosså, J.H., Furevik, D.M., 2001. Distribution, abundance and size of *Lophelia pertusa* coral reefs in mid-Norway in relation to seabed characteristics. *J. Mar. Biol. Assoc. United Kingdom* 81, 581–597. <https://doi.org/10.1017/S002531540100426X>

Mountrakis, G., Im, J., Ogole, C., 2011. Support vector machines in remote sensing: A review. *ISPRS J. Photogramm. Remote Sens.* 66, 247–259. <https://doi.org/10.1016/j.isprsjprs.2010.11.001>

Navarro, A., Young, M., Allan, B., Carnell, P., Macreadie, P., Ierodiaconou, D., 2020. The application of Unmanned Aerial Vehicles (UAVs) to estimate above-ground biomass of mangrove ecosystems. *Remote Sens. Environ.* 242, 111747. <https://doi.org/10.1016/j.rse.2020.111747>

Negahdaripour, S., Madjidi, H., 2003. Stereovision imaging on submersible platforms for 3-D mapping of benthic habitats and sea-floor structures. *IEEE J. Ocean. Eng.* 28, 625–650. <https://doi.org/10.1109/JOE.2003.819313>

Nittrouer, C.A., Wright, L.D., 1994. Transport of particles across continental shelves. *Rev. Geophys.* 32, 85–113. <https://doi.org/10.1029/93RG02603>

NPWS, 2022. NPWS Belgica Mound Province SAC (site code: 002327) Conservation objectives supporting document-Marine Habitats.

Nyimbili, P.H., Demirel, H., Seker, D.Z., Erden, T., 2016. Structure from Motion (SfM) - Approaches and Applications. *Int. Sci. Conf. Appl. Sci.*

O'Reilly, L., Fentimen, R., Butschek, F., Titschack, J., Lim, A., Moore, N., O'Connor, O.J., Appah, J., Harris, K., Vennemann, T., Wheeler, A.J., 2022. Environmental forcing by submarine canyons: Evidence between two closely situated cold-water coral mounds (Porcupine Bank Canyon and Western Porcupine Bank, NE Atlantic). *Mar. Geol.* 106930. <https://doi.org/10.1016/j.margeo.2022.106930>

Oevelen, D. van, Duineveld, G., Lavaleye, M., Mienis, F., Soetaert, K., Heip, C.H.R., 2009. The cold-water coral community as hotspot of carbon cycling on continental margins: A food-web analysis from Rockall Bank (northeast Atlantic). *Limnol. Oceanogr.* 54, 1829–1844. <https://doi.org/10.4319/lo.2009.54.6.1829>

Orejas, C., Gori, A., Lo Iacono, C., Puig, P., Gili, J.M., Dale, M.R.T.T., 2009. Cold-water corals in the Cap de Creus canyon, northwestern Mediterranean: Spatial distribution, density and anthropogenic impact. *Mar. Ecol. Prog. Ser.* 397, 37–51. <https://doi.org/10.3354/meps08314>

Orejas, C., Gori, A., Rad-Menéndez, C., Last, K.S., Davies, A.J., Beveridge, C.M., Sadd, D., Kiriakoulakis, K., Witte, U., Roberts, J.M., 2016. The effect of flow speed and food size on the capture efficiency and feeding behaviour of the cold-water coral *Lophelia pertusa*. *J. Exp. Mar. Bio. Ecol.* 481, 34–40. <https://doi.org/10.1016/j.jembe.2016.04.002>

Otero, V., Van De Kerchove, R., Satyanarayana, B., Martínez-Espinosa, C., Fisol, M.A. Bin, Ibrahim, M.R. Bin, Sulong, I., Mohd-Lokman, H., Lucas, R., Dahdouh-Guebas, F., 2018. Managing mangrove forests from the sky: Forest inventory using field data and Unmanned Aerial Vehicle (UAV) imagery in the Matang Mangrove Forest Reserve, peninsular Malaysia. *For. Ecol. Manage.* 411, 35–45. <https://doi.org/10.1016/j.foreco.2017.12.049>

Pal, M., 2005. Random forest classifier for remote sensing classification. *Int. J. Remote Sens.* 26, 217–222. <https://doi.org/10.1080/01431160412331269698>

Panagiotidis, D., Surovy, P., Kuželka, K., 2016. Accuracy of Structure from Motion models in comparison with terrestrial laser scanner for the analysis of DBH and height influence on error behaviour. *J. For. Sci.* 62, 357–365. <https://doi.org/10.17221/92/2015-JFS>

- Paradis, S., Puig, P., Masqué, P., Juan-Díaz, X., Martín, J., Palanques, A., 2017. Bottom-trawling along submarine canyons impacts deep sedimentary regimes. *Sci. Rep.* 7, 1–12. <https://doi.org/10.1038/srep43332>
- Pascoe, Kailey H., Fukunaga, A., Kosaki, R.K., Burns, J.H.R., 2021. 3D assessment of a coral reef at Lalo Atoll reveals varying responses of habitat metrics following a catastrophic hurricane. *Sci. Rep.* 11, 12050. <https://doi.org/10.1038/s41598-021-91509-4>
- Pavoni, G., Corsini, M., Callieri, M., Palma, M., Scopigno, R., 2019. SEMANTIC SEGMENTATION OF BENTHIC COMMUNITIES From ORTHO-MOSAIC MAPS. *ISPRS Ann. Photogramm. Remote Sens. Spat. Inf. Sci.* 42, 151–158. <https://doi.org/10.5194/isprs-archives-XLII-2-W10-151-2019>
- Pavoni, G., Corsini, M., Ponchio, F., Muntoni, A., Edwards, C., Pedersen, N., Sandin, S., Cignoni, P., 2022. TagLab: AI-assisted annotation for the fast and accurate semantic segmentation of coral reef orthoimages. *J. F. Robot.* 39, 246–262. <https://doi.org/10.1002/rob.22049>
- Pedregosa, F., Varoquaux, G., Gramfort, A., Michel, V., Thirion, B., Grisel, O., Blondel, M., Prettenhofer, P., Weiss, R., Dubourg, V., others, 2011. Scikit-learn: Machine learning in Python. *J. Mach. Learn. Res.* 12, 2825–2830.
- Peters, R.H., 1983. *The Ecological Implications of Body Size*. Cambridge University Press. <https://doi.org/10.1017/CBO9780511608551>
- Piazza, P., Cummings, V., Guzzi, A., Hawes, I., Lohrer, A., Marini, S., Marriott, P., Menna, F., Nocerino, E., Peirano, A., Kim, S., Schiaparelli, S., 2019. Underwater photogrammetry in Antarctica: long-term observations in benthic ecosystems and legacy data rescue. *Polar Biol.* 42, 1061–1079. <https://doi.org/10.1007/s00300-019-02480-w>
- Pierce, J., Butler, M.J.I., Rzhanov, Y., Lowell, K., Dijkstra, J.A., 2021. Classifying 3-D Models of Coral Reefs Using Structure-From-Motion and Multi-View Semantic Segmentation. *Front. Mar. Sci.* 0, 1623. <https://doi.org/10.3389/FMARS.2021.706674>

- Pittman, S.J., Costa, B.M., Battista, T.A., 2009. Using Lidar Bathymetry and Boosted Regression Trees to Predict the Diversity and Abundance of Fish and Corals. *J. Coast. Res.* 10053, 27–38. <https://doi.org/10.2112/si53-004.1>
- Pizarro, O., 2004. Large Scale Structure from Motion for Autonomous Underwater Vehicle Surveys. Massachusetts Institute of Technology.
- Pizarro, O., Eustice, R.M., Singh, H., 2009. Large area 3-D reconstructions from underwater optical surveys. *IEEE J. Ocean. Eng.* 34, 150–169. <https://doi.org/10.1109/JOE.2009.2016071>
- Pizarro, O., Friedman, A., Bryson, M., Williams, S.B., Madin, J., 2017. A simple, fast, and repeatable survey method for underwater visual 3D benthic mapping and monitoring. *Ecol. Evol.* 7, 1770–1782. <https://doi.org/10.1002/ece3.2701>
- Pontoppidan, E., 1755. The Natural History of Norway. A. Linde, Bookseller to Her Royal Highness the Princess Dowager of Wales, in Catherine-Street in the Strand.
- Poux, F., Neuville, R., Nys, G.A., Billen, R., 2018. 3D point cloud semantic modelling: Integrated framework for indoor spaces and furniture. *Remote Sens* 10. <https://doi.org/10.3390/rs10091412>
- Prado, E., Rodríguez-Basalo, A., Cobo, A., Ríos, P., Sánchez, F., 2020. 3D fine-scale terrain variables from underwater photogrammetry: A new approach to benthic microhabitat modeling in a circalittoral Rocky shelf. *Remote Sens.* 12, 2466. <https://doi.org/10.3390/RS12152466>
- Prado, E., Sánchez, F., Rodríguez-Basalo, A., Altuna, Á., Cobo, A., 2019. Analysis of the population structure of a gorgonian forest (*Placogorgia* sp.) using a photogrammetric 3D modeling approach at Le Danois Bank, Cantabrian Sea. *Deep. Res. Part I Oceanogr. Res. Pap.* 153. <https://doi.org/10.1016/j.dsr.2019.103124>
- Price, D.M., Felgate, S.L., Huvenne, V.A.I., Strong, J., Carpenter, S., Barry, C., Lichtschlag, A., Sanders, R., Carrias, A., Young, A., Andrade, V., Cobb, E., Le Bas, T., Brittain, H., Evans, C., 2022. Quantifying the Intra-Habitat Variation of Seagrass Beds with Unoccupied Aerial Vehicles (UAVs). *Remote Sens.* 14, 480. <https://doi.org/10.3390/rs14030480>

Price, D.M., Lim, A., Callaway, A., Eichhorn, M.P., Wheeler, A.J., Lo Iacono, C., Huvenne, V.A.I., 2021. Fine-Scale Heterogeneity of a Cold-Water Coral Reef and Its Influence on the Distribution of Associated Taxa. *Front. Mar. Sci.* 8. <https://doi.org/10.3389/fmars.2021.556313>

Price, D.M., Robert, K., Callaway, A., Lo Iacono, C., Hall, R.A., Huvenne, V.A.I., 2019. Using 3D photogrammetry from ROV video to quantify cold-water coral reef structural complexity and investigate its influence on biodiversity and community assemblage. *Coral Reefs* 38, 1007–1021. <https://doi.org/10.1007/s00338-019-01827-3>

Puig, P., Canals, M., Company, J.B., Martín, J., Amblas, D., Lastras, G., Palanques, A., Calafat, A.M., 2012. Ploughing the deep sea floor. *Nature* 489, 286–289. <https://doi.org/10.1038/nature11410>

Puig, P., Palanques, A., 1998. Temporal variability and composition of settling particle fluxes on the Barcelona continental margin (Northwestern Mediterranean). *J. Mar. Res.* 56, 639–654. <https://doi.org/10.1357/002224098765213612>

Purser, A., Bergmann, M., Lundälv, T., Ontrup, J., Nattkemper, T.W., 2009. Use of machine-learning algorithms for the automated detection of cold-water coral habitats: A pilot study. *Mar. Ecol. Prog. Ser.* 397, 241–251. <https://doi.org/10.3354/meps08154>

Purser, A., Orejas, C., Gori, A., Tong, R., Unnithan, V., Thomsen, L., 2013. Local variation in the distribution of benthic megafauna species associated with cold-water coral reefs on the Norwegian margin. *Cont. Shelf Res.* 54, 37–51. <https://doi.org/10.1016/j.csr.2012.12.013>

Qi, C.R., Su, H., Mo, K., Guibas, L.J., 2017. PointNet: Deep learning on point sets for 3D classification and segmentation. *Proc. - 30th IEEE Conf. Comput. Vis. Pattern Recognition, CVPR 2017* 2017-Janua, 77–85. <https://doi.org/10.1109/CVPR.2017.16>

Quincey, D.J., Bishop, M.P., Käab, A., Berthier, E., Flach, B., Bolch, T., Buchroithner, M., Kamp, U., Khalsa, S.J.S., Toutin, T., Haritashya, U.K., Racoviteanu, A., Shroder, J.F., Raup, B.H., 2014. Digital Terrain Modeling and Glacier Topographic Characterization, in: *Global Land Ice Measurements from Space*. Springer Berlin Heidelberg, Berlin, Heidelberg, pp. 113–144. https://doi.org/10.1007/978-3-540-79818-7_5

- Ragey, L., 1952. The work of Laussedat and education in photogrammetry at the National School of Arts and Crafts, Paris. *Photogramm. Eng.* 1, 21–26.
- Reaka-Kudla, M.L., 1997. The Global Biodiversity of Coral Reefs: A comparison with Rain Forests. *Biodivers. II Underst. Prot. Our Biol. Resour.* 83–108.
- Richardson, L.E., Graham, N.A.J., Hoey, A.S., 2017. Cross-scale habitat structure driven by coral species composition on tropical reefs. *Sci. Rep.* 7, 1–11. <https://doi.org/10.1038/s41598-017-08109-4>
- Ripley, B.D., 1976. The second-order analysis of stationary point processes. *J. Appl. Probab.* 13, 255–266. <https://doi.org/10.2307/3212829>
- Rizvic, S., Boskovic, D., Okanovic, V., Slijivo, S., Zukic, M., 2019. Interactive digital storytelling: bringing cultural heritage in a classroom. *J. Comput. Educ.* 6, 143–166. <https://doi.org/10.1007/s40692-018-0128-7>
- Robert, K., Huvenne, V.A.I.I., Georgiopoulou, A., Jones, D.O.B.B., Marsh, L., Carter, D.O.G., Chaumillon, L., 2017. New approaches to high-resolution mapping of marine vertical structures. *Sci. Rep.* 7, 1–14. <https://doi.org/10.1038/s41598-017-09382-z>
- Robert, K., Jones, D.O.B., Roberts, J.M., Huvenne, V.A.I., 2016. Improving predictive mapping of deep-water habitats: Considering multiple model outputs and ensemble techniques. *Deep. Res. Part I Oceanogr. Res. Pap.* 113, 80–89. <https://doi.org/10.1016/j.dsr.2016.04.008>
- Roberts, J.M., Cairns, S.D., 2014. Cold-water corals in a changing ocean. *Curr. Opin. Environ. Sustain.* 7, 118–126. <https://doi.org/10.1016/j.cosust.2014.01.004>
- Roberts, J.M., Harvey, S.M., Lamont, P.A., Gage, J.D., Humphery, J.D., 2000. Seabed photography, environmental assessment and evidence for deep-water trawling on the continental margin west of the Hebrides. *Hydrobiologia* 441, 173–183. <https://doi.org/10.1023/A:1017550612340>
- Roberts, J.M., Long, D., Wilson, J.B., Mortensen, P.B., Gage, J.D., 2003. The cold-water coral *Lophelia pertusa* (Scleractinia) and enigmatic seabed mounds along the north-east Atlantic margin: Are they related? *Mar. Pollut. Bull.* 46, 7–20. [https://doi.org/10.1016/S0025-326X\(02\)00259-X](https://doi.org/10.1016/S0025-326X(02)00259-X)

- Roberts, J.M., Peppe, O.C., Dodds, L.A., Mercer, D.J., Thomson, W.T., Gage, J.D., Meldrum, D.T., 2006. Monitoring environmental variability around cold-water coral reefs: the use of a benthic photoland and the potential of seafloor observatories, in: *Cold-Water Corals and Ecosystems*. Springer-Verlag, pp. 483–502. https://doi.org/10.1007/3-540-27673-4_24
- Roberts, J.M., Wheeler, A., Freiwald, A., Cairns, S., 2009. *Cold-Water Corals, Cold-Water Corals: The Biology and Geology of Deep-Sea Coral Habitats*. Cambridge University Press. <https://doi.org/10.1017/CBO9780511581588>
- Roberts, M., 1997. Coral in deep water | New Scientist [WWW Document]. URL <https://www.newscientist.com/article/mg15521005-500-coral-in-deep-water/> (accessed 1.25.23).
- Roberts, S., Hirshfield, M., 2004. Deep-sea corals: Out of sight, but no longer out of mind. *Front. Ecol. Environ.* 2, 123–130. [https://doi.org/10.1890/1540-9295\(2004\)002\[0123:DCOOSB\]2.0.CO;2](https://doi.org/10.1890/1540-9295(2004)002[0123:DCOOSB]2.0.CO;2)
- Roberts, Wheeler, A.J., Freiwald, A., 2006. Reefs of the Deep: The Biology and Geology of Cold-Water Coral Ecosystems. *Science* (80-.). 312, 543–547. <https://doi.org/10.1126/science.1119861>
- Rodriguez-Galiano, V.F., Ghimire, B., Rogan, J., Chica-Olmo, M., Rigol-Sanchez, J.P., 2012. An assessment of the effectiveness of a random forest classifier for land-cover classification. *ISPRS J. Photogramm. Remote Sens.* 67, 93–104. <https://doi.org/10.1016/j.isprsjprs.2011.11.002>
- Roelfsema, C.M., Lyons, M., Murray, N., Kovacs, E.M., Kennedy, E., Markey, K., Borrego-Acevedo, R., Ordoñez Alvarez, A., Say, C., Tudman, P., Roe, M., Wolff, J., Traganos, D., Asner, G.P., Bambic, B., Free, B., Fox, H.E., Lieb, Z., Phinn, S.R., 2021. Workflow for the Generation of Expert-Derived Training and Validation Data: A View to Global Scale Habitat Mapping. *Front. Mar. Sci.* 8. <https://doi.org/10.3389/fmars.2021.643381>
- Rogers, A.D., 1999. The Biology of *Lophelia pertusa* (L innaeus 1758) and Other Deep-Water Reef-Forming Corals and Impacts from Human Activities. *Int. Rev. Hydrobiol.* 84, 315–406. <https://doi.org/10.1002/iroh.199900032>

- Roynard, X., Deschaud, J.E., Goulette, F., 2018. Classification of point cloud scenes with multiscale voxel deep network. arXiv.
- Rudall, B.H., 1978. Lecture notes in computer science. Vol. 15—L-systems. *Int. J. Biomed. Comput.* 9, 242. [https://doi.org/10.1016/0020-7101\(78\)90038-7](https://doi.org/10.1016/0020-7101(78)90038-7)
- Rüggeberg, A., Flögel, S., Dullo, W.C., Hissmann, K., Freiwald, A., 2011. Water mass characteristics and sill dynamics in a subpolar cold-water coral reef setting at Stjærnsund, northern Norway. *Mar. Geol.* 282, 5–12. <https://doi.org/10.1016/j.margeo.2010.05.009>
- Russell, S.J., Norvig, P., 2010. *Artificial Intelligence: A modern Approach*, 3rd ed. Upper Saddle River, NJ: Prentice Hall.
- Samet, H., Tamminen, M.K., 1988. Efficient Component Labeling of Images of Arbitrary Dimension Represented by Linear Bintree. *IEEE Trans. Pattern Anal. Mach. Intell.* 10, 579–586. <https://doi.org/10.1109/34.3918>
- Savini, A., Corselli, C., 2010. High-resolution bathymetry and acoustic geophysical data from Santa Maria di Leuca Cold Water Coral province (Northern Ionian Sea-Apulian continental slope). *Deep. Res. Part II Top. Stud. Oceanogr.* 57, 326–344. <https://doi.org/10.1016/j.dsr2.2009.08.014>
- Savini, A., Marchese, F., Fallati, L., Corselli, C., Galli, P., 2020. Integrating acoustics and photogrammetry-based 3D point clouds for the generation of a continuous bathymetric model in coral reef environment. EGU2020. <https://doi.org/10.5194/EGUSPHERE-EGU2020-22054>
- Savini, A., Vertino, A., Marchese, F., Beuck, L., Freiwald, A., 2014. Mapping cold-water coral habitats at different scales within the Northern Ionian Sea (central Mediterranean): An assessment of coral coverage and associated vulnerability. *PLoS One* 9, 2002–2005. <https://doi.org/10.1371/journal.pone.0087108>
- Schenk, T., 2005. *Introduction to Photogrammetry*. Dep. Civ. Environ. Eng. Geod. Sci. Ohio State Univ. 79–95.
- Schlacher, T.A., Williams, A., Althaus, F., Schlacher-Hoenlinger, M.A., 2010. High-resolution seabed imagery as a tool for biodiversity conservation planning on

continental margins. *Mar. Ecol.* 31, 200–221. <https://doi.org/10.1111/j.1439-0485.2009.00286.x>

Schoening, T., Osterloff, J., Nattkemper, T.W., 2016. RecoMIA—Recommendations for Marine Image Annotation: Lessons Learned and Future Directions. *Front. Mar. Sci.* 3. <https://doi.org/10.3389/fmars.2016.00059>

Scholz, J., Smith, A.N., 2016. Augmented reality: Designing immersive experiences that maximize consumer engagement. *Bus. Horiz.* 59, 149–161. <https://doi.org/10.1016/j.bushor.2015.10.003>

Schratz, P., Muenchow, J., Iturrity, E., Richter, J., Brenning, A., 2019. Hyperparameter tuning and performance assessment of statistical and machine-learning algorithms using spatial data. *Ecol. Modell.* 406, 109–120. <https://doi.org/10.1016/j.ecolmodel.2019.06.002>

Seiler, J., Friedman, A., Steinberg, D., Barrett, N., Williams, A., Holbrook, N.J., 2012. Image-based continental shelf habitat mapping using novel automated data extraction techniques. *Cont. Shelf Res.* 45, 87–97. <https://doi.org/10.1016/j.csr.2012.06.003>

Settles, B.H., 2003. Feature Spaces. *Comput. Sci.* 540 *Introd. to Artif. Intel.*

Shang, X., Robert, K., Misiuk, B., Mackin-McLaughlin, J., Zhao, J., 2021. Self-adaptive analysis scale determination for terrain features in seafloor substrate classification. *Estuar. Coast. Shelf Sci.* 254. <https://doi.org/10.1016/j.ecss.2021.107359>

Shannon, P.M., 1991. The development of Irish offshore sedimentary basins. *J. Geol. Soc. London.* 148, 181–189. <https://doi.org/10.1144/gsjgs.148.1.0181>

Shelton, B.E., Hedley, N.R., 2004. Exploring a cognitive basis for learning spatial relationships with augmented reality. *Technol. Instr. Cogn. Learn.* 1, 323.

Shewchuk, J.R., 2002. Delaunay refinement algorithms for triangular mesh generation. *Comput. Geom.* 22, 21–74. [https://doi.org/10.1016/S0925-7721\(01\)00047-5](https://doi.org/10.1016/S0925-7721(01)00047-5)

Shihavuddin, A.S.M., Gracias, N., Garcia, R., Gleason, A., Gintert, B., 2013. Image-Based Coral Reef Classification and Thematic Mapping. *Remote Sens.* 5, 1809–1841. <https://doi.org/10.3390/rs5041809>

- Singh, H., Roman, C., Pizarro, O., Eustice, R., Can, A., 2007. Towards high-resolution imaging from underwater vehicles. *Int. J. Rob. Res.* 26, 55–74. <https://doi.org/10.1177/0278364907074473>
- Smith, M.W., Carrivick, J.L., Quincey, D.J., 2016. Structure from motion photogrammetry in physical geography. *Prog. Phys. Geogr.* 40, 247–275. <https://doi.org/10.1177/0309133315615805>
- Sorice, M.G., Oh, C.-O., Ditton, R.B., 2007. Managing scuba divers to meet ecological goals for coral reef conservation. *AMBIO A J. Hum. Environ.* 36, 316–322.
- Sotiriou, S., Bogner, F.X., 2008. Visualizing the invisible: augmented reality as an innovative science education scheme. *Adv. Sci. Lett.* 1, 114–122.
- Spetsakis, M., Aloimonos, J.Y., 1991. A multi-frame approach to visual motion perception. *Int. J. Comput. Vis.* 6, 245–255. <https://doi.org/10.1007/BF00115698>
- Spezzaferri, S., Vertino, A., Party, and the E.-C.M. cruise scientific, 2012. Cold-water coral ecosystems from the Moira Mounds (NE Atlantic): affinities and differences with modern and Pleistocene Mediterranean counterparts. *RV Belgica, Cruise No. 2012/16, EUROFLEE.*
- Squires, D.F., 1964. Fossil Coral Thickets in Wairarapa, New Zealand. *J. Paleontol.* 38, 904–915.
- Stokes, M.D., Deane, G.B., 2009. Automated processing of coral reef benthic images. *Limnol. Oceanogr. Methods* 7, 157–168. <https://doi.org/10.4319/lom.2009.7.157>
- Storlazzi, C.D., Dartnell, P., Hatcher, G.A., Gibbs, A.E., 2016. End of the chain? Rugosity and fine-scale bathymetry from existing underwater digital imagery using structure-from-motion (SfM) technology. *Coral Reefs* 35, 889–894. <https://doi.org/10.1007/s00338-016-1462-8>
- Summers, G., Lim, A., Wheeler, A.J., 2021. A Scalable, Supervised Classification of Seabed Sediment Waves Using an Object-Based Image Analysis Approach. *Remote Sens.* 13, 2317. <https://doi.org/10.3390/rs13122317>
- Sundahl, H., Buhl-Mortensen, P., Buhl-Mortensen, L., 2020. Distribution and Suitable Habitat of the Cold-Water Corals *Lophelia pertusa*, *Paragorgia arborea*, and *Primnoa*

resedaeformis on the Norwegian Continental Shelf. *Front. Mar. Sci.* 7, 1–22. <https://doi.org/10.3389/fmars.2020.00213>

Ternon, Q., Danet, V., Thiriet, P., Ysnel, F., Feunteun, E., Collin, A., 2022. Classification of underwater photogrammetry data for temperate benthic rocky reef mapping. *Estuar. Coast. Shelf Sci.* 270, 107833. <https://doi.org/10.1016/j.ecss.2022.107833>

Thierens, M., Browning, E., Pirlet, H., Loutre, M.-F., Dorschel, B., Huvenne, V.A.I., Titschack, J., Colin, C., Foubert, A., Wheeler, A.J., 2013. Cold-water coral carbonate mounds as unique palaeo-archives: the Plio-Pleistocene Challenger Mound record (NE Atlantic). *Quat. Sci. Rev.* 73, 14–30. <https://doi.org/10.1016/j.quascirev.2013.05.006>

Thornton, B., Bodenmann, A., Pizarro, O., Williams, S.B., Friedman, A., Nakajima, R., Takai, K., Motoki, K., Watsuji, T. o., Hirayama, H., Matsui, Y., Watanabe, H., Ura, T., 2016. Biometric assessment of deep-sea vent megabenthic communities using multi-resolution 3D image reconstructions. *Deep. Res. Part I Oceanogr. Res. Pap.* 116, 200–219. <https://doi.org/10.1016/j.dsr.2016.08.009>

Titschack, J., Baum, D., De Pol-Holz, R., López Correa, M., Forster, N., Flögel, S., Hebbeln, D., Freiwald, A., 2015. Aggradation and carbonate accumulation of Holocene Norwegian cold-water coral reefs. *Sedimentology* 62, 1873–1898. <https://doi.org/10.1111/sed.12206>

Titschack, J., Thierens, M., Dorschel, B., Schulbert, C., Freiwald, A., Kano, A., Takashima, C., Kawagoe, N., Li, X., 2009. Carbonate budget of a cold-water coral mound (Challenger Mound, IODP Exp. 307). *Mar. Geol.* 259, 36–46. <https://doi.org/10.1016/j.margeo.2008.12.007>

Trimble, 2018. Trimble Documentation: eCognition® Developer User Guide 1–272.

Tsang, I.W., Kwok, J.T., Cheung, P.M., 2005. Core vector machines: Fast SVM training on very large data sets. *J. Mach. Learn. Res.* 6, 363–392.

Turley, C M, Roberts, J.M., Guinotte, J.M., 2007. Corals in deep-water: will the unseen hand of ocean acidification destroy cold-water ecosystems? *Coral Reefs* 26, 445–448. <https://doi.org/10.1007/s00338-007-0247-5>

Turley, C. M., Roberts, J.M., Guinotte, J.M., 2007. Corals in deep-water: will the unseen hand of ocean acidification destroy cold-water ecosystems? *Coral Reefs* 26, 445–448. <https://doi.org/10.1007/s00338-007-0247-5>

Turner, A.K., 1997. What's the difference among 2D, 2.5D, 3D and 4D? *Appl. Geosci. Forum*.

Unity Technologies, 2021. Real-time solutions. Endless opportunities. [WWW Document]. Unity Webseite. URL <https://unity.com/>

Urbina-Barreto, I., Garnier, R., Elise, S., Pinel, R., Dumas, P., Mahamadaly, V., Facon, M., Bureau, S., Peignon, C., Quod, J.-P., Dutrieux, E., Penin, L., Adjeroud, M., 2021. Which Method for Which Purpose ? A Comparison of Line Intercept Transect and Underwater Photogrammetry Methods for Coral Reef Surveys. *Front. Mar. Sci.* 8. <https://doi.org/10.3389/fmars.2021.636902>

Urbina-barreto, I., Pinel, R., Fr, L., Mahamadaly, V., Elise, S., Kulbicki, M., Quod, J., Dutrieux, E., 2020. Quantifying the shelter capacity of coral reefs using photogrammetric 3D modeling : From colonies to reefscales. *Ecol. Indic.* 107151. <https://doi.org/10.1016/j.ecolind.2020.107151>

Urbina-Barreto, I., Elise, S., Guilhaumon, F., Bruggemann, J.H., Pinel, R., Kulbicki, M., Vigliola, L., Mou-Tham, G., Mahamadaly, V., Facon, M., Bureau, S., Peignon, C., Dutrieux, E., Garnier, R., Penin, L., Adjeroud, M., 2022. Underwater photogrammetry reveals new links between coral reefscape traits and fishes that ensure key functions. *Ecosphere* 13, 1–18. <https://doi.org/10.1002/ecs2.3934>

Van Audenhaege, L., Broad, E., Hendry, K.R., Huvenne, V.A.I., 2021. High-Resolution Vertical Habitat Mapping of a Deep-Sea Cliff Offshore Greenland. *Front. Mar. Sci.* 8. <https://doi.org/10.3389/fmars.2021.669372>

van den Bergh, J., Chirayath, V., Li, A., Torres-Pérez, J.L., Segal-Rozenhaimer, M., 2021. NeMO-Net – Gamifying 3D Labeling of Multi-Modal Reference Datasets to Support Automated Marine Habitat Mapping. *Front. Mar. Sci.* 8. <https://doi.org/10.3389/fmars.2021.645408>

Victorero, L., Blamart, D., Pons-Branchu, E., Mavrogordato, M.N., Huvenne, V.A.I.I., 2016. Reconstruction of the formation history of the Darwin Mounds, N Rockall Trough: How the dynamics of a sandy contourite affected cold-water coral growth. *Mar. Geol.* 378, 186–195. <https://doi.org/10.1016/j.margeo.2015.12.001>

VRgeoscience, 2022. Digital Outcrop Modelling [WWW Document].

Vuforia, 2015. Vuforia Engine [WWW Document]. Vuforia. URL <https://developer.vuforia.com/>

Wakita, N., Hirokawa, K., Ichikawa, T., Yamauchi, Y., 2010. Development of Autonomous Underwater Vehicle (AUV) for Exploring Deep Sea Marine Mineral Resources. *Mitsubishi Heavy Ind. Tech. Rev.* 47, 73–80.

Walbridge, S., 2018. Unified Geomorphological Analysis Workflows with Benthic Terrain Modeler. *Geosciences* 8, 94. <https://doi.org/10.3390/geosciences8030094>

Walker, J., Bennett, A.P., Thornton, B., 2021. Towards Observation Condition Agnostic Fauna Detection and Segmentation in Seafloor Imagery for Biomass Estimation, in: *OCEANS 2021: San Diego – Porto*. IEEE, pp. 1–8. <https://doi.org/10.23919/OCEANS44145.2021.9705692>

Warfield, A.D., Leon, J.X., 2019. Estimating Mangrove Forest Volume Using Terrestrial Laser Scanning and UAV-Derived Structure-from-Motion. *Drones* 3, 32. <https://doi.org/10.3390/drones3020032>

Weidner, L., Walton, G., Krajnovich, A., 2021. Classifying rock slope materials in photogrammetric point clouds using robust color and geometric features. <https://doi.org/10.13140/RG.2.2.35632.89604>

Weinmann, M., Jutzi, B., Hinz, S., Mallet, C., 2015. Semantic point cloud interpretation based on optimal neighborhoods, relevant features and efficient classifiers. *ISPRS J. Photogramm. Remote Sens.* 105, 286–304. <https://doi.org/10.1016/j.isprsjprs.2015.01.016>

Westoby, M.J., Brasington, J., Glasser, N.F., Hambrey, M.J., Reynolds, J.M., 2012. ‘Structure-from-Motion’ photogrammetry: A low-cost, effective tool for geoscience

applications. *Geomorphology* 179, 300–314.

<https://doi.org/10.1016/J.GEOMORPH.2012.08.021>

Wheeler, A.J., Beyer, A., Freiwald, A., de Haas, H., Huvenne, V.A.I.I., Kozachenko, M., Olu-Le Roy, K., Opderbecke, J., 2007a. Morphology and environment of cold-water coral carbonate mounds on the NW European margin. *Int. J. Earth Sci.* 96, 37–56. <https://doi.org/10.1007/s00531-006-0130-6>

Wheeler, A.J., Ferdelman, T., Freiwald, A., Hebbeln, D., Henriët, J.P., 2007b. Cold-Water Coral Ecosystem Functioning through Time in the Deep Sea : The example of cold-water coral carbonate mounds in the northeast Atlantic (from IODP307 to EuroMARC - CARBONATE) 9.

Wheeler, A.J., Kozachenko, M., Henry, L.-A., Foubert, A., de Haas, H., Huvenne, V.A.I.A.I., Masson, D.G.G., Olu, K., 2011. The Moira Mounds, small cold-water coral banks in the Porcupine Seabight, NE Atlantic: Part A—an early stage growth phase for future coral carbonate mounds? *Mar. Geol.* 282, 53–64. <https://doi.org/10.1016/j.margeo.2010.08.006>

Wheeler, A.J., Kozachenko, M., Masson, D.G., Huvenne, V.A.I., 2008. Influence of benthic sediment transport on cold-water coral bank morphology and growth: the example of the Darwin Mounds, north-east Atlantic. *Sedimentology* 55, 1875–1887. <https://doi.org/10.1111/j.1365-3091.2008.00970.x>

Wheeler, A.J., Beck, T., Thiede, J., Klages, M., Grehan, A., Monteys, F.X., 2005a. Deep-water coral mounds on the Porcupine Bank, Irish Margin: preliminary results from the Polarstern ARK-XIX/3a ROV cruise, in: Freiwald, A., Roberts, J.M. (Eds.), *Cold-Water Corals and Ecosystems*. Springer Berlin Heidelberg, Berlin, Heidelberg, pp. 393–402. https://doi.org/10.1007/3-540-27673-4_19

Wheeler, A.J., Bett, B., Billett, D.S., Masson, D.G., Mayor, D.J., 2005b. The Impact of Demersal Trawling on Northeast Atlantic Deepwater Coral Habitats: The Case of the Darwin Mounds, United Kingdom. *Am. Fish. Soc. Symp.* 41, 807–817.

Wheeler, A.J., Kozachenko, M., Beyer, A., Foubert, A., Huvenne, V.A.I., Klages, M., Masson, D.G., Olu-Le Roy, K., Thiede, J., 2005c. Sedimentary processes and carbonate mounds in the Belgica Mound province, Porcupine Seabight, NE Atlantic, in: *Cold-*

Water Corals and Ecosystems. Springer Berlin Heidelberg, Berlin, Heidelberg, pp. 571–603. https://doi.org/10.1007/3-540-27673-4_28

White, M., 2007. Benthic dynamics at the carbonate mound regions of the Porcupine Sea Bight continental margin. *Int. J. Earth Sci.* 96, 1–9. <https://doi.org/10.1007/s00531-006-0099-1>

White, M., Mohn, C., de Stigter, H., Mottram, G., 2005. Deep-water coral development as a function of hydrodynamics and surface productivity around the submarine banks of the Rockall Trough, NE Atlantic. *Cold-Water Corals Ecosyst.* 503–514. https://doi.org/10.1007/3-540-27673-4_25

Williams, I.D., Couch, C., Beijbom, O., Oliver, T., Vargas-Angel, B., Schumacher, B., Brainard, R., 2019. Leveraging automated image analysis tools to transform our capacity to assess status and trends on coral reefs. *Front. Mar. Sci.* 6. <https://doi.org/10.3389/fmars.2019.00222>

Wilson, 1979a. 'Patch' development of the deep-water coral *Lophelia Pertusa* (L.) on Rockall Bank. *J. Mar. Biol. Assoc. United Kingdom* 59, 165–177. <https://doi.org/10.1017/S0025315400046257>

Wilson, 1979b. The distribution of the coral *Lophelia pertusa* (L.) [*L. prolifera* (Pallas)] in the north-east Atlantic. *J. Mar. Biol. Assoc. United Kingdom* 59, 149–164. <https://doi.org/10.1017/S0025315400046245>

Wilson, A.M., 2016. Lateral transport of suspended particulate matter in nepheloid layers along the Irish continental margin - a case study of the Whittard Canyon, North-East Atlantic Ocean. *Earth Ocean Sci. Sch. Nat. Sci. Natl. Univ. Ireland, Galw.*

Wilson, M.F.J., O'Connell, B., Brown, C., Guinan, J.C., Grehan, A.J., 2007. Multiscale Terrain Analysis of Multibeam Bathymetry Data for Habitat Mapping on the Continental Slope. *Mar. Geod.* 30, 3–35. <https://doi.org/10.1080/01490410701295962>

Wolf, P.R., Dewitt, B.A., Wilkinson, B.E., 2014. *Elements of Photogrammetry with Applications in GIS*, 4th ed. 696 pp.

Wu, J., Chen, X.Y., Zhang, H., Xiong, L.D., Lei, H., Deng, S.H., 2019. Hyperparameter optimization for machine learning models based on Bayesian optimization. *J. Electron. Sci. Technol.* 17, 26–40. <https://doi.org/10.11989/JEST.1674-862X.80904120>

Xu, Y., Tuttas, S., Hoegner, L., Stilla, U., 2018. Voxel-based segmentation of 3D point clouds from construction sites using a probabilistic connectivity model. *Pattern Recognit. Lett.* 102, 67–74. <https://doi.org/10.1016/j.patrec.2017.12.016>

Young, G.C., 2018. Convolutional Neural Networks Predict Fish Abundance from Underlying Coral Reef Texture.

Young, G.C., Dey, S., Rogers, A.D., Exton, D., 2018. Cost and time-effective method for multi-scale measures of rugosity, fractal dimension, and vector dispersion from coral reef 3D models. *PLoS One* 13, 1–18. <https://doi.org/10.1371/journal.pone.0201847>

Yu, X., Ma, Y., Farrington, S., Reed, J., Ouyang, B., Principe, J.C., 2019. Fast segmentation for large and sparsely labeled coral images. *Proc. Int. Jt. Conf. Neural Networks 2019-July*. <https://doi.org/10.1109/IJCNN.2019.8852014>

Yuval, M., Alonso, I., Eyal, G., Tchernov, D., Loya, Y., Murillo, A.C., Treibitz, T., 2021a. Repeatable Semantic Reef-Mapping through Photogrammetry and Label-Augmentation. *Remote Sens.* 13, 659. <https://doi.org/10.3390/rs13040659>

Zelada Leon, A., Huvenne, V.A.I., Benoist, N.M.A., Ferguson, M., Bett, B.J., Wynn, R.B., 2020. Assessing the Repeatability of Automated Seafloor Classification Algorithms, with Application in Marine Protected Area Monitoring. *Remote Sens.* 12, 1572. <https://doi.org/10.3390/rs12101572>

Zhang, X., Chen, G., Wang, W., Wang, Q., Dai, F., 2017. Object-Based Land-Cover Supervised Classification for Very-High-Resolution UAV Images Using Stacked Denoising Autoencoders. *IEEE J. Sel. Top. Appl. Earth Obs. Remote Sens.* 10, 3373–3385. <https://doi.org/10.1109/JSTARS.2017.2672736>

Zurowietz, Martin, Langenkämper, D., Hosking, B., Ruhl, H.A., Nattkemper, T.W., 2018. MAIA-A machine learning assisted image annotation method for environmental monitoring and exploration. *PLoS One* 13. <https://doi.org/10.1371/journal.pone.0207498>

